Springer Theses
Recognizing Outstanding Ph.D. Research

Tao Ding

Power System Operation with Large Scale Stochastic Wind Power Integration

Interval Arithmetic Based Analysis and Optimization Methods

Springer

Springer Theses

Recognizing Outstanding Ph.D. Research

Aims and Scope

The series "Springer Theses" brings together a selection of the very best Ph.D. theses from around the world and across the physical sciences. Nominated and endorsed by two recognized specialists, each published volume has been selected for its scientific excellence and the high impact of its contents for the pertinent field of research. For greater accessibility to non-specialists, the published versions include an extended introduction, as well as a foreword by the student's supervisor explaining the special relevance of the work for the field. As a whole, the series will provide a valuable resource both for newcomers to the research fields described, and for other scientists seeking detailed background information on special questions. Finally, it provides an accredited documentation of the valuable contributions made by today's younger generation of scientists.

Theses are accepted into the series by invited nomination only and must fulfill all of the following criteria

- They must be written in good English.
- The topic should fall within the confines of Chemistry, Physics, Earth Sciences, Engineering and related interdisciplinary fields such as Materials, Nanoscience, Chemical Engineering, Complex Systems and Biophysics.
- The work reported in the thesis must represent a significant scientific advance.
- If the thesis includes previously published material, permission to reproduce this must be gained from the respective copyright holder.
- They must have been examined and passed during the 12 months prior to nomination.
- Each thesis should include a foreword by the supervisor outlining the significance of its content.
- The theses should have a clearly defined structure including an introduction accessible to scientists not expert in that particular field.

More information about this series at http://www.springer.com/series/8790

Tao Ding

Power System Operation with Large Scale Stochastic Wind Power Integration

Interval Arithmetic Based Analysis and Optimization Methods

Doctoral Thesis accepted by
Tsinghua University, Beijing, China

Springer

Author
Dr. Tao Ding
Xi'an Jiaotong University
Xi'an
China

Supervisor
Prof. Hongbin Sun
Tsinghua University
Beijing
China

ISSN 2190-5053 ISSN 2190-5061 (electronic)
Springer Theses
ISBN 978-981-10-2560-0 ISBN 978-981-10-2561-7 (eBook)
DOI 10.1007/978-981-10-2561-7

Library of Congress Control Number: 2016949622

Printed on acid-free paper

This Springer imprint is published by Springer Nature
The registered company is Springer Nature Singapore Pte Ltd.
The registered company address is: 152 Beach Road, #22-06/08 Gateway East, Singapore 189721, Singapore

Supervisor's Foreword

Over the past decades, overdevelopment of conventional fossil energy resulted in a range of problems, such as environmental pollution, which pose threats on human health and sustainability. In recent years, hydro, wind, solar power, natural gas, and other clean energy alternatives, which are expected to be dominant forms of energy in the future, are being developed at rapid speeds to accommodate future energy demands.

Wind power, as an alternative to fossil fuels, is one of the most important and prominent renewable resources that is under development in an unprecedented rapid pace around the world, due to the increasing electricity demands and the need for more environmentally benign electric power generation. Wind farm development in China is in fast lane too. At the end of 2012, the total installed capacity in China, excluding Taiwan, was 75.32 GW, which topped USA to become the country with most installed wind power [1, 2]. In China, however, wind resources are mainly distributed in northern and northwestern areas of the country, which are far from the major load centers in the eastern and coastal areas. Therefore, wind power is centrally collected and integrated into the power grid through long-distance transmission systems to transport the wind power to these load centers. Take Zhangbei wind farm base in North China; for example, there are nearly 20 wind farms integrated into the grid via a single 220-kV transmission line, while in the area there is neither conventional power plant nor load demand. In addition, several 10-GW-level wind power bases will be built in wind-rich areas, including Inner Mongolia, Gansu, Xinjiang, Hebei, and Jiangsu, by the end of 2020. These large wind farm bases are expected to be connected to the power grid via centralized integration.

However, large-scale wind power integrated into power system brings about a great challenge to traditional power flow analysis and economic dispatch decision. Unlike traditional thermal generators, the generation output of wind power is always uncertain and varies with natural conditions including location, wind speed and direction, air temperature, and humidity. The strong randomness of wind power makes it difficult to predict and control. Moreover, as mentioned above, when

compared to other countries, wind power consumptive problem in China is more prominent since the wind power resource distributes unevenly, mostly in areas far away from the load and difficult to achieve dispersive elimination locally; thirdly, the wind farm growth rate is much higher than that of the local power consumption. Due to the transmission capacity limitation of transmission corridors, safety and stability may be compromised, resulting in serious wind curtailment.

Therefore, it is urgent to develop new techniques to accommodate wind power in a secure and economic way. This Ph.D. dissertation mainly focuses on these topics to address uncertainties. Based on interval mathematics, the wind power uncertainties are modeled as interval numbers, which facilitates the modeling of wind power. Furthermore, this book studies the mathematical modeling and methods to interval power flow, interval economic dispatch, and interval robust economic dispatch. Its breath is impressive and seldom seen in the context of a Ph.D. dissertation.

Beijng, China
July 2016

Prof. Hongbin Sun

Preface

Large-scale wind power integrated into power system brings about a great challenge to traditional power flow analysis and economic dispatch decision. This book mainly focuses on these topics to address uncertainties. Based on interval mathematics, the wind power uncertainties are modeled as interval numbers, which facilitates the modeling of wind power. Furthermore, this book studies the mathematical modeling and methods to interval power flow, interval economic dispatch, and interval robust economic dispatch.

In Chap. 1, literature review of related works is presented, and their contributions to the book are summarized.

In Chap. 2, as the basis of this book, mathematical theories of interval calculation and optimal planning are introduced, including definition of interval number, the method for the linear equations with right-hand interval, interval optimal solution, and self-adaptive two-stage robust interval optimization.

Chapter 3 investigates the interval power flow with uncertain wind power, including DC interval flow, AC interval flow, and distribution system interval flow, in which a preprocessing iteration and parallel calculation are adopted to prevent over conservativeness; the DC power flow is taken as an example to discuss power flow calculation with constraints and dynamic interval power flow model.

In Chap. 4, the traditional economic dispatch is expanded to interval economic dispatch in which interval of wind power output is considered; in fact, interval optimization can be seen as the sensitive analysis of the traditional economic dispatch, because it provides a reference for system dispatchers about the influence of wind power uncertainty on the result of economic dispatch; interval optimization is also different from sensitive analysis because interval optimization can consider parameters that change over a wide interval while sensitive analysis usually focuses on the parameters changing within a tight range; it is worth noticing that there might be no feasible solution under the wind power uncertainty, so a minimal wind curtailment and soft transmission constraints are adopted to guarantee feasibility.

In Chap. 5, the robust optimization strategy is adopted to search for the optimal solution. The result from Chap. 3 is usually more suitable for evaluation rather than dispatching order. Dispatching order should be a concrete number instead of an

interval number, while robust optimization can provide a concrete dispatching order that satisfy security constraints in uncertain scenarios. Two types of interval robust optimization models are discussed in this chapter: One is the self-adaptive interval robust optimization that can guarantee power balance by the introduction of AGC participation factor. It is shown that this participation factor has some effect on the conservativeness of the robust optimization. If the participation factor can be regulated real time in real-time energy market (within 5 min), then the conservativeness of the robust optimization can be reduced; the second type is to perform economic dispatch under wind power uncertainty considering topology reconfiguration, which is a long-term problem in comparison with the first type, which is a real-time problem. From the perspective of mathematical modeling, two-stage robust economic dispatch is a tri-level optimization model, which can be turned into a mixed-integer optimization problem by Benders decomposition, and the optimal result can be achieved by column constraint generation that introduces cutting planes; while the self-adaptive interval robust optimization model is a bi-level problem, which can be turned to a convex second-order model by adding dummy variables; the most significant problem in the robust optimization is to reduce the conservativeness, and in this book, the concept of robust cost is introduced to reach the balance between security and economy. Finally, some practical problems in power system modeling are discussed, and their mathematical models and algorithms are provided.

In Chap. 6, improved online large-scale economic dispatch problems are studied. It is not hard to understand that real power system has a quite large scale; therefore, the dispatching problem under multiple time periods can be very complex. Such optimization problem is mostly expected to be fast ;and efficiently solved for real-time market regulation and for intraday dispatching in a rolling horizon. To do so, two perspectives are provided to improve online economic dispatching: First is to reduce redundant security constraints through offline simulation to simplify the model, and second is to use parallel optimization approaches to increase computation speed.

Chapter 7 summarizes the works and proposes future research direction.

The draft of this book is the Ph.D. dissertation of Tsinghua University. Due to our limited knowledge, this book might contain mistakes and typos. Please feel free to e-mail us whenever you find any problems within this book. We are more than happy to revise this book on your notice.

Xi'an, China Tao Ding

Parts of this thesis have been published in the following documents:

Journals

[1] **Tao Ding**, Rui Bo, Wei Gu, Hongbin Sun, "Big-M based MIQP method for economic dispatch with disjoint prohibited zones," IEEE Transactions on Power Systems, vol. 29, no. 2, pp. 976–977, March 2014.

[2] **Tao Ding**, Rui Bo, Wei Gu, Hongbin Sun, "Absolute value constraint based method for interval optimization to SCED model," IEEE Transactions on Power Systems, vol. 29, no. 2, pp. 980–981, March 2014.

[3] **Tao Ding**, Rui Bo, Fangxing Li, Hongbin Sun, et al, "Interval power flow analysis using linear relaxation and optimality-based bounds tightening (OBBT) methods," IEEE Transactions on Power Systems, vol. 30, no. 1, pp. 177–188, 2015.

[4] **Tao Ding**, Qinglai Guo, Rui Bo, Hongbin Sun, and Boming Zhang, "A Static Voltage Security Region for Centralized Wind Power Integration − Part I: Concept and Method," Energies, vol. 7, no. 1, pp. 420–443, 2014.

[5] **Tao Ding**, Qinglai Guo, Rui Bo, Hongbin Sun, and Boming Zhang, "A Static Voltage Security Region for Centralized Wind Power Integration − Part II: Applications," Energies, vol. 7, no. 1, pp. 444–461, 2014.

[6] **Tao Ding**, Rui Bo, Fangxing Li, Hongbin Sun, "Optimal Power Flow with the Consideration of Flexible Transmission Line Impedance", IEEE Transactions on Power Systems, vol. 31, no. 2, pp. 1655–1656, 2015.

[7] **Tao Ding**, Rui Bo, Qinglai Guo, Hongbin Sun, "A Robust Two-level Coordinated Static Voltage Condition for Centralized Wind Power Integration", IEEE Transactions on Smart Grid, vol. 7, no. 1, pp. 460–470, 2015.

[8] **Tao Ding**, Rui Bo, Fangxing Li, Hongbin Sun, "A Bi-level Branch and Bound Method For Economic Dispatch with Disjoint Prohibited Zones Considering Network Losses", IEEE Transactions on Power Systems, vol. 30, no. 6, pp. 2841–2855, 2015.

[9] **Tao Ding**, Rui Bo, Fangxing Li, Hongbin Sun, "Exact Penalty Function Based Constraint Relaxation Method For Optimal Power Flow Considering Wind Generation Uncertainty," IEEE Transactions on Power Systems, vol. 30, no. 3, pp. 1546–1547, 2015.

[10] **Tao Ding**, Linquan Bai, Zhaohong Bie, Fangxing Li, "An Adjustable Robust Optimal Power Flow with the Price of Robustness for Large-scale Power Systems," IET Generation, Transmission & Distribution, vol. 10, no. 1, pp. 164–174, 2016.

[11] **Tao Ding**, Zhongyu Wu, Jianjun Lv, Zhaohong Bie, Fengyu Wang, "Robust Co-optimization to Energy and Ancillary Service Joint Dispatch Considering Wind Power Uncertainties in Real-time Electricity Markets," IEEE Transactions on Sustainable Energy, In-press, 2016.

[12] **Tao Ding**, Jiajun Lv, Rui Bo, Zhaohong Bie, Fangxing Li, "Lift-and-Project MVEE Based Convex Hull for Robust SCED with Wind Power Integration Using Historical Data-Driven Modeling," Renewable Energy, vol. 92, pp. 415–427, 2016.

[13] **Tao Ding**, Kai Sun, Can Huang, Zhaohong Bie, Fangxing Li, "Mixed Integer Linear Programming-based Splitting Strategies for Power System Islanding Operation Considering Network Connectivity", IEEE Systems Journal, In-press, 2016.

[14] **Tao Ding**, Shiyu Liu, Wei Yuan, Zhaohong Bie, Bo Zeng, "A Two-Stage Robust Reactive Power Optimization Considering Uncertain Wind Power Integration in Active Distribution Networks", IEEE Transactions on Sustainable Energy, vol. 7, no. 1, pp. 301–311, 2016.

[15] **Tao Ding**, Xue Li, Fangxing Li, Hongbin Sun, "Interval Radial Power Flow Using Extended DistFlow Formulation and Krawczyk Iteration Method with Sparse Approximate Inverse Preconditioner", IET Generation, Transmission & Distribution, vol. 9, no. 14, pp.1998–2006, 2015.

[16] **Tao Ding**, Rui Bo, "Closure to Discussion on 'Interval Power Flow Analysis Using Linear Relaxation and Optimality-Based Bounds Tightening (OBBT) Methods'", IEEE Transactions on Power Systems, vol. 30., no. 4, pp. 2203–2203, 2015.

[17] Can Huang, Fangxing Li, **Tao Ding**, Yumin Jiang, Jiahui Guo, Yilu Liu, "A Bounded Model of the Communication Delay for System Integrity Protection Schemes," IEEE Transactions on Power Delivery, vol. 31, no. 4, pp. 1921–1933, 2016.

[18] Can Huang, Fangxing Li, **Tao Ding**, et al, "Second-order Cone Programming Based Robust Optimal Control for Wind Energy Conversion Systems over Complete Operating Regions", IEEE Transactions on Sustainable Energy, vol. 6, no. 1, pp. 263–271, 2015.

[19] Wei Gu, Lizi Luo, **Tao Ding**, et al, "An affine arithmetic-based algorithm for radial distribution system power flow with uncertainties," International Journal of Electrical Power & Energy Systems, vol. 58, pp. 242–245, 2014.

[20] Tao Niu, Qinglai Guo, Hongbin Sun, Qiuwei Wu, Boming Zhang, **Tao Ding**, "Autonomous Voltage Security Regions to Prevent Cascading Trip Faults in Wind Turbine Generators", IEEE Transactions on Sustainable Energy, vol. 7, no. 3, pp. 1306–1316, 2016.

[21] Zhong Zhang, Jianxue Wang, **Tao Ding**, et al, "A Two-Layer Model for Microgrid Real-Time Dispatch Based on Energy Storage System Charging/Discharging Hidden Costs", IEEE Transactions on Sustainable Energy, In-press, 2016.

[22] **Tao Ding** and Zhaohong Bie, "Parallel Augmented Lagrangian Relaxation for Multi-Period Economic Dispatch Using Diagonal Quadratic Approximation Method", IEEE Transactions on Power Systems, In-press, 2016.

[23] **Tao Ding** and Chaoyue Zhao, "Robust optimal transmission switching with the consideration of corrective actions for N–k contingencies", IET Generation, Transmission & Distribution, In-press, 2016.

[24] **Tao Ding**, Rui Bo, Zhaohong Bie and Xifan Wang, "Optimal Selection of Phase Shifting Transformer Adjustment in Optimal Power Flow", IEEE Transactions on Power Systems, In-press, 2016.

[25] **Tao Ding**, Qinglai Guo, Hongbin Sun, Rui Bo, Zhengyi Yao. "Power System Economic Dispatch Algorithm with Prohibited Zones," Tsinghua University (Science and Technology), vol. 53, no. 4, pp. 447–452, 2013. (in Chinese)

[26] **Tao Ding**, Rui Bo, Qinglai Guo, Hongbin Sun, Wenchuan Wu, Boming Zhang. "A Non-iterative Affine Arithmetic Methodology for Interval Power Flow Analysis of Transmission Network," Proceedings of the CSEE, vol. 33, no.19, pp. 76–83, 2013. (in Chinese)

[27] **Tao Ding**, Qinglai Guo, Rui Bo, Wei Gu, Hongbin Sun, Boming Zhang. "Solving of Interval DC Power Flow Using Interval Hull Algorithm with Preconditioning", Automation of Electric Power System, vol. 38, no. 3, pp. 130–136, 2014. (in Chinese)

[28] Fengda Xu, Qinglai Guo, Hongbin Sun, Boming Zhang, Bin Wang, Zhengshuo Li, **Tao Ding**. "Analysis and Simulation Research on Cascading Trips of Multiple Wind Farms," Power System Technology, vol. 38, no. 6, pp. 1426–1431, 2014. (in Chinese)

[29] **Tao Ding**, Qinglai Guo, Hongbin Sun, Fengda Xu, Xiaofei Xu, Lin Jia. A Voltage Control Strategy for Preventing Cascading Trips of Large-scale Wind Power in Centralized Area, Automation of Electric Power System, vol. 38, no.11, pp. 7–12,2014. (in Chinese)

[30] **Tao Ding**, Qinglai Guo, Rui Bo, Hongbin Sun, Wenchuan Wu, Boming Zhang, Zhengyi Yao. Two-stage Heuristic-correction for Dynamic Reactive Power Optimization Based on Relaxation-MPEC and MIQP, Proceedings of the CSEE, vol. 34, no. 13, pp. 2100–2107, 2014. (in Chinese)

[31] **Tao Ding**, Qinglai Guo, Rui Bo, Liping Zhang, Hongbin Sun, Wenchuan Wu, Boming Zhang. Interval Economic Dispatch Model with Uncertain Wind Power Injection and Spatial Branch and Bound Method, Proceedings of the CSEE, vol. 34, no. 22, pp.3707–3714, 2014. (in Chinese)

[32] **Tao Ding**, Rui Bo, Qinglai Guo, Hongbin Sun, Can Huang, Fangxing Li. Identification of Inactive Constraints for SCED Model Considering Uncertain Power Injection, Proceedings of the CSEE, vol. 34, no. 34, pp.47–50, 2014. (in Chinese)

[33] **Tao Ding**, Rui Bo, Hongbin Sun, Can Huang, Fangxing Li. "Robust Mean-Variance Optimization for Self-schedule of Thermal Producer and Its Price of Robustness," Proceedings of the CSEE, vol. 35, no. 2, pp. 319–326, 2015. (in Chinese)

[34] **Tao Ding**, Rui Bo, Zhengyi Yao, Hongbin Sun. "Real-time Economic Dispatch Model With Prohibited Zones Considering Maximum Wind Power Injection," Proceedings of the CSEE, vol. 35, no. 4, pp. 759–765, 2015. (in Chinese)

International Conferences and Workshops

[1] **Tao Ding**, Rui Bo, Fangxing Li, Hongbin Sun, "Interval Arithmetic Based Optimal Curtailment For Infeasibility of SCED in the Presence of Wind Power Uncertainty," Accepted, IEEE PES General Meeting, Denver, USA, 26–30 July, 2015.

[2] **Tao Ding**, Kai Sun, Xiubin Zhang, Fangxing Li, Honbing Sun, " Graph Theory Based Splitting Strategies for Power System Islanding Operation," Accepted, IEEE PES General Meeting, Denver, USA, 26–30 July, 2015.

[3] Linquan Bai, **Tao Ding**, Qinran Hu, Fangxing Li, Hongbin Sun, "Robust Mean-Variance Optimization Model for Grid-Connected Microgrids," Accepted, IEEE PES General Meeting, Denver, USA, 26–30 July, 2015.

[4] **Tao Ding**, Hongbin Sun, Forrest Harley, et al, "Bi-level linear programming based interval optimization for SCED in the presence of wind power uncertainty," IEEE PES General Meeting, Washington DC, USA, 27–31 July, 2014.

[5] **Tao Ding**, Qinglai Guo, Hongbin Sun, et al, "A quadratic robust optimization model for automatic voltage control of wind farm," IEEE PES General Meeting, Canada, 21–25 July, 2013.

Acknowledgements

On the completion of this book, I should like to express my heartfelt gratitude to all people those who helped me made this book possible and my alma mater—Tsinghua University, where I have spent my three-year Ph.D. life.

I am greatly indebted to my advisor Prof. Hongbin Sun for his professional guidance, constant encouragement, and patience in supervisions. His effective advice and shrewd comments have kept the study in the right direction.

During my study under the visiting Ph.D. student offered by University of Tennessee, Knoxville (UTK), I have benefited enormously from the advisor Prof. Fangxing Li. His valuable comments, guidance, and encouragement help me in all the research as well as my career development.

Besides my advisors, I would like to thank Dr. Rui Bo from Midcontinent ISO for his friendship, massive help, and constructive suggestions. He constantly encouraged me whenever I felt frustrated with this dissertation.

I offer thanks to all the professors and academic staffs at the Department of Electrical Engineering, Tsinghua University, for the courses and academic activities by them to consolidate my mathematical basis and broaden my horizon on academic research.

I also want to express my gratitude to my academic seniors, juniors, and schoolmates from Tsinghua University.

Last but not least, I am especially grateful to my dear parents and my relatives; without their unselfish and cordial support, this book would have been impossible.

The book henceforth was conducted at the Electrical Engineering, Tsinghua University, China, and was supported by the National Key Basic Research Program of China (973 Program) (2013CB228203), the Foundation for Innovative Research Groups of the National Natural Science Foundation of China (51321005), and State Key Lab of Power System of Tsinghua University (SKLD16KZ01), China Postdoctoral Science Foundation (2015M580847), National Natural Science Foundation of China (Grant 51607137) and Natural Science Basis Research Plan in Shaanxi Province of China (2016JQ5015).

Contents

Chapter 1
Introduction

Abstract Large-scale wind power integrated into power system brings about a great challenge to traditional power flow analysis and economic dispatch decision. This book mainly focuses on these topics to address uncertainties. In this chapter, we will give the brief introduction and the whole flowchart of this book.

1.1 Background and Meaning of the Research

The world is facing energy crisis and the deterioration of the natural environment. Wind power as the substitute to traditional fossil fuels with the advantages of clean non-polluting and renewable, has been widely developed and applied. Especially these years, various states support for wind power, making the wind power technology is increasingly mature and improved, whose investment price has also been reduced. The wind power industry got unprecedented development over the world [1, 2].

As can be seen from Figs. 1.1 and 1.2, by the end of 2013, the world's total installed capacity of wind power reached 318.11 GW, about 8.07 times the world's total wind power installed capacity over the past decade, which is equivalent that wind generating had developed an average annual growth rate of 26.19 % since 1996 [3–5]. Among them, China's wind power industry had made unprecedented development [6]. Figure 1.3 describes the case of the total installed capacity of wind power and the new installed capacity since 2008. By the end of 2013, China's total installed capacity of wind power had reached 91.41 GW, which had surpassed the US as the largest wind power installed capacity over the world [6].

However, large-scale wind power is facing a lot of challenges, first and foremost the wind power consumption problem [9–14]. Compared to other countries, Wind power consumptive problem in China is more prominent. First of all, China's wind power resource distribution is more concentrated, mostly in areas far away from the load, with more centralized network form. So it is difficult to achieve dispersive elimination locally, as Europe, North America and other countries; Secondly, the wind power construction growth rate is much higher than its local power

T. Ding, *Power System Operation with Large Scale Stochastic Wind Power Integration*, Springer Theses, DOI 10.1007/978-981-10-2561-7_1

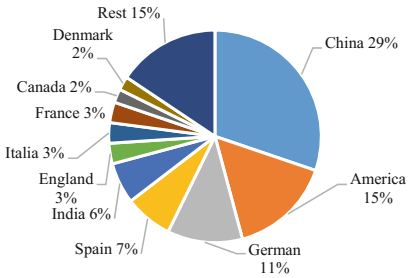

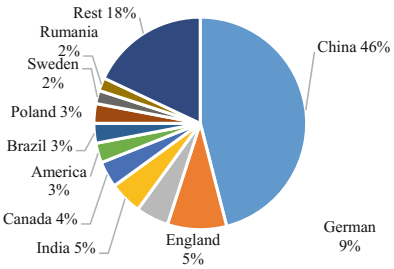

Countries	Installed capacity (MW)	Countries	New installed capacity (MW)
China	91,412	China	16,088
The US	61,091	Germany	3,238
Germany	34,250	The Great British	1,883
Spain	22,959	India	1,729
India	20,150	Canada	1,599
The Great British	10,531	The US	1,084
Italy	8,552	France	953
France	8,254	Poland	894
Canada	7,803	Sweden	724
Portugal	4,772	Romania	695
others	48,332	others	6,402
In total	318,105	In total	35,289

Fig. 1.1 By the end of 2013, the total installed capacity of wind power top 10 countries [7, 8]

consumption. Due to the transmission capacity limitation of transmission corridors, safety and stability may be reduced, resulting in serious "wind curtailment" phenomenon. By the end of 2013, total hours of wind power utilization in China is about 2046 h, while wind power plant's total "wind curtailment" losses is over 16 TWh. "Wind curtailment" has seriously affected China's large wind power base construction speed and the return on developers' investment. Third, wind power generation is different from the traditional thermal power generation is an important feature of wind power output has greater uncertainty, more difficult in prediction and difficult to control the output. Traditional thermal power output can be adjusted by adjusting the output of each turbine intake air units, while wind power output is affected by natural conditions, including location, wind speed and direction, air temperature and humidity, with strong randomness and difficult to predict and control, which brought certain challenges to the traditional schedule and operation.

To do this, how to consider the intermittency and uncertainty of large-scale wind power based on traditional operation and scheduling to ensure more economical, safer and more reliable operation in wind power is the key point of this research.

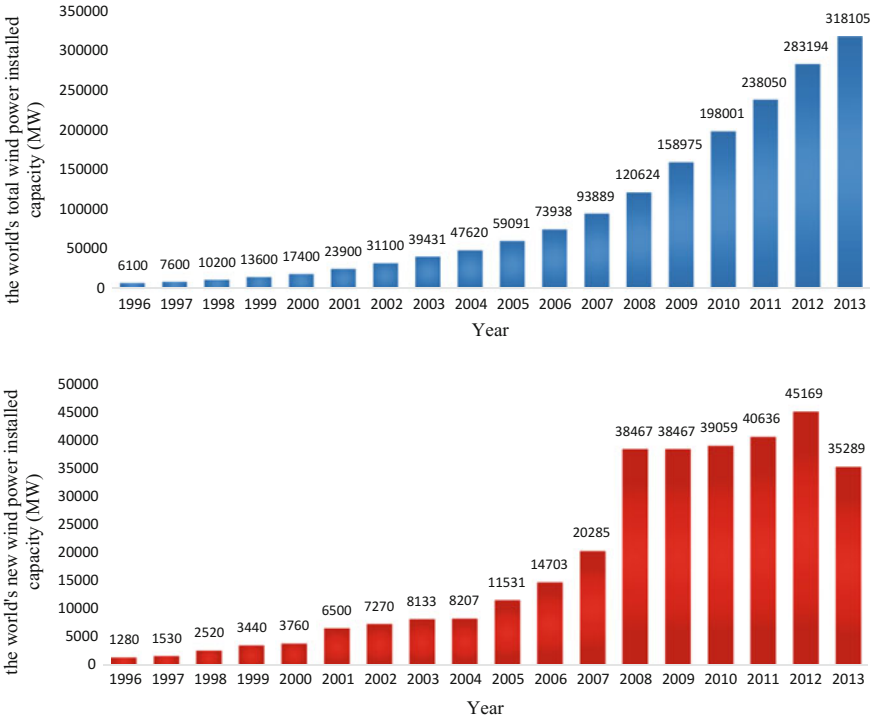

Fig. 1.2 From 1996 to 2013 the total installed capacity and new installed capacity of wind power over the world

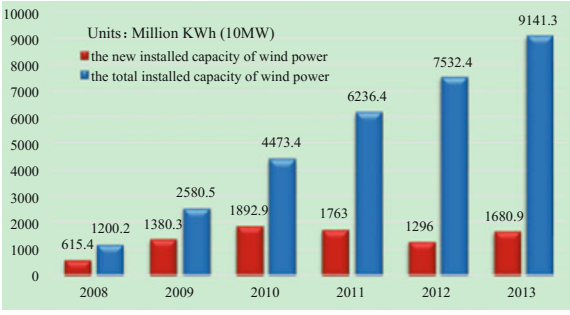

Fig. 1.3 The total installed capacity and new installed capacity of wind power in China

1.2 Research and Research Frontiers

Power flow and optimal dispatch are two important research topics in power system. After considering the uncertainty of wind power, both research got new development and application. This section of the review on the basis of traditional research, mainly reviewed the current research status in domestic and overseas of

power flow calculation and optimization dispatch, considering wind power uncertainties.

1.2.1 The Method to Power Flow Calculation with Uncertainty

Power flow calculation as the base for power system analysis, provides dispatchers intuitive and effective information and is also used as basis for security analysis and other applications.

The essence of the AC power flow is to solve nonlinear equations, solving methods including Gauss-Seidel iterative method [15–18], Newton Raphson iterative method [19–23] and etc. It is found in practical engineering applications that when using Newton's method for solving the flow, its Jacobian matrix can be decomposed into two approximately constant block matrix, which will decompose the original power flow problem into the active and reactive two sub-issues to get iterative solution, making sure to get the same solution with greatly improved speed and memory overhead saving. This method is called PQ decoupling method [24]. To further speed up the convergence of the P-Q decoupling, XB method [25] and BX method [26] has been widely used.

For high-voltage transmission grid, voltage per unit value is usually near 1.0 p.u. reactive power usually use the principle of balance locally, and most part in long-distance transmission is active power. So for the high-voltage grid, in practical applications the active distribution in network branch are usually concerned about, therefore the DC power flow has been widely used in the actual operation, especially for advanced applications of the electricity market. DC power flow is actually approximately linear of the AC power flow, whose essence is to solve linear equations and relative difficulty is greatly reduced compared with AC power flow. LU factorization method is an effective method for solving linear equations [27], which has been widely used in the power system.

To compared with transmission network, distribution network have some differences: first, resistance and reactance of the transmission line in distribution network is roughly equal size, so it often use AC power flow model; Second, its topology is very special, as a tree structure with no loop, usually the number of nodes far exceeding than the transmission network. If Newton's method is still used to solve distribution network problems, those characteristics may affect its calculation speed and Jacobian matrix will have huge memory requirements, for which the distribution network is usually solved by the use of forward and backward substitution method.

However, when large-scale renewable energy connected to the grid, its randomness and intermittent will bring new challenges to the grid dispatch, due to the traditional deterministic power flow calculation does not reflect the random information, so that potential security issues is difficult forewarned operation crew. To

this end, the birth of a series of methods for uncertain power flow, such as the stochastic load flow, fuzzy and probabilistic power flow and so on. Stochastic power flow is uncertain energy output probability distribution obtained by the historical data, usually semi-variable method to replace the current system of convolution operation to give a probability distribution. Fuzzy power flow put intermittent power output to characterize as uncertain fuzzy numbers and then follow the fuzzy number algorithms definition, using fuzzy set theory to solve. Interval power flow places interval manner to model uncertainties, giving the corresponding boundary information, so it has been widely studied [28].

Reference [29–31] used a Monte Carlo-based Newton Raphson stochastic power flow algorithm to solve stochastic power flow issues of uncertain distributed energy; [32] considered the distribution network probability function model of nodal injection power, and obtained probability distribution of power flow; [33] adopted the sigma-point transformation algorithm to solve the problem of the probability power flow, estimating nonlinear flow moments in orders by series expansion; [34] used the artificial neural network method to solve stochastic power flow uncertain confidence interval; [35] adopted the point estimates algorithm to solve the load and generation uncertain probabilistic power flow; [36] discussed the distribution network probabilistic load flow based on current injection under the forward and backward substitution algorithm framework; [37] based on semi-variable method instead of convolution to solve probabilistic power flow problem with correlation between nodal powers; Ref. [38] combined with Gram-Charlier series expansion that is semi-invariant method to solve probabilistic power flow considering static security risks of power grid; according to historical data, Ref. [39] classified load and generation capacity historical data by time, load and generation uncertain probability power flow in different periods of time; Ref. [40] use affine arithmetic to express uncertainty amount, thus, use the method based on optimizing to research calculation of probabilistic power flow; use of thus the use of based approach to the probability of the power flow; the literature [41] considered the power flow calculation of photovoltaic power generation uncertainty and respectively used Gram-Charlier, Edgeworth and Cornish-Fisher expansion to solute probabilistic power flow; [42] reviewed the stochastic load flow model, methods and safety assessment approaches with random wind power; [43] made probability model for random energy output on microgrid operated in island, and used semi-in variant method to be the power flow solution; [44] used a combination of sampling Monte Carlo algorithm for solving probability power flow problems containing large-scale random variables, and used Latin hypercube sampling to improve computational efficiency; [45] analyzed the probabilistic load flow problems based on dynamic flow, respectively considering frequency adjustment and system frequency response process to improve the practical adjacent degree.

Reference [46] reviewed fuzzy number modeling method of loads, which were respectively applied to the DC and AC power flow calculation; [47] used the Fuzzy Set Theory to describe load and power output uncertainty by trapezoidal fuzzy numbers and to get Ac fuzzy power flow by incremental model; [48] used probability theory and fuzzy number theory to build a multi-linearized fuzzy power flow

model; Ref. [49–51] considered about uncertainty of generation and load and proposed the AC non-linear fuzzy power flow which would be used in power system operation and planning; [52] used fuzzy power flow in different loads and failure scenarios to evaluate; [53] used Credibility Theory from Fuzzy Set Theory to make the uncertainty modeling, and gave out the possibility distribution, expectation and variance of power flow; [54] used fuzzy logic control to solve the fuzzy power flow for reducing computation time and the number of iterations, in order to improve solving convergence; a fuzzy power flow with constraints is put in [55], considering the constraints on transmission lines and etc. based on traditional fuzzy power flow, to correct uncertain power flow; [56] adopted trapezoid fuzzy membership to express uncertainty, and an improved fuzzy power flow calculation method based on forward and backward substitution method was put forward, which had the computing speed of linear convergence; [57] discussed that at the lack of historical information the use of traditional power flow by fuzzy power flow could considered uncertain information to provide dispatchers help of decision-making; [58] achieved fuzzy power flow based on fuzzy membership degree on the Linux operating system project; [59] established the possibility distribution of wind speed which was based on random fuzzy compatibility principle, thereby solving the fuzzy power flow problem based on linear model; [60] discussed the impact of the wind power uncertainty under a high permeability on operation and planning, using probability theory and fuzzy sets to establish power flow model of wind power uncertain with different types of wind turbine; [61] applied fuzzy set theory to research calculation method of fuzzy power flow after N-1 line operation.

References [62, 63] used interval mathematics to set an interval model of node injection power uncertainty, and then used an iterative algorithm to solve the boundary of power flow results; the literature [64] established a model for the distribution network operation uncertainty of load, capacitor and phase modifier and solved interval power flow using forward and backward substitution method; [65, 66] established a three-phase range power flow model of load, capacitor and phase modifier, and then considered the three-phase unbalanced load flow calculations; [67, 68] used Krawczyk-Moore interval iteration method to solve the problem of the interval power flow; [69, 70] pointed out that the main problem of interval arithmetic is a little conservative, for this reason, three kinds of representations were introduced into complex plane for complex interval calculation including the complex box, complex disk and complex fan, for solving interval distribution power flow with forward and backward substitution method; [71] proposed genetic algorithm based on examples learning to be introduced into the interval flow calculation; [72] considered uncertainties of the distribution network and the feeder line and used interval mathematics to make a three-phase power flow calculation; [73, 74] considered the interval uncertainty problems of static security analysis and $N-1$ security check; [75] proposed interval PQ decoupled power flow calculation method which considered about uncertainty; [76] used interval analysis method and Interval Gaussian Elimination Method for solving interval DC load flow problem; [77] established an interval load flow model of wind farm, than

analyzed the impact of wind power uncertainty on the steady-state analysis of the wind farm in quantitative; [78] coalesced interval mathematics with interval constraint traditional theory for solving nonlinear interval distribution power flow calculation; [79] used affine mathematics to describe the node inject uncertainty in order to solve the quasi-steady uncertain power flow; considering uncertainty of distributed generation, [80] proposed cutting points calculation of interconnection switch and fast failure recovery method which were based on the analysis of interval power flow; [81] proposed a method which is the combination of affine and interval for solving interval exchange; based on Krawczyk algorithm, [82] proposed a method for solving DC interval power flow, which could obtain a cover better than interval Gaussian elimination method; [83] adopted optimization algorithm and put forward an affine non-iterative calculation method for interval AC power flow; [84] proposed an interval power flow solution based on linear optimization method; [85] established uncertainty model of wind turbine and photovoltaic by interval number and used a complex affine algorithm to solve interval three-phase power flow; [86] made pretreatment on interval DC load flow, forming the main diagonally dominant coefficient matrix to improve the calculation accuracy.

1.2.2 Economic Dispatch Model and Its Solution

Power system economic dispatch is one of important part of the electricity market, according to the US Federal Energy Planning Board, to enhance the efficiency of economic dispatch of small amplitude can cause huge economic savings each year, especially for Independent System Operators (ISOs) in the new software spending, the annual cost can be controlled within 10 million dollars [87].

Potential software investment income ratio in the approximate range of 10–1000, and thus improving the economic scheduling and its solving method is very important.

Economic dispatch based on minimizing operating costs to achieve a reasonable distribution between generator units to match the constraints of generation and load balance. Its essence is to solve the problem of optimal power flow. Depending on the types of power flow equations, economic dispatch can be divided into AC power flow based and DC power flow based; depending on the optimization of time, economic dispatch can be divided into static and dynamic economic dispatch; according to the different types of electricity market, it can be divided into days of real-time market economic dispatch and days-ahead market economy dispatch.

1.2.2.1 Alternating Current (AC) and Direct Current (DC) Economic Dispatch Model

AC economic dispatch model can accurately reflect the characteristics of nonlinear network, but the optimization model has strong nonlinear and non-convex features,

which makes the model very complex and great difficult to solve. Existing some local optimum search algorithms based on Newton descent method [88–90], sequential quadratic programming method [91], the interior point method [92], trust region method [93], active-set method [94, 95] and so on. However, these methods are not particularly robust for large scale power system optimization problems which cause a convergence issues. From the research of power company in the Midwest of the U.S., we found that when using the AC economic dispatch, optimization model cannot converge for some time. Optimization Model analysis found reason why the model don't converge may be the deviation between power system input parameters and the actual case, or some constraints are too strict. Secondly, all of the above algorithms are local optimum search algorithm, which means global optimization cannot guarantee. The optimal solution is closely related to the choice of the initial value, for which reason to give a reasonable initial value in the AC economic dispatch model needs to be noticed.

Compared to AC economic dispatch model, DC economic dispatch model is based an online network to approximate the AC economic dispatch model, which makes the optimization model voltage magnitude, voltage angle, power loss and reactive power some simplify. DC model makes economic dispatch optimization model into a convex optimization, to greatly improve their convergence of solution and global optimization, especially when the objective function is linear, the linear programming model is simple model. Due to the linear programming theory becoming perfect and mature, large-scale computing and decomposition algorithms become more sophisticated, so business software for solving linear programming get rapid development, which makes the DC economic dispatch have been widely used in the actual production and operation. And based on DC optimal power flow model the analysis of the electricity market and power system planning obtain certain income and influence.

AC optimal power flow primarily to get some applications in New York ISO and California ISO, while the rest ISO are DC optimal power flow model, so the DC optimal power flow is still the mainstream applications nowadays.

1.2.2.2 Static and Dynamic Economic Dispatch

Static economic dispatch for load information of a single time section, making generation operation in this time period become the objective function to optimally distribute contribution of generator. This kind of optimization problem can be traced back to the 1930s classic economic dispatch model based on equal incremental principle.

However, the static economic dispatch does not consider the coupling between the various periods of time, in fact, power system is always in operating state of dynamic equilibrium, while the load demand changes in real time, so the output of the generator also need to be adjusted in time to meet the dynamic power balance. However, the generator regulating ability is limited, primarily adjusted the output by changing the passing gas amount of turbine, this regulating system has inertia

which cannot always fast real-time adjust. For this, if system are scheduling following the results of static economic dispatch optimization in each time period, the generator may have physical limitations that cannot transient to the security state, and the results of such scheduling is actually meaningless. To this end, in a static economic dispatch need to consider the coupling between the generator in each period of time, which means constraint climbing ability, thus to form a dynamic economic dispatch model. Dynamic economic dispatch model can be seen as a combination of static economic dispatching multiple time periods, taking into account coupling of each static economic dispatch model variables, forming a combination optimization model. The objective function of the model is to optimize the total cost of multiple time periods and to satisfy static constraints and dynamic constraints of each period of time, with some foresight ability, which can arrange for the generating units scheduling in advance and has great significance to actual scheduling operation.

Number of variables and constraints in dynamic economic dispatch model with respect to the static economic dispatch model is multiplied. Convex and linear features of the model are retained, but solving efficiency will be affected. In early times, solving large combinatorial optimization issues had various types of artificial intelligence algorithms such as particle swarm optimization [96–103], bees algorithm [104], simulated annealing algorithm [105], artificial neural networks [106, 107], genetic algorithm [108–113], evolutionary algorithm [114–117], as well as some other intelligent methods [118–120]. With the improvement and development of mathematical optimization algorithms, dynamic model will generally be pretreated and reduce dimension, so for large-scale dynamic optimization model, dimension reduction model can be solved directly, including quadratic optimization [121], Sequential quadratic programming [122, 123], dynamic programming algorithm [124].

1.2.2.3 Day-Ahead Market Economic Dispatch and Real-Time Market Economy Dispatch

Dynamic economic dispatch of power systems considered the variation of load in multiple time periods in the future and the constraint of dynamic climbing ability of generator sets, but load data in future is achieved by load forecasting. In reality, the prediction error will inevitably be brought and the power grid is also in a real-time-change state, for example, a system failure or a large disturbance, topology changes, etc., so there will also be certain error between decisions run by a dynamic model and the actual grid operation. In order to eliminate the error, the power grid usually dispatch by levels according to different time scales, generally believed that short-term prediction is more accurate than long-term projections of results, therefore, according to the real-time updated forecast information to consume error step by step.

Reference [125] divided the economic dispatch process into two sub-problems, planning and dispatch. Each sub-problem are solving as different optimization

model. On a longer time scale, dynamic economic dispatch model is adopted to give the power plan; over a shorter time scale, static economic dispatch model is adopted, according to the updated prediction information to give amendments on the plan offered by the model in the longer time scale. This method of decomposition is still used in the US electricity market, such as the American Midwest power company and the New England electricity market. The electricity market structure in the U.S. is usually divided into two markets, the day-ahead market and the real-time market. According to the load forecast of every hour, the day-ahead market builds dynamic economic dispatch model and gives the value plan of the next 24 h. The real-time market based on the value forecast of current 5 min, using static economic dispatch model to amend the plan offered by the day-ahead market. The temporal level of the real-time market execution is 5 min. And within 5 min, economic dispatch is no more use to do amendments on instructions, but use Automatic Generation Control (AGC) of the generator to track the dispatch instructions given by the real-time market.

Although China has not implemented the fully open electricity market system, in economic dispatch it also follows a model similar to the hierarchical schedule adopted by foreign countries. But the difference is, there is a time stage for roll amendments added between the day-ahead dispatch and the real-time dispatch in China [126], the in-day rolling dispatch. The most important reason for the difference is that, in the U.S., thermal power units are mostly gas-fired which has a very fast rise speed, however, most of China's thermal power units are coal-fired, whose rise rate is relatively weak. So for the weak-rise coal-fired units, as the conclusion taken before, the static dispatch is not forwarding-looking, if the rise rate constraint of generator not considered, it may not be possible to achieve the effect of optimization. The in-day rolling dispatch has a temporal level of an hour, namely the use of the latest short-term load forecasting information, and the subsequent amendments on the dispatch given by day-ahead forecast, which would relieve the pressure of real-time dispatch by smoothly linking up the plan given by day-ahead dispatch plan and the revision by real-time dispatch, and offer a coordinated control compensation balanced the long-time and short-time dispatch.

In recent years, dynamic dispatch, which is called Look-ahead, is also gradually used in real-time dispatch model. Same as the day-ahead dispatch model, it considers a combinatorial optimization model in multiple periods with unit ramp constraints, but the difference lies in the application of results. The day-ahead dispatch delivers the optimized plan issue of all the periods, but when the Look-ahead real-time dynamic dispatch produce the optimization issues of several periods, it will deliver only the optimization issue of first five minutes, but not the all after. Then in the next period, according to the amended predicted value, the multi-period dynamic dispatch model analysis the optimization issue and deliver optimization point of the first 5 min. This kind of optimization control method is called Model Prediction Control (MPC) in control theory. The MPC theory is widely applied in latest study, but considering its computational complexity, the main focus is how to complete the large-scale combination dispatch algorithm

within a time scale of 5-min, so the key to implement the Look-ahead method is to develop quick and efficient algorithm.

1.2.3 Economic Dispatch Issues Considered the Security Constraints

Traditional models of economic dispatch considered only power balancing constraint of generation with load and output constraint of generator sets. In early stage the economic dispatch is considered without security constraint of network transmission line, even the security constraints of N − 1 [125]. Thus, although the results obtained could offer the best economy, still the security will be lost. Especially in the peak load, there may be overloaded on transmission lines, which will lead to out of operation of lines and transfer of the network power flow, and induce to overload of other lines and to form a chain of off-grid crash. Therefore, the application of rational models is quite effective in small-scale network system, but for the online operation of large-scale system, security issues become increasingly serious. Conventional methods use offline security check to do amendments on dispatch plans which do not meet the security check, but this often takes a lot of time and the revised dispatch plans is not necessarily the global optimal solution, and therefore the economy of the dispatch optimization is also decreased.

In order to coordinate security and economy of the system, Security Constrained Economic Dispatch (SCED), which take security constraint as consider, is gradually replacing the traditional economic dispatch which do not have security constraint. But compared to the traditional optimization model, SCED model adds a lot of linear constraints to keep the system security on transmission cross section, which makes the optimization model becomes relatively complicated, especially the economic dispatch optimization model with dynamic security constraint on consideration of the multi-period system, which greatly increased the difficulty of solution. Fortunately, in recent years decomposition-coordination algorithms are developed. These algorithms typically decompose large-scale combinatorial optimization problem into several sub-problems, which usually has the same structure and can be solved in parallel. Coupled with the development of parallel computing, the solving speed of combinatorial optimization has been further improved. The most representative ones are the Lagrangian relaxation algorithm [127], Augmented Lagrangian relaxation algorithm [128].

1.2.4 Economic Dispatch Problems Considering Wind Power Uncertainty

The uncertainty from wind output has brought unprecedented challenges to the optimal operation of the power system. The power system operation has been dealing with the uncertainty of load, different from load uncertainty, however, wind output is characterized with large uncertainties and low prediction precision [129–131], while load uncertainty has an intrinsic pattern, and the load prediction, especially the short term 24 h load prediction has a significantly high forecast accuracy [132–135]. Therefore, the optimal operation and dispatching model considering stochastic wind power output has been a hot topic for research.

Reference [136] studied the effect of wind integration and wind uncertainty on power system reliability, using an ARMA model to analyze short term wind forecast; Ref. [137] studied the effect of stochastic wind power on the unit commitment (UC) problem, and constructed a UC stochastic optimization problem with the objective to minimize the expected operation cost; Ref. [138] tackled the influence of distribution generation on a heavily loaded distribution system with a wind forecast model based on statistics; a mixed integer stochastic optimization model is established in [139], where the wind uncertainty is modeled with ARMA as well as Latin hypercube sampling, and a scenario reduction method is adopted to simplify the computation; in [140], an multi-agent framework for microgrids has been proposed to coordinate distributed resources with distributed smart control algorithm; Ref. [141] maximized renewable integration and minimized power loss using an optimal AC power flow for renewable energy planning and operation; in addition, the $N - 1$ security constraint and coupling among different time intervals are considered; a multi-objective stochastic optimization problem which aims to minimize generation cost and pollution emission is proposed in [142], which employed a chance constraint for wind power output and is solved by a two stage method; Ref. [143] studies the influence of wind power uncertainty on economic dispatch, and a comparison between chance constraint and CVaR is presented; Ref. [144] proposes a probability distribution model to economically dispatch combined heat and power plants employing a scenario reduction technique; a security constrained stochastic optimization model considering large scale wind integration in [145] is proposed and verified on a real world power system; Based on ARMA, Ref. [146] introduced GARCH model to facilitate analysis of dynamic economic dispatch problem considering wind power; the stochastic optimization is employed in [147] to investigate the spinning reserve planning problem in a wind integrated power system; Ref. [148] adopted a Differential Evolution method to solve the multi-objective optimization problems in the power system with wind integration; revenue and peak load regulating capacity were investigated in [149] that put forward a multi-objective optimization problem considering demand response; another multi-objective optimization problem was proposed in [150] that coordinated revenue and peak load regulating capacity, and used a fuzzy optimization method to solve the problem; Ref. [151] applied Latin hypercube sampling and

simultaneous backward substitution method to perform microgrid energy optimal dispatch while considering economy and fluctuation at the microgrid connection point; based on α-superquantile stochastic optimization, Ref. [152] considered combined cooling heating and power optimization model with wind power, and a discussion of different confidence intervals of wind power is put forward.

Generally speaking, to investigate wind uncertainty, the first step is to model the uncertain wind output, while often used methods include probability distribution model, fuzzy model, and interval number model. Furthermore, based on different modeling, stochastic planning theory, fuzzy optimization theory, and robust optimization theory are proposed.

Stochastic optimization is to sample renewable energy output based on probability distribution, find typical output scenarios, and construct stochastic planning modeling; fuzzy optimization is to describe the uncertain characteristics as fuzzy membership functions, and add these functions into the optimization model; robust optimization, on the other hand, is to use uncertain sets to represent wind power uncertain output, and find an optimal solution that will not violate the security constraint in the worst case scenario. In particular, if the uncertain set is modeled as an interval, then the robust optimization can be termed as interval robust optimization.

1.2.4.1 Stochastic Planning Theory

Reference [153] established different forms of linear stochastic optimal power flow model, and compared their computation complexity; Ref. [154] investigated the influence of uncertain power output from wind on the reactive power optimization and built chance constraint stochastic planning problem based on probability distribution model; Ref. [155] considered load and wind uncertainty, and used particle swarm optimization (PSO) to perform day ahead stochastic dispatch problem; for renewable energy in microgrids, Ref. [156] used a heuristic stochastic optimization that combined PSO with Monte Carlo simulation; Ref. [157] studied the stochastic dispatch problem for multiple wind farms; based on wind power uncertainty, stochastic optimization model for post-fault situations was established in [158]; Ref. [159] considered the influence of stochastic nature of EV charging/discharging and wind power on power system, and used Weibull distribution for wind power and normal distribution for EV to build a stochastic optimization model; a stochastic two stage stochastic unit commitment considering wind power was proposed in [160], which employed a scenario reduction technique; Ref. [161] discussed the optimal power flow model considering wind power probability distribution under security constraint; based on wide area measurement [162], constructed a dynamic stochastic power flow model for high penetration of renewable power, and to solve the nonlinear optimal control problem, a dual heuristic dynamic optimization was employed; Ref. [163] investigated hydro-power-wind cogeneration optimization model that calculated parameters by Maximum Likelihood Estimation; Ref. [164] adopted T-S fuzzy neural network to study stochastic optimal dispatch problem, in

which a nonlinear evolution process is presented for evolution in generations; on the basis of Copula function, a stochastic optimal dispatch model for renewable energy is proposed in [165] and PSO is employed for solution; load elasticity and wind power uncertainty were considered in [166], for which a stochastic optimization model was proposed and was solved by Empire competition algorithm. Ref. [167] proposed a stochastic power flow model based on Gaussian Mixture Model for distribution system with uncertain factors; Ref. [168] established a stochastic optimization model considering voltage stability and small-signal stability constraints, and applied second order relaxation, using Cornish-Fisher to solve the problem. A bi-level dynamic stochastic optimization for high penetrating renewable energy was constructed in [169], and a self-adaptive design algorithm was used to solve the model; Ref. [170] dealt with power system operation and planning, in which the stochastic model combined a multi-period UC and AC optimal power flow to guarantee system security; N-1 security economic dispatch model was proposed in [171], in which the AC power flow was relaxed and the chance constraint convex optimization was used to deal with uncertainty; the optimal power flow problem for flexible AC transmission was discussed in [172] to optimize wind power shedding, in which the wind power output was modeled with multiple scenarios, therefore a two stage stochastic optimization model was used; Ref. [173] adopted a second-order relaxation for the AC power flow, and on that basis a stochastic second-order optimization considering wind power output uncertainty was proposed and solved by interior point method; Ref. [174] considered high voltage DC transmission for a multi-period stochastic optimization model, considering double fed induction wind turbines to solve active and reactive combined optimization problems; the reactive power control considering wind power uncertainty was considered in [175] and solved with PSO-based fast probabilistic power flow algorithm; the reactive optimization with uncertain nodal injection was investigated in [176], similar to active power optimization, the model also adopted a point estimation transformation under chance constraint, and used a genetic algorithm to solve the model; Ref. [177] considered wind and PV output uncertainty by using multi-scenario generation technique, and a multi-objective optimization stochastic model was provided for microgrids.

1.2.4.2 Fuzzy Optimization Theory

Reference [178] modeled the uncertain nodal injection as fuzzy number and solved a DC fuzzy power flow model using Dantzig Wolfe decomposition and dual simplex method; Ref. [179] employed fuzzy set theory to build a cost minimization power planning model, and solved the problem with dynamic genetic algorithm. The fuzzy power flow was used to check security constraint and fuzzy energy loss costs in fault scenarios; a multi-objective model considering voltage security was proposed in [180], a fuzzy model is used to overcome the limitation of weights. The model was solved with nonlinear primal dual interior point method; In [181] and [182], the short term transmission system planning considering Credibility Theory

and fuzzy power flow was proposed, and the genetic algorithm was employed to reach optimality; Ref. [183] built a mix integer linear optimization model that can consider multiple scenarios for optimal distribution planning; Ref. [184] analyzed the influence of renewable energy and fault uncertainty on microgrid energy management, and built a multi-objective economic dispatch model which was solved by PSO; Ref. [185] studied the influence of load and wind power uncertainty on capacitor planning, using fuzzy number for voltage constraints; Ref. [186] established a fuzzy logic controller for maximum wind power tracking, which can track the maximum wind power by considering wind power uncertainty and provide real time control parameters; Ref. [187] carried out analysis on the influence of wind power uncertainty on system sustaining cost, and therefore proposed a probabilistic model to minimize pollution and costs for static stochastic economic dispatch, and adopted fuzzy set theory and entropy weight method to solve the model; concerning renewable energy uncertainty, [188] introduced fuzzy number theory, and combined the fuzzy number and optimal power flow together to form fuzzy optimal power flow model, which is turned to deterministic optimization problem by weighted shift and is solved by primal dual interior point method; Ref. [189] provided a novel method towards fuzzy stochastic optimal power flow problem, and used interval constraint to fuzzify the initial population in the genetic algorithm, and used probability distribution to describe the fuzzy distribution of the feasible solutions, therefore the optimal solution set can be reached; Ref. [190] used the demand response to smooth the wind output fluctuation, and proposed a multi-objective problem of minimizing operating cost and power loss, and used fuzzy number theory to turn the problem into a single objective problem.

1.2.4.3 Robust Optimization Theories

Reference [191] studied the impact of the uncertain nodal power price on the self-regulation of power generation. A robust optimization model was established, the Value-at-risk was taken as a chance constraint, and the model was turned to a second-order-cone model and solved by the primal dual interior point method; considering the uncertainty of load and energy price, the robust optimization problem for generators in an energy market was proposed in [192]; Ref. [193] discussed the robust unit commitment problem considering wind power uncertainty, and establish a security constrained mixed integer optimization model; Ref. [194] proposed a robust wind farm planning problem considering the penetrating power limit; Ref. [195] introduced the concept of Virtual Power Plant (VPP) to deal with uncertain renewable power optimization problems, and used robust optimization and PSO to solve the model; Ref. [196] built a robust unit commitment to deal with wind power forecast errors, at the same time, this model also considered reserve constraint and transmission power loss; the objective in [197] was to minimize power loss while satisfying all constraints, and further, a robust reactive power optimization model was established, which was turned to a linear optimization by dual theory; Ref. [198] considered wind power uncertainty and proposed to convex

robust optimization based on linear theory for system reserve planning; Ref. [199] studied the two stage unit commitment optimization problem for renewable energy and demand side response, and adopted cutting plane method to solve the model; Ref. [200] proposed a robust unit commitment problem considering renewable energy and storage, and introduced new variables to control the level of conservativeness; Ref. [201] proposed a new real time economic dispatch algorithm that can consider security and reliability with renewable energy; Ref. [202] studied the combined dispatch optimization problem, in which a two stage mixed integer robust planning model was used to consider renewable energy uncertainty; Ref. [203] investigated the renewable energy uncertainty and its relationship to wind power, natural gas system and coal system, and built a robust optimization model; Ref. [204] built a two-stage self-adaptive robust unit commitment problem to consider the uncertain nodal injection, and adopted a Benders decomposition to solve the problem; Ref. [205] proposed a Affine robust optimization to determine the best planning value, the output of thermal plant was presented as a uncertain renewable energy source, a second-order cone with interior point method is used to reach the optimal solution; based on wind power uncertainty, [206] took a step further and considered the elastic demand response, and proposed a multi-level robust mixed integer planning model, which was solved by Benders decomposition. A robust cost function was employed to overcome conservativeness brought by the algorithm; to reduce the issue of over conservativeness brought by robust optimization, [207] introduced maxmin regret degree into the robust optimization problem and adopted the Benders decomposition to solve the model; Ref. [208] used robust optimization for power system reactive optimization; Ref. [209] considered the situation where wind uncertainty can cause no feasible solution to economy, and proposed multi-period rolling horizon robust dispatch to minimize wind curtailment; Ref. [210] introduced dynamic uncertain set for two stage self-adaptive robust optimization and considered the correlation of variables in different time period and locations; Ref. [211] proposed an efficient microgrid operation algorithm for wind and storage integration based on optimal order theory; a robust model considering natural gas pipeline congestion and fast startup/shutdown units was studied in [212], in which the pipeline constraints were linearized; the robust unit commitment model with consideration for wind and load uncertainty was put forward in [213], which did no settle for the worst case scenario, but optimize the base value so as to have enough regulatory capacity for a certain range of uncertainty; Ref. [214] came up with a sparse affine robust optimization model to process a multi-period storage optimization problem that can guarantee real time power balance by constraining generators; a robust optimal power flow was presented in [215] and an evolutionary algorithm was adopted to solve the model; to tackle long term planning problem of microgrid, a two stage robust optimization to determine the size and location of renewable energy was presented in [216], and was solved by column generation algorithm; game theory was used in [217] to deal with large scale wind integration in power system, which was formulated as a two stage relaxed min-max problem; Ref. [218] adopted robust optimization for AC optimal power flow and nodal price considering wind and PV uncertainty; the objective in [219] was to minimize wind

curtailment while finding the robust operating condition of the power system under security consideration; references [220, 221] introduced robust optimization model for automatic generation control (AGC) to guarantee the system security by controlling ACG units; In [222, 223] the robust economic dispatch model was divided into pre-adjustment and re-adjustment, and by adding feasible conditions into the pre-adjustment problem to achieve the optimal results.

1.3 Limits of Existing Works and Research Motivation for This Book

Energy management has been widely studied over decades; therefore the algorithms and application are well developed. However, the large scale integration of renewable energy, especially wind power, causes large impact on the current energy management system by their stochastic nature. Consequently a new energy management system that can accommodate such new features is urgently required. According to the literature review, intensive study has been carried out in this area, but some key points remain unsolved.

As mentioned in 1.2, compared with probability distribution or fuzzy formulation, interval number is an easier way to model the uncertain parameters, because the distribution of the uncertain parameters are not straightforward to get, but the upper and lower limits are relatively easier to obtain, thus making the interval method more accessible.

Through interval power flow, the results are in intervals; though the probabilistic distribution of variables are not deduced, the interval provides clear upper and lower limits to system operators, which are important Ref. for optimal control; for optimal operating and dispatching, interval robust optimization is widely used to guarantee the system security in all possible wind power output intervals;

But there also exits some problems for interval robust power flow, which are following:

(i) **the conservativeness of interval algorithm** (**algorithm design**)

Though interval expression is very straightforward, its calculation has conservativeness issues. For example, assume two interval numbers $[-1, +1]$ and $[-2, +2]$, then $[-1, +1] + [-2, +2] = [-3, +3]$, but $[-3, +3] - [-2, +2] = [-5, +5] \neq [-1, +1]$. This means that after some rounds of calculation, the interval would be expanded, which is called the conservativeness. The interval number calculation is different from real number calculation, such as $1 + 2 = 3$ or $3 - 2 = 1$. Therefore how to reduce the conservativeness of the interval calculation is a very important topic. In Chap. 2 the algorithm for solving interval linear and nonlinear functions are illustrated in detail.

Secondly, robust optimization in essence is to optimize in the worst case scenarios for uncertain factors; however, if the worst case scenario does not happen,

the economy of the system operation is compromised, which can be considered as conservativeness. Robust economic dispatch must reduce this conservativeness.

(ii) **interval calculation and high efficiency of optimization algorithm (algorithm design)**

First, another goal of interval calculation is to find highly efficient algorithm for interval linear and nonlinear functions. Though iteration algorithm has some advantages in calculation efficiency, it is not ideal concerning convergence. It is therefore worth investigating the highly efficient algorithms with good convergence;

Second, speaking from the perspective of algorithm, robust optimization, especially the max-min model for economic dispatch is hard to solve compared with traditional linear problem or second order problem. For interval economic dispatch, it is also worth learning how to reach optimal solution and optimize objective interval;

Finally, most power systems are of a large scale, therefore the scale of variables can be huge, and more dummy variables can be introduced when considering uncertain parameters. Methods to reduce computation scale for online dispatch by parallel calculation is urgently needed.

(iii) **modeling of power system practical problems and algorithms (physical model)**

First, in the traditional power flow calculation, the unbalanced power is balanced at the slack bus. However, in reality the unbalance is taken by all the generators, thus the dynamic power flow calculation is practical in this sense. Similarly, in interval power flow all the uncertainty of the wind power output is balanced at the slack bus, if certain constraints are added to make sure all generators share the uncertainty, then interval power flow is transformed into a constrained interval power flow;

Second, with the integration of uncertain wind power, there might be no feasible solution to the traditional economic dispatch model. It is worth investigating how to relax certain constraints or produce a closed-loop control strategy to perform wind shed, or turn constraints into short-term soft constraints;

There are some specific practical problems in the power system operation, such as the wind turbine has a non-operational range, or $N - 1$ outage often happens in mass integration of wind power. Therefore it is worth investigating how to form the robust economic dispatch model while considering security constraints, e.g. the non-operational range and $N - 1$ security.

References

1. Deng S (2006) The study of the enterprise innovation incentive mode. Master Degree thesis, Southwest Jiaotong University
2. Fang C (2007) Analysis on developing objectives and prospects of wind power in China. Energy China 29(12):30–34

3. Shi J (2009) Status of world wind power development and opportunity to wind turbine manufacturing industry of China. Renew Energy Resour 27(3):1–3
4. Yin M, Wang C, Ge X et al (2010) Comparison and analysis of wind power development between China and Germany. Trans China Electrotech Soc 25(9):157–162
5. Zhou Y, Wang Q, Fang T et al (2010) Spain's wind power development: experience and message to China. Energy Technol Econ 22(4):9–14
6. Li J, Cai F, Qiao L (2014) China wind power development report in 2014
7. GWEC (2012) Global wind report: annual market update 2012
8. The World Wind Energy Association (2012) Annual report
9. Wang Y (2008) Wind power capacity analysis and strategies in Jiangsu Province. Master thesis, Nanjing Normal University
10. Qiu WD, Wang ZD, Li J (2008) Analysis on issues related to wind power development in China. Electr Power Technol Econ 20(1):19–23
11. Jiang L (2009) Review on global wind power development in 2008. Electr Power Technol Econ 21(2):12–15
12. Zhang M, Deng K, Chen B et al (2010) Status and development of chinese wind power industry. J Mech Electr Eng 27(1):1–3
13. Wang NB (2010) Analysis on the wind power development bottleneck and its strategies. Energy China 32(3):17–20
14. Tan Z, Ju L (2013) Review of China's wind power development: history, current status, trends and policy. J North China Electr Power Univ (Social Sciences) 02:1–7
15. Huang G, Ongsakul W (1994) Managing the bottlenecks in parallel Gauss-Seidel type algorithms for power flow analysis. IEEE Trans Power Syst 9(2):677–684
16. Huang G, Ongsakul W (1993) Managing the bottlenecks of a parallel Gauss-Seidel algorithm for power flow analysis. In: Power industry computer application conference, Newport, CA
17. Jong-Ho B, Ravindran A, Mukherjee A et al (2009) Accelerating the Gauss-Seidel power flow solver on a high performance reconfigurable computer. In: Field programmable custom computing machines, Napa, CA
18. Huang G, Ongsakul W (1993) Managing the bottlenecks in parallel Gauss-Seidel type algorithms for power flow analysis. In: Power industry computer application conference, Scottsdale, AZ
19. Penido DRR, Araujo LR, Pereira JLR et al (2004) Four wire Newton-Raphson power flow based on the current injection method. In: IEEE PES power systems conference and exposition
20. Panosyan A, Oswald BR (2004) Modified Newton-Raphson load flow analysis for integrated AC/DC power systems. In: 39th international universities power engineering conference, Bristol, UK
21. Bjelogrlic M, Calovic MS, Babic BS et al (1989) Application of Newton's optimal power flow in voltage/reactive power control. In: Power industry computer application conference, Seattle, WA, USA
22. Crisan O, Mohtadi MA (1992) Efficient identification of binding inequality constraints in optimal power flow Newton approach. In: IEE Proceedings C-generation, transmission and distribution, vol 139(5), pp 365–370
23. Zhang Y, Chiang HD (2010) Fast Newton-FGMRES solver for large-scale power flow study. IEEE Trans Power Syst 25(2):769–776
24. Stott B (1972) Decoupled Newton load flow. IEEE Trans Power Apparatus Syst PAS-91 (5):1955–1959
25. Despotovic ST (1974) A new decoupled load flow method. IEEE Trans Power Apparatus Syst PAS-93(3):884–891
26. Wu F (1977) Theoretical study of the convergence of the fast decoupled load flow. IEEE Trans Power Apparatus Syst 96(1):268–275

27. Cai D, Chen Y (2002) Solving power flow equations with in exact Newton methods preconditioned by incomplete LU factorization with partially fill-in. Autom Electr Power Syst 26(8):11–14
28. Alvarado F, Hu Y, Adapa R (1992) Uncertainty in power system modeling and computation. In: IEEE international conference on man and cybernetics systems, Chicago, IL
29. El-Khattam W, Hegazy YG, Salama MMA (2003) Stochastic power flow analysis of electrical distributed generation systems. IEEE PES power engineering society general meeting
30. Duan Y, Gong Y, Tan X et al (2011) Probabilistic power flow calculation in microgrid based on Monte-Carlo simulation. Trans China Electrotech Soc 26(1):274–278
31. Gonzalez-Longatt F, Roldan J M, Rueda J L, et al. Evaluation of power flow variability on the Paraguaná; transmission system due to integration of the first venezuelan wind farm. IEEE PES power engineering society general meeting, San Diego, CA
32. Krynsky J, Janecek E, Janecek P (2004) A new stochastic model of the electric distribution network. In: International conference on probabilistic methods applied to power systems, Ames, IA
33. Liu S, Zhou X, Fan M et al. Probabilistic power flow calculation using sigma-point transform algorithm. In: International conference on Chongqing Power System Technology
34. Jain A, Tripathy SC, Balasubramanian R et al (2006) Stochastic load flow analysis using artificial neural networks. IEEE PES power engineering society general meeting, Montreal, Que
35. Morales JM, Perez-Ruiz J (2007) Point estimate schemes to solve the probabilistic power flow. IEEE Trans Power Syst 22(4):1594–1601
36. Haesen E, Driesen J, Belmans R (2007) Stochastic, computational and convergence aspects of distribution power flow algorithms. In: IEEE Lausanne power tech, Lausanne
37. Hu Z, Wang X (2009) Error Analysis of the probabilistic load flow based on cumulant method. Power Syst Technol 33(18):32–37
38. Liu Y, Zhang B, Li J et al (2011) Probabilistic load flow algorithm considering static security risk of the power system. Proc CSEE 31(01):59–64
39. Goza J, Wedeward K, Smith M (2011) A probabilistic study of electric power systems considering the uncertainties of renewable generation and loads. In: International conference on system of systems engineering (SoSE), Albuquerque, NM
40. Pirnia M, Canizares CA, Bhattacharya K et al (2012) An affine arithmetic method to solve the stochastic power flow problem based on a mixed complementarity formulation. IEEE PES power engineering society general meeting, San Diego, CA
41. Miao F, Vittal V, Heydt GT et al (2012) Probabilistic power flow studies for transmission systems with photovoltaic generation using cumulants. IEEE Trans Power Syst 27(4):2251–2261
42. Zhu X, Liu W, Zhang J et al (2013) Reviews on power system stochastic load flow and its applications in safety evaluation. Trans China Electrotech Soc 28(10):257–270
43. Liu M, Jian G, Dong P (2014) Stochastic power flow calculation of islanded microgrids. J South China Univ Technol (Natural Science Edition) 42(4):13–18
44. Peng H, Cao Y, Huang X et al (2014) Probabilistic load flow calculation based on combination sampling for power system containing distributed generations. Electr Power Autom Equip 34(5):28–34
45. Zhu X, Liu W, Zhang J et al (2014) Probabilistic load flow method considering function of frequency modulation. Proc CSEE 01:168–178
46. Tome Saraiva J, Duarte FO (1996) Enhanced fuzzy power flow models integrating correlation between nodal injections. In: Electrotechnical conference, Bari
47. Zhang Y, Chen Z (1998) Algorithm of AC fuzzy load flow incorporating uncertainties. Power Syst Technol 22(2):22–24
48. Sun HB, Yu DC, Xie YS (2000) Application of fuzzy set theory to power flow analysis with uncertain power injections. IEEE power engineering society winter meeting

49. Pajan PA, Paucar VL (2002) Fuzzy power flow: considerations and application to the planning and operation of a real power system. In: International conference on power system technology
50. Hao J, Shi L B, Xu GY et al (2004) Study on the fuzzy AC power flow model. In: Fifth World Congress on intelligent control and automation
51. Saraiva JT, Fonseca N, Matos MA (2004) Fuzzy power flow-an AC model addressing correlated data. In: International conference on probabilistic methods applied to power systems, Ames, IA
52. Shishir D, Srivastava L, Agnihotri G (2006) Power flow analysis using fuzzy logic. In: IEEE power India conference, New Delhi
53. Wang H, Wu W, Zhang B et al (2007) Fuzzy power flow based on credibility theory. Autom Electr Power Syst 31(17):21–25
54. Gajalakshmi P, Rajesh S (2007) Fuzzy modeling of power flow solution. In: Telecommunications energy conference, Rome
55. Gouveia E, Matos MA (2007) Constrained fuzzy power flow. In: IEEE Power Tech, Lausanne
56. Sun Q, Zhang H, Liu Z (2008) Fuzzy flow calculation in power distribution system and its convergence. Proc CSEE 28(10):46–50
57. Matos MA, Gouveia EM (2008) The Fuzzy Power Flow Revisited. IEEE Trans Power Syst 23(1):213–218
58. Barboza LV, de Vargas RR, de Farias CM (2009) Uncertainties in power flow analyzed via a fuzzy number based method. In: Intelligent system applications to power systems, Curitiba
59. Hong L, Shi L, Yao L et al (2010) Fuzzy modelling and solution of load flow incorporating uncertainties of wind farm generation. Trans China Electrotech Soc 25(8):116–122
60. Weng ZX, Shi LB, Xu Z et al (2012) Effects of wind power variability and intermittency on power flow. In: IEEE PES power engineering society general meeting, San Diego, CA
61. Li H, Pan X, Liu D et al (2013) Fuzzy power flow calculation of line returned based on uncertainties. Electr Power Constr 34(2):6–10
62. Wang Z, Alvarado FL (1992) Interval arithmetic in power flow analysis. IEEE Trans Power Syst 7(3):1341–1349
63. Wang Z, Alvarado FL (1991) Interval arithmetic in power flow analysis. In: Conference proceedings power industry computer application conference, Baltimore, MD
64. Wang S, Wang C, Liu R (2000) Fuzzy interval algorithm based computation of power flow in distribution network. Autom Electr Power Syst 24(20):19–22
65. Wang S, Wang C (2002) Distribution three-phase power flow based on interval algorithm. Proc CSEE 22(02):53–59
66. Wang S, Wang C (2002) Distribution three-phase power flow based on interval algorithm and test results. Proc CSEE 22(03):59–63
67. Pei A, Liu M, Zhang C (2004) Interval algorithm for power flow calculation with uncertain load. Proc CSU-EPSA 16(06):24–27
68. Barboza L V, Dimuro G P, Reiser R H S. Towards interval analysis of the load uncertainty in power electric systems. In: Probabilistic methods applied to power systems, Ames, IA
69. Wang S, Zhang G, Wang C (2005) Solution to conservative property of complex interval power flow. Autom Electr Power Syst 29(19):25–30
70. Zhang G (2006) Study of complex interval power flow and solution to its conservative property. Master thesis, Tianjin University
71. Zhang Y, Yu Y, Yan X et al (2005) Distribution network planning based on interval algorithm and paradigm learning. Autom Electr Power Syst 29(17):40–44
72. Das B (2006) Consideration of input parameter uncertainties in load flow solution of three-phase unbalanced radial distribution system. IEEE Trans Power Syst 21(3):1088–1095
73. Wang S, Zhao W, Wang C et al (2007) Automatic contingency selection based on interval method considering uncertainty of generation and load condition. Autom Electr Power Syst 31(20):27–31

74. Wu Z (2007) Static security analysis considering uncertainty in power system. Master thesis, Tianjin University
75. Zhao G (2007) Power system P-Q decoupled load flow using interval method under uncertainty. Master thesis, Tianjin University
76. Wang S, Wu Z, Wang C (2007) Interval algorithm of DC power flow considering uncertainty in power systems. Autom Electr Power Syst 31(05):18–22
77. Wang S, Xu Q, Zhang G et al (2009) Modeling of wind speed uncertainty and interval power flow analysis for wind farms. IEEE Trans Power Syst 33(21):82–86
78. Vaccaro A, Villacci D (2009) Radial power flow tolerance analysis by interval constraint propagation. IEEE Trans Power Syst 24(1):28–39
79. Vaccaro A, Canizares CA, Villacci D (2010) An affine arithmetic-based methodology for reliable power flow analysis in the presence of data uncertainty. IEEE Trans Power Syst 25 (2):624–632
80. Li Z, Wang G, Chen Z et al (2011) An interval load Flos based algorithm for service restoration in distribution network with distributed generations. Autom Electr Power Syst 35 (24):53–58
81. Ding T, Cui H, Gu W et al (2012) An uncertainty power flow algorithm based on interval and affine arithmetic. Autom Electr Power Syst 36(13):51–55
82. Zheng Z, Wang S, Zhao L et al (2012) An interval algorithm for DC power flow calculations based on Krawczyk algorithm. Autom Electr Power Syst 36(20):50–53
83. Ding T, Bo R, Guo Q et al (2013) A non-iterative affine arithmetic methodology for interval power flow analysis of transmission network. Proc CSEE 19:76–83
84. Vaccaro A, Ca XF, Izares CA et al (2013) A range arithmetic-based optimization model for power flow analysis under interval uncertainty. IEEE Trans Power Syst 28(2):1179–1186
85. Han L, Wang S (2013) Affine algorithm based calculation of three-phase power flow in distribution network connected with PV generation and wind generation. Power Syst Technol 12:3413–3418
86. Ding T, Guo Q, Bo R et al (2014) Solving of interval DC power flow using interval hull algorithm with preconditioning. Autom Electr Power Syst 03:130–136
87. O'Neill RP (2011) Recent ISO software enhancements and future software and modeling plans. Staff report
88. Santos A Jr, Da Costa GRM (1995) Optimal-power-flow solution by Newton's method applied to an augmented Lagrangian function. IEE Proc-Gener Transm Distrib 142(1):33–36
89. Sun D, Ashley B, Brewer B et al (1984) Optimal power flow by newton approach. IEEE Power Eng Rev PER-4(10):39
90. Hong Y (1992) Enhanced Newton optimal power flow approach: experiences in Taiwan power system. IEE Proc C-Gen Transm Distrib 139(3):205–210
91. Burchett RC, Happ HH, Vierath DR (1984) Quadratically convergent optimal power flow. IEEE Trans Power Apparatus Syst PAS-103(11):3267–3275
92. Wei H, Sasaki H, Kubokawa J et al (1998) An interior point nonlinear programming for optimal power flow problems with a novel data structure. IEEE Trans Power Syst 13(3):870–877
93. Sousa AA, Torres GL (2007) Globally convergent optimal power flow by trust-region interior-point methods. In: IEEE Lausanne Power Tech, Lausanne
94. Momoh JA, Adapa R, El-Hawary ME (1999) A review of selected optimal power flow literature to 1993. I. Nonlinear and quadratic programming approaches. IEEE Trans Power Syst 14(1):96–104
95. Momoh JA, El-Hawary ME, Adapa R (1999) A review of selected optimal power flow literature to 1993. II. Newton, linear programming and interior point methods. IEEE Trans Power Syst 14(1):105–111
96. Praveena P, Vaisakh K, Rao SRM (2010) A bacterial foraging PSO-DE algorithm for solving dynamic economic dispatch problem with security constraints. In: Joint international conference on power electronics, drives and energy systems, New Delhi

97. Zhao B, Chuangxin G, Yijia C (2004) Dynamic economic dispatch in electricity market using particle swarm optimization algorithm. Intell Control Autom
98. Muneender E, Vinodkumar DM (2012) A new hybrid fuzzy dynamic velocity feedback PSO for non-convex economic dispatch problem. In: Sustainable utilization and development in engineering and technology, Kuala Lumpur
99. Praveena P, Vaisakh K, Rao SRM (2010) A bacterial foraging and PSO-DE algorithm for solving dynamic economic dispatch problem with valve-point effects. In: Integrated intelligent computing, Bangalore
100. Vaisakh K, Praveena P, Rao SRM (2009) PSO-DV and bacterial foraging optimization based dynamic economic dispatch with non-smooth cost functions. Trivandrum, Kerala
101. Zhang T, Cai J (2009) A new chaotic PSO with dynamic inertia weight for economic dispatch problem. In: International conference on sustainable power generation and supply, Nanjing
102. Zwe-Lee G (2004) Constrained dynamic economic dispatch solution using particle swarm optimization. IEEE power engineering society general meeting
103. Niknam T, Golestane F, Bahmanifirouzi B (2011) Modified adaptive PSO algorithm to solve dynamic economic dispatch. In: IEEE power engineering and automation conference, Wuhan
104. Niknam T, Golestaneh F (2013) Enhanced bee swarm optimization algorithm for dynamic economic dispatch systems. J IEEE 7(4):754–762
105. Ongsakul W, Ruangpayoongsak N (2001) Constrained dynamic economic dispatch by simulated annealing/genetic algorithms. in: Power industry computer applications, Sydney, NSW
106. Kumar SS, Palanisamy V (2006) A new dynamic programming based Hopfield neural network to unit commitment and economic dispatch. In: International conference on industrial technology, Mumbai
107. Abdelaziz AY, Mekhamer SF, Kamh MZ et al (2008) A hybrid Hopfield neural network-quadratic programming approach for dynamic economic dispatch problem. In: International middle-east power system conference, Aswan
108. Shang X, Lu J, Sun Y (2008) A preference-based non-dominated sorting genetic algorithm on dynamic economic dispatch. World Congress on Intelligent Control and Automation, Chongqing
109. Zhang G, Lu H, Li G et al (2006) A new hybrid real-coded genetic algorithm and application in dynamic economic dispatch. In: The Sixth World Congress on intelligent control and automation, Dalian
110. Zhang G, Lu H, Li G et al (2005) Dynamic economic load dispatch using hybrid genetic algorithm and the method of fuzzy number ranking. In: Proceedings of 2005 international conference on machine learning and cybernetics, Guangzhou, China
111. Hosseini SH, Kheradmandi M (2004) Dynamic economic dispatch in restructured power systems considering transmission costs using genetic algorithm. In: Conference on electrical and computer engineering, Canadian
112. Li F, Morgan R, Williams D (1997) Towards more cost saving under stricter ramping rate constraints of dynamic economic dispatch problems—a genetic based approach. In: Genetic algorithms in engineering systems: innovations and applications, Glasgow
113. Gwo-Ching L, Jia-Chu L (2010) Application novel immune genetic algorithm for solving bid-based dynamic economic power load dispatch. In: International conference on power system technology, Hangzhou
114. Babu GSS, Das DB, Patvardhan C (2008) Dynamic economic dispatch solution using an enhanced real-quantum evolutionary algorithm. In: Joint international conference on power system technology, New Delhi
115. Joned AMAA, Musirin I, Rahman TKA (2006) Solving dynamic economic dispatch using evolutionary programming. In: IEEE international power and energy conference, Putra Jaya
116. Shailti Swamp K, Natarajan A (2005) Constrained optimization using evolutionary programming for dynamic economic dispatch. In: International conference on intelligent sensing and information processing

117. Zwe-Lee G, Ting-Chia O (2009) Dynamic economic dispatch solution using fast evolutionary programming with swarm direction. In: IEEE conference on industrial electronics and applications, Xi'an
118. Arul R, Velusami S, Ravi G (2013) Chaotic differential harmony search algorithm to solve dynamic economic dispatch problem with emission and security constraints. In: International conference on energy efficient technologies for sustainability, Nagercoil
119. Arul R, Velusami S, Ravi G (2013) Solving security constrained dynamic economic dispatch problem using chaotic differential harmony search algorithm. In: International conference on circuits, power and computing technologies, Nagercoil
120. Kundu R, Mukherjee R, Das S et al (2013) Adaptive differential evolution with difference mean based perturbation for dynamic economic dispatch problem. In: IEEE symposium on differential evolution, Singapore
121. Benhamida F, Ziane I, Souag S et al (2013) A quadratic programming optimization for dynamic economic load dispatch: comparison with GAMS. In: International conference on systems and control, Algiers
122. Attaviriyanupap P, Kita H, Tanaka E et al (2002) A hybrid EP and SQP for dynamic economic dispatch with nonsmooth fuel cost function. IEEE Trans Power Syst 17(2):411–416
123. Attaviriyanupap P, Kita H, Tanaka E et al (2002) A hybrid EP and SQP for dynamic economic dispatch with nonsmooth fuel cost function. IEEE Power Eng Rev 22(4):77
124. Rabiee A, Mohammadi-Ivatloo B, Moradi-Dalvand M (2014) Fast dynamic economic power dispatch problems solution via optimality condition decomposition. IEEE Trans Power Syst 29(2):982–983
125. Carpentier J (1979) Optimal power flows. Int J Electr Energy Syst 1(1):3–15
126. Zhang B, Wu W, Zheng T et al (2011) Design o fa multi-time scale coordinated active power dispatching system for accommodating large scale wind power penetration. Autom Electr Power Syst 35(1):1–6
127. Li Z, Wu W, Zhang B et al (2013) Dynamic economic dispatch with spinning reserve constraints considering wind power integration. IEEE power engineering society general meeting, Vancouver, BC
128. Lai X, Xie L, Xia Q et al (2014) Decentralized multi-area economic dispatch via dynamic multiplier-based lagrangian relaxation. IEEE Trans Power Syst 1–9
129. Sun D (2014) Research on dispatching for wind farm integrated system based on power forcasting. Master thesis, Beijing Jiaotong University
130. Zou J, Lai X, Wang N (2014) Time series model of stochastic wind power generation. Power Syst Technol 09:2416–2421
131. Shi J, Lee WJ (2012) Weighted parallel algorithm to improve the performance of short-term wind power forecasting. IEEE power and energy society general meeting, San Diego, CA
132. Kang C, Mu T, Xia Q (2008) Power system multilevel load forecasting and coordinating part one research framework. Autom Electr Power Syst 32(07):34–38
133. Chen Y, Ma L, Mu G et al (2003) Comparison studies on two types of accuracy criteria for short-term load forecast. Autom Electr Power Syst 27(17):73–77
134. Kang C, Xia Q, Zhang B (2004) Review of power system load forecasting and its development. Autom Electr Power Syst 17:1–11
135. Mu T, Kang C, Xia Q et al (2008) Power system multilevel load forecasting and coordinating part two basic coordinating model. Autom Electr Power Syst 08:14–18
136. Zhang Y, Ka WC (2008) The impact of wind forecasting in power system reliability. In: Third international electric utility deregulation and restructuring and power technologies, Nanjing
137. Tuohy A, Meibom P, Denny E et al (2009) Unit commitment for systems with significant wind penetration. IEEE Trans Power Syst 24(2):592–601
138. Kroposki B, Sen PK, Malmedal K (2009) Selection of distribution feeders for implementing distributed and renewable energy applications. In: IEEE rural electric power conference, Fort Collins, CO

139. Yan Y, Wen F, Yang S et al (2010) Generation scheduling with fluctuating wind power. Autom Electr Power Syst 34(6):79–88
140. Zhang W, Cai J (2010) A multi-agent system for distributed energy resources control in microgrid. In: 2010 5th international conference on critical infrastructure, Beijing
141. Ochoa LF, Harrison GP (2010) Using AC optimal power flow for DG planning and optimisation. IEEE power and energy society general meeting, Minneapolis, MN
142. Qiu W, Zhang J, Liu N (2011) Model and solution for environmental/economic dispatch considering large-scale wind power penetration. Proc CSEE 31(19):8–16
143. Yao L (2011) Study of conditional risk method for security economic dispatch in power system with wind power. Master thesis, Changsha University of Science & Technology
144. Xu L, Yang Y, Xu Z et al (2011) Combined scheduling of electricity and heat in a microgrid with volatile wind power. Autom Electr Power Syst 35(9):53–60
145. Jigoria-Oprea D, Kilyeni S, Barbulescu C et al (2011) Integration of large wind farms within the Romanian power system. In: International conference on environment and electrical engineering, Rome
146. Jiang W (2012) Research on reliability and dynamic economic dispatch of power system considering wind Powe. Doctoral dissertation, Shanghai Jiaotong University
147. Fan W (2012) Research of conditional risk method for spinning reserve in wind power integrated system. Master thesis, Changsha University of Science & Technology
148. Qiu W (2012) Multi-objective optimal active power dispatch with intermittent energy integration and operation security. Doctoral dissertation, North China Electric Power University
149. Liu X, Chen H, Fang K (2012) Research on demand response for wind power integration into smart grid. Electr Power 45(4):10–14
150. Hu Y (2013) Study on wind power storage technology and the intelligent dispatch method. Master thesis, Lanzhou University of Technology
151. Liu D, Li Q, Yuan X (2014) Economic and optimal dispatching of power microgrid with renewable energy resources based on stochastic optimization. Power Syst Prot Control 11:112–117
152. Zhou R, Yin Q, Kang X et al (2014) Optimization operation control for wind power access to CCHP system. J Electr Power Sci Technol 03:45–51
153. Yong TY, Lasseter RH (2000) Stochastic optimal power flow: formulation and solution. IEEE power engineering society summer meeting, Seattle, WA
154. Li H, Lin L, Shi S (2009) Stochastic optimization model and its hybrid intelligent algorithm for wind power station. Huadian Technol 31(12):73–76
155. Pappala VS, Erlich I, Rohrig K et al (2009) A stochastic model for the optimal operation of a wind-thermal power system. IEEE Trans Power Syst 24(2):940–950
156. Haghi HV, Hakimi SM, Tafreshi SMM (2010) Optimal sizing of a hybrid power system considering wind power uncertainty using PSO-embedded stochastic simulation. In: IEEE 11th international conference on probabilistic methods applied to power systems, Singapore
157. Wang S (2011) Research on stochastic optimal dispatch of power system with multiple wind farms. Master thesis, Changsha University of Science & Technology
158. Entriken R, Tuohy A, Brooks D (2011) Stochastic optimal power flow in systems with wind power. IEEE power and energy society general meeting, San Diego, CA
159. Chen J (2012) Stochastic optimal dispatch of power system based on V2G technology. Master thesis, Changsha University of Science & Technology
160. Lei Y, Yang M, Han X (2012) A two-stage stochastic optimization of unit commitment considering wind power based on scenario analysis. Power Syst Prot Control 23:58–67
161. Banerjee B, Jayaweera D, Islam SM (2012) Probabilistic optimisation of generation scheduling considering wind power output and stochastic line capacity. In: 22nd Australasian Universities power engineering conference, Bali
162. Liang JQ, Venayagamoorthy GK, Harley RG (2012) Wide-area measurement based dynamic stochastic optimal power flow control for smart grids with high variability and uncertainty. IEEE Trans Smart Grid 3(1):59–69

163. Li X (2013) Research on stochastic optimal dispatch of hydro-wind integrated operation. Master thesis, Changsha University of Science & Technology
164. Li A (2013) Multi-objective Stochastic optimal dispatch of power system considering the uncertainty output of wind power. Master thesis, Changsha University of Science & Technology
165. Yang H, Wang S, Yi D et al (2013) Stochastic optimal dispatch of power system considering multi-wind power correlation. Electr Power Autom Equip 33(01):114–120
166. Yang N, Wang B, Liu D et al (2013) Large-scale wind power stochastic optimization scheduling method considering flexible load peaking. Trans China Electrotech Soc 28 (11):231–238
167. Valverde G, Saric AT, Terzija V (2013) Stochastic monitoring of distribution networks including correlated input variables. IEEE Trans Power Syst 28(1):246–255
168. Perninge M, Hamon C (2013) A stochastic optimal power flow problem with stability constraints-Part II: the optimization problem. IEEE Trans Power Syst 28(2):1849–1857
169. Liang JQ, Molina DD, Venayagamoorthy GK et al (2013) Two-level dynamic stochastic optimal power flow control for power systems with intermittent renewable generation. IEEE Trans Power Syst 28(3):2670–2678
170. Murillo-Sanchez CE, Zimmerman RD, Anderson CL et al (2013) Secure planning and operations of systems with stochastic sources, energy storage, and active demand. IEEE Trans Smart Grid 4(4):2220–2229
171. Vrakopoulou M, Katsampani M, Margellos K et al (2013) Probabilistic security-constrained AC optimal power flow. Grenoble
172. Nasri A, Conejo AJ, Kazempour SJ et al (2014) Minimizing wind power spillage using an OPF with FACTS devices. IEEE Trans Power Syst 29(5):2150–2159
173. Baradar M, Hesamzadeh MR (2014) A stochastic SOCP optimal power flow with wind power uncertainty. National Harbor, MD
174. Rabiee A, Soroudi A (2014) Stochastic multiperiod OPF model of power systems with HVDC-connected intermittent wind power generation. IEEE Trans Power Deliv 29(1):336–344
175. Hong YY, Lin FJ, Lin YC et al (2014) Chaotic PSO-based VAR control considering renewables using fast probabilistic power flow. IEEE Trans Power Deliv 29(4):1666–1674
176. Fang SD, Cheng HZ, Song Y et al (2014) Stochastic optimal reactive power dispatch method based on point estimation considering load margin. IEEE PES general meeting, National Harbor, MD
177. Ichoua S (2014) A stochastic approach for the integration of distributed energy resources. In: IEEE international technology management conference, Chicago, IL
178. Miranda V, Saraiva JT (1992) Fuzzy modelling of power system optimal load flow. IEEE Trans Power Syst 7(2):843–849
179. Zhang Y, Chen Z, Tan W (1999) An approach for transmission system planning incorporating uncertainties. Power Syst Technol 23(3):16–19
180. Liu X, Li J, Li H et al (2005) Fuzzy modeling and interior point algorithm of multi-objective OPF with voltage security margin. In: IEEE/PES transmission and distribution conference and exhibition: Asia and Pacific, Dalian
181. Wang H, Wu W, Zhang B et al (2008) Short-term planning algorithm considering fuzziness of load. Power Syst Technol 32(21):26–31
182. Zhang K, Tian J, Xu M et al (2010) Transmission planning based on credibility theory. J Beijing Jiaotong Univ 34(05):37–42
183. Khodr HM, Vale Z, Ramos C et al (2009) Optimization techniques for power distribution planning with uncertainties: a comparative study. IEEE Power & energy society general meeting, Calgary, AB
184. Ji M (2010) Research of multi-objective economic dispatch model for a mrico-grid based on particle swarm optimization. Master thesis, Hefei University of Technology

185. Dukpa A, Venkatesh B, Liuchen C (2011) Fuzzy stochastic programming method: capacitor planning in distribution systems with wind generators. IEEE Trans Power Syst 26(4):1971–1979
186. Petrila D, Blaabjerg F, Muntean N et al (2012) Fuzzy logic based MPPT controller for a small wind turbine system. In: 13th international conference on optimization of electrical and electronic equipment (OPTIM), Brasov
187. Sun H, Peng C, Yi H (2012) Multi-objective stochastic optimal dispatch of power system with wind farms. Electr Power Autom Equip 32(5):123–128
188. Liao Y, Gan D, Chen X et al (2012) Fuzzy optimal power flow analysis considering indeterminacy of distributed generation for urban power grid. Electr Power Autom Equip 32 (9):35–39
189. Ma R, Kang R, Jiang F et al (2013) Multi-objective dispatch planning of power system considering the stochastic and fuzzy wind power. Power Syst Protect Control 01:150–156
190. Liu W, Wen J, Xie C et al (2014) Multi-objective fuzzy optimal dispatch based on source-load interaction for power system with wind farm. Electr Power Autom Equip 34 (10):56–63
191. Jabr RA (2005) Robust self-scheduling under price uncertainty using conditional value-at-risk. IEEE Trans Power Syst 20(4):1852–1858
192. Wen Q (2010) The research of self-scheduling in pool for generators based on robust optimization. Master thesis. Changsha University of Science and Technology
193. Zhang S, Song Y H, Hu Z C et al (2011) Robust optimization method based on scenario analysis for unit commitment considering wind uncertainties. In: IEEE power and energy society general meeting, San Diego, CA
194. Li S (2011) Robust optimization research on penetration power limit of wind farm connected to grid. Master thesis. Changsha University of Science and Technology
195. Hropko D, Ivanecky J, Turcek J (2012) Optimal dispatch of renewable energy sources included in virtual power plant using accelerated particle swarm optimization. ELEKTRO, Rajeck Teplice
196. Jiang H, Zhang S, Hu Z et al (2012) Robust optimization method for unit commitment with network losses considering wind uncertainties. In: IEEE power and energy society general meeting, San Diego, CA
197. Yang Y, Zhou R, Ran X (2012) Robust optimization with box set for reactive power optimization in wind power integrated system. In: IEEE power and energy society general meeting, San Diego, CA
198. Warrington J, Goulart P J, Mariethoz S et al (2012) Robust reserve operation in power systems using affine policies. In: IEEE 51st annual conference on decision and control (CDC), Maui, HI
199. Zhao L, Zeng B (2012) Robust unit commitment problem with demand response and wind energy. In: IEEE power and energy society general meeting, San Diego, CA
200. Jiang R, Wang J, Guan Y (2012) Robust unit commitment with wind power and pumped storage hydro. IEEE Trans Power Syst 27(2):800–810
201. Sasaki Y, Hristov EP, Yorino N et al (2013) A real-time robust dynamic ELD against uncertainties of renewable energy sources. IEEE/PES innovative smart grid technologies Europe, Lyngby
202. Yang Y, Zhai Q, Guan X (2013) A robust hydro-thermal scheduling problem for a system integrated with wind resource. In: International conference on the European energy market (EEM), Stockholm
203. Martinez-Mares A, Fuerte-Esquivel CR (2013) A robust optimization approach for the interdependency analysis of integrated energy systems considering wind power uncertainty. IEEE Trans Power Syst 28(4):3964–3976
204. Bertsimas D, Litvinov E, Sun XA et al (2013) Adaptive robust optimization for the security constrained unit commitment problem. IEEE Trans Power Syst 28(1):52–63
205. Jabr RA (2013) Adjustable robust OPF with renewable energy sources. IEEE Trans Power Syst 28(4):4742–4751

206. Zhao C, Wang J, Watson JP et al (2013) Multi-stage robust unit commitment considering wind and demand response uncertainties. IEEE Trans Power Syst 28(3):2708–2717
207. Jiang R, Wang J, Zhang M et al (2013) Two-stage minimax regret robust unit commitment. IEEE Trans Power Syst 28(3):2271–2282
208. . Yang Y. Research on Reactive Power /Voltage Control for in Power System Considering Wind Uncertainties with Robust Linear Optimization: [Master Thesis]. Changsha University of Science & Technology, 2013
209. Wu W, Chen J, Zhang B et al (2014) A robust wind power optimization method for look-ahead power dispatch. Sustainable Energy, IEEE Transactions on 5(2):507–515
210. Lorca A, Sun XA (2014) Adaptive robust optimization with dynamic uncertainty sets for multi-period economic dispatch under significant wind. IEEE Trans Power Syst 1–12
211. Xu Q, Zhang N, Kang C et al (2014) Day-ahead battery scheduling in microgrid considering wind power uncertainty using ordinal optimization. In: North American power symposium, Pullman, WA, USA
212. Liu C, Lee C, Shahidehpour M (2014) Look ahead robust scheduling of wind-thermal system with considering natural gas congestion. IEEE Trans Power Syst 1–2
213. Hu BQ, Wu L, Marwali M (2014) On the robust solution to SCUC with load and wind uncertainty correlations. IEEE Trans Power Syst 29(6):2952–2964
214. Jabr RA, Karaki S, Korbane JA (2014) Robust multi-period OPF with storage and renewables. IEEE Trans Power Syst 1–10
215. Marin S, Garces A (2014) Robust optimal power flow in distribution systems with high penetration of wind energy using a model-based evolutionary strategy. In: IEEE PES transmission & distribution conference and exposition, Medellin, Colombia
216. Wang ZY, Bokan C, Wang JH et al (2014) Robust optimization based optimal DG placement in microgrids. IEEE Trans Smart Grid 5(5):2173–2182
217. Mei SW, Zhang D, Wang YY et al (2014) Robust optimization of static reserve planning with large-scale integration of wind power: a game theoretic approach. IEEE Trans Sustain Energy 5(2):535–545
218. Samakpong T, Ongsakul W, Polprasert J (2014) Robust optimization-based AC optimal power flow considering wind and solar power uncertainty. In: International conference and utility exhibition on green energy for sustainable development, Pattaya
219. Chen J, Wu W, Zhang B et al (2014) A robust interval wind power dispatch method considering the tradeoff between security and economy. Proc CSEE 7:1033–1040
220. Li Z, Wu W, Zhang B (2014) A robust interval economic dispatch method accommodating large-scale wind power generation part one dispatch scheme and mathematical model. Autom Electr Power Syst 20:33–39
221. Li Z, Wu W, Zhang B et al (2014) A look-ahead generation dispatch method considering discrete generation regulation constraints with large-scale wind power integration. Autom Electr Power Syst (10):36–42
222. Wei W, Liu F, Mei W (2013) Robust and economical scheduling methodology for power systems part two application examples. Autom Electr Power Syst 37(18):60–67
223. Wei W, Liu F, Mei W (2013) Robust and economical scheduling methodology for power systems part one theoretical foundations. Autom Electr Power Syst 37(17):37–43

Chapter 2
Mathematics for Interval Algebra and Optimization

Abstract This chapter introduces some mathematical algorithms for solving interval linear equations, interval nonlinear equations, interval nonlinear equations and interval robust optimization models.

2.1 Definition of Intervals

Definition: An interval $\langle x \rangle$ is a non-empty set of real numbers, satisfying $\langle x \rangle = [\underline{x}, \overline{x}] = \{x \in \mathrm{R} : \underline{x} \le x \le \overline{x}\}$, where $\underline{x}$ and $\overline{x}$ are called as the upper and lower bound of the interval. Moreover, we have $\underline{x}, \overline{x} \in \mathrm{R}$ and $\underline{x} \le \overline{x}$. In particular, when $\underline{x} = \overline{x}$, the interval is degenerated into a real number. The set of all intervals are called interval space, denoted by IR.

Interval arithmetic operations are defined on interval space IR. Given two intervals $\langle x \rangle$ and $\langle y \rangle$, we have

Absolute value of intervals: $|\langle x \rangle| \triangleq \mathrm{mag}(\langle x \rangle) \triangleq \max\{|\underline{x}|, |\overline{x}|\}$;

Inclusion of intervals: $\langle x \rangle \subseteq \langle y \rangle \triangleq \underline{y} \le \underline{x}$ and $\overline{y} \ge \overline{x}$;

Basic arithmetic operations of intervals:

Addition $\langle x \rangle + \langle y \rangle \triangleq \left[\underline{x} + \underline{y}, \overline{x} + \overline{y}\right]$;

Subtraction $\langle x \rangle - \langle y \rangle \triangleq \left[\underline{x} - \overline{y}, \overline{x} - \underline{y}\right]$;

Multiplication $\langle x \rangle \times \langle y \rangle \triangleq \left[\min\left\{\underline{x}\underline{y}, \underline{x}\overline{y}, \overline{x}\underline{y}, \overline{x}\,\overline{y}\right\}, \max\left\{\underline{x}\underline{y}, \underline{x}\overline{y}, \overline{x}\underline{y}, \overline{x}\,\overline{y}\right\}\right]$;

Division $\langle x \rangle \div \langle y \rangle \triangleq [1/\overline{x}, 1/\underline{x}] \times \langle y \rangle$, where $0 \notin \langle y \rangle$

Intersection of intervals: $\langle x \rangle \cap \langle y \rangle = [\max(\underline{x}, \underline{y}), \min(\overline{x}, \overline{y})]$;

Union of intervals: $\langle x \rangle \cup \langle y \rangle = [\min(\underline{x}, \underline{y}), \max(\overline{x}, \overline{y})]$;

Comparison of intervals: $\langle x \rangle < \langle y \rangle \Leftrightarrow \overline{x} < \underline{y}$;

The interval length: $length(\langle x \rangle) \triangleq \overline{x} - \underline{x}$;

For an interval vector $\langle \boldsymbol{x} \rangle \in \mathrm{IR}^{n \times 1}$, a norm of an interval vector is given by $\|\langle \boldsymbol{x} \rangle\| = \max\{|\langle \boldsymbol{x}_i \rangle| : i = 1, \ldots, n\}$. According to the definition of norm followed by (i)–(iv), we will show that $\|\langle \boldsymbol{x} \rangle\|$ defined above is a norm of $\langle \boldsymbol{x} \rangle$:

T. Ding, *Power System Operation with Large Scale Stochastic Wind Power Integration*, Springer Theses, DOI 10.1007/978-981-10-2561-7_2

(i) Subadditivity: $\|\langle \boldsymbol{x}\rangle\| = \max\{|\langle \boldsymbol{x}_i\rangle| : i = 1, \ldots, n\} \geq 0 \Rightarrow \|\langle \boldsymbol{x}\rangle\| \geq 0$;

(ii) Existence of zeros: $\|\langle \boldsymbol{x}\rangle\| = 0 \Rightarrow \max(|\overline{\boldsymbol{x}}|, |\underline{\boldsymbol{x}}|) = 0 \Rightarrow |\overline{\boldsymbol{x}}| = |\underline{\boldsymbol{x}}| = 0 \Rightarrow \langle \boldsymbol{x}\rangle = [0, 0]$;

(iii) Homogeneity: $\|c \cdot \langle \boldsymbol{x}\rangle\| = \max(|c\overline{\boldsymbol{x}}|, |c\underline{\boldsymbol{x}}|) = |c|\max(|\overline{\boldsymbol{x}}|, |\underline{\boldsymbol{x}}|) = |c|\|\langle \boldsymbol{x}\rangle\|$;

(iv) Positivity:

$$\|\langle \boldsymbol{x}\rangle + \langle \boldsymbol{y}\rangle\| = \max\left(|\overline{\boldsymbol{x}} + \overline{\boldsymbol{y}}|, \left|\underline{\boldsymbol{x}} + \underline{\boldsymbol{y}}\right|\right) \leq \max\left(|\overline{\boldsymbol{x}}| + |\overline{\boldsymbol{y}}|, |\underline{\boldsymbol{x}}| + \left|\underline{\boldsymbol{y}}\right|\right)$$
$$\leq \max(|\overline{\boldsymbol{x}}|, |\underline{\boldsymbol{x}}|) + \max\left(|\overline{\boldsymbol{y}}|, \left|\underline{\boldsymbol{y}}\right|\right) = \|\langle \boldsymbol{x}\rangle\| + \|\langle \boldsymbol{y}\rangle\|$$

The aforementioned definitions of intervals are simple and understood, however, it needs to know that the interval space is not satisfied with the definition of linear space.

Example 1: $\langle x\rangle - \langle x\rangle = [2\underline{x}, 2\overline{x}] \neq 0$. It shows that interval space is not a closure for subtraction.

Example 2: $\langle x\rangle(\langle y\rangle + \langle z\rangle) \neq \langle x\rangle\langle y\rangle + \langle x\rangle\langle z\rangle$, instead $\langle x\rangle(\langle y\rangle + \langle z\rangle) \subseteq \langle x\rangle\langle y\rangle + \langle x\rangle\langle z\rangle$. It shows that the distributive law does not hold in interval space.

The two examples above show interval space does not follow operational rules of linear space, such that the interval solution will be calculated greater and greater, especially when the same intervals appear several times in one expression, the range of interval will become conservative. Therefore, it is significant to study how to reduce the conservatism of interval arithmetic.

Furthermore, define two special interval matrices (M-matrix and H-matrix) and a special real matrix (comparison matrix). Given an interval matrix $\langle \boldsymbol{A}\rangle \in \mathrm{IR}^{n\times n}$, $\langle \boldsymbol{A}\rangle$ is called an M-matrix if and only if $\langle \boldsymbol{A}\rangle_{ij} \leq 0$ for all $i \neq j$ and $\langle \boldsymbol{A}\rangle \boldsymbol{u} > 0$ for some positive vector $\boldsymbol{u} \in \mathbf{R}^n$; the comparison matrix $\boldsymbol{A}^c$ of $\langle \boldsymbol{A}\rangle$ is defined as (2.1), if $\boldsymbol{A}^c$ is an M-matrix, then $\langle \boldsymbol{A}\rangle$ is said to be an H-matrix. Additionally, the central matrix $\boldsymbol{A} \in \mathrm{R}^{n\times n}$ of interval matrix $\langle \boldsymbol{A}\rangle \in \mathrm{IR}^{n\times n}$ is defined as: for $\forall[a_{ij}] \in \langle \boldsymbol{A}\rangle$, $a_{ij} = \left(\overline{a_{ij}} + \underline{a_{ij}}\right)/2 \in \boldsymbol{A}$

$$\boldsymbol{A}^c = \begin{cases} \mathrm{mig}(\langle a_{ii}\rangle) & i = j \\ -\mathrm{mag}(\langle a_{ij}\rangle) & i \neq j \end{cases} \quad \forall[a_{ij}] \in \boldsymbol{A} \tag{2.1}$$

2.2 Solutions of Algebraic Equations with Right-Hand Intervals

2.2.1 *Linear Equations with Right-Hand Intervals Using Kraw Operator Iteration Method with Preconditioner*

Given $\langle \boldsymbol{A}\rangle \in \mathrm{IR}^{n\times n}$ and $\langle \boldsymbol{b}\rangle \in \mathrm{IR}^{n\times 1}$, traditional interval linear equations are defined as $\langle \boldsymbol{A}\rangle\langle \boldsymbol{x}\rangle = \langle \boldsymbol{b}\rangle$ to solve $\langle \boldsymbol{x}\rangle$. To solve general interval linear equations, four solution methods are discussed in the paper including interval Gauss elimination

method, Kraw operator iteration method, interval hull method and optimality-based method. The details and flow chart of aforementioned four methods can be found in Appendix A.

Howerver, if the coefficient matrix of interval linear equations is a constant matrix, the traditional interval linear equations can be simplified as linear equations with right-hand intervals, such that $\boldsymbol{A}\langle \boldsymbol{x} \rangle = \langle \boldsymbol{b} \rangle$. Thus, the special structural interval linear equations obviously can be solved by four traditional methods:

(i) For interval Gauss elimination method, interval operations of coefficient matrix $\langle \boldsymbol{A} \rangle$ in the method directly replace by operations of traditional deterministic coefficient matrix $\boldsymbol{A}$ in the real space, and right-hand intervals still adopt interval operations. However, the nature of interval Gauss elimination method is a direct method, and time complexity of the method is excessive.

(ii) For Kraw operator iteration method and interval hull method, they both need to compute and express the inverse of central matrix $(\boldsymbol{A}^c)^{-1}$. However, for large system, it is difficult to directly compute the inverse of the matrix.

(iii) For optimality-based method, it is effective to solve this problem, because interval linear equations can be transformed into linear programming followed by (2.2)–(2.3). The linear programming is easy to solve, but we can find that the interval of every variable need to compute separately. Certainly, the interval of every variable is independent and can use parallel implementation. However, if the number of variables are relatively large, it will need large parallel cores to implement while (i) and (ii) can solve intervals of all variables simultaneously.

$$\min_{\boldsymbol{x},\boldsymbol{A}} / \max \quad x_i, \quad i = 1, \ldots, n \tag{2.2}$$

$$\underline{b_j} \leq \sum_{i=1}^{n} a_{ij} x_i \leq \overline{b_j}, \quad j = 1, \ldots, n \tag{2.3}$$

With respect to conservatism problem, because interval operations are not satisfied with distributive law, LU decomposition will also expand the range of the interval solution even for interval linear equations with constant coefficient. To reduce the conservatism of the interval arithmetic, four methods in Appendix A can overcome conservatism for interval linear equations with constant coefficient. Therefore, the high efficiency of solution method should be focused on.

Reviewing the four methods, interval hull method needs to solve inverse central matrix of coefficient matrix, so the complexity of computation is more difficult than other methods; the relatively direct method (interval Gauss elimination method) and the general iteration method (Kraw operator iteration method) has a faster solution speed and a lower space complexity, but iteration method usually has poor

convergence. Kraw operator iteration method needs to solve inverse of central matrix to guarantee the convergence. However, the book to compute inverse of a matrix is much great, and it hard to implement for a large system in practice. According to the iteration expression of Kraw operator iteration method, we only need to find a better matrix which is defined to guarantee the convergence, so krawczyk iteration method with approximate inverse preconditioner can be used [1, 2]. For coefficient matrix $\boldsymbol{A}$, a state-of-the-art method is to minimize the Frobenius norm of the residual matrix $\|\boldsymbol{I} - \boldsymbol{CA}\|_F^2$ to seek an approximate inverse $\boldsymbol{C}$. Generally, we can take the 2-norm into consideration. In addition, the 2-norm can be decoupled as the sum of the squares, which can be utilized for the parallel computation. The optimization model is formulated as following:

$$\min_{\boldsymbol{C}} \quad \|\boldsymbol{I} - \boldsymbol{CA}\|_2^2 = \sum_{i=1}^{n} \|\boldsymbol{e}_i - \boldsymbol{C}_i\boldsymbol{A}\|_2^2 \tag{2.4}$$

where $\boldsymbol{C}_i^{k+1}$ denotes ith row of $\boldsymbol{C}$ at $k + 1$ iteration, n is the dimension of coefficient matrix $\boldsymbol{A}$, and $\boldsymbol{e}_i$ is the ith raw of the identity matrix.

Furthermore, an approximate inverse can be computed using Newton's method with the iteration as

$$\boldsymbol{C}^{k+1} = \boldsymbol{C}^k - \left(\boldsymbol{I} - \boldsymbol{C}^k\boldsymbol{A}\right)\left(-\boldsymbol{C}^k\right) = \boldsymbol{C}^k\left(2\boldsymbol{I} - \boldsymbol{AC}^k\right) \tag{2.5}$$

$$\boldsymbol{C}_i^{k+1} = \boldsymbol{C}_i^k - \left(\boldsymbol{e}_i - \boldsymbol{C}_i^k\boldsymbol{A}\right)\left(-\boldsymbol{C}^k\right) = \boldsymbol{C}_i^k\left(2\boldsymbol{I} - \boldsymbol{AC}^k\right), \quad i = 1, \ldots, n \tag{2.6}$$

Theorem 2.1 *To guarantee the convergence of Kraw operator iteration method, constant matrix* $\boldsymbol{C}$ *should satisfy* $\|\boldsymbol{I} - \boldsymbol{CA}\| = \beta < 1$

Proof According to Kraw operator iteration expression, define an interval sequence $\left\{\left\langle \boldsymbol{x}^k \right\rangle\right\}$ which satisfies $\left\langle \boldsymbol{x}^{k+1} \right\rangle = \left(\boldsymbol{C}\langle \boldsymbol{b} \rangle + (\boldsymbol{I} - \boldsymbol{CA})\left\langle \boldsymbol{x}^k \right\rangle\right) \cap \left\langle \boldsymbol{x}^k \right\rangle \subseteq \left(\boldsymbol{C}\langle \boldsymbol{b} \rangle + (\boldsymbol{I} - \boldsymbol{CA})\left\langle \boldsymbol{x}^k \right\rangle\right)$.

Then, we introduce a new sequence $\left\{\left\langle \boldsymbol{y}^k \right\rangle\right\}$ with $\left\langle \boldsymbol{y}^{k+1} \right\rangle = \left(\boldsymbol{C}\langle \boldsymbol{b} \rangle + (\boldsymbol{I} - \boldsymbol{CA})\left\langle \boldsymbol{y}^k \right\rangle\right)$. We can easily derive that $0 \le \left\|\left\langle \boldsymbol{x}^k \right\rangle\right\| \le \left\|\left\langle \boldsymbol{y}^k \right\rangle\right\|$, so if $\left\{\left\langle \boldsymbol{y}^k \right\rangle\right\}$ converges, $\left\{\left\langle \boldsymbol{x}^k \right\rangle\right\}$ will be bounded by the limit of $\{\langle \boldsymbol{y}^\infty \rangle\}$.

For the sequence $\left\{\left\langle \boldsymbol{y}^k \right\rangle\right\}$, it derives

$$\begin{cases} \left\langle \boldsymbol{y}^{k+1} \right\rangle = \left(\boldsymbol{C}\langle \boldsymbol{b} \rangle + (\boldsymbol{I} - \boldsymbol{CA})\left\langle \boldsymbol{y}^k \right\rangle\right), \left\|\left\langle \boldsymbol{y}^{k+1} \right\rangle\right\| = \left\|\boldsymbol{C}\langle \boldsymbol{b} \rangle + (\boldsymbol{I} - \boldsymbol{CA})\left\langle \boldsymbol{y}^k \right\rangle\right\| \\ \left\langle \boldsymbol{y}^k \right\rangle = \left(\boldsymbol{C}\langle \boldsymbol{b} \rangle + (\boldsymbol{I} - \boldsymbol{CA})\left\langle \boldsymbol{y}^{k-1} \right\rangle\right), \left\|\left\langle \boldsymbol{y}^k \right\rangle\right\| = \left\|\boldsymbol{C}\langle \boldsymbol{b} \rangle + (\boldsymbol{I} - \boldsymbol{CA})\left\langle \boldsymbol{y}^{k-1} \right\rangle\right\| \end{cases} \tag{2.7}$$

Take the difference of the two equations, and we have

$$\left\|\left\langle \boldsymbol{y}^{k+1} \right\rangle - \left\langle \boldsymbol{y}^k \right\rangle\right\| \le \lambda\left\|\left\langle \boldsymbol{y}^k \right\rangle - \left\langle \boldsymbol{y}^{k-1} \right\rangle\right\| \le \lambda^2\left\|\left\langle \boldsymbol{y}^{k-1} \right\rangle - \left\langle \boldsymbol{y}^{k-2} \right\rangle\right\| \le \cdots \le \lambda^k\left\|\langle \boldsymbol{y}^1 \rangle - \langle \boldsymbol{y}^0 \rangle\right\| \tag{2.8}$$

Next, we will show that if n, $m \geq N$ for an any given number N (assuming $n > m$), then it holds that

$$\|\langle \boldsymbol{y}^n \rangle - \langle \boldsymbol{y}^m \rangle\| \leq \frac{\lambda^n}{1-\lambda} \|\langle \boldsymbol{y}^1 \rangle - \langle \boldsymbol{y}^0 \rangle\| \tag{2.9}$$

It can be proved as following:

$$\begin{aligned}
&\|\langle \boldsymbol{y}^{m+1} \rangle - \langle \boldsymbol{y}^m \rangle\| \leq \lambda^m \|\langle \boldsymbol{y}^1 \rangle - \langle \boldsymbol{y}^0 \rangle\| \\
&\|\langle \boldsymbol{y}^m \rangle - \langle \boldsymbol{y}^{m+2} \rangle\| \leq \|\langle \boldsymbol{y}^{m+2} \rangle - \langle \boldsymbol{y}^m \rangle\| \leq \|\langle \boldsymbol{y}^{m+1} \rangle - \langle \boldsymbol{y}^m \rangle\| \\
&\quad + \|\langle \boldsymbol{y}^{m+2} \rangle - \langle \boldsymbol{y}^{m+1} \rangle\| \leq (\lambda^m + \lambda^{m+1}) \|\langle \boldsymbol{y}^1 \rangle - \langle \boldsymbol{y}^0 \rangle\| \cdots \\
&\|\langle \boldsymbol{y}^n \rangle - \langle \boldsymbol{y}^m \rangle\| \leq (\lambda^m + \lambda^{m+1} + \cdots + \lambda^{n-1}) \|\langle \boldsymbol{y}^1 \rangle - \langle \boldsymbol{y}^0 \rangle\| \\
&\quad = \lambda^m (1 + \lambda + \cdots + \lambda^{n-m-1}) \|\langle \boldsymbol{y}^1 \rangle - \langle \boldsymbol{y}^0 \rangle\| \\
&\quad \leq \lambda^n (1 + \lambda + \lambda^2 + \cdots) \|\langle \boldsymbol{y}^1 \rangle - \langle \boldsymbol{y}^0 \rangle\| = \frac{\lambda^n}{1-\lambda} \|\langle \boldsymbol{y}^1 \rangle - \langle \boldsymbol{y}^0 \rangle\|
\end{aligned}$$

(Q.E.D.)

Thus, we can conclude that if $\lambda < 1$, $\{\langle \boldsymbol{y}^k \rangle\}$ is a Cauchy sequence, which converges to a point $\langle \boldsymbol{y}^* \rangle$ that belongs to IR space. Thus, $\{\langle \boldsymbol{x}^k \rangle\}$ will be bound by $\{\langle \boldsymbol{y}^* \rangle\}$, such that $0 \leq \|\langle \boldsymbol{x} \rangle\| \leq \|\langle \boldsymbol{y}^* \rangle\|$.

On the other hand

$$\langle \boldsymbol{x}^{k+1} \rangle = (\boldsymbol{C}\langle \boldsymbol{b} \rangle + (\boldsymbol{I} - \boldsymbol{CA})\langle \boldsymbol{x}^k \rangle) \cap \langle \boldsymbol{x}^k \rangle \subseteq \langle \boldsymbol{x}^k \rangle \Rightarrow \|\langle \boldsymbol{x}^{k+1} \rangle\| \leq \|\langle \boldsymbol{x}^k \rangle\|$$

As a result, we can see that $\{\langle \boldsymbol{x}^k \rangle\}$ is a monotonously decreasing and bounded sequence; therefore, it must be converged after several iterations.

(Q.E.D.)

According to Corollary 2.1, the spectral radius of $\boldsymbol{I} - \boldsymbol{C}_0\boldsymbol{A}$ must be less than one with the aim of convergence. Therefore, if the initial guess of $\boldsymbol{C}^0$ is chosen as $\boldsymbol{C}^0 = \delta \boldsymbol{A}^T$, it yields

$$\rho(\boldsymbol{I} - \delta \boldsymbol{A}^T \boldsymbol{A}) < 1 \Rightarrow 0 \leq \delta \leq \frac{2}{\rho(\boldsymbol{A}^T \boldsymbol{A})} \tag{2.10}$$

where ρ denotes the spectral radius of a matrix.

It is easily known from [3] that $\rho(\boldsymbol{A}^T \boldsymbol{A}) \leq \|\boldsymbol{A}^T \boldsymbol{A}\|$, where $\|\cdot\|$ is any subordinate norm. In practice, we use

$$\delta = 1/\|\boldsymbol{A}^T \boldsymbol{A}\|_1 \tag{2.11}$$

Finally, it is important to point out that the approximate inverse matrix may become denser and denser as the iterations progress, which will need additional

communication with memory and will have a side effect on the computation efficiency. Meanwhile, some nonzero elements with small value is extremely close to zero, but they can not be fully equal to zero because of calculation error. Therefore, the sparsity representation should be performed during each iteration by dropping some elements with small value in the approximate inverse matrix. The flowchart of proposed Kraw operator iteration method with minimum norm preconditioner is shown in Table 2.1.

Table 2.1 The flowchart of Kraw operator iteration method with minimum norm preconditioner

Approximate Inverse Preconditioner-based Kraw Operator Iteration Method	
Input:	ε is a preset convergence precision, n is the dimension of coefficient matrix $\boldsymbol{A}$, and η is the dropping tolerance.
Output:	The interval solution $\langle \boldsymbol{x} \rangle$ of $\boldsymbol{A}\langle \boldsymbol{x} \rangle = \langle \boldsymbol{b} \rangle$
Step 1:	Compute δ by (2-11), such that $\delta = 1/\left\| \boldsymbol{A}^T \boldsymbol{A} \right\|_1$;
Step 2:	Let $\boldsymbol{C}^0 \leftarrow \delta \boldsymbol{A}^T$, $\lambda \leftarrow +\infty$, and $k \leftarrow 1$;
Step 3:	**while** $\lambda > 1$
Step 4:	**for** i=1:n
Step 5:	$TempC_i^k \leftarrow C_i^{k-1}(2\boldsymbol{I} - \boldsymbol{A}\boldsymbol{C}^k)$;
Step 6:	$TCmax_i^k \leftarrow \max(TempC_i^k)$;
Step 7:	**for** j=1:n
Step 8:	**if** $TempC_{i,j}^k / TCmax_i^k \le \eta$
Step 9:	$TempC_{i,j}^k \leftarrow 0$;
Step 10:	**end**
Step 11:	**end**
Step 12:	**end**
Step 13:	$\boldsymbol{C}^k \leftarrow \boldsymbol{TempC}^k$ and $k \leftarrow k+1$;
Step 14:	$\lambda \leftarrow \| \boldsymbol{I} - \boldsymbol{C}^k \boldsymbol{A} \|_2$;
Step 15:	**end**
Step 16:	Let $\boldsymbol{b} \leftarrow \boldsymbol{C}\boldsymbol{b}$, $\boldsymbol{A} \leftarrow \boldsymbol{I} - \boldsymbol{C}\boldsymbol{A}$;
Step 17:	Compute $\lambda \leftarrow \|\boldsymbol{A}\|$ and $\alpha = \left\| \boldsymbol{C}\langle \boldsymbol{b} \rangle \right\| / (1-\lambda)$;
Step 18:	Let $\left\langle \boldsymbol{x}^0 \right\rangle \leftarrow ([-\alpha, +\alpha], [-\alpha, +\alpha], \ldots, [-\alpha, +\alpha])^T$, $s^0 \leftarrow 2n\alpha$, $\tau \leftarrow +\infty$ and $k \leftarrow 1$;
Step 19:	**while** $\tau \le \varepsilon$
Step 20:	$\left\langle \boldsymbol{x}^{k+1} \right\rangle \leftarrow \left(\boldsymbol{C}\langle \boldsymbol{b} \rangle + (\boldsymbol{I} - \boldsymbol{C}\boldsymbol{A}) \left\langle \boldsymbol{x}^k \right\rangle \right) \cap \left\langle \boldsymbol{x}^k \right\rangle$
Step 21:	$s^{k+1} \leftarrow sum(length(\left\langle \boldsymbol{x}^{k+1} \right\rangle))$;
Step 22:	$\tau \leftarrow (s^k - s^{k+1}) / s^{k+1}$;
Step 23:	**end**

Partially Parallel

2.2.2 Nonlinear Equations with Right-Hand Intervals Using Optimality-Based Method

It should be noted that the interval nonlinear equations are more difficult than interval linear equations to be handled. If the intervals only exist in the right hand of the nonlinear equations, the interval nonlinear equations can be compactly formulated as $\boldsymbol{F}(\langle \boldsymbol{x} \rangle) = \langle \boldsymbol{p} \rangle$, where $\boldsymbol{p}$ is the input interval parameters and $\langle \boldsymbol{x} \rangle$ is the interval solution of the nonlinear equations. Generally, the interval nonlinear equations can be solved by the interval nonlinear Kraw operator iteration method, the flowchart of which can be found in the Appendix B.

However, the conservatism problem of interval nonlinear equations are more serious. As Sect. 1.2.1 mentioned, when the same intervals appear several times in one expression, the range of interval will become conservative. However, in the computation of interval nonlinear equations, it may have many same elements in Jacobian matrix and initial equations, so the interval solutions may be greatly expanded after several iterations, which will lead to serious conservatism problem. Therefore, the biggest challenge to solve interval nonlinear equations is to overcome conservatism of interval operations.

Similarly, optimality-based method of interval linear equations can be used. If $\boldsymbol{p}$ is regarded as a new variable, then in a high-dimensional space with the optimal variable of $(\boldsymbol{p}, \boldsymbol{x})$, the optimization model is formulated as following:

$$\min_{\boldsymbol{x},\boldsymbol{p}} / \max \quad x_i \quad s.t. \quad \underline{\boldsymbol{p}} \leq \boldsymbol{F}(\boldsymbol{x},\boldsymbol{p}) \leq \overline{\boldsymbol{p}}, \quad i = 1, \ldots, n \tag{2.12}$$

With the objective function of min and max respectively, the lower and upper bound of the variable i can be solved. Similarly, because the solution of every variable is independent, it can be divided into n optimizer with parallel implementation. Compared with Kraw operator iteration method, optimality-based method is able to attain compact range of interval. However, the aforementioned model is generally a nonlinear optimization model, and it is hard to compute global optimal solution. Then, our discussion is based on the common interval quadratic nonlinear equations.

2.2.2.1 Linear Relaxation Model for Interval Quadratic Equations with Optimality-Based Method

Consider interval quadratic nonlinear equations $\boldsymbol{x}^T \boldsymbol{Q}_j \boldsymbol{x} + \boldsymbol{c}_j^T \boldsymbol{x} = \left[\underline{d_j}, \overline{d_j}\right], j = 1, \ldots, m.$ The optimization model based the aforementioned method is formulated as

$$\max_{\boldsymbol{x} \in \mathrm{R}^{n \times 1}} / \min \quad \boldsymbol{x}^T \boldsymbol{Q}_0 \boldsymbol{x} + \boldsymbol{c}_0^T \boldsymbol{x} \tag{2.13}$$

$$s.t. \quad \underline{d_j} \le \boldsymbol{x}^T \boldsymbol{Q}_j \boldsymbol{x} + \boldsymbol{c}_j^T \boldsymbol{x} \le \overline{d_j}, \quad j = 1, \ldots, m \tag{2.14}$$

It notes that the independent variable x generally has a reasonable given range of interval. Let the range of interval is $l_i \le x_i \le u_i, i = 1, \ldots, n$, then we can get a general quadratically constrained quadratic programming (QCQP) model:

$$(\mathbf{QCQP}) \quad \max_{\boldsymbol{x} \in \mathrm{R}^{n \times 1}} / \min \quad \boldsymbol{x}^T \boldsymbol{Q}_0 \boldsymbol{x} + \boldsymbol{c}_0^T \boldsymbol{x} \tag{2.15}$$

$$s.t. \quad \underline{d_j} \le \boldsymbol{x}^T \boldsymbol{Q}_j \boldsymbol{x} + \boldsymbol{c}_j^T \boldsymbol{x} \le \overline{d_j}, \quad j = 1, \ldots, m \tag{2.16}$$

$$l_i \le x_i \le u_i, \quad i = 1, \ldots, n \tag{2.17}$$

where n denotes the number of quadratic constraints, Q_j (j = 1,…,m) are indefinite $n \times n$ matrices, $\boldsymbol{c}_j$ (j = 0,…,m) are n-dimensional vectors, the set $\bigcup_{i=1}^{n} [l_i, u_i]$ is assumed to be nonempty and bounded.

$\phi(x,y)$ is called bilinear function if $\phi(x,\cdot)$ and $\phi(\cdot,y)$ are both linear functions. For example, $\phi(x,y) = xy$ is a bilinear function. Let a mapping f: $\Omega \rightarrow$ R be a bilinear function, then $\mathrm{vex}_\Omega(f)$ is the convex envelope of f over Ω, if it is the point-wise supremum of convex underestimation of f over Ω. Similarly, $\mathrm{cav}_\Omega(f)$ is the concave envelope of f over Ω, if it is the point-wise infimum of concave overestimation of f over Ω, then a theorem is given as following.

Theorem 2.2: *xy is a bilinear function given in a bounded closed set Ψ. The convex envelope $vex_\Omega(xy)$ and concave envelope $cav_\Omega(xy)$ are determined by* (2.58) *and* (2.59)*, and then we can arrive at $vex_\Omega(xy) \le xy \le cav_\Omega(xy)$.*

$$\Psi \stackrel{def}{=} \left\{ (x, y) \in \mathrm{R}^2 \middle| l_x \le x \le u_x, l_y \le y \le u_y \right\} \tag{2.18}$$

$$vex_\Omega(xy) = \max\{l_y x + l_x y - l_x l_y, u_y x + u_x y - u_x u_y\} \tag{2.19}$$

$$cav_\Omega(xy) = \min\{u_y x + l_x y - l_x u_y, l_y x + u_x y - u_x l_y\} \tag{2.20}$$

Let dummy variable $\boldsymbol{Z} = \boldsymbol{x}\boldsymbol{x}^T \in \mathrm{R}^{n \times n}$ and substitute $\boldsymbol{Z}$ for $\boldsymbol{x}\boldsymbol{x}^T$ in QCQP model, the objective and constraints become bilinear. Furthermore, the convex envelopes and concave envelopes as defined in Theorem 2.2 are introduced to obtain the tractable linear relaxation (LR) model of the non-convex problem QCQP, formulated as follows:

$$(\mathbf{QCQP{-}LR}) \quad \max_{\boldsymbol{x} \in \mathrm{R}^{n \times n}, \boldsymbol{z} \in \mathrm{R}^{n \times n}} / \min \quad \boldsymbol{c}^T \boldsymbol{x} + \boldsymbol{Q}_0 \cdot \boldsymbol{Z} \tag{2.21}$$

$$s.t. \quad \underline{d_j} \le \boldsymbol{c}_j^T \boldsymbol{x} + \boldsymbol{Q}_j \cdot Z \le \overline{d_j}, \quad j = 1, \ldots, m \tag{2.22}$$

$$z_{ij} - l_i x_j - l_j x_i + l_i l_j \geq 0, \quad j = 1, \ldots, m \quad i = 1, \ldots, n \tag{2.23}$$

$$z_{ij} - u_i x_j - u_j x_i + u_i u_j \geq 0, \quad j = 1, \ldots, m \quad i = 1, \ldots, n \tag{2.24}$$

$$z_{ij} - l_i x_j - u_j x_i + l_i u_j \leq 0, \quad j = 1, \ldots, m \quad i = 1, \ldots, n \tag{2.25}$$

$$z_{ij} - u_i x_j - l_j x_i + u_i l_j \leq 0, \quad j = 1, \ldots, m \quad i = 1, \ldots, n \tag{2.26}$$

$$l_i \leq x_i \leq u_i, \quad i = 1, \ldots, n \tag{2.27}$$

where $\forall A, B \in \mathrm{R}^{n \times n}$, $A \cdot B = \sum_{i=1}^{n} \sum_{j=1}^{n} a_{ij} b_{ij}$.

For minimization problem of the original QCQP, the QCQP-LR is a relaxed linear programming model and therefore provides a lower bound of the original QCQP. Similarly, it provides an upper bound for the maximization problem of the original QCQP.

2.2.3 Optimality-Based Bounds Tightening Method

It can be observed that the relaxed QCQP-LR model is dependent on the hyper-rectangular variable domain. At the beginning, the initial domain is usually so large that leads to a conservational interval solution, so it is desirable to schedule a more rigorous hyper-rectangle domain to achieve an optimal interval solution. For this reason, the optimality-based bounds tightening (OBBT) method proposed in [4–6] is employed to solve the QCQP-LR model, which will tighten the relaxed model QCQP-LR based on linear optimality by cycling through each participating variable until the volume fails to improve.

Define $\boldsymbol{x}^k = (\boldsymbol{e}^k, \boldsymbol{f}^k, \boldsymbol{y}^k)$ to represent the variable set in the kth iteration. Let $LR_{\Omega}^{k}(\boldsymbol{x}^k)$ denote the constraints of QCQP-LR model and let $(\varphi_{\Omega})^k(\cdot)$ be the optimal objective value of (QCQP-LR) in the feasible domain $\Omega^k = \left\{ \underline{\boldsymbol{x}^k} \leq \boldsymbol{x} \leq \overline{\boldsymbol{x}^k} \right\}$. Then, the hyper-rectangular variable domain can be tightened or 'squeezed' through an iterative linear programming solver, which is illustrated in the following three steps.

(a) The initial matrix domain is set as Ω^0, set $k \leftarrow 0$;

(b) Solve $\begin{cases} \overline{x}_i^{k+1} \leftarrow \{\max x_i \quad s.t. \quad LR_{\Omega^k}(\boldsymbol{x}^k) \cap \Omega^k\} \\ \underline{x}_i^{k+1} \leftarrow \{\min x_i \quad s.t. \quad LR_{\Omega^k}(\boldsymbol{x}^k) \cap \Omega^k\} \end{cases}$ for $\forall I$, set $k \leftarrow k+1$;

(c) $\Omega^k \leftarrow \{ \underline{\boldsymbol{x}^k} \leq \boldsymbol{x} \leq \overline{\boldsymbol{x}^k} \}$, if $\Omega^k = \Omega^{k-1}$ stop; otherwise, go to (b).

From iteration process above, we know that interval power flow computation includes 'min' and 'max' models simultaneously solved. Based on OBBT method, the variable domain Ω^i satisfies $\Omega^{i-1} \subseteq \Omega^i$, and as such the domain sequence $\{\Omega^0, \Omega^1, \Omega^2, \ldots, \Omega^i, \ldots\}$, obtained from step (b), is monotonously decreasing and geometrically a nested sequence of hyper-rectangles, so the domain sequence is a

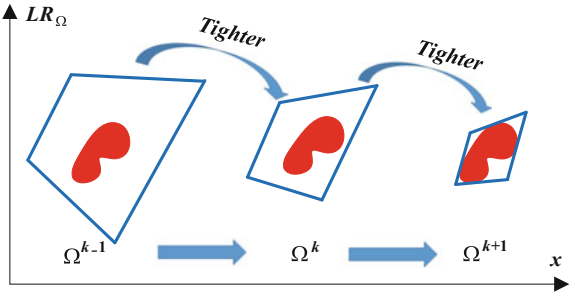

Fig. 2.1 The process of gradually tightened variable domain using OBBT-based method

Cauchy sequence and has a limit. Additionally, QCQP-LR model is a linear programming in a bounded closed set (compact set). For any given solution $\boldsymbol{x}$ and $\boldsymbol{y}$, we have $\|(\varphi_\Omega)(\boldsymbol{x}) - (\varphi_\Omega)(\boldsymbol{y})\|_\infty = \|(\boldsymbol{x}^T\boldsymbol{Q}_0\boldsymbol{x} + c_0^T\boldsymbol{x}) - (\boldsymbol{y}^T\boldsymbol{Q}_0\boldsymbol{y} + c_0^T\boldsymbol{y})\|_\infty \le \|\boldsymbol{u} - \boldsymbol{l}\|_\infty \cdot \|\boldsymbol{Q}_0\|_\infty \cdot \|\boldsymbol{u} - \boldsymbol{l}\|_\infty < +\infty$, which means operator $(\varphi_\Omega)^i(\cdot)$ is a bounded operator. Therefore, $\|(\varphi_\Omega)^{i+1}(\boldsymbol{x}) - (\varphi_\Omega)^i(\boldsymbol{x})\|_\infty \le \|(\varphi_\Omega)^i(\boldsymbol{x})\|_\infty \cdot \|\Omega^{i+1} - \Omega^i\|_\infty$, where $\|\Omega^i\|_\infty = \left\|\overline{\boldsymbol{x}^i} - \underline{\boldsymbol{x}^i}\right\|_\infty$. According to functional analysis, the aforementioned expression denotes that a Cauchy sequence is mapped to a Cauchy sequence by bounded operator. Therefore, the sequence $\{(\varphi_\Omega)^0(\boldsymbol{x}), \ldots, (\varphi_\Omega)^i(\boldsymbol{x}), \ldots\}$ is also a Cauchy sequence and has a limit, which demonstrates that the proposed OBBT-based algorithm can converge after finite number of iterations. Furthermore, the process of gradually tightened hyper-rectangular variable domain is illustrated in Fig. 2.1, where the solid red area represents the feasible region of the original non-convex QCQP problem.

After the process stops (and OBBT algorithm converges), the optimally tightened hyper-rectangular variable domain Ω^* and the corresponding interval solution are obtained.

2.3 Optimization Solutions Based Intervals

2.3.1 Optimization Solutions with Right-Hand Intervals

Interval linear optimization model with right-hand interval uncertainties is formulated as

$$\text{Min} \quad Z = \boldsymbol{c}^T\boldsymbol{x} \tag{2.28}$$

$$s.t.\ \boldsymbol{A}\boldsymbol{x} = [\boldsymbol{w}^-, \boldsymbol{w}^+] \tag{2.29}$$

$$\boldsymbol{B}\boldsymbol{x} \le [\boldsymbol{d}^-, \boldsymbol{d}^+] \tag{2.29}$$

$$\boldsymbol{l} \leq \boldsymbol{x} \leq \boldsymbol{u} \tag{2.30}$$

where, $\boldsymbol{A} \in \mathrm{R}^{s\times n}, \boldsymbol{B} \in \mathrm{R}^{m\times n}$, $\boldsymbol{c} \in \mathrm{R}^{n\times 1}, \boldsymbol{x} \in \mathrm{R}^{n\times 1}$; m represents the number of interval inequations, s represents the number of interval equations, n represents the dimension of variable.

The objective of interval optimization is to find out the optimistic value and pessimistic value of objective functions and range of interval variables. For $\forall \boldsymbol{w} \in [\boldsymbol{w}^-, \boldsymbol{w}^+]$, $\forall \boldsymbol{d} \in [\boldsymbol{d}^-, \boldsymbol{d}^+]$, solve the deterministic optimization model as following, and obtain the objective value and the optimal solution. if uncertainty variables are taken as any possible combinations of intervals, then we can obtain any possible objective values and optimal interval solutions, and the upper and lower bounds of which are called the optimal interval function value and the optimal interval solution, where the upper bound of optimal interval function value is called pessimistic value and the lower bound is called optimistic value.

$$\text{Min} \quad Z = \boldsymbol{c}^T \boldsymbol{x} \tag{2.31}$$

$$s.t. \quad \boldsymbol{A}\boldsymbol{x} = \boldsymbol{w} \tag{2.32}$$

$$\boldsymbol{B}\boldsymbol{x} \leq \boldsymbol{d} \tag{2.33}$$

$$\boldsymbol{l} \leq \boldsymbol{x} \leq \boldsymbol{u} \tag{2.34}$$

We can see that independent variable $\boldsymbol{x}$ and objective value Z of model (2.28)–(2.30) is the function of uncertainties, which is an optimization model. From this perspective, interval optimization is a special kind of interval mathematical operation, which is hard to obtain an explicit expression. Considering to overcome the conservatism of interval operations, it can be solved by the optimization method. Therefore, interval optimization can be regarded as the optimization of optimization, that is, bi-level programming.

Firstly, assume the interval optimization model is solvable, such that for $\forall \boldsymbol{w} \in [\boldsymbol{w}^-, \boldsymbol{w}^+]$, $\forall \boldsymbol{d} \in [\boldsymbol{d}^-, \boldsymbol{d}^+]$, the optimization model (2.31)–(2.34) is feasible. Based on the assumption, the solution models of optimistic value and pessimistic value are obtained according to the two standard bi-level optimization model (2.35)–(2.39) and (2.40)–(2.44), where optimistic value denotes the optimal value among the range of uncertain disturbance interval, which is expressed as "min-min" form while pessimistic value denotes the worst value among the range of uncertain disturbance interval, which is expressed as "max-min" form

$$(\text{Optimistic value}) \min_{\boldsymbol{w},\boldsymbol{d}} \min_{\boldsymbol{x}} \quad Z^- = \boldsymbol{c}^T \boldsymbol{x} \tag{2.35}$$

$$s.t. \quad \boldsymbol{A}\boldsymbol{x} = \boldsymbol{w} \tag{2.36}$$

$$\boldsymbol{Bx} \leq \boldsymbol{d} \tag{2.37}$$

$$\boldsymbol{l} \leq \boldsymbol{x} \leq \boldsymbol{u} \tag{2.38}$$

$$\forall \boldsymbol{w} \in [\boldsymbol{w}^-, \boldsymbol{w}^+], \quad \forall \boldsymbol{d} \in \left[\boldsymbol{d}^-, \boldsymbol{d}^+\right] \tag{2.39}$$

$$\text{(Pessimistic value)} \quad \max_{\boldsymbol{w},\boldsymbol{d}} \min_{\boldsymbol{x}} \quad Z^+ = \boldsymbol{c}^T\boldsymbol{x} \tag{2.40}$$

$$s.t. \quad \boldsymbol{Ax} = \boldsymbol{w} \tag{2.41}$$

$$\boldsymbol{Bx} \leq \boldsymbol{d} \tag{2.42}$$

$$\boldsymbol{l} \leq \boldsymbol{x} \leq \boldsymbol{u} \tag{2.43}$$

$$\forall \boldsymbol{w} \in [\boldsymbol{w}^-, \boldsymbol{w}^+], \quad \forall \boldsymbol{d} \in \left[\boldsymbol{d}^-, \boldsymbol{d}^+\right] \tag{2.44}$$

A. The solution of optimistic model

Because the inner and outer level of bi-level optimistic model are both "min" problems, it can be combined as single-level programming, and we hope the feasible region is as large as possible to guarantee the lower bound of interval solution. Then, the inequality constraint is relaxed to the maximum bound $\boldsymbol{d}^+$, and the simplified single-level optimization is formulated as (2.45)–(2.48). Therefore, the linear programming problem can be solved effectively by simplex method.

$$\text{(Optimistic value)} \quad \min_{\boldsymbol{x}} \quad Z^- = \boldsymbol{c}^T\boldsymbol{x} \tag{2.45}$$

$$s.t. \, \boldsymbol{w}^- \leq \boldsymbol{Ax} \leq \boldsymbol{w}^+ \tag{2.46}$$

$$\boldsymbol{Bx} \leq \boldsymbol{d}^+ \tag{2.47}$$

$$\boldsymbol{l} \leq \boldsymbol{x} \leq \boldsymbol{u} \tag{2.48}$$

B. The solution of pessimistic model

However, for bi-level pessimistic model, the inner level is "min" model while the outer level is "max" model. Because the objectives of inner and outer levels are different, it can not be transformed as a single-level programming. Generally, it is easy to handle interval inequality constraints and hard to handle interval equality constraints. From the view of mathematics, strong duality theorem is employed to express the inner model as its dual model and a "max" model is obtained. Then the "max-max" model is transformed into a single-level "max" model is according to the solution of two-level optimistic model. To pessimistic model, we hope the feasible region is as small as possible, so the inequality constraint is shrunk to the

minimum bound $\boldsymbol{d}^{-}$. In the inner model, the uncertain value is regarded as a constant and dual model is used, then we have,

$$Z^{+} = \underset{\boldsymbol{b}^{-} \le \boldsymbol{w} \le \boldsymbol{b}}{\text{Max}} \begin{cases} \underset{\boldsymbol{x}}{\text{Min}} & Z = \boldsymbol{c}^{T}\boldsymbol{x} \\ s.t. & \boldsymbol{B}\boldsymbol{x} \le \boldsymbol{d}^{-} \quad \text{the number of constraints is } m \\ & \boldsymbol{A}\boldsymbol{x} = \boldsymbol{w} \quad \text{the number of constraints is } s \\ & \boldsymbol{I}\boldsymbol{x} \ge \boldsymbol{l} \quad \text{the number of constraints is } n \\ & \boldsymbol{I}\boldsymbol{x} \ge \boldsymbol{u} \quad \text{the number of constraints is } n \end{cases}$$

$$\overset{\Leftrightarrow}{Z^{+} = \underset{\boldsymbol{b}^{-} \le \boldsymbol{w} \le \boldsymbol{b}}{\text{Max}}} \begin{cases} \underset{\boldsymbol{y}_1,\boldsymbol{y}_2,\boldsymbol{y}_3,\boldsymbol{y}_4}{\text{Max}} & (d^{-})^{T}\boldsymbol{y}_1 + \boldsymbol{w}^{T}\boldsymbol{y}_2 + \boldsymbol{l}^{T}\boldsymbol{y}_3 + \boldsymbol{u}^{T}\boldsymbol{y}_4 \\ s.t. & \left[\boldsymbol{E}^{T}, \boldsymbol{A}^{T}, \boldsymbol{I}, \boldsymbol{I}\right] \begin{bmatrix} \boldsymbol{y}_1 \\ \boldsymbol{y}_2 \\ \boldsymbol{y}_3 \\ \boldsymbol{y}_4 \end{bmatrix} = \boldsymbol{c} \quad \text{the number of constraints is } n \\ & \boldsymbol{y}_1 \le 0 \quad \text{the number of constraints is } m \\ & -\infty < \boldsymbol{y}_2 < +\infty \quad \text{the number of constraints is } s \\ & \boldsymbol{y}_3 \ge 0 \quad \text{the number of constraints is } n \\ & \boldsymbol{y}_4 \le 0 \quad \text{the number of constraints is } n \end{cases} \tag{2.49}$$

where $\boldsymbol{y}_1 = (y_i)_{m\times 1}, \boldsymbol{y}_2 = (y_i)_{s\times 1}, \quad \boldsymbol{y}_3 = (y_i)_{n\times 1}, \boldsymbol{y}_4 = (y_i)_{n\times 1}$ and $\boldsymbol{y} = \left(\boldsymbol{y}_1^{T}, \boldsymbol{y}_2^{T}, \boldsymbol{y}_3^{T}, \boldsymbol{y}_4^{T}\right)^{T}$.

It is obvious from model (2.49) that transformed "max" model is not a linear programming, but a nonlinear programming with inner product of different variables (wTy2). This special optimization model is also called bilinear programming. Certainly, the interior point method of nonlinear programming is only to obtain local optimal solution, but it is a NP difficult problem to obtain global optimal solution. For NP difficult problem, a unified and effective method to solve the problem is not proposed at present. In general, different approximate methods are used to solve the problem, and the artificial intelligence method and branch and bound method are mainly used to search. Two branch and bound methods are proposed in the paper to solve this problem.

Method One: *Spatial branch and bound method*

The first method to search global optimal solution is to use branch and bound method based linear relaxation technique. It is branched for continuous variables, so it is also called spatial branch and bound method or simplicial branch and bound method [7, 8].

Generally, the objective function of standard model is normalized as "min" form. Therefore, (2.49) is replaced by (2.50), which have same optimal solutions, and the model with "min" form is used to analyze and discuss below.

$$\underset{\boldsymbol{w},\boldsymbol{y}}{\min} \quad -Z^{+} = -\boldsymbol{w}^{T}\boldsymbol{y}_1 - (\boldsymbol{d}^{-})^{T}\boldsymbol{y}_2 - \boldsymbol{l}^{T}\boldsymbol{y}_3 - \boldsymbol{u}^{T}\boldsymbol{y}_4 \tag{2.50}$$

Firstly, spatial branch and bound method need to relax (2.49) in the continuous space to find the strict lower bound of the model. Of course, there are many ways to relax, and we hope to find a linear relaxation model which can be easily solved. According to Theorem 2.2, the original optimization model (2.49) can be linearly relaxed on any bounded closed set to obtain global lower bound. However, the lower bound is not necessarily the infimum, so the branch and bound method is used to approaching. The initial bounded closed set can be selected as the whole feasible region. However, because $\boldsymbol{y}_1$ has no limit, a big number $Q = 10^6$ is used to restrict, such that $R^0 = \left\{\boldsymbol{w}^- \le \boldsymbol{w}^0 \le \boldsymbol{w}^+, -Q < y_{1,i}^0 < +Q\right\}$, $i = 1, \ldots, N_g$. If f^* denotes exact optimal solution, for the kth region, the feasible region is expanded after relaxation, so the solution $f^{r,k}$ is obtained and $f^{r,k} \le f^*$. If the bounded closed set is halved into two regions shown in Fig. 2.2 and each region is linearly relaxed, the new feasible region obtained is smaller than the one after direct relaxation, and the relaxation solution $f^{r,k}$ is improved. However, the relaxation model is used to solve after branching, so the solution is always the lower bound of original model, so that $f^{r,k} \le f^*$ is always satisfied. After each halving, the subregion with minimum value is chosen to be branched again, so the sequence solution $f^{r,k}$ is monotonically increasing with continuous branching.

On the other hand, the solution $f^{r,k}$ of relaxation model can be selected as the initial value, and interior point method is used to solve model (2.55) directly. Because only local optimal solution $f^{l,k}$ is obtained by interior point method, and the local optimal solution must be greater than or equal to global optimal solution, such that $f^* \le f^{l,k}$. Therefore, the upper bound is limited by $\min(f^{l,k})$ in the solving process, and the upper bound value is continuously decreased.

Considering the upper bound solution sequence and the lower bound solution sequence, we know that the upper bound solution is continuously decreased and lower bound solution is continuously increased. The global optimal solution is between upper and lower bound, and the distance between upper and lower bound is called gap. Therefore, with the number of branches increased, the gap is deceased gradually, and if the gap is smaller than the predefined error, then the branching is stopped and upper bound solution is the global optimal solution, which is the branch and bound method proceeding in the continuous space.

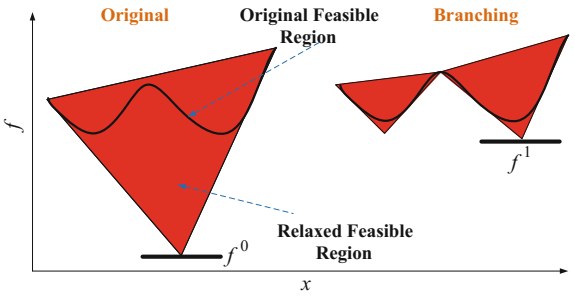

Fig. 2.2 The influence of bounded closed set halved on feasible region

In the kth bounded closet set R^k, the linear relaxation model of (2.49) is formulated as following:

$$\min_{\boldsymbol{w},\boldsymbol{y}} \quad -Z^+ = -\boldsymbol{s} - (\boldsymbol{d}^-)^T\boldsymbol{y}_2 - \boldsymbol{l}^T\boldsymbol{y}_3 - \boldsymbol{u}^T\boldsymbol{y}_4 \tag{2.51}$$

$$set \quad \boldsymbol{A}^T\boldsymbol{y}_1 + \boldsymbol{B}^T\boldsymbol{y}_2 + \boldsymbol{y}_3 + \boldsymbol{y}_4 = \boldsymbol{c} \tag{2.52}$$

$$\boldsymbol{y}_2 \le 0 \quad \boldsymbol{y}_3 \ge 0 \quad \boldsymbol{y}_4 \le 0 \tag{2.53}$$

$$s_i^k \ge l_{y_1,i}^k w_i + l_{w,i}^k y_{1,i} - l_{w,i}^k l_{y_1,i}^k \tag{2.54}$$

$$s_i^k \ge u_{y_1,i}^k w_i + u_{w,i}^k y_{1,i} - u_{w,i}^k u_{y_1,i}^k \tag{2.55}$$

$$s_i^k \le u_{y_1,i}^k w_i + l_{w,i}^k y_{1,i} - l_{w,i}^k u_{y_1,i}^k \tag{2.56}$$

$$s_i^k \le l_{y_1,i}^k w_i + u_{w,i}^k y_{1,i} - u_{w,i}^k l_{y_1,i}^k \tag{2.57}$$

$$R^k = \left\{ \boldsymbol{w}^k, \boldsymbol{y}_1^k \in \mathrm{R}^{N_g \times 1} \middle| l_w^k \le \boldsymbol{w}^k \le u_w^k, l_{y_1}^k \le \boldsymbol{y}_1^k \le u_{y_1}^k \right\} \tag{2.58}$$

The flow chart of spatial branch and bound method is given in Table 2.2. To express conveniently, $\Psi_{\mathrm{lb}}(\Omega)$ denotes the lower bound solution of region Ω obtained by relaxtion model (2.43), and $\Psi_{\mathrm{ub}}(\Omega)$ denotes the upper bound solution obtained by interior point method.

Method Two: *Integral branch and bound method*

Theorem 2.3 [9]: *If the polyhedral feasible region* $\boldsymbol{W}$ *and* $\boldsymbol{Y}$ *are bounded and separable, the optimal solution* $(\boldsymbol{w}^*, \boldsymbol{y}^*)$ *of bi-linear programming with* $\boldsymbol{w} \in \boldsymbol{W}$ *and* $\boldsymbol{y} \in \boldsymbol{Y}$ *is satisfied with* $\boldsymbol{w}^* \in V(\boldsymbol{W})$ *and* $\boldsymbol{y}^* \in V(\boldsymbol{Y})$, *where* $V(\boldsymbol{W})$ *and* $V(\boldsymbol{Y})$ *denotes the vertexes (poles) of polyhedral feasible region* $\boldsymbol{W}$ *and* $\boldsymbol{Y}$, *respectively, then we have*

Table 2.2 The flow chart of spatial branch and bound method

Spatial Branch and Bound Method	
Step 1	$k \leftarrow 0$, initial region Ω_0 and precision ε is given;
Step 2	$L_0 = \mathrm{L_{b.}}(\Omega_0)$, $U_0 = \Psi_{\mathrm{ub}}(\Omega_0)$, List$=\{\Omega_0\}$;
Step 3	**while** $U_k - L_k > \varepsilon$
Step 4	$k = \arg_j(\Psi_{\mathrm{ub}}(\Omega_j) == L_k), \forall\ \Omega_j \in$ List;
Step 5	Halve region Ω_k, and form two new region Ω_{I} and Ω_{II};
Step 6	Remove Ω_k of List, and add Ω_{I} and Ω_{II};
Step 7	$L_{k+1} \leftarrow \min \Psi_{\mathrm{lb}}(\Omega_j)$, $\forall\ \Omega_j \in$ List
Step 8	$U_{k+1} \leftarrow \min \Psi_{\mathrm{ub}}(\Omega_j)$, $\forall\ \Omega_j \in$ List
Step 9	$k \leftarrow k+1$;
Step 10	**end**

$$\max_{\boldsymbol{w}\in\boldsymbol{W}} f(\boldsymbol{w},\boldsymbol{y}^*) = f(\boldsymbol{w}^*,\boldsymbol{y}^*) = \max_{\boldsymbol{y}\in\boldsymbol{Y}} f(\boldsymbol{w}^*,\boldsymbol{y}) \tag{2.59}$$

Proof If the value of fixed vector $\boldsymbol{y}$ is $\boldsymbol{y}^*$, the bilinear programming model is transformed into a linear programming with variable $\boldsymbol{w}$ and its optimal solution $\boldsymbol{w}^*$ must be at the poles of the feasible region of $\boldsymbol{W}$. Similarly, if the value of fixed vector $\boldsymbol{w}$ is $\boldsymbol{w}^*$, then the bilinear programming model is transformed into a linear programming with variable $\boldsymbol{y}$ and its optimal solution $\boldsymbol{y}^*$ must be at the poles of the feasible region of $\boldsymbol{Y}$. It notes that the optimal solution $(\boldsymbol{w}^*, \boldsymbol{y}^*)$ of the bilinear programming model is satisfied with $\boldsymbol{w}^* \in V(\boldsymbol{W})$ and $\boldsymbol{y}^* \in V(\boldsymbol{Y})$, where $V(\boldsymbol{W})$ and $V(\boldsymbol{Y})$ represents the vertexes (poles) of polyhedral feasible region $\boldsymbol{W}$ and $\boldsymbol{Y}$, respectively.

Based on this theorem, for the bilinear programming model of (2.49). The feasible region of uncertainties is a boxed polyhedron feasible region, so the optimal solution must be achieved at the interval upper or lower bounds of the uncertainties. Therefore, "or" constraint can be used to express. Furthermore, with a dummy integer variable z, "or" constraint can be transformed into a mixed integer linear programming model, such that

$$\begin{array}{l} w_i = b_i^- \quad or \quad w_i = b_i^+ \\ for \quad \forall i = 1,\ldots,s \end{array} \quad \Leftrightarrow \quad w_i = \underline{b_i} + z_i\left(\overline{b}_i - \underline{b_i}\right), z_i \in \{0,1\}, \quad \forall i = 1,\ldots,s \tag{2.60}$$

Furthermore, the pessimistic model of (2.49) can be transformed into

$$\text{(Pessimistic value)} \quad \begin{array}{ll} \max\limits_{\boldsymbol{y}_1,\boldsymbol{y}_2,\boldsymbol{y}_3,\boldsymbol{y}_4,\boldsymbol{w}} & Z^+ = (\boldsymbol{d}^-)^T\boldsymbol{y}_1 + \boldsymbol{w}^T\boldsymbol{y}_2 + \boldsymbol{L}^T\boldsymbol{y}_3 + \boldsymbol{U}^T\boldsymbol{y}_4 \\ s.t. & \boldsymbol{E}^T\boldsymbol{y}_1 + \boldsymbol{A}^T\boldsymbol{y}_2 + \boldsymbol{y}_3 + \boldsymbol{y}_4 = \boldsymbol{c} \\ & \boldsymbol{y}_1 \le 0 \quad -\infty < \boldsymbol{y}_2 < +\infty \quad \boldsymbol{y}_3 \ge 0 \quad \boldsymbol{y}_4 \le 0 \\ & w_i = b_i^- + z_i\left(b_i^+ - b_i^-\right), \quad z_i \in \{0,1\} \end{array} \tag{2.61}$$

We can know that, the model (2.61) is a mixed integer bilinear programming. Fortunately, based on big M theory, the product zy_2 of integer variable and continuous variable can be introduced some dummy variables, and the model is simplified as a simple dummy integer variable as following:

$$\text{(Pessimistic value)} \quad \begin{array}{ll} \max\limits_{\boldsymbol{y}_1,\boldsymbol{y}_2,\boldsymbol{y}_3,\boldsymbol{y}_4,\boldsymbol{w}} & Z^+ = (\boldsymbol{d}^-)^T\boldsymbol{y}_1 + \sum\limits_{i=1}^{s}\left(y_{2,i}b_i^- + x_i\left(b_i^+ - b_i^-\right)\right) + \boldsymbol{L}^T\boldsymbol{y}_3 + \boldsymbol{U}^T\boldsymbol{y}_4 \\ s.t. & \boldsymbol{E}^T\boldsymbol{y}_1 + \boldsymbol{A}^T\boldsymbol{y}_2 + \boldsymbol{y}_3 + \boldsymbol{y}_4 = \boldsymbol{c} \\ & \boldsymbol{y}_1 \le 0 \quad -\infty < \boldsymbol{y}_2 < +\infty \quad \boldsymbol{y}_3 \ge 0 \quad \boldsymbol{y}_4 \le 0, \quad z_i \in \{0,1\} \\ & y_{2,i} - M(1-z_i) \le x_i \le y_{2,i} + M(1-z_i), \quad -Mz_i \le x_i \le Mz_i \end{array} \tag{2.62}$$

where M is a sufficient large number. We can know that if $z_i = 0$, x_i is 0, and the value of $w_i y_{2i}$ is $y_{2,i} b_i^-$; if $z_i = 1$, x_i is $y_{2,I}$, and the value of $w_i y_{2i}$ is $y_{2,i} b_i^+$.

The general solution of mixed integer programming is to relax integer variables into continuous variables, branch and bound next, and stop searching when the upper bound and lower bound are almost equal. Because the optimal solution of (2.49) is solution of the dual problem of model (2.40)–(2.44), the optimal solution of original model (2.40)–(2.44) can be solved by complementary relaxation condition. Another method is to obtain the optimal solution $\boldsymbol{w}^p$ of uncertainties based on (2.62), then fix and bring it into model (2.49). Due to uncertainties defined, the model can be transformed into:

(Pessimistic value)

$$\min_{\boldsymbol{x}} \quad Z^+ = \boldsymbol{c}^T \boldsymbol{x} \tag{2.63}$$

$$\text{s.t.} \quad \boldsymbol{A}\boldsymbol{x} = \boldsymbol{w}^p \tag{2.64}$$

$$\boldsymbol{B}\boldsymbol{x} \le \boldsymbol{d}^- \tag{2.65}$$

$$\boldsymbol{l} \le \boldsymbol{x} \le \boldsymbol{u} \tag{2.66}$$

It is necessary to know that optimistic value and pessimistic value of interval optimization model are obtained according to (2.45)–(2.48) and (2.63)–(2.66), respectively, and the optimal interval of objective function is $[Z^l, Z^u]$. Interval optimization mainly focus on the interval upper and lower bound information of objective function, so the optimal solution $\boldsymbol{x}^{opt}$ and $\boldsymbol{x}^{opt}$ of interval independent variables reflect the objective change from the optimistic value to the pessimistic value, which can not define interval range of optimal independent variables strictly. To obtain interval of optimal independent variables, a bi-level optimization model can be formulated as:

$$\begin{aligned} x_i^{\pm} = \max_{\boldsymbol{x},\boldsymbol{w},\boldsymbol{d}} / \min_{\boldsymbol{x},\boldsymbol{w},\boldsymbol{d}} \quad & x_i \\ s.t. \quad & x_i^{\min} \le x_i \le x_i^{\max} \\ & \boldsymbol{w}^- \le \boldsymbol{w} \le \boldsymbol{w}^+ \\ & \boldsymbol{d}^- \le \boldsymbol{d} \le \boldsymbol{d}^+, \quad i = 1, \ldots, n \\ & x_i = \arg\min_{\boldsymbol{x}} \boldsymbol{c}^T \boldsymbol{x} \\ s.t. \quad & \boldsymbol{A}\boldsymbol{x} = \boldsymbol{w} \\ & \boldsymbol{B}\boldsymbol{x} \le \boldsymbol{d} \end{aligned} \tag{2.67}$$

The combinatorial nature of bi-level programming can be observed by studying the single-level reformulation obtained by replacing the inner level problem with its KKT (Karush-Kuhn-Tucker) condition, which is a necessary and sufficient optimality conditions when the inner optimization model is actually a convex problem.

However, KKT condition is a set of nonlinear and non-convex equations; therefore, though KKT condition is used, ti is hard to guarantee the global optimality of programming. Then we consider to transform the KKT condition into an expression of mixed integer, and by introducing some dummy variables, nonlinear and non-convex equations can be replaced by non-convex equations of mixed integer linear programming, which is easier to solve. Furthermore, combined big M theory, the general complementarity slackness constraints can be exactly linearized with dummy integer variables z, such that (2.68) is equivalently transformed as (2.69).

$$\begin{gathered} \boldsymbol{Ax} = \boldsymbol{w} \\ \boldsymbol{Bx} \le \boldsymbol{d} \\ \boldsymbol{c} + \boldsymbol{A}^T\boldsymbol{\mu} + \boldsymbol{B}^T\boldsymbol{\lambda} = \boldsymbol{0} \\ (\boldsymbol{Bx} - \boldsymbol{d}) \cdot * \boldsymbol{\lambda} = \boldsymbol{0} \\ \boldsymbol{\lambda} \ge 0 \end{gathered} \tag{2.68}$$

$$\begin{gathered} \boldsymbol{Ax} = \boldsymbol{w} \\ \boldsymbol{c} + \boldsymbol{A}^T\boldsymbol{\mu} + \boldsymbol{B}^T\boldsymbol{\lambda} = \boldsymbol{0} \\ -M(1 - \boldsymbol{z}) \le (\boldsymbol{Bx} - \boldsymbol{d}) \le \boldsymbol{0} \\ M\boldsymbol{z} \ge \boldsymbol{\lambda} \ge 0, \boldsymbol{z} \in \{\boldsymbol{0}, \boldsymbol{1}\} \end{gathered} \tag{2.69}$$

Furthermore, the model (2.67) is transformed into

$$x_i^{\pm} = \max_{\boldsymbol{x}} / \min_{\boldsymbol{x}} \quad x_i \quad s.t. \quad \begin{gathered} x_i^{\min} \le x_i \le x_i^{\max} \\ \boldsymbol{w}^- \le \boldsymbol{w} \le \boldsymbol{w}^+ \\ \boldsymbol{d}^- \le \boldsymbol{d} \le \boldsymbol{d}^+ \\ \boldsymbol{Ax} = \boldsymbol{w} \\ \boldsymbol{c} + \boldsymbol{A}^T\boldsymbol{\mu} + \boldsymbol{B}^T\boldsymbol{\lambda} = \boldsymbol{0} \\ -M(1 - \boldsymbol{z}) \le \boldsymbol{Bx} - \boldsymbol{d} \le \boldsymbol{0} \\ M\boldsymbol{z} \ge \boldsymbol{\lambda} \ge 0, \quad \boldsymbol{z} \in \{0, 1\} \end{gathered}, \quad i = 1, \ldots, n \tag{2.70}$$

Moreover, the mixed integer linear programming can be solved by branch and bound method to obtain upper and lower bound of optimal solution as well as its interval $\left[x_i^-, x_i^+\right]$.

However, when conducting interval optimization, it is necessary to consider such a problem that whether the objective function and optimal solution are continuous functions of uncertainties or not. In other words, when the uncertainties are changed in the range of interval, the objective function and the optimal solution are also changed in a certain range, but whether they are filled with the entire range of interval. Next, we will prove that if the objective function and optimal solution are continuous functions of uncertainties, then they can be filled with the entire range of interval.

Mathematically, linear programming (2.28)–(2.30) can be formulated as

$$\min_{\boldsymbol{x}\in\mathrm{R}^n} \quad \boldsymbol{q}^T\boldsymbol{x}+r \tag{2.71}$$

$$s.t. \quad \boldsymbol{B}_{eq}\boldsymbol{x}=\boldsymbol{g}_{eq}+\boldsymbol{F}_{eq}\boldsymbol{\theta} \tag{2.72}$$

$$\boldsymbol{B}_{ieq}\boldsymbol{x}\le\boldsymbol{g}_{ieq}+\boldsymbol{F}_{ieq}\boldsymbol{\theta} \tag{2.73}$$

$$\boldsymbol{\theta}\in\left[\boldsymbol{\theta}^-,\boldsymbol{\theta}^+\right] \tag{2.74}$$

where $\boldsymbol{x}$ is an $n\times 1$ vector; $\boldsymbol{\theta}$ is an $t\times 1$ parametric vector with its upper bound $\boldsymbol{\theta}^+$ and lower bound $\boldsymbol{\theta}^-$, respectively; $\boldsymbol{Q}$ is an $n\times n$ positive definite matrix; $\boldsymbol{q}$ is an $n\times 1$ vector; $\boldsymbol{B}_{eq}$ is an $m\times n$ coefficient matrix; m is the number of equality constraints; $\boldsymbol{g}_{eq}$ is an $m\times 1$ constant vector; $\boldsymbol{F}_{eq}$ is an $m\times t$ coefficient matrix; $\boldsymbol{B}_{ieq}$ is an $l\times n$ coefficient matrix; l is the number of inequality constraints; $\boldsymbol{g}_{ieq}$ is an $l\times 1$ constant vector; $\boldsymbol{F}_{ieq}$ is an $l\times t$ coefficient matrix.

The KKT conditions of model (2.71)–(2.74) are formulated as

$$\boldsymbol{B}_{eq}^T\boldsymbol{\pi}+\boldsymbol{B}_{ieq}^T\boldsymbol{\mu}+\boldsymbol{q}=\boldsymbol{0} \tag{2.75}$$

$$\boldsymbol{B}_{eq}\boldsymbol{x}-\boldsymbol{g}_{eq}-\boldsymbol{F}_{eq}\boldsymbol{\theta}=\boldsymbol{0} \tag{2.76}$$

$$\boldsymbol{B}_{ieq}\boldsymbol{x}-\boldsymbol{g}_{ieq}-\boldsymbol{F}_{ieq}\boldsymbol{\theta}\le\boldsymbol{0} \tag{2.77}$$

$$\mu^i\left(B_{ieq}^i\boldsymbol{x}-g^i+F^i\boldsymbol{\theta}\right)=0 \tag{2.78}$$

$$\boldsymbol{\pi}\ge\boldsymbol{0} \tag{2.79}$$

Definition: For each constraint of (2.75), we define the ith constraint to be an active constraint with $B_{ieq}^i\boldsymbol{x}-g^i+F^i\boldsymbol{\theta}=0$, and inactive constraint with $B_{ieq}^i\boldsymbol{x}-g^i+F^i\boldsymbol{\theta}<0$. Furthermore, the optimal active set $\mathcal{A}$ is defined as the set of indices of active constraints at the optimum, such that $\mathcal{A}=\left\{i\middle|B_{ieq}^i\boldsymbol{x}-g^i+F^i\boldsymbol{\theta}=0\right\}$ and the optimal inactive set $\mathcal{I}$ is defined as the set of indices of active constraints at the optimum, such that $\mathcal{I}=\left\{i\middle|B_{ieq}^i\boldsymbol{x}-g^i+F^i\boldsymbol{\theta}<0\right\}$.

For the active set $\mathcal{A}$, we have (2.80) and the corresponding Lagrange multipliers are $\boldsymbol{\mu}^{\mathcal{A}}\ge\boldsymbol{0}$.

$$\boldsymbol{B}_{ieq}^{\mathcal{A}}\boldsymbol{x}-\boldsymbol{g}_{ieq}^{\mathcal{A}}-\boldsymbol{F}_{ieq}^{\mathcal{A}}\boldsymbol{\theta}=\boldsymbol{0} \tag{2.80}$$

For the inactive set $\mathcal{I}$, we have (2.81) and the corresponding Lagrange multipliers are $\boldsymbol{\mu}^{\mathcal{I}}=\boldsymbol{0}$.

$$\boldsymbol{B}_{ieq}^{\mathcal{I}}\boldsymbol{x}-\boldsymbol{g}_{ieq}^{\mathcal{I}}-\boldsymbol{F}_{ieq}^{\mathcal{I}}\boldsymbol{\theta}<\boldsymbol{0} \tag{2.81}$$

Furthermore, we assume the original linear optimization model is feasible and the constraints are satisfied, such that $\begin{pmatrix}\boldsymbol{B}_{eq}\\ \boldsymbol{B}_{ieq}^{\mathcal{A}}\end{pmatrix}$ has full row rank. According to (2.76) and (2.80), we have

$$\begin{pmatrix}\boldsymbol{B}_{eq}\\ \boldsymbol{B}_{ieq}^{\mathcal{A}}\end{pmatrix}\boldsymbol{x}=\begin{pmatrix}\boldsymbol{g}_{eq}\\ \boldsymbol{g}_{ieq}^{\mathcal{A}}\end{pmatrix}+\begin{pmatrix}\boldsymbol{F}_{eq}\\ \boldsymbol{F}_{ieq}^{\mathcal{A}}\end{pmatrix}\boldsymbol{\theta} \tag{2.82}$$

Then $\boldsymbol{x}$ yields

$$\boldsymbol{x}=\begin{pmatrix}\boldsymbol{B}_{eq}\\ \boldsymbol{B}_{ieq}^{\mathcal{A}}\end{pmatrix}^{-1}\begin{pmatrix}\boldsymbol{g}_{eq}\\ \boldsymbol{g}_{ieq}^{\mathcal{A}}\end{pmatrix}+\begin{pmatrix}\boldsymbol{B}_{eq}\\ \boldsymbol{B}_{ieq}^{\mathcal{A}}\end{pmatrix}^{-1}\begin{pmatrix}\boldsymbol{F}_{eq}\\ \boldsymbol{F}_{ieq}^{\mathcal{A}}\end{pmatrix}\boldsymbol{\theta} \tag{2.83}$$

From (2.83), we can find that the active set $\mathcal{A}$ changes with parameter $\boldsymbol{\theta}$. Furthermore, the optimal solution $\boldsymbol{x}$ is a piecewise linear function. According to KKT conditions, because the model is a convex programming, the optimal solution of (2.75)–(2.79) obtained by KKT conditions is the global optimal solution of linear programming (2.71)–(2.74) sufficiently and necessarily, and the optimal solution is unique. Therefore, the optimal solution $\boldsymbol{x}$ is a piecewise linear continuous function, which further illustrates the optimal solution is the continuous function of uncertainties and they must be able to fill the entire interval range. Take the optimal solution $\boldsymbol{x}$ into the objective function of (2.71), we can know the objective function is a piecewise linear continuous function about $\boldsymbol{\theta}$, which can also fill the entire interval range.

2.3.2 *Traditional Interval Robust Optimization Method*

Firstly, a traditional robust optimization model is formulated as

$$\min_{\boldsymbol{x}} \quad \boldsymbol{a}^T\boldsymbol{x} \tag{2.84}$$

$$s.t. \quad \boldsymbol{b}\leq\boldsymbol{A}\boldsymbol{x}+\boldsymbol{B}\boldsymbol{u}\leq\boldsymbol{d} \tag{2.85}$$

$$\boldsymbol{x}\in\Omega_{\boldsymbol{x}} \tag{2.86}$$

$$\forall\boldsymbol{u}\in\Omega_{\boldsymbol{u}} \tag{2.87}$$

where $\Omega_{\boldsymbol{u}}$ denotes the set of uncertainties, if it is an interval number, such as $\Omega_{\boldsymbol{u}}=\{\boldsymbol{u}|\boldsymbol{u}^-\leq\boldsymbol{u}\leq\boldsymbol{u}^+\}$, the model is called a traditional interval robust

optimization model. The objective of model is to search an optimal $\boldsymbol{x}$, and satisfy constraint (2.85) with any change of uncertainty $\boldsymbol{u}$. The model (2.84)–(2.87) can be transformed into a bi-level programming model as following:

$$\min_{\boldsymbol{x}} \max_{\boldsymbol{u}\in\Omega_u} \quad \boldsymbol{a}^T\boldsymbol{x} \tag{2.88}$$

$$s.t. \quad \boldsymbol{b} \le \boldsymbol{A}\boldsymbol{x} + \boldsymbol{B}\boldsymbol{u} \le \boldsymbol{d} \tag{2.89}$$

$$\boldsymbol{x} \in \Omega_{\boldsymbol{x}} \tag{2.90}$$

Because the objective function is not related to $\boldsymbol{u}$, then (2.88)–(2.90) is equivalent to:

$$\min_{\boldsymbol{x}} \quad \boldsymbol{a}^T\boldsymbol{x} \tag{2.91}$$

$$s.t.\ \boldsymbol{A}\boldsymbol{x} + \max_{\boldsymbol{u}\in\Omega_u}(\boldsymbol{B}\boldsymbol{u}) \le \boldsymbol{d} \tag{2.92}$$

$$\boldsymbol{A}\boldsymbol{x} + \min_{\boldsymbol{u}\in\Omega_u}(\boldsymbol{B}\boldsymbol{u}) \ge \boldsymbol{b} \tag{2.93}$$

$$\boldsymbol{x} \in \Omega_{\boldsymbol{x}} \tag{2.94}$$

Considering the interval form of uncertainties in model (2.92) and (2.93), $\max_{\boldsymbol{u}\in\Omega_u}(\boldsymbol{B}\boldsymbol{u}) = \boldsymbol{B}^+\boldsymbol{u}^+ + \boldsymbol{B}^-\boldsymbol{u}^-$, $\min_{\boldsymbol{u}\in\Omega_u}(\boldsymbol{B}\boldsymbol{u}) = \boldsymbol{B}^+\boldsymbol{u}^- + \boldsymbol{B}^-\boldsymbol{u}^+$, where $\boldsymbol{B}^+ = \max(\boldsymbol{B}, \boldsymbol{0})$, such that $\boldsymbol{B}^+$ is the positive elements of $\boldsymbol{B}$, and $\boldsymbol{B}^- = \min(\boldsymbol{B}, \boldsymbol{0})$, such that $\boldsymbol{B}^-$ is the negative elements of $\boldsymbol{B}$. Furthermore, (2.91)–(2.94) is translated into a bi-level optimization model:

$$\min_{\boldsymbol{x}} \quad \boldsymbol{a}^T\boldsymbol{x} \tag{2.95}$$

$$s.t.\ \boldsymbol{A}\boldsymbol{x} + \max(\boldsymbol{B}, \boldsymbol{0})\boldsymbol{u}^+ + \min(\boldsymbol{B}, \boldsymbol{0})\boldsymbol{u}^- \le \boldsymbol{d} \tag{2.96}$$

$$\boldsymbol{A}\boldsymbol{x} + \max(\boldsymbol{B}, \boldsymbol{0})\boldsymbol{u}^- + \min(\boldsymbol{B}, \boldsymbol{0})\boldsymbol{u}^+ \ge \boldsymbol{b} \tag{2.97}$$

$$\boldsymbol{x} \in \Omega_{\boldsymbol{x}} \tag{2.98}$$

It notes that an important characteristic of the model is no equality constraints, because traditional robust optimization model requires that constraints can not be violated with any change of uncertainty $\boldsymbol{u}$. if equality constraints are existed, they must be violated and robust optimal solution can be obtained. On the other hand, from model (2.88)–(2.90),we find that the transformation result is the same as the pessimistic value of interval optimization without equality constraints. It illustrates that although pessimism value has some sacrifices of objective, it can ensure all constraints are satisfied with any change of uncertainties.

An simple example:

$$\min_{x_1+x_2} \quad 0.1x_1 + 0.2x_2 \quad s.t \begin{cases} 0 \le 2x_1 + x_2 + u \le 6 \\ 0 \le x_1 \le 3 \\ 0 \le x_2 \le 3 \end{cases}, \quad \forall u \in [-1, +1]$$

The objective of the optimization model is to obtain an optimal solution (x_1^*, x_2^*), which can ensure all constraints satisfied for any given $u \in [-1 + 1]$. The model is equivalent to:

$$\min_{x_1^* x_2^*} \quad 0.1x_1^* + 0.2x_2^* \quad s.t. \begin{cases} \max\limits_{-1 \le u \le +1}(-u) \le 2x_1^* + x_2^* \le \min\limits_{-1 \le u \le +1}(6-u) \\ 0 \le x_1^* \le 3 \\ 0 \le x_2^* \le 3 \end{cases}, \text{furthermore, simplified as}$$

$$\min_{x_1^* x_2^*} \quad 0.1x_1^* + 0.2x_2^* \quad s.t. \begin{cases} 1 \le 2x_1^* + x_2^* \le 5 \\ 0 \le x_1^* \le 3 \\ 0 \le x_2^* \le 3. \end{cases}$$

2.3.3 Adaptive Interval Robust Optimization Method

In traditional interval robust optimization model, equality constraints can not be considered because the model need to obtain an optimal solution $\boldsymbol{x}$ which can satisfy all constraints with any change of uncertainty $\boldsymbol{u}$; therefore, equality constraints are not always satisfied. On the other hand, traditional interval robust optimization requires that optimal variable $\boldsymbol{x}$ is not related to uncertainty $\boldsymbol{u}$. If equality constraints are existed, we can obtain an optimal variable $\boldsymbol{x}$ irrelevant to $\boldsymbol{u}$.

However, considering that the independent variable $\boldsymbol{x}$ in the model can follow the change of uncertainty $\boldsymbol{u}$, such that $\widetilde{\boldsymbol{x}}(\boldsymbol{x},\boldsymbol{u})$, then the optimal $\boldsymbol{x}$ can be solved only if the adjusted variable $\widetilde{\boldsymbol{x}}(\boldsymbol{x},\boldsymbol{u})$ can guarantee that all constraints are not violated with any given uncertainty $\boldsymbol{u}$. In such situation, after the change of uncertainty $\boldsymbol{u}$, the equality constraint can be satisfied because the independent variable $\boldsymbol{x}$ is changed accordingly. Such model is called adaptive robust optimization model shown following:

$$\min_{\boldsymbol{x}} \quad \boldsymbol{a}^T\boldsymbol{x} \tag{2.99}$$

$$s.t.\ \boldsymbol{A}\widetilde{\boldsymbol{x}}(\boldsymbol{x},\boldsymbol{u}) + \boldsymbol{B}\boldsymbol{u} = \boldsymbol{w} \tag{2.100}$$

$$\boldsymbol{b} \le \boldsymbol{C}\widetilde{\boldsymbol{x}}(\boldsymbol{x},\boldsymbol{u}) + \boldsymbol{D}\boldsymbol{u} \le \boldsymbol{d} \tag{2.101}$$

$$\boldsymbol{x} \in \Omega_{\boldsymbol{x}} \tag{2.102}$$

$$\forall \boldsymbol{u} \in \Omega_{\boldsymbol{u}} \tag{2.103}$$

Similarly, if the set of uncertainties is an interval form, the model is called an adaptive interval robust optimization model which has challenge to be solved. Generally, the equality constraints should be analyzed and $\widetilde{\boldsymbol{x}}(\boldsymbol{x},\boldsymbol{u})$ related to uncertainty is strictly expressed, according to the physically practical problems or the structural characteristics of the model. If $\boldsymbol{u}^0$ is the given value of the uncertainty, satisfied with $\boldsymbol{A}\boldsymbol{x}+\boldsymbol{B}\boldsymbol{u}^0=\boldsymbol{w}$, then consider $\widetilde{\boldsymbol{x}}(\boldsymbol{x},\boldsymbol{u})=\boldsymbol{x}+\boldsymbol{L}(\boldsymbol{u}^0-\boldsymbol{u})$, and satisfy $\boldsymbol{A}\boldsymbol{L}(\boldsymbol{u}^0-\boldsymbol{u})=\boldsymbol{B}(\boldsymbol{u}^0-\boldsymbol{u})$. It illustrates that when the uncertainty is deviated from $\boldsymbol{u}^{\boldsymbol{0}}$, the independent variable $\widetilde{\boldsymbol{x}}(\boldsymbol{x},\boldsymbol{u})$ can be adjusted accordingly to guarantee the equality constraints, where $\boldsymbol{L}$ is usually a linear function called the affine expansion of uncertainty $\boldsymbol{u}$. Nevertheless, if $\boldsymbol{L}$ is given, with any change of $\boldsymbol{u}$ in the $\Omega_{\boldsymbol{u}}$, we should guarantee that $\widetilde{\boldsymbol{x}}(\boldsymbol{x},\boldsymbol{u})$ can always satisfy equality constraints as well as inequality constraints. Furthermore, the adaptive robust optimization model can be transformed into traditional robust optimization model as following:

$$\min_{\boldsymbol{x}} \quad \boldsymbol{a}^T\boldsymbol{x} \tag{2.104}$$

$$s.t.\ \boldsymbol{A}\boldsymbol{x}+\boldsymbol{B}\boldsymbol{u}^0=\boldsymbol{w} \tag{2.105}$$

$$\boldsymbol{b} \le \boldsymbol{C}\boldsymbol{x}+\left(\boldsymbol{C}\boldsymbol{L}\left(\boldsymbol{u}^0-\boldsymbol{u}\right)+\boldsymbol{D}\boldsymbol{u}\right) \le \boldsymbol{d} \tag{2.106}$$

$$\boldsymbol{x} \in \Omega_{\boldsymbol{x}} \tag{2.107}$$

$$\forall \boldsymbol{u} \in \Omega_{\boldsymbol{u}} \tag{2.108}$$

We should know that the biggest challenge of adaptive robust optimization model is how to find the strict expression of $\widetilde{\boldsymbol{x}}(\boldsymbol{x},\boldsymbol{u})$ about uncertainty, such that. If it can be obtained, then the problem is easily solved.

A simple example:

$$\min_{x_1,x_2} \quad 0.1x_1+0.2x_2 \quad s.t \begin{cases} x_1+x_2+u=4 \\ 0 \le 2x_1+x_2+u \le 6 \\ 0 \le x_1 \le 3 \\ 0 \le x_2 \le 3 \end{cases}, \quad \forall u \in [-1,+1]$$

The objective of the optimization model is also to obtain an optimal solution (x_1^*, x_2^*), which can ensure all constraints satisfied for any given $u \in [-1\ +\ 1]$. However, due to equality constraints, constraints are not always satisfied; therefore, the traditional robust optimization model can not be obtained. Considering the change of uncertainties, x_1 and x_2 is changed accordingly, such that $\begin{cases} x_1=x_1^*+L_1(u^0-u) \\ x_2=x_2^*+L_2(u^0-u) \end{cases}$.

Considering the linear expansion of L_1 and L_2, such as $\begin{cases} x_1 = x_1^* + 0.2(u^0 - u) \\ x_2 = x_2^* + 0.8(u^0 - u) \end{cases}$, then we find $x_1 + x_2 + u = x_1^* + x_2^* + u^0$. Therefore, no matter how uncertainty u changes, as long as $x_1^* + x_2^* + u^0$ is satisfied, equality constraints will be always satisfied with the linear adjustment of x_1 and x_2. To guarantee inequality constraints satisfied, we have $\min\limits_{x_1^*, x_2^*} \quad 0.1x_1^* + 0.2x_2^*$ *s.t.* $\begin{cases} x_1^* + x_2^* + u^0 = 4 \\ 0 \le 2\left(x_1^* + 0.2(u^0 - u)\right) + x_2^* + 0.8(u^0 - u) + u \le 6 \\ 0 \le x_1^* \le 3 \\ 0 \le x_1^* \le 3 \end{cases}$, $\forall u \in [-1, +1]$ it can be further simplified as $\min\limits_{x_1^*, x_2^*} \quad 0.1x_1^* + 0.2x_2^*$ *s.t.* $\begin{cases} x_1^* + x_2^* + u^0 = 4 \\ 0 \le 2x_1^* + x_2^* + 1.2u^0 - 0.2u \le 6 \\ 0 \le x_1^* \le 3 \\ 0 \le x_1^* \le 3 \end{cases}$, $\forall u \in [-1, +1]$. We can know that the model is the same as traditional robust optimization and uncertainty is only existed in the inequality constrain, so it can be transformed into $\min\limits_{x_1^*, x_2^*} \quad 0.1x_1^* + 0.2x_2^*$ *s.t.* $\begin{cases} x_1^* + x_2^* + u^0 = 4 \\ 0.2 \le 2x_1^* + x_2^* + 1.2u^0 \le 5.8 \\ 0 \le x_1^* \le 3 \\ 0 \le x_1^* \le 3 \end{cases}$. Generally, u^0 is considered as the desired value of u, for example $u^0 = 0$, and the model is formulated as $\min\limits_{x_1^*, x_2^*} \quad 0.1x_1^* + 0.2x_2^*$ *s.t.* $\begin{cases} x_1^* + x_2^* = 4 \\ 0.2 \le 2x_1^* + x_2^* \le 5.8 \\ 0 \le x_1^* \le 3 \\ 0 \le x_1^* \le 3 \end{cases}$. It notes that L_1, L_2 and u^0 of the model should be determined based on the actual situation, and the different choices of L_1, L_2 and u^0 lead to different optimal results.

2.3.4 Two-Stage Interval Robust Optimization Method

Generally, a two-stage robust optimization model can be formulated as

$$\min_{\boldsymbol{y} \in \Omega_y} \boldsymbol{c}^T \boldsymbol{y} + \max_{\boldsymbol{u} \in \Omega_u} \min_{\boldsymbol{x} \in \Omega_x} \boldsymbol{a}^T \boldsymbol{x} \tag{2.109}$$

where Ω_y and Ω_u are both bounded convex sets and $\Omega_x = \{\boldsymbol{x} | \boldsymbol{A}\boldsymbol{x} \ge \boldsymbol{d} - \boldsymbol{B}\boldsymbol{y} - \boldsymbol{C}\boldsymbol{u}\}$. If uncertainty set is an interval number, then the model is call two-stage interval robust optimization model.

The objective of two-stage robust optimization is to obtain optimal variable $\boldsymbol{y}$ in the first stage and optimal variable $\boldsymbol{x}^*$ in the second stage. Actually, $\boldsymbol{x}^*$ is a function of uncertainty $\boldsymbol{u}$, such that $\boldsymbol{x}^*(\boldsymbol{u})$, so the optimal variable and objective function are changed accordingly with the uncertainties. Robust optimization is to choose $\boldsymbol{u}$ which can obtain the best $\boldsymbol{y}$ when $\boldsymbol{x}^*(\boldsymbol{u})$ achieves the worst case. If the uncertainty

set is modeled with intervals, the two-stage robust optimization model based intervals is formed.

The first-stage variable of the two-stage interval robust optimization model is generally discrete variable, and the second-stage variable is continuous variable. Therefore, the two-stage interval robust optimization model is a large-scale combinatorial optimization problem which can be solved by decomposition algorithms, where Benders decomposition method is an effective method and is widely used [10–13]. For Benders decomposition method, the original problem is decomposed into master problem and subproblem, by solving each subproblem, generating Benders cut and adding it to the master problem, and the master problem is solved to get a better objective function, through several iterations, then the optimal solution is obtained. In the flow chart of Benders, the most important step is to form Benders cut, and different cut generation methods have different computational complexity. Two kinds of Benders cut generation methods are presented.

The inner level of "max-min" is the same as pessimistic model of interval optimization, so the corresponding method can be used, which is to solve the duality of "min" model in the "max-min". The dual model is

$$(\mathrm{SP}) \quad \Theta(\boldsymbol{y}) = \max_{\boldsymbol{u},\pi} \quad \pi^T (\boldsymbol{d} - \boldsymbol{B}\boldsymbol{y} - \boldsymbol{C}\boldsymbol{u}) \tag{2.110}$$

$$s.t. \quad \boldsymbol{A}^T \boldsymbol{\pi} \leq \boldsymbol{a}^T \tag{2.111}$$

$$\boldsymbol{u} \in \Omega_{\boldsymbol{u}}, , \quad \boldsymbol{\pi} \geq \boldsymbol{0} \tag{2.112}$$

It shows that (SP) is the subproblem of Benders which is an iterative algorithm. In the kth iteration, for a given $\boldsymbol{y}_k^*$, the subproblem $\Theta(\boldsymbol{y}_k^*)$ can be solve to obtain the optimal solution $(\boldsymbol{u}_k^*, \boldsymbol{\pi}_k^*)$. Then two kinds of cuts are designed for iterations.

A. Benders decomposition method based on dual cut

By solving subproblem SP, the dual information $\boldsymbol{\pi}_k^*$ of inner problem is obtained. Based on weak duality theorem, the dual problem of the linear programming model must be a lower bound of the original problem, so the dual cut is

$$\eta \geq (\boldsymbol{\pi}_k^*)^T (\boldsymbol{d} - \boldsymbol{B}\boldsymbol{y} - \boldsymbol{C}\boldsymbol{u}_k^*) \tag{2.113}$$

Add the dual cut (2.113) to Benders main problem, we have

$$(\mathrm{MP1}) \quad \min_{\boldsymbol{y},\eta} \quad \boldsymbol{c}^T \boldsymbol{y} + \eta \tag{2.114}$$

$$s.t. \quad \eta \geq (\boldsymbol{\pi}_l^*)^T (\boldsymbol{d} - \boldsymbol{B}\boldsymbol{y} - \boldsymbol{C}\boldsymbol{u}_l^*), \quad l = 1, 2, \ldots, k \tag{2.115}$$

$$\boldsymbol{y} \in \Omega_{\boldsymbol{y}} \tag{2.116}$$

We can see the main problem is a simple mixed integer programming model, which can be solved by branch and bound method, and $\left(\boldsymbol{y}_{k+1}^{*}, \eta_{k+1}^{*}\right)$ denotes to the optimal solution. The objective functions $\boldsymbol{c}^{T}\boldsymbol{y}_{k}^{*} + \Theta\left(\boldsymbol{y}_{k}^{*}\right)$ and $\boldsymbol{c}^{T}\boldsymbol{y}_{k+1}^{*} + \eta_{k+1}^{*}$ of MP1 give the upper and lower bound of original optimization model, respectively. By continuous iterations, subproblem increases optimal cuts gradually and the upper bound and lower bound are finally reaching consistently, so the algorithm converges to the global optimal solution.

B. Benders decomposition method based on original cut

The inner-level "max-min" model of original three-level optimization problem is transformed into a max bilinear programming with duality. The specific structure of bilinear programming discussed in the interval optimization is that the bilinear variable $(\boldsymbol{u}, \boldsymbol{\pi})$ can be separable, which illustrates that the global optimal solution must be achieved at the vertices (or poles) of the defined feasible region $\boldsymbol{u}$ and $\boldsymbol{\pi}$. The optimal solution $\left(\boldsymbol{u}_{k}^{*}, \boldsymbol{\pi}_{k}^{*}\right)$ obtained in kth the iteration is only an optimal solution with the given $\boldsymbol{y}_{k}$, so an original cut is designed as

$$\boldsymbol{A}\boldsymbol{x}^{l} \geq \boldsymbol{d} - \boldsymbol{B}\boldsymbol{y} - \boldsymbol{C}\boldsymbol{u}_{l}^{*}, \quad \eta \geq \boldsymbol{a}^{T}\boldsymbol{x}^{l} \tag{2.117}$$

Add the original cut (2.117) to Benders main problem, we have

$$(\text{MP2}) \quad \min_{\boldsymbol{y},\eta,\boldsymbol{x}^{l}} \quad \boldsymbol{c}^{T}\boldsymbol{y} + \eta \tag{2.118}$$

$$s.t. \quad \eta \geq \boldsymbol{a}^{T}\boldsymbol{x}^{l}, \quad \boldsymbol{A}\boldsymbol{x}^{l} + \boldsymbol{B}\boldsymbol{y} \geq \boldsymbol{d} - \boldsymbol{C}\boldsymbol{u}_{l}^{*}, \quad l = 1, 2, \ldots, k \tag{2.119}$$

$$\boldsymbol{y} \in \Omega_{\boldsymbol{y}} \tag{2.120}$$

We can see the main problem is a simple mixed integer programming model, which can be solved by branch and bound method, and denotes to the optimal solution. Similarly, the objective functions $\boldsymbol{c}^{T}\boldsymbol{y}_{k}^{*} + \Theta\left(\boldsymbol{y}_{k}^{*}\right)$ and $\boldsymbol{c}^{T}\boldsymbol{y}_{k+1}^{*} + \eta_{k+1}^{*}$ of MP2 give the upper and lower bound of original optimization model, respectively. By continuous iterations, subproblem increases optimal cuts gradually and the upper bound and lower bound are finally reaching consistently, so the algorithm converges to the global optimal solution. The difference between MP1 is when increasing the original cuts, the extra variables will be added. Therefore, with the increase of iterations, the number of variables in the model (MP2) is more and more, and the scale of the model will be increased, but the total number of iterations will be greatly reduced.

Theorem 2.4 [14] *if p is the pole number of uncertainty set Ω_u, q is the pole number of simplex $\{ \boldsymbol{A}^T\boldsymbol{\pi} \le \boldsymbol{a}^T, \boldsymbol{\pi} \ge \boldsymbol{0} \}$, then the iteration number of Benders decomposition method based on dual cut is $\mathcal{O}(pq)$; the iteration number of Benders decomposition method based on original cut is $\mathcal{O}(p)$.*

From 2.4, it is obvious that by using original cut, the computation complexity is greatly reduced, and the solving efficiency is Q times higher. Therefore, the method based on original cut is mainly used in this paper. Of course, in the actual calculation, we can also add the original cut and the dual cut into the model, while preserving the characteristics of the original cut and the dual cut. Next, Benders decomposition method based on original cut is refined, given convergence precisionε, and the flow chart is shown following:

(i) Set $LB = -\infty$, $UB = +\infty$, $k = 0$;
(ii) Solve main problem (MP2), and obtain the optimal solution $\left(\boldsymbol{y}_{k+1}^*, \eta_{k+1}^*, \boldsymbol{x}_1^*, \ldots, \boldsymbol{x}_k^*\right)$ and lower bound of model $LB = \eta^*$;
(iii) Fix $\boldsymbol{y}^*$ to solve subproblem (SP), if subproblem is feasible, obtain optimal solution $\left(\boldsymbol{u}_k^*, \boldsymbol{\pi}_k^*\right)$ and objective value $\Theta(\boldsymbol{y}^*)$; if not, $\Theta(\boldsymbol{y}^*) = +\infty$. Furthermore, update upper bound of model with $UB = \min\{UB, \Theta(\boldsymbol{y}^*)\}$;
(iv) If $(UB\text{-}LB) \le \varepsilon$, return $\boldsymbol{y}^*$ and stop iterations; otherwise $k = k+1$, fix $\boldsymbol{u}_k^*$, design original cut:

(a) If the subproblem of (iii) is feasible, generate new variable $\boldsymbol{x}^l$, and add cut shown in (2.121) to the main problem (MP);

$$\boldsymbol{A}\boldsymbol{x}^l \ge \boldsymbol{d} - \boldsymbol{B}\boldsymbol{y} - \boldsymbol{C}\boldsymbol{u}_l^*, \quad \eta \ge \boldsymbol{a}^T\boldsymbol{x}^l \tag{2.121}$$

(b) If the subproblem of (iii) is infeasible, generate new variable $\boldsymbol{x}^l$ and add cut shown in (2.122) to the main problem (MP);

$$\boldsymbol{A}\boldsymbol{x}^l \ge \boldsymbol{d} - \boldsymbol{B}\boldsymbol{y} - \boldsymbol{C}\boldsymbol{u}_l^* \tag{2.122}$$

(v) Go to (ii).

According to the flow chart of Benders decomposition method based on original cut, in the fourth step, if the subproblem is feasible, the added original cut is called optimal cut from the mathematical structure, because it is obtained with the information of optimal solution; but if the subproblem is infeasible, the original cut is changed and called feasible cut which is only to guarantee the feasibility of problem.

Another important problem is how to solve the inner-level "maxmin" optimization model. It has been illustrated anteriorly that if the uncertainty set is an interval form, the "maxmin" optimization is the same as the pessimistic model of interval optimization. Furthermore, it is proved that optimal solution must be obtained when uncertainties reach the bounds, so it can be transformed into a mixed linear programming model to solve. However, if the robust cost is considered, the

structure of uncertainty set is changed, and optimal solution is not achieved at the bound (but achieved at the vertices of the simplex). Therefore, new methods need to solve.

Assume the dual variable of second stage is $\boldsymbol{\pi}$. Because the "maxmin" can be regarded as a bilinear programming where inner-level model is a linear programming, if the inner-level model is feasible, then KKT condition is the sufficient and necessary condition of optimal solution and we have optimization model as following:

$$\max_{\boldsymbol{x},\boldsymbol{u},\boldsymbol{\pi}} \quad 0 \tag{2.123}$$

$$s.t. \quad \boldsymbol{A}^T\boldsymbol{\pi} \le \boldsymbol{a}^T \tag{2.124}$$

$$\boldsymbol{Ax} \ge \boldsymbol{d} - \boldsymbol{By} - \boldsymbol{Cu} \tag{2.125}$$

$$\boldsymbol{u} \in \Omega_{\boldsymbol{u}}, \quad \boldsymbol{\pi} \ge \boldsymbol{0} \tag{2.126}$$

$$\pi_i(\boldsymbol{Ax} - \boldsymbol{d} + \boldsymbol{By} + \boldsymbol{Cu})_i = 0, \quad \forall i \tag{2.127}$$

$$x_j\left(\boldsymbol{a}^T - \boldsymbol{A}^T\boldsymbol{\pi}\right)_j = 0, \quad \forall j \tag{2.128}$$

$$\boldsymbol{u} \in \Omega_{\boldsymbol{u}}, \quad \boldsymbol{\pi} \ge \boldsymbol{0} \tag{2.129}$$

where constraints (2.127) and (2.128) are complementary, which can be transformed into mixed integer programming to solve based on big M theory, and we have:

$$\max_{\boldsymbol{x},\boldsymbol{u},\boldsymbol{\pi},\boldsymbol{v},\boldsymbol{w}} \quad 0 \tag{2.130}$$

$$s.t. \quad \boldsymbol{A}^T\boldsymbol{\pi} \le \boldsymbol{a}^T \tag{2.131}$$

$$\boldsymbol{Ax} \ge \boldsymbol{d} - \boldsymbol{By} - \boldsymbol{Cu} \tag{2.132}$$

$$\boldsymbol{u} \in \Omega_{\boldsymbol{u}}, \quad \boldsymbol{\pi} \ge \boldsymbol{0} \tag{2.133}$$

$$\pi_i \le Mw_i, \quad (\boldsymbol{Ax} - \boldsymbol{d} + \boldsymbol{By} + \boldsymbol{Cu})_i \le M(1 - w_i), \quad \forall i \tag{2.134}$$

$$0 \le x_j \le Mv_j, \quad \left(\boldsymbol{a}^T - \boldsymbol{A}^T\boldsymbol{\pi}\right)_j \le M\left(1 - v_j\right), \quad \forall j \tag{2.135}$$

$$\boldsymbol{u} \in \Omega_{\boldsymbol{u}}, \quad \boldsymbol{\pi} \ge \boldsymbol{0}, \quad \boldsymbol{w} \in \{0,1\}, \quad \boldsymbol{v} \in \{0,1\} \tag{2.136}$$

2.4 Summary

Mathematical theory based on interval computation and optimization is mainly introduced in this chapter. Interval computation includes interval linear equations, interval nonlinear equations; optimization methods based interval include interval optimization and robust optimization, where interval robust optimization include adaptive interval robust optimization and two-stage interval robust optimization. This chapter does not involve specific application model in power system, but use abstract mathematical expressions to describe and obtain some general solution methods. These methods provide the mathematical basis to solve the power system model created later in the paper, and can be widely used in other fields referring to interval models, such as water conservancy, transportation, aviation and so on. In addition, it notes that each mathematical model has its own solution which may be more than one, and the computational complexity or result precision may vary with each method. This paper contains many kinds of mathematical solution method which will be compared and discussed in the following application.

References

1. Guessous N, Souhar O (2004) Recursive two-level ILU preconditioner for nonsymmetric M-matrices. J Appl Math Comput 16(1–2):19–35
2. Cui X, Hayami K (2009) Generalized approximate inverse preconditioners for least squares problems. Jpn J Ind Appl Math 26(1):1–14
3. Griffel DH (2002) Applied functional analysis. G. P. C. Press, Canada
4. Al-Khayyal FA, Larsen C, Van Voorhis T (1995) A relaxation method for nonconvex quadratically constrained quadratic programs. J Global Optim 6(3):215–230
5. Androulakis IP, Maranas CD, Floudas CA (1995) αBB: a global optimization method for general constrained nonconvex problems. J Global Optim 7(4):337–363
6. Maranas CD, Floudas CA (1995) Finding all solutions of nonlinearly constrained systems of equations. J Global Optim 7(2):143–182
7. Raber U (1998) A simplicial branch-and-bound method for solving nonconvex all-quadratic programs. J Global Optim 13(4):417–432
8. Linderoth J (2005) A simplicial branch-and-bound algorithm for solving quadratically constrained quadratic programs. Math Program 103(2):251–282
9. Floudas CA, Pardalos PM, Nahapetyan AG (2009) Bilinear programming. In: Floudas CA, Pardalos PM (eds) Encyclopedia of optimization. Springer, US, pp 279–282
10. Shapiro JF (1984) A note on node aggregation and Benders' decomposition. Math Program 29 (1):113–119
11. Henry J, Yvon J, Lahdelma R et al (1994) A modified benders' decomposition technique for solving large scale unit commitment problems. In: Henry J, Yvon J (eds) System modelling and optimization. Springer, Berlin, pp 737–745
12. Floudas CA, Pardalos PM, Floudas CA (2001) Generalized benders decomposition. In: Floudas CA, Pardalos PM (eds) Encyclopedia of optimization. Springer, US, pp 747–758
13. Gass SI, Fu MC (2013) Benders decomposition method. In: Gass SI, Fu MC (eds) Encyclopedia of operations research and management science. Springer, US, p 115
14. Zeng B, Zhao L (2013) Solving two-stage robust optimization problems using a column-and-constraint generation method. Oper Res Lett 41(5):457–461

Chapter 3
The Research and Application of Interval Power Flow

Abstract Interval power flow extends deterministic power flow to an interval based power flow. Mathematically, interval power flow aims to solve interval linear and nonlinear equations. In this book, Kraw iteration method with approximated inverse preconditioner is proposed to solve interval linear equations, which is applied to interval DC power flow and Distflow based interval radial power flow. Besides, optimization based method is proposed to for solve interval nonlinear equations, especially for interval quadratic equations, which is applied to interval AC power flow.

3.1 Summary

As its name implies, the interval power flow is the interval results of power flow acquired by modeling some parameters as interval numbers based on traditional power flow. The interval power flow, probabilistic load flow and fuzzy power flow are belonging to category of uncertainty power flow analysis, and the difference among them is the modeling for uncertainties.

Considering the randomness and intermittent when a large-scale wind power integrated to power system, the probability density function is usually difficult to accurately obtain, which brings about the challenge to probabilistic power flow and fuzzy power flow analysis. However, the interval number is easier than probability distribution and fuzzy numbers. With the modeling of interval numbers, there only need upper and lower bounds which can be acquired by the information of prediction and confidence intervals, while there is no need to find probability density function. At last, the upper and lower bounds of power flow can be obtained, which provide intuitive bound information for operators, which can be utilized for the further optimization of operation.

Traditional power flow analysis includes DC power flow, AC power flow and power flow in radial network, the essence of which is to solve linear and nonlinear equations. Therefore, Sect. 2.2 in Chap. 2 will study the mathematical methods for each model. Specifically, Kraw operator iterative algorithm with approximately

T. Ding, *Power System Operation with Large Scale Stochastic Wind Power Integration*, Springer Theses, DOI 10.1007/978-981-10-2561-7_3

inverse pretreatment is proposed to DC interval power flow analysis, Distflow approximation is introduced to distribution network interval power flow analysis, and optimization based method is developed to interval AC power flow analysis. Particularly, according to the quadratic characteristic of power flow equations, the method by relaxing the feasible region to a convex set, and interval solutions are obtained by tightening bounds. Furthermore, from the perspective of actual physical modeling of power systems, the power flow result is related to the selection of slack bus. To obtain the result without the relation to slack bus, dynamic power flow analysis has been researched and applied.

Interval power flow analysis can obtain the upper and lower bounds of power flow solution, provide operators intuitive information of upper and lower bounders and offer the advanced applications in power system. This section will extend traditional deterministic power flow analysis to an interval flow analysis, forming DC interval power flow, AC interval power flow, interval distribution power flow and constrained interval power flow analysis. The flowchart of methods in this chapter is as follows (Fig. 3.1):

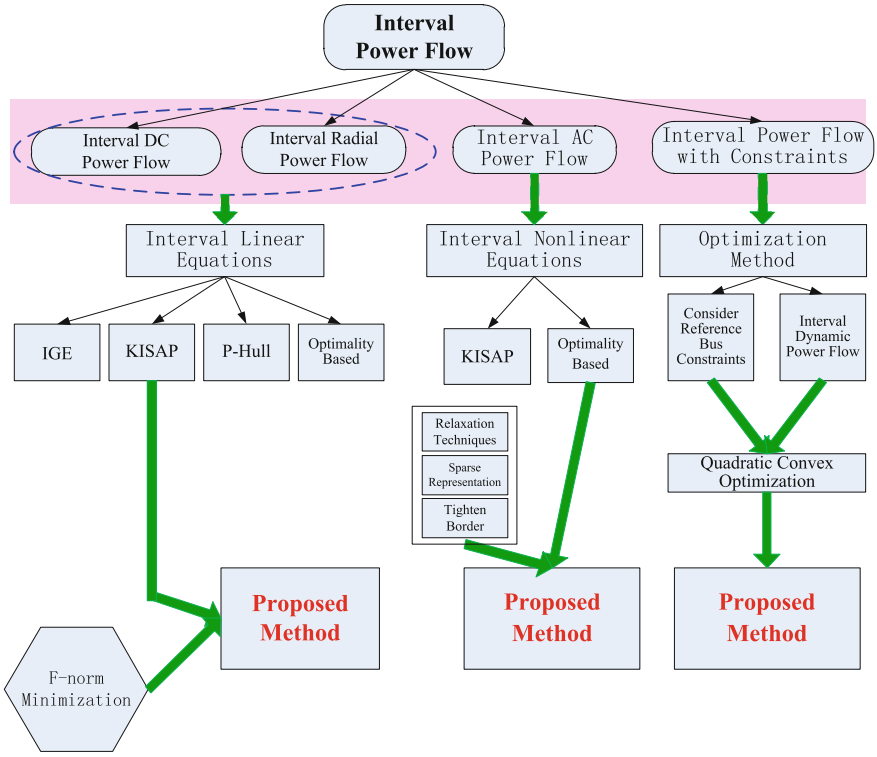

Fig. 3.1 The framework of this chapter

3.2 The Application of Interval Power Flow

3.2.1 The Interval DC Power Flow

3.2.1.1 Modeling of Interval DC Power Flow

The uncertainty of interval power flow mainly focused on the uncertain wind power output. Thus, it can put generator output, load demand and wind power output together to form the injection power at each bus, and then the injection power of each bus could be expressed as an interval number. Furthermore, the mathematical description of interval DC flow is (3.1), where B is susceptance matrix and $\left[\underline{\boldsymbol{P}}, \overline{\boldsymbol{P}}\right]$ is interval injection power at each bus. Interval DC flow can obtain interval transmission flow and interval phase angle based on interval injection power at each bus.

Since the system always maintains the power balance, we will arrive at $\sum \left[\underline{\boldsymbol{P}}, \overline{\boldsymbol{P}}\right] = 0$. Usually when calculating power flow, the voltage phase angle slack bus is known (usually is 0), therefore the reduced admittance matrix is used to solver interval DC flow, such as (3.2), where, Ω is a collection of PV and PQ buses, ref are slack bus. Then the reduced admittance matrix B is invertible matrix.

$$\boldsymbol{B}\left[\underline{\boldsymbol{\theta}}, \overline{\boldsymbol{\theta}}\right] = \left[\underline{\boldsymbol{P}}, \overline{\boldsymbol{P}}\right] \tag{3.1}$$

$$\boldsymbol{B}_{\Omega\times\Omega}\left[\underline{\boldsymbol{\theta}}, \overline{\boldsymbol{\theta}}\right]_{\Omega\times 1} = \left[\underline{\boldsymbol{P}}, \overline{\boldsymbol{P}}\right]_{\Omega\times 1} - \boldsymbol{B}_{\Omega\times ref}\theta_{ref\times 1} = \left[\underline{\boldsymbol{P}}, \overline{\boldsymbol{P}}\right]_{\Omega\times 1} \tag{3.2}$$

If we suppose $\left[\underline{\boldsymbol{P}^{\dagger}}, \overline{\boldsymbol{P}^{\dagger}}\right] = \left[\underline{\boldsymbol{P}}, \overline{\boldsymbol{P}}\right]_{\Omega\times 1}$ to be injection vector of power injection, $\boldsymbol{B}^{\dagger}_{\Omega\times\Omega} = \boldsymbol{B}_{\Omega\times\Omega}$ and $\left[\underline{\boldsymbol{\theta}^{\dagger}}, \overline{\boldsymbol{\theta}^{\dagger}}\right] = \left[\underline{\boldsymbol{\theta}}, \overline{\boldsymbol{\theta}}\right]_{\Omega\times 1}$ as the phase angle of each bus, then

$$\boldsymbol{B}^{\dagger}\left[\underline{\boldsymbol{\theta}^{\dagger}}, \overline{\boldsymbol{\theta}^{\dagger}}\right] = \left[\underline{\boldsymbol{P}^{\dagger}}, \overline{\boldsymbol{P}^{\dagger}}\right], \quad \text{and} \quad \left\langle \theta_{ref} \right\rangle = [0, 0] \tag{3.3}$$

While $\left[\underline{P_{g,ref}}, \overline{P_{g,ref}}\right]$ is interval flow of slack bus. As the power system needs to meet the balance of power at each time, so the flow of slack bus can be obtained by (3.4).

$$\left[\underline{P_{g,ref}}, \overline{P_{g,ref}}\right] + \sum \left[\underline{\boldsymbol{P}^{\dagger}}, \overline{\boldsymbol{P}^{\dagger}}\right] = [0, 0] \tag{3.4}$$

According to the definition of power flow, the flow on branch l can be expressed as $P_{T,l} = \frac{\theta_i - \theta_j}{x_{ij}}$, where i and j are the index of "from" and "to" buses of the branch l;

xij is reactance of branch l. If considering the interval expression, the interval flow can be expressed as

$$\left[\underline{P_{T,l}}, \overline{P_{T,l}}\right] = \frac{[\theta_i] - [\theta_j]}{x_{ij}} \tag{3.5}$$

However, it should be noted that, when using (3.5) to solve the interval power flow, the interval phase angle information is needed, and the phase angle range is obtained by (3.3). Thus, the calculation of interval phase angle appears more than once, which will inevitably lead to an enlarged interval. In order to overcome conservativeness of interval arithmetic, the network distribution shift factors can be used, and we can obtain

$$\left[\underline{\boldsymbol{P}_T}, \overline{\boldsymbol{P}_T}\right] = \boldsymbol{H}\left[\underline{\boldsymbol{P}}, \overline{\boldsymbol{P}}\right] \tag{3.6}$$

where H is the network distribution shift factors and PT is transmission flow vector. Since the interval expression is conducted only once, so the conservativeness resulted from the interval operation will be greatly reduced. But taking (3.6) into application also have some challenges, because H is a full array, which needs to account for much memory space.

3.2.1.2 Method for DC Interval Power Flow

It can be observed from (3.3) that the interval linear equations are very special in that the intervals only exist in the right hand of equations, and the coefficient matrix of equations is constant. Intuitively, interval flow of (3.3) can be obtained directly from (3.7), but computing the inverse of a constant matrix is very difficult.

$$\left[\underline{\boldsymbol{\theta}^{\dagger}}, \overline{\boldsymbol{\theta}^{\dagger}}\right] = \left(\boldsymbol{B}^{\dagger}\right)^{-1}\left[\underline{\boldsymbol{P}^{\dagger}}, \overline{\boldsymbol{P}^{\dagger}}\right], \quad \text{with } \langle\theta_{ref}\rangle = [0,0] \tag{3.7}$$

For traditional deterministic power flow, LU decomposition is widely used to solve the DC power equations, but unfortunately LU decomposition cannot apply to interval flow equations, since it solves linear equations of upper triangular and lower triangular matrices, which will bring about the conservativeness. Using a simple linear system as an example:

Given $\boldsymbol{A} = \begin{bmatrix} 0.5973 & 0.7009 & 0.7400 \\ 0.0493 & 0.09623 & 0.4319 \\ 0.5711 & 0.7505 & 0.6343 \end{bmatrix}$, $\langle \boldsymbol{b} \rangle = \begin{bmatrix} [-1, +4] \\ [+2, +5] \\ [-3, -1] \end{bmatrix}$, Solving $\boldsymbol{A}\langle \boldsymbol{x} \rangle = \langle \boldsymbol{b} \rangle$.

Exact Solutions is:

$$\langle \boldsymbol{x} \rangle = \boldsymbol{A}^{-1}\langle \boldsymbol{b} \rangle = \begin{bmatrix} -4.9898 & -1.9325 & 7.1374 \\ -3.7546 & 0.7619 & 3.8617 \\ 8.9354 & 0.8384 & -9.4190 \end{bmatrix} \begin{bmatrix} [-1, +4] \\ [+2, +5] \\ [-3, -1] \end{bmatrix} = \begin{bmatrix} [-51.0338, -6.0125] \\ [-25.0801, 3.7025] \\ [2.1603, 68.1903] \end{bmatrix}$$

With LU decomposition, we can obtain:

$$\boldsymbol{L} = \begin{bmatrix} 1 & 0 & 0 \\ 0.0825 & 1 & 0 \\ 0.9560 & 0.0890 & 1 \end{bmatrix}, \quad \boldsymbol{U} = \begin{bmatrix} 0.5973 & 0.7009 & 0.7400 \\ 0 & 0.9045 & 0.3708 \\ 0 & 0 & -0.1062 \end{bmatrix}$$

Solutions using LU decomposition for interval linear equations is

$$\langle \boldsymbol{y} \rangle = \boldsymbol{L}^{-1}\langle \boldsymbol{b} \rangle = \begin{bmatrix} 1 & 0 & 0 \\ -0.0825 & 1 & 0 \\ -0.9487 & -0.0890 & 1 \end{bmatrix} \begin{bmatrix} [-1, +4] \\ [+2, +5] \\ [-3, -1] \end{bmatrix} = \begin{bmatrix} [-1, +4] \\ [1.6700, 5.0825] \\ [-7.2397, -0.2293] \end{bmatrix}$$

$$\langle \boldsymbol{x} \rangle = \boldsymbol{U}^{-1}\langle \boldsymbol{y} \rangle = \begin{bmatrix} 1.6741 & -1.2972 & 7.1374 \\ 0 & 1.1056 & 3.8617 \\ 0 & 0 & -9.4190 \end{bmatrix} \begin{bmatrix} [-1, +4] \\ [1.6700, 5.0825] \\ [-7.2397, -0.2293] \end{bmatrix} = \begin{bmatrix} [-59.9392, 2.8929] \\ [-26.1112, 4.7336] \\ [2.1603, 68.1903] \end{bmatrix}$$

It can be observed that for interval linear equations with constant coefficients, the LU decomposition method will expand the range of the interval solutions. Therefore, in order to reduce conservativeness of interval arithmetic, four methods to solve interval linear equations in Appendix A can be used. Furthermore, we can compare the corresponding efficiency with the preprocessing Kraw operator iterative method presented in Sect. 2.2.

3.2.1.3 Simulation Results

In this book, 9-bus system [1] is used to test the proposed method, where there are 3 loads, 3 generators and 9 branches. Considering power injection of each bus to be within 10 % of normal condition, the results of the interval power flow solved by several methods can be presented in Table 3.1, where all the four methods can accurately solve interval flow, and for the 9-bus small systems, the computational speed of several methods is nearly the same. Then, the large-scale test system is

Table 3.1 Result of interval DC power flow by different methods

Bus no.	Deterministic power flow (MW)	Interval Gauss elimination (MW)	Kraw Iteration (MW)	Optimization based method (MW)	Matrix inverse (MW)
1	0.0000	[0.0000, 0.0000]	[0.0000, 0.0000]	[0.0000, 0.0000]	[0.0000, 0.0000]
2	9.7960	[4.1146, 15.4775]	[4.1146, 15.4775]	[4.1146, 15.4775]	[4.1146, 15.4775]
3	5.0605	[0.0207, 10.1004]	[0.0207, 10.1004]	[0.0207, 10.1004]	[0.0207, 10.1004]
4	−2.2111	[−4.0692,−0.3531]	[−4.0692,−0.3531]	[−4.0692,−0.3531]	[−4.0692,−0.3531]
5	−3.7380	[−6.9210,−0.5551]	[−6.9210,−0.5551]	[−6.9210,−0.5551]	[−6.9210,−0.5551]
6	2.2066	[−2.5478, 6.9611]	[−2.5478, 6.9611]	[−2.5478, 6.9611]	[−2.5478, 6.9611]
7	0.8224	[−4.3729, 6.0178]	[−4.3729, 6.0178]	[−4.3729, 6.0178]	[−4.3729, 6.0178]
8	3.9590	[−1.1388, 9.0568]	[−1.1388, 9.0568]	[−1.1388, 9.0568]	[−1.1388, 9.0568]
9	−4.0634	[−7.4393,−0.6875]	[−7.4393,−0.6875]	[−7.4393,−0.6875]	[−7.4393,−0.6875]

Table 3.2 Computational time of each method for interval DC power flow

Deterministic power flow (MW)	Interval Gauss elimination (MW)	Kraw iteration (MW)	Optimization based method (MW)	Matrix inverse (MW)
0.03 s	33.12 s	0.12 s	0.08 s (each bus)	0.24 s

introduced to test the algorithm complexity of several methods. For IEEE 300-bus system [1], the uncertainty of power injection is set to be 10 %, and the computational complexity by four methods is shown in Table 3.2. It can be found that Gaussian elimination method requires the most computing time. Moreover, with the increasing of the system size, the time of direct inverse method will increase significantly, especially when solving the matrix inverse on a system with thousands of buses, direct matrix inverse will be a great challenge. Although optimization based method has a fast speed, this method obtains the interval solution only one bus. That means, we need to solve this optimization model for several times to obtain the whole intervals for all buses. However, if the hardware is available for parallel computation, the computational complexity will be greatly improved. Besides, similar to the direct inverse method, traditional Kraw operator method also needs to solve inverse of the center matrix, which is not practical for large-scale test systems. For the IEEE 300-bus system, the computational speed of the proposed Kraw Method with F-norm preconditioning is twice less than the direct inverse method, which ensures the convergence by 11 iterations.

Finally, we will study the interval branch flow, which can obtain by (3.6). In contrast, in accordance with interval phase angle in Table 3.1, interval branch flow can also be calculated by (3.5). The comparison of the results by the two methods is shown in Table 3.3. The results show that the traditional deterministic flow by (3.5) and (3.6) are exactly the same. But for the interval branch flow, the results of (3.5) have a much larger range than the results of (3.6), It is because (3.6) deals with uncertain power flow only once, whereas (3.5) needs to get an implicit result of the

Table 3.3 Comparison of interval branch flow by two methods

Branch no.	Deterministic power flow		Interval power flow	
	By (3–6) (MW)	By (3–5) (MW)	By (3–6) (MW)	By (3–5) (MW)
1	67.0000	67.0000	[10.6999, 123.3001]	[10.6999, 123.3001]
2	28.9673	28.9673	[3.8332, 54.1015]	[−66.6642, 124.5989]
3	−61.0326	−61.0326	[−79.5992, −42.4660]	[−142.5223, 20.4571]
4	85.0000	85.0000	[76.5000, 93.5001]	[−206.7088, 376.7088]
5	23.9673	23.9673	[7.3585, 40.5763]	[−148.3099, 196.2447]
6	−76.0326	−76.0326	[−93.2996, −58.7657]	[−325.5427, 173.4775]
7	−163.0000	−163.0000	[−179.3001, −146.6999]	[−464.0101, 138.0101]
8	86.9673	86.9673	[65.1801, 108.7547]	[−4.8909, 178.8256]
9	−38.0326	−38.0326	[−69.1986, −6.8667]	[−145.5016, 69.4364]

power angle, and then calculate the branch flow. Thus, interval matrix operations carry out twice, which will result in an enlarged range. Therefore, using (3.6) to calculate interval branch flow is very necessary.

3.2.2 Interval AC Power Flow

3.2.2.1 Modeling for Optimization Based Interval Power Flow

For the interval AC power flow, this book proposes an optimization based method. First, we will define some symbolic variables of interval AC flow as follows:

e_i, f_i	Real and imaginary part of voltage magnitude of bus i
G_{ij}, B_{ij}	real and imaginary part of $(i,j)th$ element of bus admittance matrix $Y_{bus} = G + \mathrm{j}B$
n	total number of buses
N_P	set of PQ and PV buses
N_{PQ}	set of PQ buses
N_{PV}	set of PV buses
N_{REF}	reference bus

(continued)

(continued)

$\underline{P_i}$, $\overline{P_i}$	lower and upper bound of P_i
P_i, Q_i	active and reactive power injection at bus i
$\underline{Q_i}$, $\overline{Q_i}$	lower and upper bound of Q_i
s	total number of branches

The energy balance equation in polar coordinates including active and reactive power flow are represented as (3.8)–(3.9).

The energy balance equation in polar coordinates including active and reactive power flow are represented as (3.8)–(3.9).

$$P_i = U_i \sum_{j=1}^{n} U_j \left(G_{ij} \cos\theta_{ij} + B_{ij} \sin\theta_{ij}\right) \quad i \in N_P \tag{3.8}$$

$$Q_i = U_i \sum_{j=1}^{n} U_j \left(G_{ij} \sin\theta_{ij} - B_{ij} \cos\theta_{ij}\right) \quad i \in N_{PQ} \tag{3.9}$$

Note that the energy balance equations contain strong nonlinear functions such as sin(·) and cos(·), which are difficult to deal with when obtaining the AA form of the injected powers [2]. Usually, the linear polynomials using Taylor series or Horner's rule are introduced to linearize the equation system at the operating point with respect to the variables, where the omitted remainders in the approximation might cause additional level of inaccuracy. An iterative method was proposed in [3] that eliminates the effect of remainders with an initial guess of deviation so as to narrow the solution's bounds.

In order to overcome the approximation errors caused by strong nonlinear energy balance equations in polar coordinates, we transform the original problem into Cartesian coordinates form in (3.10)–(3.12), which only contain quadratic polynomials.

$$P_i = e_i \sum_{j=1}^{n} \left(G_{ij} e_j - B_{ij} f_j\right) + f_i \sum_{j=1}^{n} \left(G_{ij} f_j + B_{ij} e_j\right) \quad i \in N_P \tag{3.10}$$

$$Q_i = f_i \sum_{j=1}^{n} \left(G_{ij} e_j - B_{ij} f_j\right) - e_i \sum_{j=1}^{n} \left(G_{ij} f_j + B_{ij} e_j\right) \quad i \in N_{PQ} \tag{3.11}$$

$$U_i^2 = e_i^2 + f_i^2 \quad i \in N_{PV} \tag{3.12}$$

In interval power flow analysis, power injections are volatile and can be represented using intervals, such that $P_i = \left[\underline{P_i}, \overline{P_i}\right]$ and $Q_i = \left[\underline{Q_i}, \overline{Q_i}\right]$. However, the

maximum (or minimum) voltage magnitude cannot be directly obtained due to the nonlinear characteristics of the power flow equations. Therefore, we solve the interval information for each bus one at a time. Take voltage magnitudes for example (and the branch flow will be studied later): the interval power flow (IPF) problem can be formulated as a non-convex and nonlinear programming (NP) in (3.13)–(3.17) with quadratic objective and constraints, which is a standard QCQP problem and is labeled IPF-QCQP in this paper.

$$(\mathbf{IPF-QCQP}) \quad \max_{e,f}/\min \quad e_i^2 + f_i^2 \quad i \in N_{PQ} \tag{3.13}$$

$$s.t. \quad \underline{P_i} \le e_i \sum_{j=1}^{n} \left(G_{ij}e_j - B_{ij}f_j\right) + f_i \sum_{j=1}^{n} \left(G_{ij}f_j + B_{ij}e_j\right) \le \overline{P_i} \quad i \in N_P \tag{3.14}$$

$$\underline{Q_i} \le f_i \sum_{j=1}^{n} \left(G_{ij}e_j - B_{ij}f_j\right) - e_i \sum_{j=1}^{n} \left(G_{ij}f_j + B_{ij}e_j\right) \le \overline{Q_i} \quad i \in N_{PQ} \tag{3.15}$$

$$U_i^2 = e_i^2 + f_i^2 \quad i \in N_{PV} \tag{3.16}$$

$$e_i = e^{ref}, f_i = f^{ref} \quad i \in N_{REF} \tag{3.17}$$

It can be deduced that the total number of decision variables (e, f) is 2n − 2 according to the linear relaxation model of interval quadratic equations model which can be solved by the method is Sect. 2.2.2.1 with bound tightening algorithm.

However, from the model in Sect. 2.3, it can be found that dummy variables as well as convex and concave envelope will be introduced when using linear relaxation techniques, which leads the relaxed QCQP model to be a linear programming problem. Intuitively, Z has 2n × 2n elements, because any two variables will add a dummy variable. However, for a large-scale power system, this will greatly increase the computational burden for computing interval power flow. Fortunately, the power systems always have a sparse characteristic, so that Zij between any two variables should only be introduced for the branch lines, because in power flow equations, the admittance produced by Zij without connected lines is 0. So this will greatly reduce the computational complexity of linear relaxation model with the help of sparsity technique.

3.2.2.2 Sparsity Technique for Relaxed Model of Interval Power Flow

Let B be a finite set and denote the pairs of B by L (B) in (3.18).

$$L(B) = \{(u, v) | u, v \in B, u \neq v\} \tag{3.18}$$

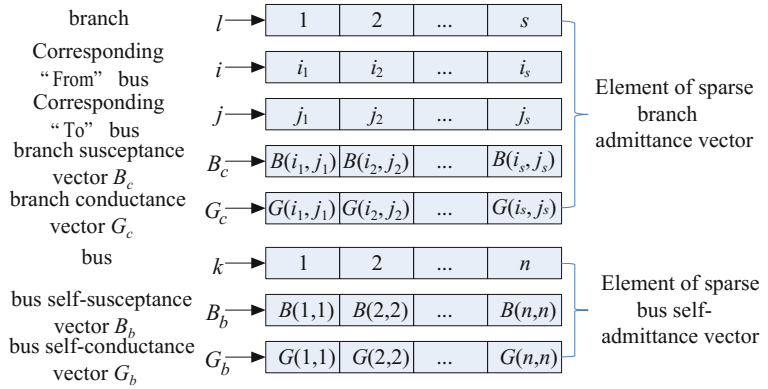

Fig. 3.2 Data structure of sparse susceptance and conductance vector

For a given power network graph G = (B, L) with L ⊆ L(B) [4], where the elements of B are the vertices of G representing all the buses, and the elements of L are the edges of G representing transmission lines and transformers. According to the energy functions in (3.10)–(3.11), the quadratic terms in P and Q have the same structure except for the constant G, B and the operator sign. Note that only up to six additional dummy variables eiej, eifj, fiej, fifj, eiei and fifi are needed for each edge l = (i, j) ∈ L, and bilinear terms are not needed for l = (i, j) ∉ L. Meanwhile, in order to reduce the number of additional dummy variables, the bus admittance matrix Ybus = (yij)n × n, describing the bus-bus relationship, should be converted into bus-branch relationship. An n × s sparse connection matrix Sc is defined such that its (k, l) element is 1 if branch l is connected to bus k and 0 otherwise.

We firstly define Bc and Gc as the susceptance vector and conductance vector of the branch admittance, respectively, and define Bb and Gb as the susceptance vector and conductance vector of the bus self-admittance. Then, utilizing the connection matrix Sc, we convert those vectors into four matrices WG ∈ Rn × s, WB ∈ Rn × s, KG ∈ Rn × n and KB ∈ Rn × n, as formulated in (3.19)–(3.22). Figure 3.2 illustrates the data structure of the sparse susceptance and conductance vectors.

$$\left(\boldsymbol{W}^{G}\right)_{n\times s}=\left(\boldsymbol{S}_c\right)_{n\times s}\times\left(diag\left(\boldsymbol{G}_c\right)\right)_{s\times s} \tag{3.19}$$

$$\left(\boldsymbol{W}^{B}\right)_{n\times s}=\left(\boldsymbol{S}_c\right)_{n\times s}\times\left(diag\left(\boldsymbol{B}_c\right)\right)_{s\times s} \tag{3.20}$$

$$\left(\boldsymbol{K}^{G}\right)_{n\times n}=\left(diag\left(\boldsymbol{G}_b\right)\right)_{n\times n} \tag{3.21}$$

$$\left(\boldsymbol{K}^{B}\right)_{n\times n}=\left(diag\left(\boldsymbol{B}_b\right)\right)_{n\times n} \tag{3.22}$$

Further, we define xl = eiej, yl = fifj, ml = eifj, nl = fiej, rl = eiei, hl = fifj, ∀l = (i, j) ∈ L. Then dummy variable vectors are created, X = (xl)s × 1, Y = (yl)

s × 1, M = (ml)s×1, N = (nl)s × 1, R = (rl)n × 1, H = (hl)n × 1. With the four susceptance and conductance matrices WG, WB, KG and KB, and the dummy variable vectors, Eqs. (3.10)–(3.11) can be converted into Eqs. (3.24)–(3.25). Based on the linear relaxation method for QCQP model introduced in section III-A, the IPF-QCQP can be converted into IPF-LR expressed in (3.23)–(3.50).

Through this sparse matrix technique, the number of added matrix variable Z is reduced from 2n × 2n elements to 4s + 2n, which is particularly important for applications to large-scale systems.

$$(\mathbf{IPF}-\mathbf{LR}) \quad \max_{\{\boldsymbol{X},\boldsymbol{Y},\boldsymbol{M},\boldsymbol{N},\boldsymbol{R},\boldsymbol{H},\boldsymbol{e},\boldsymbol{f}\}}/\min \quad Z_i + H_i \quad i \in N_{PQ} \tag{3.23}$$

$$\text{s.t.} \quad \underline{P_i} \le \sum_{l=1}^{s} \left(W_{i,l}^{G} X_l - W_{i,l}^{B} M_l + W_{i,l}^{G} Y_l + W_{i,l}^{B} N_l \right) + K_i^{G} R_i + K_i^{G} H_i \le \overline{P_i} \quad i \in N_P \tag{3.24}$$

$$\underline{Q_i} \le \sum_{l=1}^{s} \left(W_{i,l}^{G} N_l - W_{i,l}^{B} Y_l - W_{i,l}^{G} M_l - W_{i,l}^{B} X_l \right) + K_i^{B} R_i + K_i^{B} H_i \le \overline{Q_i} \quad i \in N_{PQ} \tag{3.25}$$

$$R_i + H_i = \widehat{U}_i^2 \quad i \in N_{PV} \tag{3.26}$$

$$e_i = \widehat{e}, \quad f_i = \widehat{f} \quad i \in N_{REF} \tag{3.27}$$

$$X_l - \underline{e_i}\, e_j - \underline{e_j}\, e_i + \underline{e_i}\, \underline{e_j} \ge 0 \quad l \in L \tag{3.28}$$

$$X_l - \overline{e_i}\, e_j - \overline{e_j}\, e_i + \overline{e_i}\, \overline{e_j} \ge 0 \quad l \in L \tag{3.29}$$

$$X_l - \underline{e_i}\, e_j - \overline{e_j}\, e_i + \underline{e_i}\, \overline{e_j} \le 0 \quad l \in L \tag{3.30}$$

$$X_l - \overline{e_i}\, e_j - \underline{e_j}\, e_i + \overline{e_i}\, \underline{e_j} \le 0 \quad l \in L \tag{3.31}$$

$$Y_l - \underline{f_i} f_j - \underline{f_j} f_i + \underline{f_i}\, \underline{f_j} \ge 0 \quad l \in L \tag{3.32}$$

$$Y_l - \overline{f_i} f_j - \overline{f_j} f_i + \overline{f_i}\, \overline{f_j} \ge 0 \quad l \in L \tag{3.33}$$

$$Y_l - \underline{f_i} f_j - \overline{f_j} f_i + \underline{f_i}\, \overline{f_j} \le 0 \quad l \in L \tag{3.34}$$

$$Y_l - \overline{f_i} f_j - \underline{f_j} f_i + \overline{f_i}\, \underline{f_j} \le 0 \quad l \in L \tag{3.35}$$

$$M_l - \underline{e_i} f_j - \underline{f_j} e_i + \underline{e_i}\, \underline{f_j} \ge 0 \quad l \in L \tag{3.36}$$

$$M_l - \overline{e_i}f_j - \overline{f_j}e_i + \overline{e_i}\,\overline{f_j} \geq 0 \quad l \in L \tag{3.37}$$

$$M_l - \underline{e_i}f_j - \overline{f_j}e_i + \underline{e_i}\,\overline{f_j} \leq 0 \quad l \in L \tag{3.38}$$

$$M_l - \overline{e_i}f_j - \underline{f_j}e_i + \overline{e_i}\,\underline{f_j} \leq 0 \quad l \in L \tag{3.39}$$

$$N_l - \underline{f_i}e_j - \underline{e_j}f_i + \underline{f_i}\,\underline{e_j} \geq 0 \quad l \in L \tag{3.40}$$

$$N_l - \overline{f_i}e_j - \overline{e_j}f_i + \overline{f_i}\,\overline{e_j} \geq 0 \quad l \in L \tag{3.41}$$

$$N_l - \underline{f_i}e_j - \overline{e_j}f_i + \underline{f_i}\,\overline{e_j} \leq 0 \quad l \in L \tag{3.42}$$

$$N_l - \overline{f_i}e_j - \underline{e_j}f_i + \overline{f_i}\underline{e_j} \leq 0 \quad l \in L \tag{3.43}$$

$$R_i - 2\underline{e_i}e_i + \underline{e_i^2} \geq 0 \quad i \in B \tag{3.44}$$

$$R_l - 2\overline{e_i}e_i + \overline{e_i^2} \geq 0 \quad i \in B \tag{3.45}$$

$$R_i - \left(\underline{e_i} + \overline{e_i}\right)e_i + \underline{e_i}\,\overline{e_i} \leq 0 \quad i \in B \tag{3.46}$$

$$H_i - 2\underline{f_i}f_i + \underline{f_i^2} \geq 0 \quad i \in B \tag{3.47}$$

$$H_i - 2\overline{f_i}f_i + \overline{f_i^2} \geq 0 \quad i \in B \tag{3.48}$$

$$H_l - \left(\underline{f_i} + \overline{f_i}\right)f_i + \underline{f_i}\,\overline{f_i} \leq 0 \quad i \in B \tag{3.49}$$

$$\underline{e_i} \leq e_i \leq \overline{e_i}, \quad \underline{f_i} \leq f_i \leq \overline{f_i} \quad i \in N_P \tag{3.50}$$

where $\widehat{U_i}$ is the scheduled voltage magnitude for PV bus i; $\widehat{e}$ and $\widehat{f}$ are the given real and imaginary parts of reference bus voltage.

It should be noted that (3.23) formulates the interval voltage magnitude of each bus. Intervals of other system statuses including voltage angle, branch reactive and active power of power flow, can be established through changing the model's objective as follows and adding additional constraints.

(a) **Voltage angle**

The voltage angle interval can be obtained by solving the original IPF-QCQP problem with replaced objective function $\theta_i = \arctan\left(\frac{f_i}{e_i}\right)$.

Note that voltage angles are normally between $[-\pi/2, +\pi/2]$, in which tangent function is monotonous. Therefore, we can firstly solve an IPF-QCQP problem with (3.51) as objective function to get the interval of a new dummy vector y, where yi = fi/ei, and then calculate the voltage angle interval using θi = arctan(yi). After

reformulating yi = fi/ei as a quadratic constraint fi = eiyi, linear relaxation method in Chap. 2 is used again for eiyi to generate (3.52)–(3.55). Combining (3.24)–(3.50) and (3.52)–(3.55) together with the objective (3.51), we can obtain the improved interval solution of yi.

$$\max/\min_{\{\boldsymbol{X},\boldsymbol{Y},\boldsymbol{M},\boldsymbol{N},\boldsymbol{R},\boldsymbol{H},\boldsymbol{e},\boldsymbol{f}\}} \quad y_i \tag{3.51}$$

$$f_i - \underline{e_i} y_i - \underline{y_i} e_i + \underline{e_i}\,\underline{y_i} \geq 0 \quad i \in B \tag{3.52}$$

$$f_i - \overline{e_i} y_i - \overline{y_i} e_i + \overline{e_i}\,\overline{y_i} \geq 0 \quad i \in B \tag{3.53}$$

$$f_i - \underline{e_i} y_i - \overline{y_i} e_i + \underline{e_i}\,\overline{y_i} \leq 0 \quad i \in B \tag{3.54}$$

$$f_i - \overline{e_i} y_i - \underline{y_i} e_i + \overline{e_i}\,\underline{y_i} \leq 0 \quad i \in B \tag{3.55}$$

(b) **Branch active and reactive power**

The original form of branch active and reactive power is formulated in (3.56) and (3.57). Using the aforementioned susceptance and conductance matrices as well as the dummy variable vectors, (3.56) and (3.57) can be expressed in linear representation as in (3.58) and (3.59) respectively.

$$\max/\min \quad P_{ij} = e_i G_{ij} e_j - e_i B_{ij} f_j + f_i G_{ij} f_j + f_i B_{ij} e_j \tag{3.56}$$

$$\max/\min \quad Q_{ij} = f_i G_{ij} e_j - f_i B_{ij} f_j - e_i G_{ij} f_j - e_i B_{ij} e_j \tag{3.57}$$

$$\max/\min_{\{\boldsymbol{X},\boldsymbol{Y},\boldsymbol{M},\boldsymbol{N},\boldsymbol{R},\boldsymbol{H},\boldsymbol{e},\boldsymbol{f}\}} \quad W_{i,l}^G X_l - W_{i,l}^B M_l + W_{i,l}^G Y_l + W_{i,l}^B N_l \tag{3.58}$$

$$\max/\min_{\{\boldsymbol{X},\boldsymbol{Y},\boldsymbol{M},\boldsymbol{N},\boldsymbol{R},\boldsymbol{H},\boldsymbol{e},\boldsymbol{f}\}} \quad W_{i,l}^G N_l - W_{i,l}^B Y_l - W_{i,l}^G M_l - W_{i,l}^B X_l \tag{3.59}$$

(c) **Generator's reactive power**

As for generator's reactive power, the original form is formulated in (3.60). Similarly, (3.60) can be expressed in linear representation as in (3.61) according to the aforementioned method. Under power injection variations, generators' reactive power output may exceed its limit, given the scheduled voltage. In this situation, the PV bus will be converted to PQ bus with reactive power assigned to the limiting value, and the solution needs to be recalculated.

$$\max/\min \quad f_i \sum_{j=1}^{n} \left(G_{ij} e_j - B_{ij} f_j\right) - e_i \sum_{j=1}^{n} \left(G_{ij} f_j + B_{ij} e_j\right) \tag{3.60}$$

$$\max/\min_{\{\boldsymbol{X},\boldsymbol{Y},\boldsymbol{M},\boldsymbol{N},\boldsymbol{R},\boldsymbol{H},\boldsymbol{e},\boldsymbol{f}\}} \quad K_i^B R_i + K_i^B H_i + \sum_{l=1}^{s}\left(W_{i,l}^G N_l - W_{i,l}^B Y_l - W_{i,l}^G M_l - W_{i,l}^B X_l\right) \quad i \in N_{PV} \tag{3.61}$$

3.2.2.3 Optimality Based Bound Tightening Technique

An initial estimation of the solution interval is obtained as follows by linearizing power flow at a given operating point (e0, f0) with the Jacobi matrix J calculated by (3.63) and applying an offset ($\left[\underline{\boldsymbol{e}^{ED}}, \overline{\boldsymbol{e}^{ED}}\right], \left[\underline{\boldsymbol{f}^{ED}}, \overline{\boldsymbol{f}^{ED}}\right]$) to ensure optimal solution bound is within the initial estimation.

$$\begin{bmatrix} [\underline{\boldsymbol{e}}^0, \overline{\boldsymbol{e}}^0] \\ [\underline{\boldsymbol{f}}^0, \overline{\boldsymbol{f}}^0] \end{bmatrix} = \begin{bmatrix} [\boldsymbol{e}_0, \boldsymbol{e}_0] \\ [\boldsymbol{f}_0, \boldsymbol{f}_0] \end{bmatrix} + \boldsymbol{J}^{-1} \begin{bmatrix} [\underline{\boldsymbol{P}}, \overline{\boldsymbol{P}}] \\ [\underline{\boldsymbol{Q}}, \overline{\boldsymbol{Q}}] \end{bmatrix} + \begin{bmatrix} \left[\underline{\boldsymbol{e}^{ED}}, \overline{\boldsymbol{e}^{ED}}\right] \\ \left[\underline{\boldsymbol{f}^{ED}}, \overline{\boldsymbol{f}^{ED}}\right] \end{bmatrix} \tag{3.62}$$

$$\boldsymbol{J} = \begin{bmatrix} \frac{\partial \underline{\boldsymbol{P}}}{\partial \boldsymbol{e}} & \frac{\partial \underline{\boldsymbol{P}}}{\partial \boldsymbol{f}} \\ \frac{\partial \underline{\boldsymbol{Q}}}{\partial \boldsymbol{e}} & \frac{\partial \underline{\boldsymbol{Q}}}{\partial \boldsymbol{f}} \end{bmatrix}\Bigg|_{\boldsymbol{e}_0, \boldsymbol{f}_0} \tag{3.63}$$

After the process stops (and OBBT algorithm converges), the optimally tightened convex hull LRΩ* with hyper-rectangular variable domain Ω* and the corresponding interval solution are obtained. Because the dummy vector y is a component of x, the interval solution of bus angle is immediately available. Linear programming models in (3.64)–(3.67) are solved for interval solution of bus voltage, branch active and reactive power and generator's reactive power respectively. Linear programming models instead of interval operation using (2.23), (2.58) and (2.59) are utilized to avoid conservative operations of IA due to the correlation among dummy variables X, M, Y, N, R and H.

$$\left[\underline{U_i^2}, \overline{U_i^2}\right] = \begin{cases} \overline{U_i^2} \leftarrow \{\max\ (29) \quad s.t.\ LR_{\Omega^*}(\boldsymbol{x}) \cap \Omega^*\} \\ \underline{U_i^2} \leftarrow \{\min\ (29) \quad s.t.\ LR_{\Omega^*}(\boldsymbol{x}) \cap \Omega^*\} \end{cases} \text{for } \forall\, i \in N_{PQ} \tag{3.64}$$

$$\left[\underline{P_l}, \overline{P_l}\right] = \begin{cases} \overline{P_l} \leftarrow \{\max\ (91) \quad s.t.\ LR_{\Omega^*}(\boldsymbol{x}) \cap \Omega^*\} \\ \underline{P_l} \leftarrow \{\min\ (91) \quad s.t.\ LR_{\Omega^*}(\boldsymbol{x}) \cap \Omega^*\} \end{cases} \text{for } \forall\, l \in L \tag{3.65}$$

$$\left[\underline{Q_l}, \overline{Q_l}\right] = \begin{cases} \overline{Q_l} \leftarrow \{\max\ (92) \quad s.t.\ LR_{\Omega^*}(\boldsymbol{x}) \cap \Omega^*\} \\ \underline{Q_l} \leftarrow \{\min\ (92) \quad s.t.\ LR_{\Omega^*}(\boldsymbol{x}) \cap \Omega^*\} \end{cases} \text{for } \forall\, l \in L \tag{3.66}$$

$$\left[\underline{Q_k}, \overline{Q_k}\right] = \begin{cases} \overline{Q_k} \leftarrow \{\max\ (94) \quad s.t.\ LR_{\Omega^*}(\boldsymbol{x}) \cap \Omega^*\} \\ \underline{Q_k} \leftarrow \{\min\ (94) \quad s.t.\ LR_{\Omega^*}(\boldsymbol{x}) \cap \Omega^*\} \end{cases} \text{for } \forall\, l \in L \tag{3.67}$$

It should be noted that, (3.64)–(3.67) represent an improved and tighter outer hull of original feasible space. Besides, as the interval solutions of bus voltage and branch active and reactive power can be solved independently, parallel computing can be utilized to further improve the computing efficiency.

3.2.2.4 Numerical Results

A. *9-bus System and Comparison with Monte Carlo Simulation*

A 9-bus test system available in [1] was analyzed using the proposed methodology, with a ±10 % variation on load and generation. The computation was performed using MATPOWER, YALMIP and CPLEX 12.4 on a personal computer with Intel® Core™ i5 Duo Processor T420 (2.50 GHz) and 8 GB RAM. The interval solutions obtained by solving for the maximum and minimum of voltage magnitudes and angles for load bus (a.k.a. PQ buses) and generator bus (a.k.a. PV buses), as well as line flows, were listed in Tables 3.4 and 3.5 Results for transmission buses were not presented for simplicity. The results were verified by comparing with Monte Carlo (MC) stochastic simulation results, which randomly samples power injection for 5000 trials to get maximum/minimum voltage magnitude and angle of each bus. Here, we assume Monte Carlo simulation (MC) with sufficient number of samples can yield the "correct" interval solutions.

From the comparison between proposed method and Monte Carlo simulation, it's seen that the proposed method can estimate the upper/lower bound of voltage magnitude with maximum error no more than 0.5 %. Furthermore, the ratio between the length of intervals obtained from the MC simulation and those obtained from the proposed method is presented in the last column of Tables 3.4 and 3.5. The ratio is mostly in the range of 60–90 %, indicating the estimated interval length is reasonably enlarged compared to that from MC method.

It should also be noted that, when one variable happens to sit at the interval lower or upper bound at a given scenario, the other variables don't necessarily sit at their respective interval bounds.

B. *57-bus System and Comparison with Affine Arithmetic Method and Monte Carlo Simulation Method*

The proposed method was also verified on the IEEE 57-bus system, with a ±20 % variation on load and generator powers. The results were compared with those of Monte Carlo (MC) simulation with 5000 sample size. Figures 3.3 and 3.4 depict the interval lower and upper bounds for voltage magnitudes and angles; Figs. 3.5 and 3.6 show the interval results of branch active and reactive power flows. The comparison between QCQP and MC simulation illustrates the effectiveness of the proposed method, and the maximum error of voltage magnitude is no more than 3 % and average error is about 1 %. The error of active/reactive power flow intervals is also very small, which demonstrates the effectiveness of the proposed method.

Table 3.4 Interval solutions of voltage magnitudes and angles obtained from proposed method and Monte Carlo simulation method

Bus	Certain power flow		Proposed method		Monte Carlo simulation		Ratio	
	Voltage magnitude	Voltage angle	Voltage magnitude	Voltage angle	Voltage magnitude	Voltage angle	Voltage magnitude	Voltage angle
2	1.0000	9.669	[1.0000, 1.0000]	[6.9500, 12.0149]	[1.0000, 1.0000]	[7.7890, 11.5835]	1.0000	0.7492
3	1.0000	4.771	[1.0000, 1.0000]	[2.1429, 7.0130]	[1.0000, 1.0000]	[2.9662, 6.6251]	1.0000	0.7513
5	0.975	−4.017	[0.9671, 0.9824]	[−6.0676, −2.2632]	[0.9706, 0.9803]	[−5.3230, −2.4996]	0.6340	0.7421
7	0.986	0.622	[0.9795, 0.9906]	[−2.3491, 3.1513]	[0.9815, 0.9890]	[−1.4711, 2.6737]	0.6757	0.7535
9	0.958	−4.350	[0.9458, 0.9669]	[−6.5374, −2.4981]	[0.9473, 0.9645]	[−5.8153, −2.6864]	0.8152	0.7746

Table 3.5 Interval solutions of active and reactive line flows obtained from proposed method and Monte Carlo simulation method

Line	Certain power flow		Proposed method		Monte Carlo simulation		Ratio	
	Active power	Reactive power	Active power	Reactive power	Active power	Reactive power	Active power	Reactive power
1–4	71.95	24.07	[45.25, 101.41]	[16.97,31.66]	[47.63, 98.14]	[18.01, 29.96]	0.8994	0.8135
4–5	30.73	−0.59	[16.85, 44.76]	[−4.63, 3.51]	[18.42, 42.62]	[−3.52, 2.23]	0.8671	0.7064
5–6	−59.45	−16.31	[−66.68, −52.17]	[−18.96, −13.97]	[−65.95, −54.05]	[−17.87, −14.77]	0.8201	0.6212
3–6	85.00	−3.65	[84.94, 85.19]	[−8.07, 0.92]	[85.00,85.00]	[−6.72,−0.33]	–	0.8937
6–7	24.11	4.54	[16.48, 31.71]	[2.07, 7.08]	[17.26, 29.77]	[2.67, 6.38]	0.8214	0.7405
7–8	−75.99	−10.60	[−84.11, −67.87]	[−13.95, −7.17]	[−82.43, −69.16]	[−12.99,−8.15]	0.8171	0.7139
8–2	−163.00	2.28	[−163.07, −162.96]	[−2.59, 6.93]	[−163.00, −163.00]	[−1.45, 5.77]	–	0.7584
8–9	86.50	−2.53	[78.31,94.69]	[−6.34, 1.51]	[79.98, 93.42]	[−5.31, 0.78]	0.8205	0.7758
9–4	−40.96	−35.72	[−58.25, −23.84]	[−40.68, −30.78]	[−55.38, −26.53]	[−39.63, −31.97]	0.8384	0.7737

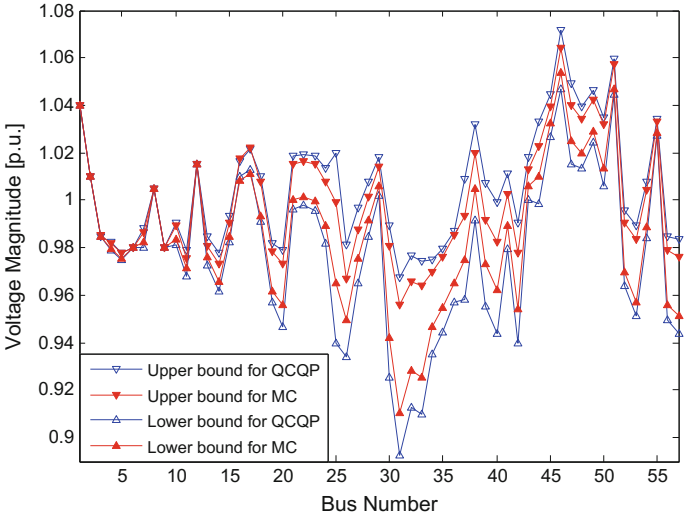

Fig. 3.3 Bounds of voltage magnitudes under 20 % variation

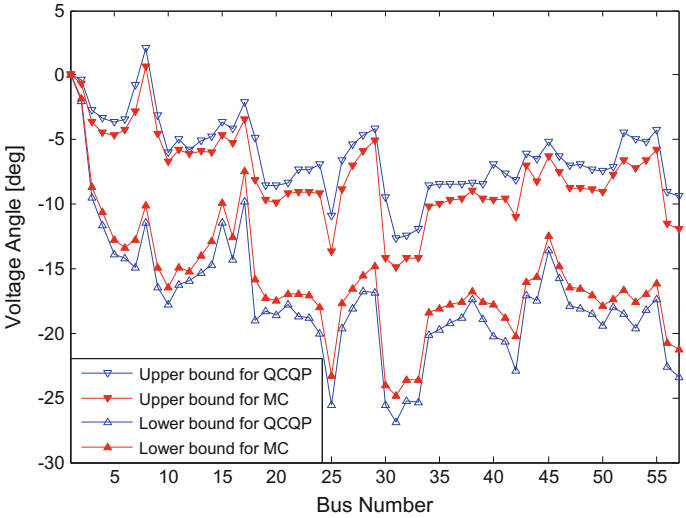

Fig. 3.4 Bounds of voltage angles under 20 % variation

Furthermore, in comparison to Affine Arithmetic method [2], we can see that the proposed method produces lower bounds and upper bounds that are significantly closer to the true lower and upper bounds obtained from Monte Carlo Simulation method, than AA method does. Particularly, estimated intervals for some buses

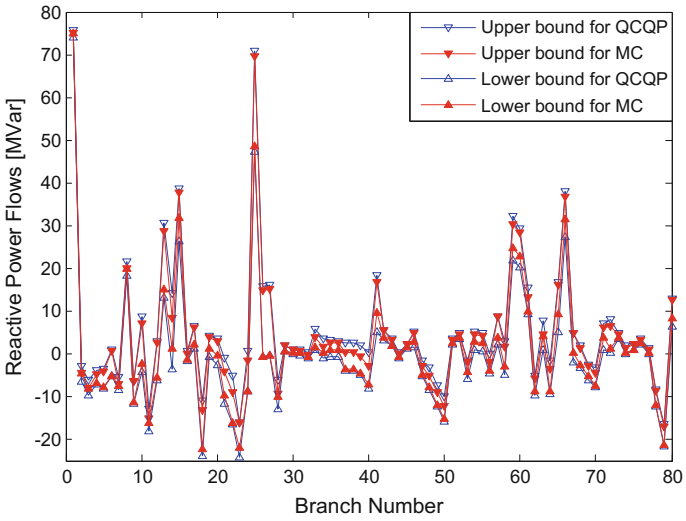

Fig. 3.5 Bounds of active power flows under 20 % variation

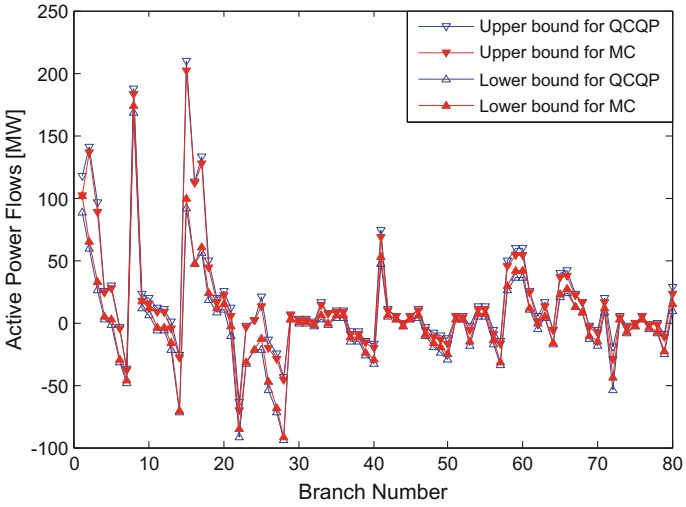

Fig. 3.6 Bounds of reactive power flows under 20 % variation

such as bus 23, 31, and 37 using the proposed method are much better than those using AA method. The performance improvement of the proposed method over AA method has been observed in both voltage magnitude bounds and voltage angle bounds, which is because the proposed method only involves very limited interval arithmetic operations.

It should also be pointed out that, the proposed method arrives at a better solution than AA method at the cost of more computation time. For example, it took the proposed method about 19 s (8 % of simulation time by MC simulation) to obtain the interval solution whereas it only took AA method 7 s (3 % of simulation time by MC simulation).

C. *Reactive Power Limit*

Table 3.6 lists the generator reactive power limit and scheduled voltage, the initial interval analysis results for reactive power and voltage magnitude before bus type conversion, and the final interval analysis results after bus type conversion. The 'Initial solution' column represents the case without considering reactive power limit, and 'Final solution' column shows the case with reactive power limit considered. Table 3.6 also shows reactive power outputs of generator 3, 9 and 12 are out of limit, as highlighted in red and bold font. Therefore, the bus types for those generator buses are changed from PV to PQ and the solution is recalculated.

Taking generator 9 as an example, the interval results of the proposed method are compared with those of MC simulation in Figs. 3.7 and 3.8. With the violation of reactive power limit, generation 9's bus type is switched to PQ bus, and the generator bus voltage magnitude will not hold constant any more. Rather, it becomes an interval [0.977, 0.984] as shown in Fig. 3.7, whereas the true interval of voltage magnitude is [0.9775, 0.9821].

Figure 3.8 illustrates that estimated reactive power interval for generator bus with bus type conversion is also very close to the true interval. Furthermore, Fig. 3.9 and 3.10 show the impact of different uncertainty level on voltage

Table 3.6 Interval solution of generator reactive power and voltage magnitude with reactive power limit enforced

Gen No.	Limit		Initial solution		Final solution	
	Reactive power	Voltage	Reactive power	Voltage	Reactive power	Voltage
1	[−140,200]	1.040	[114.82,146.72]	[1.040, 1.040]	[114.82,146.72]	[1.040, 1.040]
2	[−17,50]	1.010	[−2.14,1.74]	[1.010, 1.010]	[−2.14,1.74]	[1.010, 1.010]
3	[−10,60]	0.985	[−13.20,15.54]	[0.985, 0.985]	[−10.00,15.54]	[0.980, 0.994]
6	[−8,25]	0.980	[−7.46,10.15]	[0.980, 0.980]	[−7.46,10.15]	[0.980, 0.980]
8	[−140,200]	1.005	[51.34,73.56]	[1.005, 1.005]	[51.34,73.56]	[1.005, 1.005]
9	[−3,9]	1.000	[−11.19,16.75]	[1.000, 1.000]	[−3.00,9.00]	[0.977, 0.984]
12	[−150,155]	1.015	[95.66,169.87]	[1.015, 1.015]	[95.66,155.00]	[1.006, 1.022]

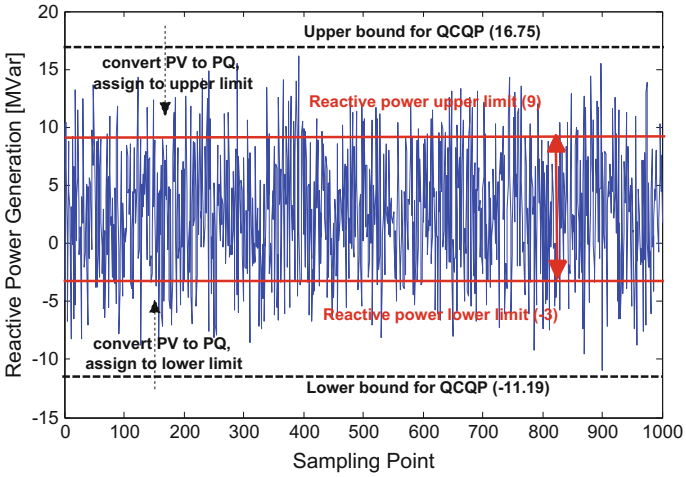

Fig. 3.7 Generator 9's reactive power of proposed method and Monte

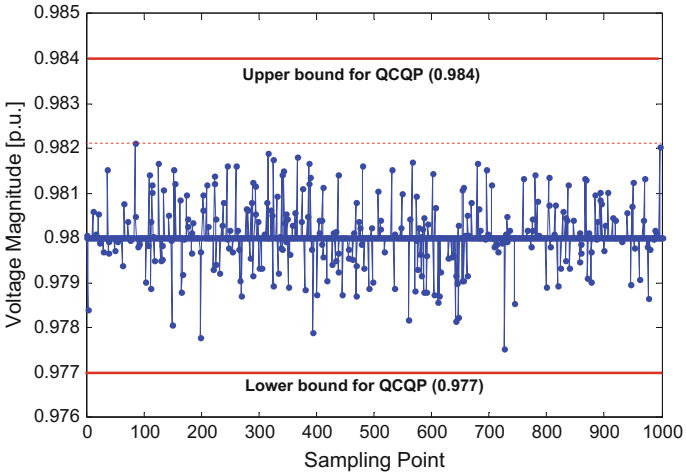

Fig. 3.8 generator 9's voltage magnitude of proposed method and Carlo simulation method Monte Carlo simulation method

magnitude without/with reactive power limit respectively. It is observed that more generators may reach to their limits with the increase of power injection uncertainty, and the voltage magnitude intervals of all buses become wider, especially for bus 3 to bus 15 which are close to the generator buses that are converted to PQ buses.

Lastly, it should be pointed out the interval solution from MC method by its nature is a subset of the true interval, while the solutions from the proposed method and AA method are supersets of the true interval, as illustrated in Fig. 3.11. In other

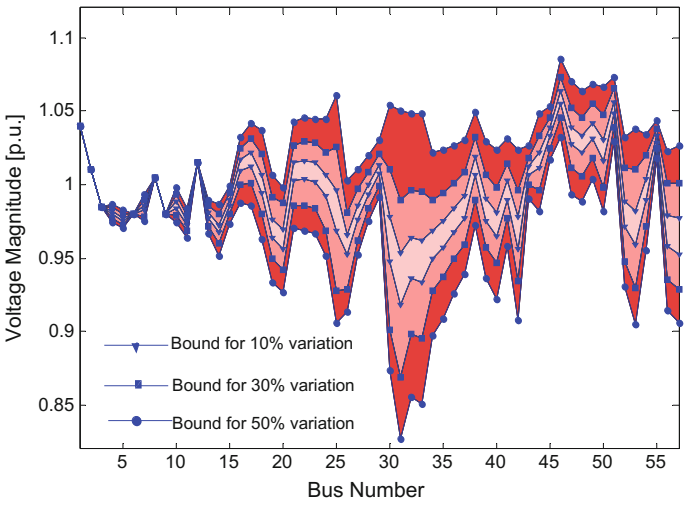

Fig. 3.9 Impact of variation level on voltage magnitude

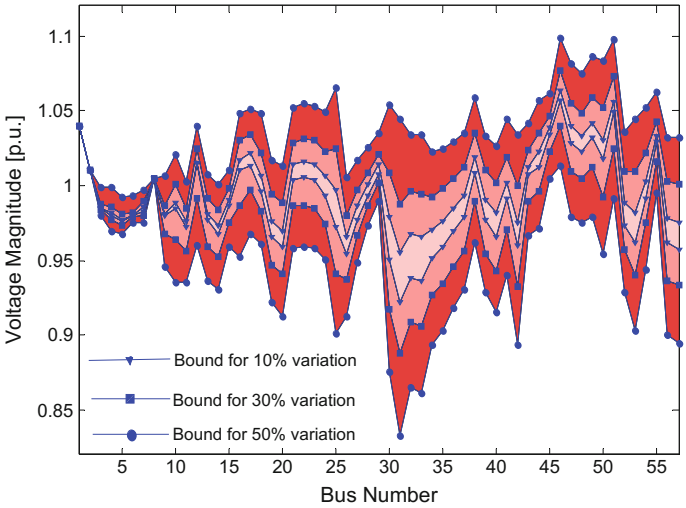

Fig. 3.10 Impact of variation level on voltage magnitude without reactive power limit with reactive power limit

words, MC method gives an underestimated interval length and the proposed method produces an overestimated interval length. Therefore, the proposed method is suitable for application where the full range of the true interval needs to be captured.

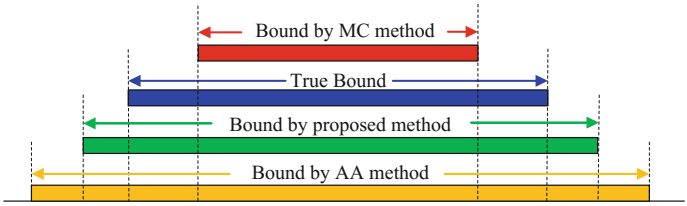

Fig. 3.11 Illustration of interval solution from different methods

3.2.3 Interval Radial Power Flow

3.2.3.1 Modeling of Interval Distribution Power Flow

It has been well recognized that the power flow in a radial network can be formed by a set of recursive equations, which was proposed in [5], called DistFlow. Please keep in mind that a radial network with n buses has n − 1 branches, since there is no circle; this is also recognized as a spanning tree in the graph theory.

However, the exact DistFlow equations take on a nonlinear characteristic due to the nonlinear network loss. In order to approximate the nonlinear term to fast compute the radial power flow, two simplified DistFlow methods had been proposed and identified in [6]. The first method is to directly drop the nonlinear network loss, and the other method is to approximate the nonlinear term to a quadratic one. These two simplified methods will be explicitly addressed in the following work.

Moreover, with the consideration of uncertain active and reactive power injection, the interval numbers are employed. The uncertain active and reactive power injection of ith bus are represented by an interval number, respectively (i.e., $\langle P_i \rangle$ and $\langle Q_i \rangle$). The interval power flow is therefore intended to obtain the interval voltage magnitude of each bus, active and reactive power of each branch.

A. Dropping network loss

For a simple radial network with n + 1 buses and n branches in Fig. 3.12, the simplified equations without considering the network loss can be written as

$$\begin{cases} \langle P_{i+1} \rangle = \langle H_{i+1} \rangle - \langle H_i \rangle \\ \langle Q_{i+1} \rangle = \langle G_{i+1} \rangle - \langle G_i \rangle \\ \left\langle U_{i+1}^2 \right\rangle = \left\langle U_i^2 \right\rangle - 2(r_i \langle H_i \rangle + x_i \langle G_i \rangle) \end{cases}, \quad i = 1, \ldots, n \tag{3.68}$$

where ri and xi denote the resistance and reactance of the i-th branch; $<H_i>$ and $<G_i>$ denote the interval active and reactive power on i-th branch; $<U_i>$, $<P_i>$, and $<Q_i>$ denote the voltage magnitude, injected active power, and reactive power at i-th bus, respectively. It can be observed that the power flow on the i-th branch is from i-th bus to $(i + 1)$-th bus.

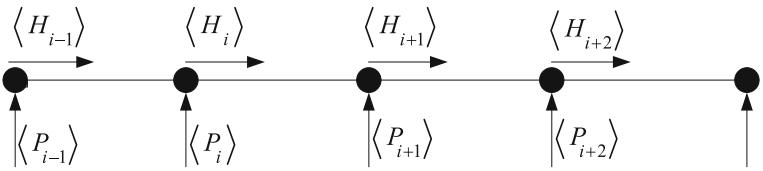

Fig. 3.12 A simple radial network with active power flow

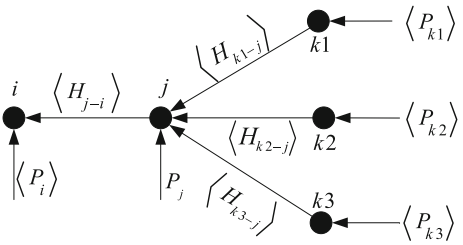

Fig. 3.13 A general radial network with active power flow

However, there may be multiple feeders for one bus, and the bus and branch order may not be the same as that in Fig. 3.12. Therefore, in order to obtain a versatile expression for a general radial network, we will first set up a direction topology where we let the positive direction of branch power flow from "from" bus to "to" bus, shown in Fig. 3.13. Furthermore, the simplified DistFlow can be extended to (3.69).

$$\begin{cases} \langle P_i\rangle = \sum\limits_{l\in L_f^i}\langle H_l\rangle - \sum\limits_{l\in L_t^i}\langle H_l\rangle \\ \langle Q_i\rangle = \sum\limits_{l\in L_f^i}\langle G_l\rangle - \sum\limits_{l\in L_t^i}\langle G_l\rangle \\ \left\langle U_{l-f}^2\right\rangle = \langle U_{l-t}^2\rangle + 2(r_l\langle H_l\rangle + x_l\langle G_l\rangle) \end{cases}, \quad \begin{matrix} i = 1,\ldots,n+1 \\ l = 1,\ldots,n \end{matrix} \tag{3.69}$$

where <Ul-f> and <Ul-t> are the "from" and "to" bus of l-th branch; Lif and Lit are the branch sets with its "from" and "to" bus connected to the i-th bus, respectively.

In the matrix form, Eq. (3.69) can be reformulated as

$$\begin{cases} \langle \overline{\boldsymbol{P}}\rangle = \overline{\boldsymbol{S}}^T\langle \boldsymbol{H}\rangle, \quad \langle \overline{\boldsymbol{Q}}\rangle = \overline{\boldsymbol{S}}^T\langle \boldsymbol{G}\rangle \\ \overline{\boldsymbol{S}}\left\langle \overline{\boldsymbol{U}}^2\right\rangle = 2\boldsymbol{R}\langle \boldsymbol{H}\rangle + 2\boldsymbol{X}\langle \boldsymbol{G}\rangle \end{cases} \tag{3.70}$$

with $(\overline{\boldsymbol{S}})_{n\times(n+1)} = \left[\boldsymbol{S}_1, \underset{ref}{\boldsymbol{e}}, \boldsymbol{S}_2\right]$, $(\boldsymbol{S})_{n\times n} = [\boldsymbol{S}_1, \boldsymbol{S}_2]$, where $\overline{\boldsymbol{S}}$ denotes the connection matrix whose (i, j)-th element equals to 1 if the branch i connects to "from" bus j; otherwise, it equals to −1 if the branch i connects to "to" bus j, and all other

elements are zero (e.g., R = diag(r1,…,rn) and X = diag(x1,…,xn)). However, the voltage magnitude of reference bus is already given; therefore, the reduced system is derived by

$$\begin{cases} \langle \boldsymbol{P} \rangle = \boldsymbol{S}^T \langle \boldsymbol{H} \rangle, \quad \langle \boldsymbol{Q} \rangle = \boldsymbol{S}^T \langle \boldsymbol{G} \rangle \\ \boldsymbol{S} \langle \boldsymbol{U}^2 \rangle = -\langle U_0^2 \rangle \boldsymbol{e} + 2\boldsymbol{R} \langle \boldsymbol{H} \rangle + 2\boldsymbol{X} \langle \boldsymbol{G} \rangle \end{cases} \tag{3.71}$$

Where $\langle U_0^2 \rangle = [U_0^2, U_0^2]$, U_0 is the voltage magnitude of the reference bus, and e is the column of $\overline{\boldsymbol{S}}$ corresponding to the reference bus. Therefore, the final interval radial power flow can be written in a matrix form as

$$\begin{pmatrix} \boldsymbol{S} & -2\boldsymbol{R} & -2\boldsymbol{X} \\ \boldsymbol{0} & \boldsymbol{S}^T & \boldsymbol{0} \\ \boldsymbol{0} & \boldsymbol{0} & \boldsymbol{S}^T \end{pmatrix} \begin{pmatrix} \langle \boldsymbol{U}^2 \rangle \\ \langle \boldsymbol{H} \rangle \\ \langle \boldsymbol{G} \rangle \end{pmatrix} = \begin{pmatrix} -\langle U_0^2 \rangle \boldsymbol{e} \\ \langle \boldsymbol{P} \rangle \\ \langle \boldsymbol{Q} \rangle \end{pmatrix} \tag{3.72}$$

B. Linearized approximation for network loss

While considering the nonlinear network loss, the exact DistFlow at the receiving end of the branch for a simple radial network in Fig. 3.13 can be presented as

$$\begin{cases} \langle P_i \rangle = \sum\limits_{l \in L_f^i} \langle H_l \rangle - \sum\limits_{l \in L_t^i} \left(\langle H_l \rangle - r_l \frac{\langle H_l^2 \rangle + \langle G_l^2 \rangle}{\langle U_i^2 \rangle} \right) \\ \langle Q_i \rangle = \sum\limits_{l \in L_f^i} \langle G_l \rangle - \sum\limits_{l \in L_t^i} \left(\langle G_l \rangle - x_l \frac{\langle H_l^2 \rangle + \langle G_l^2 \rangle}{\langle U_i^2 \rangle} \right) \\ \left\langle U_{l-f}^2 \right\rangle = \langle U_{l-t}^2 \rangle + 2(r_l \langle H_l \rangle + x_l \langle G_l \rangle) + \left(r_l^2 + x_l^2 \right) \frac{\langle H_l^2 \rangle + \langle G_l^2 \rangle}{\langle U_i^2 \rangle} \end{cases} \tag{3.73}$$

where the nonlinear term $\frac{\langle H_l^2 \rangle + \langle G_l^2 \rangle}{\langle U_i^2 \rangle}$ is approximated as

$$\frac{\langle H_l^2 \rangle + \langle G_l^2 \rangle}{\langle U_t^2 \rangle} \approx \frac{\langle H_l \rangle H_l^* + \langle G_l \rangle G_l^*}{\left(U_t^* \right)^2} \tag{3.74}$$

where Hl* and Gl* denote the normal deterministic active and reactive power of l-th branch; Ui* denotes the normal deterministic voltage magnitude of i-th bus.

In the matrix form, it is derived as

$$\begin{cases} \langle \boldsymbol{P} \rangle = \boldsymbol{S}^T \langle \boldsymbol{H} \rangle + \boldsymbol{C}^T (\boldsymbol{R}\boldsymbol{K}_H \langle \boldsymbol{H} \rangle) + \boldsymbol{C}^T (\boldsymbol{R}\boldsymbol{K}_G \langle \boldsymbol{G} \rangle) \\ \langle \boldsymbol{Q} \rangle = \boldsymbol{S}^T \langle \boldsymbol{G} \rangle + \boldsymbol{C}^T (\boldsymbol{X}\boldsymbol{K}_H \langle \boldsymbol{H} \rangle) + \boldsymbol{C}^T (\boldsymbol{X}\boldsymbol{K}_G \langle \boldsymbol{G} \rangle) \\ \boldsymbol{S} \langle \boldsymbol{U}^2 \rangle = -\langle U_0^2 \rangle \boldsymbol{e} + 2\boldsymbol{R} \langle \boldsymbol{H} \rangle + 2\boldsymbol{X} \langle \boldsymbol{G} \rangle + \left(\boldsymbol{X}^T \boldsymbol{X} + \boldsymbol{R}^T \boldsymbol{R} \right) (\boldsymbol{K}_H \langle \boldsymbol{H} \rangle + \boldsymbol{K}_G \langle \boldsymbol{G} \rangle) \end{cases} \tag{3.75}$$

where C is a matrix with (i, j)-th element being 1, assuming that branch i connects to “to” bus j and zero; otherwise, KH and KG refer to

$$\boldsymbol{K}_H = \mathrm{diag}\left(\frac{H_1^*}{\left(U_{1-t}^*\right)^2}, \ldots, \frac{H_n^*}{\left(U_{n-t}^*\right)^2}\right),\ \boldsymbol{K}_G = \mathrm{diag}\left(\frac{G_1^*}{\left(U_{1-t}^*\right)^2}, \ldots, \frac{G_n^*}{\left(U_{n-t}^*\right)^2}\right)$$

For simplification, we will arrive at

$$\begin{pmatrix} \boldsymbol{S} & -2\boldsymbol{R} - \left(\boldsymbol{X}^T\boldsymbol{X} + \boldsymbol{R}^T\boldsymbol{R}\right)\boldsymbol{K}_H & -2\boldsymbol{X} - \left(\boldsymbol{X}^T\boldsymbol{X} + \boldsymbol{R}^T\boldsymbol{R}\right)\boldsymbol{K}_G \\ \boldsymbol{0} & \boldsymbol{S}^T + \boldsymbol{C}^T\boldsymbol{R}\boldsymbol{K}_H & \boldsymbol{C}^T\boldsymbol{R}\boldsymbol{K}_G \\ \boldsymbol{0} & \boldsymbol{C}^T\boldsymbol{X}\boldsymbol{K}_H & \boldsymbol{S}^T + \boldsymbol{C}^T\boldsymbol{X}\boldsymbol{K}_G \end{pmatrix} \begin{pmatrix} \langle \boldsymbol{U}^2 \rangle \\ \langle \boldsymbol{H} \rangle \\ \langle \boldsymbol{G} \rangle \end{pmatrix} = \begin{pmatrix} -\langle U_0^2 \rangle \boldsymbol{e} \\ \langle \boldsymbol{P} \rangle \\ \langle \boldsymbol{Q} \rangle \end{pmatrix} \tag{3.76}$$

Interestingly, it can be found from (3.75) and (3.76) that the interval DistFlow with and without considering network loss have the same mathematical formulation, i.e., $\boldsymbol{A}\langle \boldsymbol{x} \rangle = \langle \boldsymbol{b} \rangle$. Moreover, it can be found that the formulation is similar to the interval DC power flow, where the coefficient matrices are constant and the intervals exist only in the right hand side. The difference is that the matrix in this formulation is asymmetric and non-diagonal dominant matrix.

3.2.3.2 Numerical Results

The proposed method in Sect. 2.2 is compared with Monte Carlo Simulation and interval Gauss elimination method on 33-bus, 69-bus, 123-bus, and several large radial network test systems, available from [1], where the proposed methodology is implemented with uncertainties on load and generator powers. The computational tasks were performed using the MATPOWER toolbox of Matlab on a 2.0 GHz personal computer with 2 GB RAM.

(a) **33-bus system**

A 33-bus radial system was plotted in Fig. 3.14, where the bus 1 is the reference bus and the others are all load buses (a.k.a., PQ bus). Considering the ±20 % variation on load demands, it could be observed that this would define an interval wide enough to properly evaluate the proposed method. Compared with the 5000 Monte Carlo simulation (MCS), interval solutions defined by the upper endpoint and power endpoint of the voltage magnitude of all buses—as well as line flows—were obtained by the proposed method in Figs. 3.15, 3.16, and 3.17, respectively. Here, the method ignoring the transmission loss refers to "M1," the method with approximate transmission loss is denoted as "M2," and the Monte Carlo simulation is "M3." Note that we assume results from the MCS are the true value. Observe that the lower and upper bounds of power flow from the proposed method are very close to that of the MCS. Notably, the method with approximate transmission loss is more realistic to the true value—compared to ignoring the loss and the maximum and

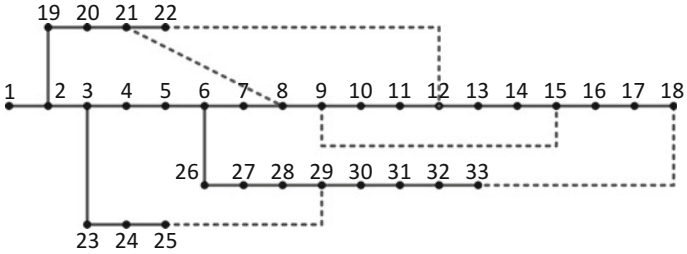

Fig. 3.14 A 33-bus radial network topolog

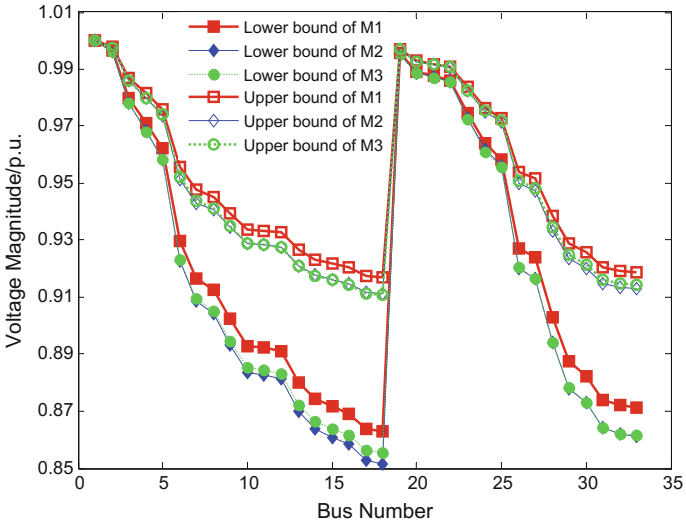

Fig. 3.15 Bounds of voltage magnitude

average error of the two methods—for voltage magnitude U, branch active power H, and branch reactive power G (shown in Table 3.7).

Next, we will study the impact of dropping tolerance on the convergence performance and the sparsity of approximate inverse matrices. Consider the method ignoring the network loss for instance, and the four choices of tolerance are given as 5, 1, 0.5, and 0 % (no dropping). Figure 3.18 depicts the convergence process of approximation inverse matrix (left figure) and Krawczyk iteration (right figure). It shows that the norm λ increases at the beginning and further decreases below 1. Moreover, it needs more iteration for a larger η, since the dropping technology may destroy the Newton iteration form of the original 2-norm optimization model. As for Krawczyk iteration, it can be institutively found from the proof of Corollary 1 that smaller λ for Krawczyk method (i.e., the last value of left by the figure) seems

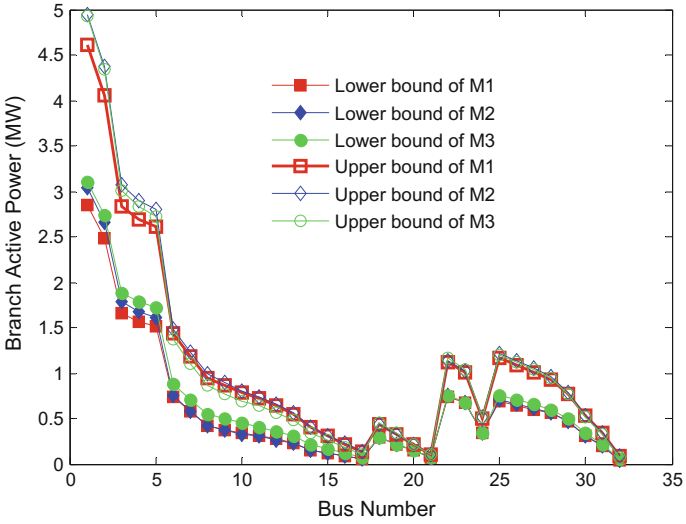

Fig. 3.16 Bounds of branch active power

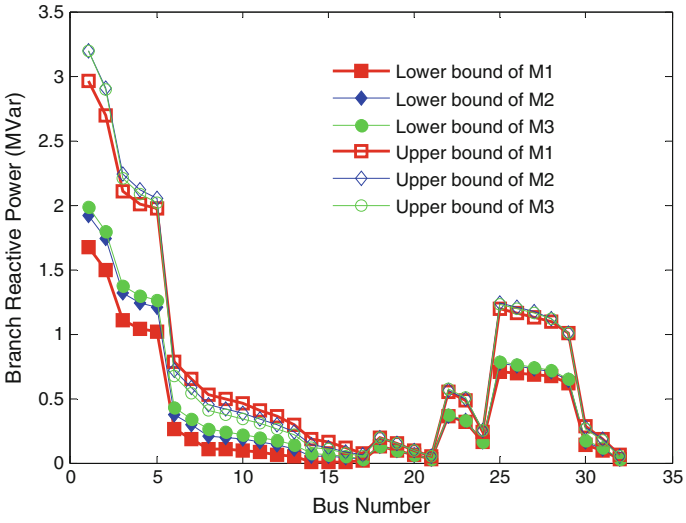

Fig. 3.17 Bounds of branch reactive power

to have faster convergence. Perhaps it is true for most conditions, but it fails in the case of $\eta = 5\ \%$ and $1\ \%$.

Importantly, it should be noted that $\eta = 5\ \%$ comes out with more iterations, but the computation time for each iteration may be reduced due to the sparsity. In addition, the number of nnz elements is employed to measure the sparsity of the

Table 3.7 Error of the proposed methods for interval power flow

	M1				M2			
	Upper bound		Lower bound		Upper bound		Lower bound	
	Max. (%)	Ave. (%)	Max. (%)	Ave. (%)	Max. (%)	Ave. (%)	Max. (%)	Ave. (%)
U	0.65	0.41	2.22	0.13	0.36	0.19	0.35	0.09
H	1.65	0.79	2.38	1.18	1.27	0.54	1.72	0.87
G	2.42	0.79	4.18	1.42	1.19	0.30	1.71	0.49

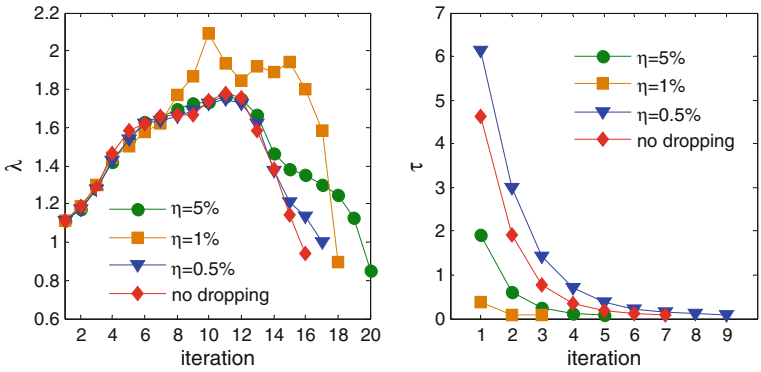

Fig. 3.18 Influence of dropping tolerance (η) on convergence performance

approximate inverse matrix. It is interesting from Fig. 3.19 that the exact inverse matrix is also a sparse matrix with nnz = 2813 (i.e., the density is 30.52 %), while the approximate inverse matrix without dropping will lead to a density matrix with nnz = 9216 (i.e., 100 %). In contrast, the approximate matrix with larger dropping tolerance results in sparser approximate inverse matrix (i.e., smaller nnz). Unfortunately, η should not be chosen too large, which would make the Newton iteration for approximate inverse matrix divergent (e.g., η > 7 %).

(b) **69-bus system**

For 69-bus system in Fig. 3.20, we consider 10 renewable resources, which can be taken as a negative load for power flow at a steady state; the ratio of total renewable resource generation to the total load demand is 11.4 %. Certainly, the uncertainties on renewable resources are larger than load demand, so we define βr and βl to represent the variation on them, respectively. Generally, βr is about 20–40 % and βl is about 5–10 %. We set three scenarios such that S1 denotes (βr = 20 %, βl = 5 %), S2 denotes (βr = 40 %, βl = 5 %), and S3 denotes (βr = 20 %, βl = 10 %). The three scenarios are simulated by the proposed method with the consideration of the network loss. Figure 3.21 shows that the interval range of voltage magnitude will be enlarged with an increase of both βr and βl, and in this case, the load uncertainties have more impact on the bounds of voltage magnitude.

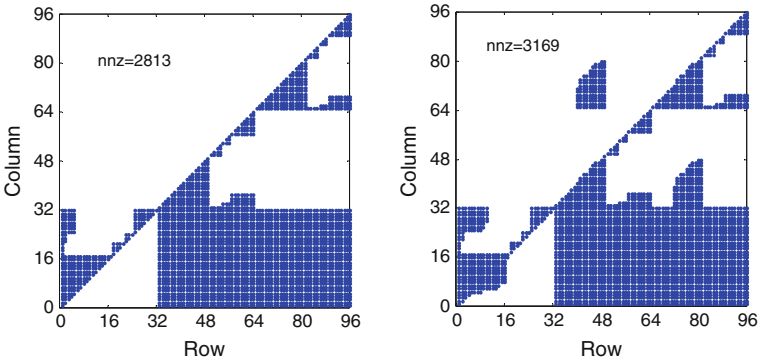

(a) Exact inverse matrix

(b)Approximate inverse matrix (η=5%)

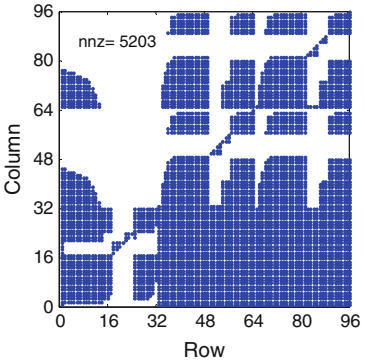

(c) Approximate inverse matrix (η=1%)

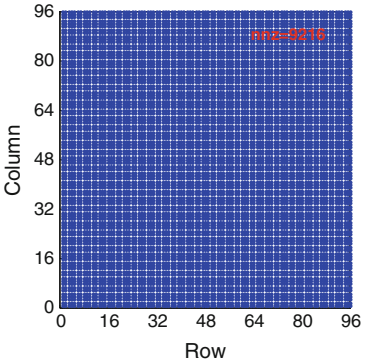

(d) Approximate inverse matrix (η=0.5%)

Fig. 3.19 Influence of dropping tolerance (η) on convergence performance

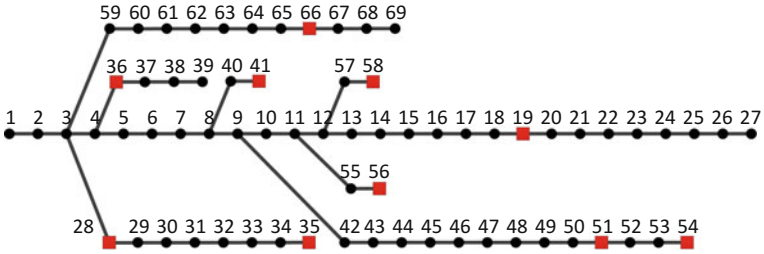

Fig. 3.20 A 69-bus radial network topology

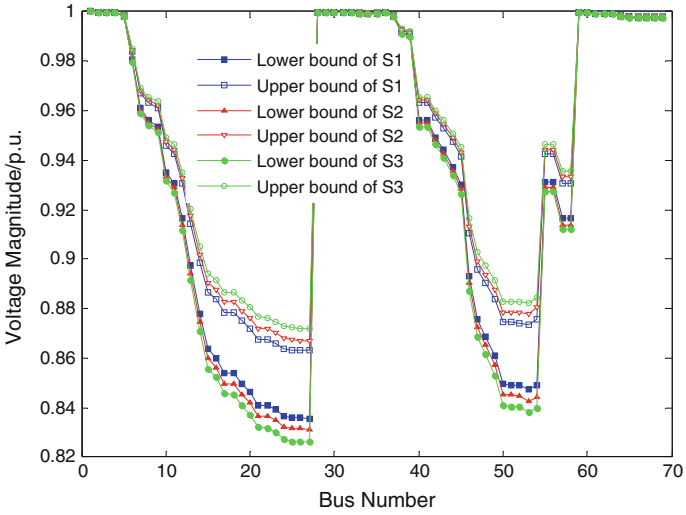

Fig. 3.21 Impact of uncertain degree on the interval voltage magnitude

Additionally, the exact and approximate inverse matrix for the method with and without network loss by $\eta = 5$ % are shown in Fig. 3.22, where we can find that the inverse matrix becomes denser if considering network loss. Likewise, the inverse matrix is a full matrix without the dropping strategy (nnz = 416616). That means the dropping strategy can save nearly half of its memory space (i.e., 57.69 % for the method without network loss and 47.09 % with network loss).

(c) **Computation time on several test systems**

Last but not the least, we will focus on computation time so that three large test systems [including 246-, 615-, and 861-bus systems [4] that derive from a 123-bus system (seen Fig. 3.23)] are employed to compare the proposed method (KISAP) considering network loss with the interval Gauss elimination (IGE) method which can still be given the same rigorous interval solution, and the Monte Carlo simulation with 5000 trials by the forward/backward sweep method. In the simulation, we only understand the simple serial-computing machine, although the partial parallel computation is feasible. Furthermore, the results of the three methods are presented in Table 3.8, where it shows that the computation time of IGE is more than 100 times significantly slower than KISAP. Additionally, for small systems, IGE is better than MCS; for large systems, the superior is lost. As for the proposed KISAP method, it is always the best choice—of the three methods—for all test systems. However, it should be pointed out the interval solution from MCS method by its nature is only a subset of the true interval. Therefore, more trials by MCS are needed to capture the true interval solution.

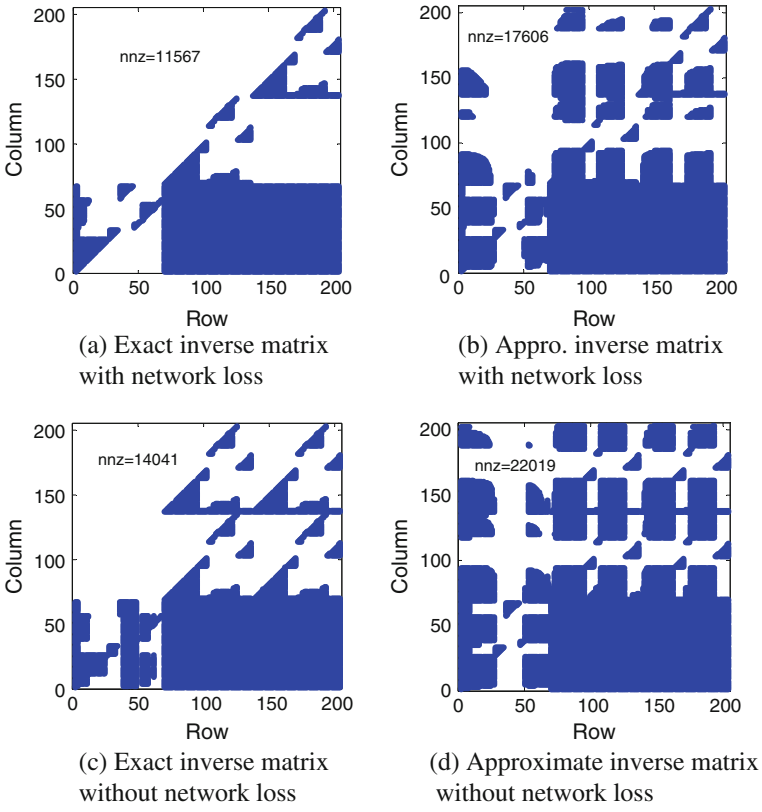

(a) Exact inverse matrix with network loss

(b) Appro. inverse matrix with network loss

(c) Exact inverse matrix without network loss

(d) Approximate inverse matrix without network loss

Fig. 3.22 Comparison of exact and approximate inverse matrix

3.2.4 Interval DC Power Flow with Constraints

Power system operation needs to consider the specific physical constraints, such as generator output limits, and etc. Traditionally, interval flow problem should consider some constraints, which have not been addressed, such as generation output limits. Therefore, the interval power flow solution must be conservative, and even some interval values have no physical meaning. In addition, the interval results are often related to the selection the slack bus, for which the dynamic flow has been widely studied [7]. This paper takes interval DC power flow as an example and set up the interval DC flow model with the constraints to balance machine output and dynamic adjustment constraints. We can observe that the results of interval DC flow model with constraints are closer to the actual physical meaning, and overcome the

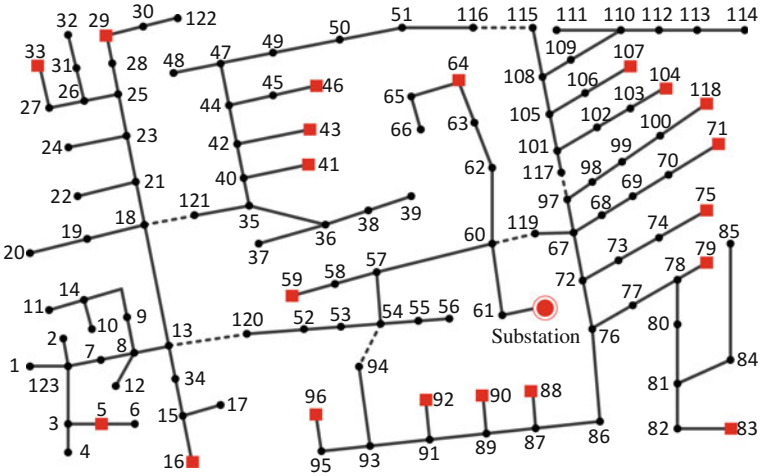

Fig. 3.23 A 123-bus radial network topology

Table 3.8 Comparison of the proposed method, interval Gauss method, and MCS

Test systems	MCS (s)	IGE (s)	KISAP (s)
33-bus	74.6882	1.5608	0.0128
69-bus	137.2393	7.2391	0.0675
123-bus	197.5357	24.3609	0.2493
246-bus	364.7247	111.8038	0.6545
615-bus	862.4503	979.9895	3.1557
861-bus	1397.5201	1890.4819	6.1490

conservativeness. In addition, after considering the dynamic adjustment of the generators, the results of interval power flow are no longer related to the selection of slack bus.

3.2.4.1 Modeling of Interval Power Flow with Constraints

After given the interval expression of power injection, interval branch flow can be obtained directly by (3.6). In fact, for the interval DC power flow described in (3.3), the uncertainty of power injection at each bus is within a given interval. However, in the practical power grid, the power output of generation is often subject to the physical limit, so that the power output of the slack bus is not arbitrary. This actually reflects a certain degree of correlation between generation output, which is not a simple positive and negative correlation among a few units and other units output, but a more general correlation. That is, besides power flow equations defined in (3.3), the output of the generator also needs to meet certain additional equations or inequality (including linear or nonlinear) constraints. The interval DC

flow equations defined in (3.3) with these additional equality and inequality constraints, gives the interval DC flow with constraints.

Due to this correlation, the generator output is not independent which results in different interval flow results, and these results are closer to the realistic power flow operation than the traditional uncorrelated interval power flow solution. Furthermore, divide the interval DC power flow equations into two parts: network load (i.e. the superimposition of wind power and load power injection) and power generation, giving (3.77). Here, loads are free variables that can be arbitrarily changed in the interval, and the generator output is required to meet some constraints. Accordingly, the slack bus can be described as (3.78).

$$\left[\underline{\boldsymbol{P}_T}, \overline{\boldsymbol{P}_T}\right] = \boldsymbol{HC}_g \left[\underline{\boldsymbol{P}_g}, \overline{\boldsymbol{P}_g}\right] - \boldsymbol{HC}_l \left[\underline{\boldsymbol{P}_l}, \overline{\boldsymbol{P}_l}\right] \tag{3.77}$$

$$\left[\underline{P_{g,ref}}, \overline{P_{g,ref}}\right] = \sum_{k=1}^{M} \left[\underline{P_{l,k}}, \overline{P_{l,k}}\right] - \sum_{i=1, i\neq ref}^{N} \left[\underline{P_{g,i}}, \overline{P_{g,i}}\right] \tag{3.78}$$

where N is the number of the generators, M is the number of load sites; $Cg \in RV \times N$ is an adjacency matrix of generator bus to other buses; $Cg \in RV \times M$ is an adjacency matrix of load buses to other buses; Pg is generator output and Pl is equivalent power injection.

(a) With linear inequalities

Similar to traditional power flow computation, interval DC power flow equations defined in (3.3) does not involve the slack bus. From the physical modeling of the interval power flow, we can find that the total imbalanced power should be taken by the slack bus. However, the power output of slack bus should be restricted by its maximum and minimum range, i.e.

$$P_{g,ref}^{\min} \leq \left[\underline{P_{g,ref}}, \overline{P_{g,ref}}\right] \leq P_{g,ref}^{\max} \tag{3.79}$$

where $P_{g,ref}^{\min}$ and $P_{g,ref}^{\max}$ are minimum and maximum output of the slack bus. Taking (3.78) into (3.7) obtains

$$P_{g,ref}^{\min} \leq \sum_{k=1}^{M} \left[\underline{P_{l,k}}, \overline{P_{l,k}}\right] - \sum_{i=1, i\neq ref}^{N} \left[\underline{P_{g,i}}, \overline{P_{g,i}}\right] \leq P_{g,ref}^{\max} \tag{3.80}$$

For branch flow constituted by (3.77) and (3.80), the equations of interval DC power flow with constraints are as follows:

$$\begin{cases} \left[\underline{\boldsymbol{P}_T}, \overline{\boldsymbol{P}_T}\right] = \boldsymbol{HC}_g\left[\underline{\boldsymbol{P}_g}, \overline{\boldsymbol{P}_g}\right] - \boldsymbol{HC}_l\left[\underline{\boldsymbol{P}_l}, \overline{\boldsymbol{P}_l}\right] \\ \left[\underline{\boldsymbol{P}_g}, \overline{\boldsymbol{P}_g}\right] \subseteq \left[\boldsymbol{P}_g^{\min}, \boldsymbol{P}_g^{\max}\right] \\ \left[\underline{P_{g,ref}}, \overline{P_{g,ref}}\right] = \sum_{k=1}^{M}\left[\underline{P_{l,k}}, \overline{P_{l,k}}\right] - \sum_{i=1,i\neq ref}^{N}\left[\underline{P_{g,i}}, \overline{P_{g,i}}\right] \\ P_{g,ref}^{\min} \le \left[\underline{P_{g,ref}}, \overline{P_{g,ref}}\right] \le P_{g,ref}^{\max} \end{cases} \tag{3.81}$$

Optimization based interval arithmetic method proposed in Sect. 2.2 can still be used for interval DC power flow equations with constraints. First, consider interval variables as optimizing decision variables, due to the goal of interval power flow is to solve the bound of branch flow, so the objective functions are maximizing and minimizing branch flow, obtaining $\overline{\boldsymbol{Z}}$ and $\underline{\boldsymbol{Z}}$ respectively, and the branch interval flow can be expressed as

$$\left[\underline{P_{T,l}}, \overline{P_{T,l}}\right] = \left[\underline{Z_l}, \overline{Z_l}\right], \quad l = 1, \ldots, L \tag{3.82}$$

Based on the interval DC power flow with constraint defined by (3.77), $\overline{\boldsymbol{Z}}$ and $\underline{\boldsymbol{Z}}$ can be obtained by optimization model (3.83), such that

$$\begin{aligned} &\underline{Z_i} = \min_{\boldsymbol{P}_g, \boldsymbol{P}_l} / \overline{Z_i} = \max_{\boldsymbol{P}_g, \boldsymbol{P}_l} \quad P_{T,i} \\ &s.t. \quad P_{T,i} = \left(\boldsymbol{HC}_g\boldsymbol{P}_g - \boldsymbol{HC}_l\boldsymbol{P}_l\right)_i \\ &P_{g,ref}^{\min} \le \sum_{k=1}^{M} P_{l,k} - \sum_{i=1,i\neq ref}^{N} P_{g,i} \le P_{g,ref}^{\max}, \quad l = 1, \ldots, L \\ &\max\left(\underline{P_{g,i}}, P_{g,i}^{\min}\right) \le P_{g,i} \le \min\left(\overline{P_{g,i}}, P_{g,i}^{\max}\right), \quad i = 1, \ldots, N \,\&\, i \neq ref \\ &\underline{P_{l,k}} \le P_{l,k} \le \overline{P_{l,k}}, \quad k = 1, \ldots, M \end{aligned} \tag{3.83}$$

(b) With linear equality

Model (3.83) considers all the imbalanced power to be taken only by the slack bus. However, in the practical power system, the imbalance power is actually shared by all generators, thereby forming a dynamic power flow. In general, the generator output is controllable, and the imbalanced power will lead to the dynamic changes of the generation output to meet the real-time balance. In this term, considering the imbalance power allocate proportion of generator i to be βi and $\sum_{i=1}^{n} \beta_i = 1$. Thus, the interval power flow with the equality constraints based on the original definition in (3.3) can be expressed as

$$\begin{cases} \left[\underline{\boldsymbol{P}_T}, \overline{\boldsymbol{P}_T}\right] = \boldsymbol{HC}_g\left[\underline{\boldsymbol{P}_g}, \overline{\boldsymbol{P}_g}\right] - \boldsymbol{HC}_l\left[\underline{\boldsymbol{P}_l}, \overline{\boldsymbol{P}_l}\right] \\ \left[\underline{\boldsymbol{P}_g}, \overline{\boldsymbol{P}_g}\right] \subseteq \left[\boldsymbol{P}_g^{\min}, \boldsymbol{P}_g^{\max}\right] \\ \left[\underline{\boldsymbol{P}_g}, \overline{\boldsymbol{P}_g}\right] = \beta_i\left(\sum_{k=1}^{M}\left[\underline{P_{l,k}}, \overline{P_{l,k}}\right] - \sum_{i=1}^{N}\left[P_{g,i}^*, P_{g,i}^*\right]\right) + \left[P_{g,i}^*, P_{g,i}^*\right] \end{cases} \tag{3.84}$$

where $P_{g,i}^*$ is active power of the generator i in base case. Based on the interval DC flow equations with constraints defined in (3.84), $\overline{\boldsymbol{Z}}$ and $\underline{\boldsymbol{Z}}$ can be obtained by optimization model

$$\begin{aligned} &\underline{Z_l} = \min_{\boldsymbol{P}_g, \boldsymbol{P}_l} / \overline{Z_l} = \max_{\boldsymbol{P}_g, \boldsymbol{P}} \quad P_{T,i} \\ &s.t. \quad P_{T,i} = \left(\boldsymbol{HC}_g\boldsymbol{P}_g - \boldsymbol{HC}_l\boldsymbol{P}_l\right)_i \\ &P_{g,i} = \beta_i\left(\sum_{k=1}^{M} P_{l,k} - \sum_{i=1}^{N} P_{g,i}^*\right) + P_{g,i}^*, \quad l = 1, \ldots, L \\ &\max\left(\underline{P_{g,i}}, P_{g,i}^{\min}\right) \le P_{g,i} \le \min\left(\overline{P_{g,i}}, P_{g,i}^{\max}\right), \quad i = 1, \ldots, N \\ &\underline{P_{l,k}} \le P_{l,k} \le \overline{P_{l,k}}, \quad k = 1, \ldots, M \end{aligned} \tag{3.85}$$

Of course, the interval power flow with constraints is not limited to the above two cases. According to the practical power system operating conditions, other constraints can be proposed, such as wind power correlation constraints, network losses and so on.

3.2.4.2 Numerical Analysis

At first, a 9-bus system in [1] is employed to test the proposed method, where bus 1 is slack bus, and the injection power of each generator and load buses change randomly within ±30 % range, while the upper and lower bounds of the slack bus is [50, 150] MW. Comparing with traditional interval power flow without constraints, results are shown in Table 3.9. As it can be found, interval power flow with constraints is a sub-range of the traditional interval power flow, this is because after being constrained by the slack bus output, the generator output is not so free, showing a certain relevance, so that the actual interval branch flow decreases.

To further study the influence of uncertainty on the traditional interval power flow and interval power flow with constraints, we set the uncertainty degree as ±10, ±30 and ±50 %, respectively. The width of the interval power flow is shown in Figs. 3.24 and 3.25. With the increase of uncertainties, the length of intervals of both the traditional interval power flow and interval power flow with constraints will monotonously increase. But the length of interval power flow with constraints is very smaller than that of the traditional interval power flow, since the constraints of slack bus is considered. In addition, the interval of branch 1 (connect to the slack bus) takes on a significant improvement.

Table 3.9 Comparison of the traditional interval power flow and the interval power flow with constraints

Branch no.	Traditional interval power flow (MW)	Interval power flow with constraints (MW)
1	[−101.90, 235.90]	[50.00, 150.00]
2	[−46.43, 104.37]	[−9.28, 91.07]
3	[−116.73, −5.33]	[−99.09, −9.32]
4	[59.50, 110.50]	[59.50, 110.50]
5	[−25.86, 73.79]	[−20.00, 73.79]
6	[−127.83, −24.23]	[−127.83, −24.23]
7	[−211.90, −114.10]	[−211.90, −114.10]
8	[21.61, 152.33]	[23.08, 136.22]
9	[−131.53, 55.47]	[−111.96, 3.55]

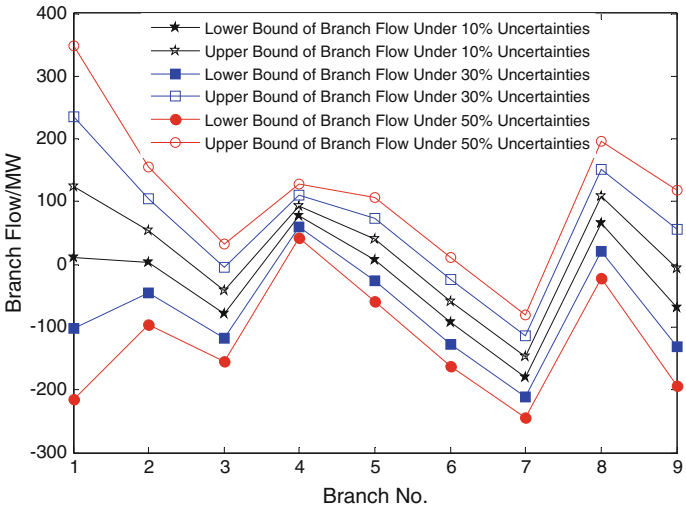

Fig. 3.24 Impact of uncertainty degree on traditional interval power flow

Similarly, considering the dynamic allocation for imbalance power with same proportion on bus-9 system, we can obtain the dynamic interval power flow with 30 % uncertainty using the linear optimization model in (3.23)–(3.50), which is shown in Table 3.10. The interval range is relatively narrowed and the output of all generators requires dynamic allocation, representing the correlation between the multiple generators. As shown in Fig. 3.26, with the increase of the uncertainty degree, the change of the interval width of the dynamic interval power flow is relatively small. In addition, the results of selecting a different slack bus results in the different interval solution of the traditional interval power flow, while the same dynamic interval power flow solution. This implies that the results of dynamic

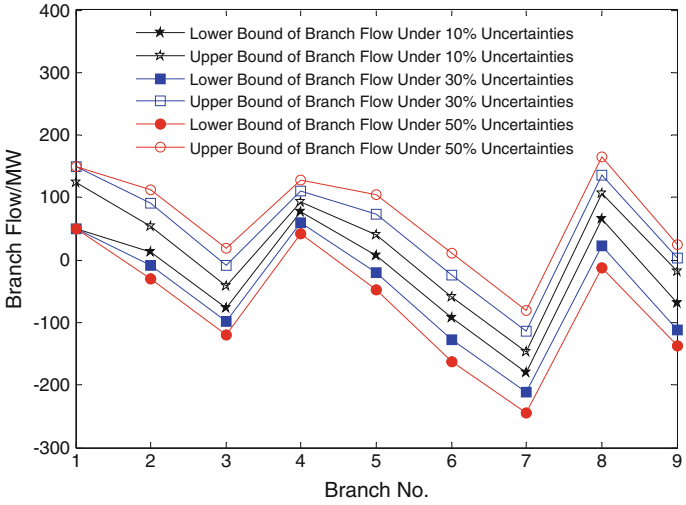

Fig. 3.25 Impact of uncertainty degree on interval power flow with constraints

Table 3.10 Comparison of traditional interval power flow and dynamic interval power flow

Branch no.	Traditional interval power flow (MW)			Dynamic interval power flow (MW)
	Slack 1	Slack 2	Slack 3	
1	[−101.90, 235.90]	[46.90, 87.10]	[46.90, 87.10]	[50.00, 92.50]
2	[−46.43, 104.37]	[−10.40, 68.34]	[−25.38, 83.31]	[2.63, 55.30]
3	[−116.73, −5.33]	[−100.21, −21.85]	[−128.90, 6.83]	[−85.24, −36.82]
4	[59.50, 110.50]	[59.50, 110.50]	[−78.50, 248.50]	[68.00, 110.50]
5	[−25.86, 73.79]	[−27.77, 75.70]	[−71.67, 119.60]	[1.31, 46.63]
6	[−127.83, −24.23]	[−151.42, −0.64]	[−150.55, −1.51]	[−100.20, −51.87]
7	[−211.90, −114.10]	[−303.10, −22.90]	[−211.90, −114.10]	[−188.50, −146.00]
8	[21.61, 152.33]	[22.26, 151.68]	[36.52, 137.41]	[58.18, 115.76]
9	[−131.53, 55.47]	[−82.98, 6.91]	[−87.75, 11.68]	[−69.37, −6.69]

interval power flow are not related to the choice of the slack bus and the interval solution obtained by traditional interval power flow will be larger than dynamic interval power flow.

Furthermore, when using different dynamic allocation coefficient, the results of the dynamic interval power flow are compared in Table 3.11. Case 1 represents allocation with same proportion, case 2 is the allocation with proportion of 3: 1: 1, case 3 is allocation with proportion of 1: 3: 1, case 4 is allocation with proportion of 1: 1: 3. With the different dynamic allocation, the correlation coefficient between generators will change and the results will change as well.

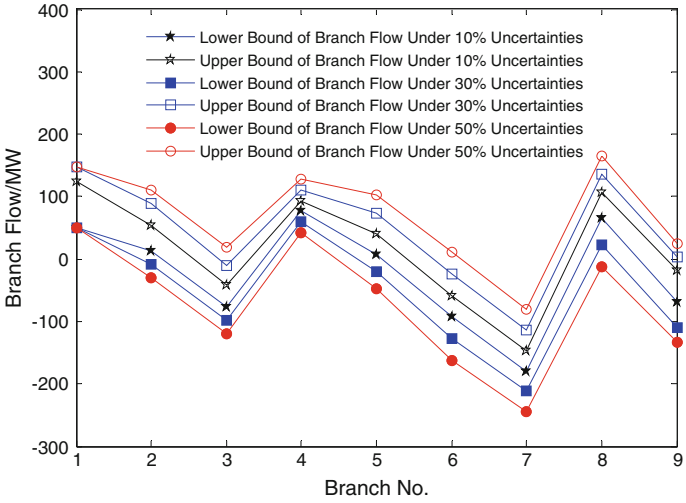

Fig. 3.26 Impact of uncertainty on dynamic interval power flow

Table 3.11 Impact of different allocation coefficient on dynamic interval power flow

Branch no.	Case 1 (MW)	Case 2 (MW)	Case 3 (MW)	Case 4 (MW)
1	[50.00, 92.50]	[50.00, 150.00]	[50.00, 94.17]	[52.83, 81.17]
2	[2.63, 55.30]	[−18.02, 77.09]	[−14.46, 72.39]	[−11.16, 69.09]
3	[−85.24, −36.82]	[−93.89, −30.22]	[−102.21, −19.86]	[−108.04, −14.02]
4	[68.00, 110.50]	[79.33, 112.67]	[68.00, 112.17]	[42.50, 127.50]
5	[1.31, 46.63]	[−8.51, 61.52]	[−5.71, 53.64]	[−24.06, 71.99]
6	[−100.20, −51.87]	[−116.41, −36.20]	[−122.65, −30.17]	[−113.52, −38.54]
7	[−188.50, −146.00]	[−190.67, −157.33]	[−244.50, −112.00]	[−177.17, −148.83]
8	[58.18, 115.76]	[48.86, 127.11]	[32.14, 141.79]	[37.98, 135.96]
9	[−69.37, −6.69]	[−99.48, 10.56]	[−82.23, 6.17]	[−89.09, 13.02]

Finally, IEEE-118 bus system is used to further compare the two interval DC power flow with constraints, where each generator uses same proportion to allocate imbalanced power, and the load uncertainty is 30 %.Simulation results are shown in Fig. 3.27, which suggests that the traditional interval DC power flow is conservative in large part in (a), and (b) can obtained minimum interval range, since the generator output is most relevant in this case.

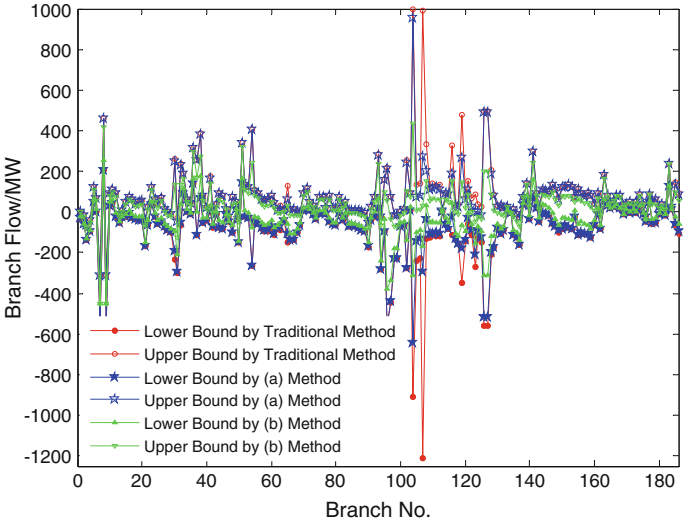

Fig. 3.27 Comparison of interval power flow by hree methods under 30 % uncertainty degree

3.3 Chapter Summary

This chapter applied the methods for solving interval linear equations and nonlinear equations in the second chapter to power flow calculation, formed an interval AC power flow, interval DC power flow and interval distribution power flow models. Interval AC power flow is based optimization method, at first relaxing the traditional flow equations, and then using boundary tightening method. Interval DC power flow and interval distribution power flow models utilizes Kraw iteration method with preconditioning. In addition, the paper also studied the interval power flow with constraints and discussed the impact of slack bus on the interval power flow. Finally, several test systems are studied to verify the effectiveness of the proposed method for solving interval power flow. Moreover, the results show that power flow considering constraints can be address the correlation between uncertain variables, so that the interval range will greatly reduce, and the results of dynamic interval power flow are not related to the selection of slack node.

References

1. Zimmerman RD, Murillo-Sa X, Nchez CE et al (2011) MATPOWER: steady-state operations, planning, and analysis tools for power systems research and education. IEEE Trans Power Syst 26(1):12–19
2. Vaccaro A, Canizares CA, Villacci D (2010) An affine arithmetic-based methodology for reliable power flow analysis in the presence of data uncertainty. IEEE Trans Power Syst 25 (2):624–632

3. Grabowski D, Olbrich M, Barke E (2008) Analog circuit simulation using range arithmetics. Seoul
4. Bondy JAM (1978) USR graph theory with applications. Macmillan Press, Britain
5. Baran ME, Wu FF (1989) Network reconfiguration in distribution systems for loss reduction and load balancing. IEEE Trans Power Deliv 4(2):1401–1407
6. Baran ME, Wu FF (1989) Network reconfiguration in distribution systems for loss reduction and load balancing. Power Eng Rev IEEE 9(4):101–102
7. Zhang B, Chen S, Yan Z, et al (2008) Power network analysis, Tsinghua University press

Chapter 4
Interval Economic Dispatch and the Tackling of Infeasible Model

Abstract Interval economic dispatch is derived from the traditional economic dispatch considering the interval numbers for wind power uncertainties to achieve the upper and lower bound of the optimal objective and generation output. Mathematically, the interval economic dispatch is to solve the interval optimization with the right-hand interval numbers. In this book, a general algorithm is proposed to solve this kind of mathematical problem, which can be extended to other research area. Furthermore, the infeasibility of interval economic dispatch is dealt with by two strategies to avoid the loss of dispatch instructions in the close-loop control. One is to find the optimal curtailment of wind power and the other is transmission constraints softened using exact penalty function based triple-level optimization model.

4.1 Introduction

Chapter 3 has discussed the algorithm of power flow considering the interval output of the uncertain wind power output. In this chapter, we will mainly discuss on optimal power flow with respect to uncertain wind generation output. Optimal power flow in power system is widely used in electricity market to schedule and dispatch the generation units in which the objective is to minimize the costs and maximize the benefits. In electricity market, DC power flow is often used which is also called economic dispatch (ED). Consider wind generation output variation is modeled by intervals, the corresponding objective function and the optimal results are also in terms of intervals. That is exactly the so-called interval economic dispatch. Interval economic dispatch can also be understood in this way: if wind generation output is an exact value which is contained in the given interval, we can solve the optimization model to get the optimal objective and the optimal generation output schedules; if wind generation output takes all the possibilities in the interval, we can get the corresponding intervals of optimal objectives and optimal generation outputs schedules respectively. Interval economic dispatch is exactly to get the optimal interval results.

T. Ding, *Power System Operation with Large Scale Stochastic Wind Power Integration*, Springer Theses, DOI 10.1007/978-981-10-2561-7_4

On the other hand, the economic dispatch model may be infeasible when the wind generation output takes some value of the given interval. Therefore, we must take some special actions to make the model feasible to avoid the failure in the closed-loop control when the model is infeasible. In this chapter we will implement two approaches to guarantee the infeasibility of the model: optimal curtailment of wind generation to guarantee the economic dispatch model to be feasible; another approach is to utilize the constraint relaxation method in the online dispatch model. In fact, the real-life power system is operating in a closed-loop framework; so the power system will take an action to prevent the violations of the transmission constraints in the next dispatch interval. Now, we can construct the economic dispatch model with exact penalty function to guarantee the feasibility of the model. In a word, the economic dispatch model is feasible using the above two approaches when the wind generation output varies within the given interval. The concrete research idea is as follows:

4.2 Interval Economic Dispatch Optimization Model

4.2.1 Modeling the Interval Economic Dispatch

Interval economic dispatch optimization model is similar to the conventional economic dispatch model. Specifically, we usually take linear or quadratic cost function as the objective, subjected to the energy balance constraints, generator ramp-up and ramp-down constraints, generator output constraints and transmission capacity constraints. The difference is that the right-hand parameters are modeled by interval numbers, instead of deterministic values, because the uncertain wind generation output are included in the right-hand parameter of the economic dispatch optimization model. If the wind generation output is deterministic (within the deterministic uncertain interval), then we can get the corresponding optimal objectives. For any given the wind power output, we can obtain the optimal dispatch and optimal objective value with respect to the economic dispatch. If we take all the value of the possible wind power output (may be infinite), we can have the final optimal interval dispatch and interval objective values. For the decision-makers, they can get the intuitive interval estimation of the cost, as well as the generation outputs of each of the thermal units' variation tendency with the objectives varying from the optimistic solution to the pessimistic ones. Furthermore, the interval optimization model is as follows:

Objective function:

$$\min \sum_{t=1}^{T} \left[\sum_{i=1}^{N_g} (a_i P_i(t) + c_i) \right] \tag{4.1}$$

where a_i and c_i are the coefficients of piecewise linear function of the costs; T is the total number of the time intervals. N_g is the total number of the conventional thermal units in the power system; $P_i(t)$ is the generation output of the thermal unit i at time t.

Constraints:

(i) *Energy balance constraints*:

$$\sum_{i=1}^{N_g} P_i(t) + \sum_{k=1}^{N_w} \left[W_k^-(t), W_k^+(t)\right] = \sum_{j=1}^{N_d} D_j(t), \quad t = 1, 2 \ldots T \tag{4.2}$$

Where $D_j(t)$ refers to the load demand for the site j at time t; and the non-dispatchable wind power generation of farm k at time t is $W_k(t)$, which is within its forecasted upper and lower bounds $W_k^+(t)$ and $W_k^-(t)$, such that $W_k(t) \in \left[W_k^-(t), W_k^+(t)\right]$. Generally $\left[W_k^-(t), W_k^+(t)\right]$ is equivalent to $\left[W_k^f - W_k^e, W_k^f + W_k^e\right]$, where W_k^f and W_k^e are the forecasted values and forecasted error of the wind farm k respectively. N_w and N_d are the total numbers of the wind farms and load sites respectively.

(ii) *Thermal unit outputs constraint conditions*:

$$P_i^{\min}(t) \le P_i(t) \le P_i^{\max}(t), \quad t = 1, 2 \ldots T \tag{4.3}$$

where $P_i^{\min}(t)$ and $P_i^{\max}(t)$ are generation output upper and lower bounds of the thermal unit i at time t.

(iii) *Thermal unit ramp-up and ramp-down constraints*:

$$-Rd_i \le P_i(t) - P_i(t-1) \le Ru_i, \quad t = 1, 2 \ldots T \tag{4.4}$$

where $-Rd_i$ and Ru_i are the ramp-up and ramp-down constraints of i-th unit.

(iv) *Transmission capacity constraints*:

$$-F_{ij}^{\max}(t) \le F_{ij}(t) \le F_{ij}^{\max}(t), \quad t = 1, 2 \ldots T \tag{4.5}$$

where $F_{ij}^{max}(t)$ refers to the transmission capacity limit of line $l = (i, j)$ at time t. i and j are the starting and ending bus of line l. Furthermore, the transmission capacity constrains can be rewritten with the network distribution shift factors as follows:

$$\begin{aligned} -F_l^{\max} \le & \sum_{i=1}^{N_g} S_{l,i} P_i(t) + \sum_{k=1}^{N_w} G_{l,k}\left[W_k^-(t), W_k^+(t)\right] \\ & - \sum_{j=1}^{N_d} H_{l,j} D_j(t) \le F_l^{\max}, \quad t = 1, \ldots T,\ l = 1, \ldots, N_l \end{aligned} \tag{4.6}$$

where $\boldsymbol{S}$, $\boldsymbol{G}$ and $\boldsymbol{H}$ are generator, wind farm and load site distribution shift factors of the network, respectively. $S_{l,i}$ is the distribution shift factor of power injection at generator bus i on line l; $H_{l,i}$ is the distribution shift factor of power injection at load site j on line l, and $G_{l,i}$ is the distribution shift factor of power injection at wind farm bus k on line l. N_l is the total number of the transmission lines. The distribution shift factor is related to the structures and parameters of the network and it can be obtained from the node impedance matrix [1, 2].

Therefore, the above mathematical expressions formulate the interval economic dispatch optimization model. Without the consideration of the correlation of each wind farm, we can obtain (4.7) and (4.12) by combining (4.2) and (4.6). It is obvious that the uncertain wind generation outputs, which are the inputs of the model, only occur in the right hand side of both the equality constraints and the inequality constraints in the optimization model. Therefore, we can write an interval optimization model with the special structure as follows:

$$\min \sum_{t=1}^{T} \left[\sum_{i=1}^{N_g} (a_i P_i(t) + c_i) \right] \tag{4.7}$$

$$s.t. \quad \sum_{i=1}^{N_g} P_i(t) + \sum_{k=1}^{N_w} \left[W_k^-(t), W_k^+(t) \right] = \sum_{j=1}^{N_d} D_j(t), \quad t = 1, 2 \ldots T \tag{4.8}$$

$$P_i^{\min}(t) \le P_i(t) \le P_i^{\max}(t), \quad t = 1, 2 \ldots T \tag{4.9}$$

$$-Rd_i \le P_i(t) - P_i(t-1) \le Ru_i, \quad t = 1, 2 \ldots T \tag{4.10}$$

$$-\sum_{i=1}^{N_g} S_{l,i} P_i(t) + \sum_{j=1}^{N_d} H_{l,j} D_j(t) - F_l^{\max} \le \left[\sum_{k=1}^{N_w} G_{l,k} W_k^-(t), \sum_{k=1}^{N_w} G_{l,k} W_k^+(t) \right], \tag{4.11}$$
$$t = 1, \ldots T, \; l = 1, \ldots, N_l$$

$$\sum_{i=1}^{N_g} S_{l,i} P_i(t) - \sum_{j=1}^{N_d} H_{l,j} D_j(t) - F_l^{\max} \le \left[\sum_{k=1}^{N_w} -G_{l,k} W_k^+(t), \sum_{k=1}^{N_w} -G_{l,k} W_k^-(t) \right],$$
$$t = 1, \ldots T, \; l = 1, \ldots, N_l \tag{4.12}$$

where (4.7)–(4.12) formulate a classic interval linear optimization model, and the variables in the intervals can be easily transposed to the right hands of the equality and inequality constraints. So we can utilize the interval optimization theory with right hand intervals mentioned in Chap. 2 to solve the problem (Fig. 4.1).

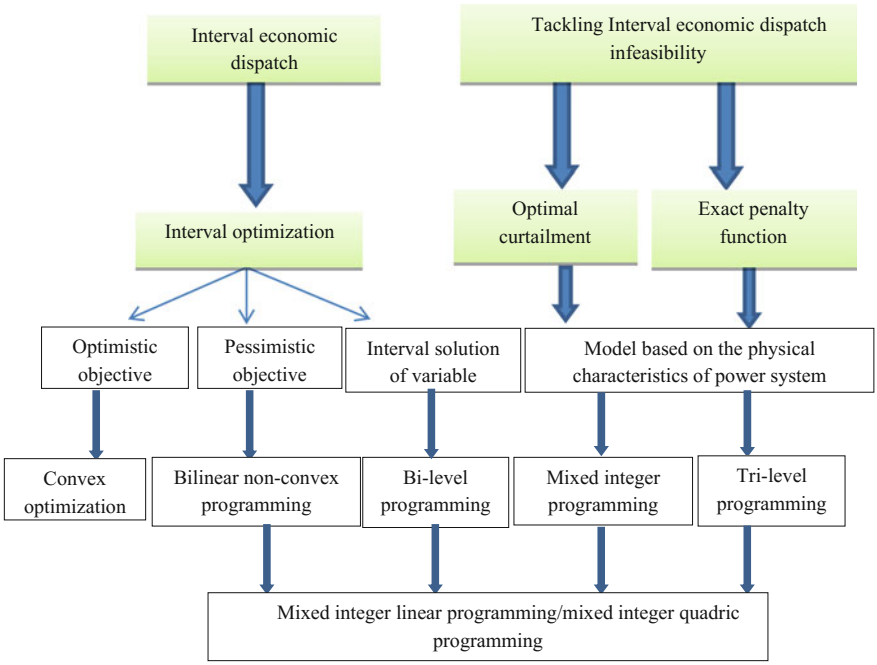

Fig. 4.1 Framework and writing ideas of this chapter

4.2.2 Numerical Results and Discussion

In this section, the IEEE 118-bus test system with 24 time periods is studied to investigate the effectiveness of proposed interval SCED model using bi-level programming. The detailed parameters information of network and generators can be found in MATPOWER [3], where the 19 units are in-service for SCED model with 6 wind farms. The maximum capacity of each wind farm is 100 MW. Besides, the total load demand and wind generation forecasting is shown in Fig. 4.2 where the shapes are similar to the real operation condition in Jilin province in north China. The proposed approach is performed using YALMIP, MATLAB and CPLEX 12 on a personal computer with Intel® Core™ i5 Duo Processor T420 (2.50 GHz) and 8 GB RAM.

Besides, two scenarios are selected as 'Loose' and 'Tight', to represent different level of solution condition. The security constraints are not considered in 'Loose' case while they are strictly guaranteed in 'Tight' case. Furthermore, three different uncertain levels denoted as α (0,Æ10,Æ20 %) are studied to discuss the impact of uncertainties on the solution of SCED. Table 4.1 lists the upper and lower bound of interval SCED under different scenarios and α, as well as the computational performance. It can be observed that the gap between upper and lower bound becomes larger with the increasing of uncertainty degree. As the lower bound is a simple

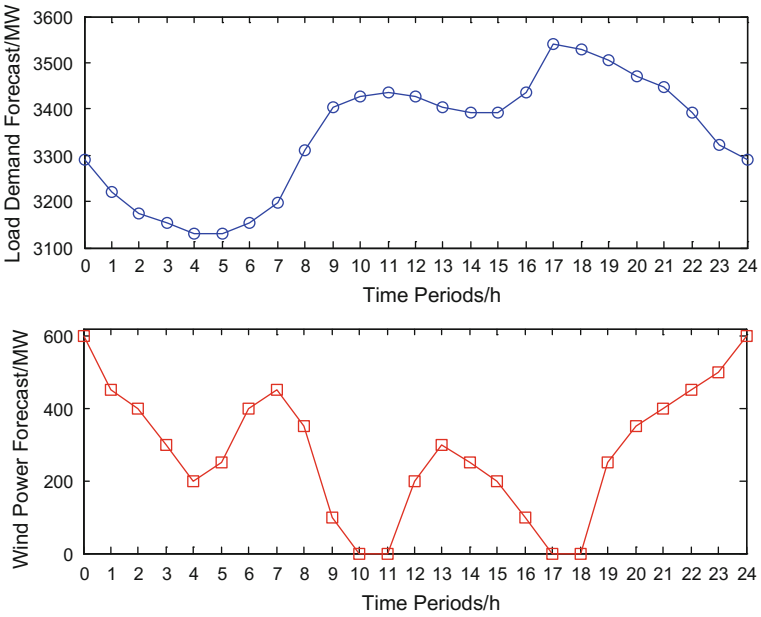

Fig. 4.2 The forecast of load demand and wind power generation

Table 4.1 Solution of interval SCED under different scenarios and α

		$\alpha = 0$		$\alpha = 0.1$		$\alpha = 0.2$	
		Tight	Loose	Tight	Loose	Tight	Loose
Upper bound	Obj/10^5\$	5.298	4.960	6.360	5.206	7.564	5.658
	Time (s)	2.79	2.74	3.85	3.31	14.61	13.17
Lower bound	Obj/10^5\$	5.298	4.960	5.441	4.797	5.277	4.660
	Time (s)	0.586	0.463	0.652	0.477	0.694	0.407

quadratic programming, the computational time is nearly the same about 0.5 s, whereas the upper is actually an NP-hard problem, which needs more time consumption under 'Tight' case with large uncertainties.

Furthermore, the interval optimal generation of each unit is computed by (4.11). The results with two scenarios under $\alpha = 0.1$ are shown in Fig. 4.3, where Fig. 4.3a, b depict the generation of all units during 11:00–12:00 a.m.; Fig. 4.3c, d depict the generation of unit 5 during 24 h. It can be observed that the generation of each unit only has a small variation for 'Loose' case, but it may be large for 'Tight' case, such as unit 7, 8 and 9 at 11:00–12:00 a.m.. In addition, the impact on upper

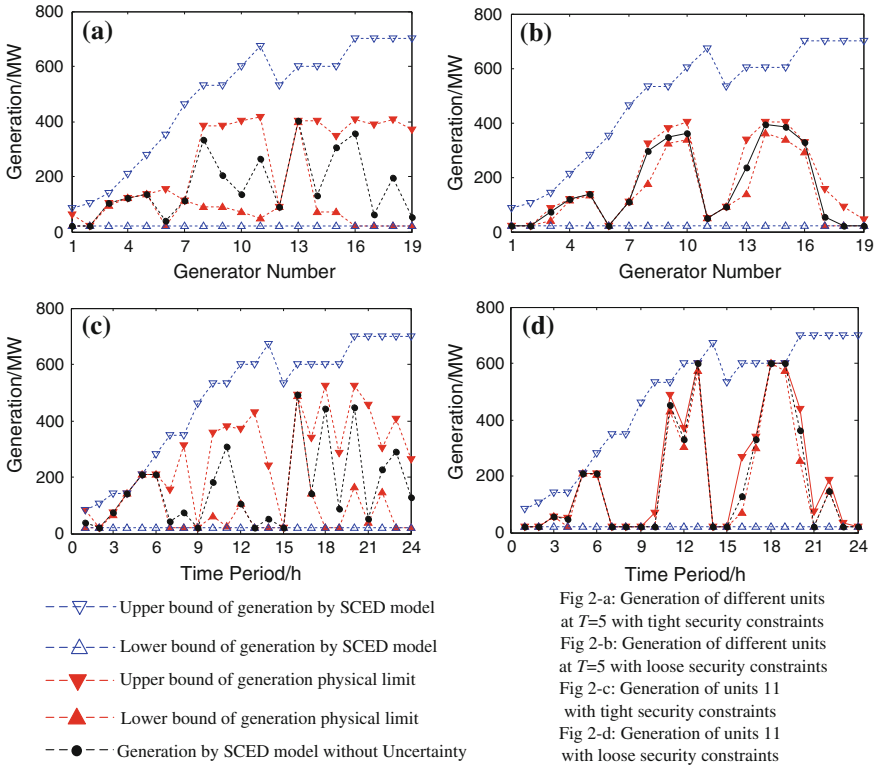

Fig. 4.3 Comparison of upper and lower bound of generation with tight and loose security constraints

and lower bound is studied under different α in Figs. 4.4 and 4.5. It is interesting to find that in order to achieve the optimal objective value (minimum fuel costs), different units at different time period would have probably different response to the wind variation. Take Fig. 4.4 for instance, under wind power variation, unit 5 during 11:00–12:00 a.m. always ramps down, unit 3 sometimes ramps down and sometimes ramps up, unit 18 always ramps up and unit 7 always keeps constant. In other words, it can be known in day-ahead market that the units have different sensitivity to wind power variation for achieving the optimal objective value. For example, under different α, the lower bound of unit 14 is different, which illustrates that the lower bound is sensitive to wind power variation but upper bound is not; unit 18 is just the opposite. These results could give us some institutive useful information for a better dispatch in real-time market. Therefore, this should be further studied in the future work.

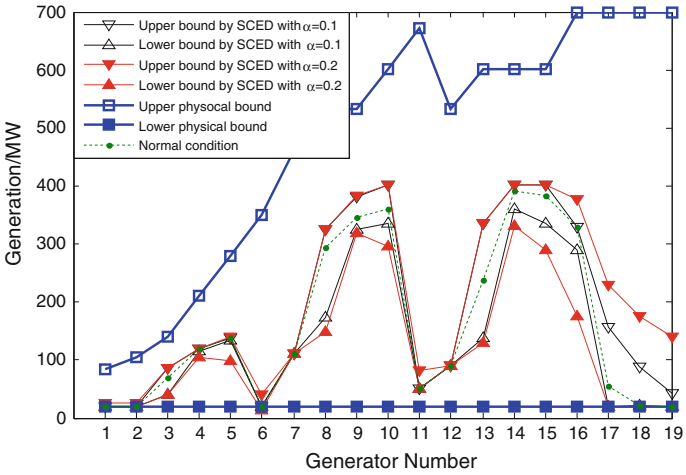

Fig. 4.4 Upper/lower bound with different α (unit 5)

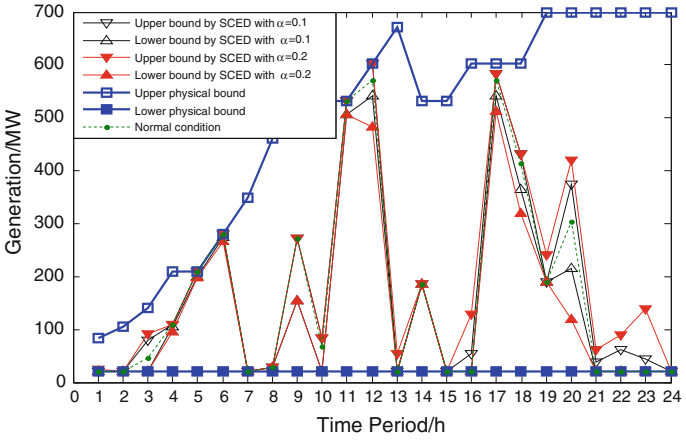

Fig. 4.5 Upper/lower bound with different α (during 11:00–12:00 a.m.)

4.3 Methods for Infeasible Economic Dispatch

The prerequisite assumption of solving the interval economic dispatch by bi-level programming is to ensure the infeasibility of the economic dispatch model with any given uncertainties. However, the assumption may not always hold, so we need some measures to guarantee a solution for economic dispatch model. In this book, we will utilize two different methods to handle this problem under two different given economic dispatch model: for the day-ahead multi-period economic dispatch model, we utilize optimal curtailment of the wind generation output to ensure the

feasibility of the model. Since the curtailment of wind generation output will increase the generation of thermal units and decrease the renewable energy generation, minimizing the curtailment of wind generation output is considered; for the real-time single-period economic dispatch model, relaxing the transmission security constraints is implemented to ensure the feasibility of the model. In real-time electricity market, transmission constraints could be violated in short term, and we can get the redispatch in the next dispatch interval. However, the short term violation of the transmission constraints must be confined within a certain range. Therefore, how to define the degree of the violation and the exact penalty function is needed to be studied.

4.3.1 Optimal Curtailment Model

4.3.1.1 Optimal Curtailment for Infeasibility of SCED in the Presence of Wind Power Uncertainties

In practice, the optimal solution of SCED with wind power generation is related to the wind power output and the optimal generation will be adjustable under wind power uncertainties. Then, a question arises: "Is the SCED problem in (4.1) always feasible for any given wind power output?" If not, the wind power needs to be curtailed so that SCED is feasible.

To clearly answer the above question, the feasible region of the SCED under a given wind power output $W_k(t) \in \left[W_k^-(t), W_k^+(t)\right]$, $t = 1, \ldots, T$, $k = 1, \ldots, N_w$, is defined as

$$\Gamma(\boldsymbol{W}) = \left\{ \boldsymbol{P} \left| \left\{ \begin{array}{c} \sum_{i=1}^{N_g} P_{i,t} + \sum_{k=1}^{N_w} W_{k,t} = \sum_{j=1}^{N_d} D_{j,t}; t = 1, \ldots, T \\ P_{i,t}^{\min} \le P_{i,t} \le P_{i,t}^{\max}; i = 1, \ldots, N_g; t = 1, \ldots, T \\ -Rd_{i,t} \le P_{i,t} - P_{i,t-1} \le Ru_{i,t}; i = 1, \ldots, N_g; t = 1, \ldots, T \\ -F_{l,t}^{\max} \le \sum_{i=1}^{N_g} S_{l,i} P_{i,t} + \sum_{k=1}^{N_w} G_{l,k} W_{k,t} - \sum_{j=1}^{N_d} H_{l,j} D_{j,t} \le F_{l,t}^{\max} \\ t = 1, \ldots, T; \; l = 1, \ldots, N_l \end{array} \right. \right\} \tag{4.13}$$

Here, the feasible region $\Gamma(\boldsymbol{W})$ is related to the given wind power outputs $\boldsymbol{W}$ and then the above question can be mathematically stated as "Is $\Gamma(\boldsymbol{W})$ always nonempty for $\forall W_k(t) \in \left[W_k^-(t), W_k^+(t)\right]$?" If so, $\forall W_k(t) \in \left[W_k^-(t), W_k^+(t)\right]$, $\exists \boldsymbol{P} \in \Gamma(\boldsymbol{W})$.

Obviously, $\Gamma(\boldsymbol{W})$ can be empty under certain wind power outputs and the generation dispatch $\boldsymbol{P}$ cannot always fully satisfy the constraints (4.13). In this case,

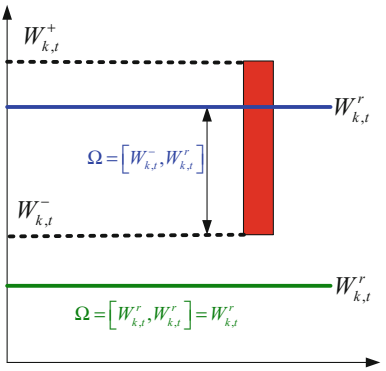

Fig. 4.6 Impact of curtailment on the uncertainty set

the proper curtailment is required with the objective of changing the wind power uncertainty set and guaranteeing $\Gamma(\boldsymbol{W})$ nonempty.

To be specific, the impact of curtailment on the uncertainty set is depicted in Fig. 4.6, in which $W_{k,t}^{r}$ is the restricted wind power output for k-th wind farm at time period t.

As shown in Fig. 4.6: (i) $W_{k,t}^{r}$ is smaller than the maximum wind power output as $W_{k,t}^{r} \le W_{k,t}^{+}$; (ii) if $W_{k,t}^{+} \ge W_{k,t}^{r} \ge W_{k,t}^{-}$, the uncertainty set $\Omega_{k,t} = [W_{k,t}^{-}, W_{k,t}^{r}]$; and (iii) if $W_{k,t}^{r} \le W_{k,t}^{-}$, the uncertainty set $\Omega_{k,t} = \left[W_{k,t}^{r}, W_{k,t}^{r}\right] = W_{k,t}^{r}$. The curtailment can be expressed as $W_{k,t}^{+} - W_{k,t}^{r}$ and $W_{k,t}^{+} = W_{k,t}^{r}$ means no curtailment. Thus, with the consideration of curtailment, the SCED in this paper aims to find the optimal restricted wind power $W_{k,t}^{r}$ for each wind farm, so that $\forall W_k(t) \in \Omega_{k,t}$, $\exists \boldsymbol{P} \in \Gamma(\boldsymbol{W})$.

Also, (4.13) suggests that the uncertainty only affect the first and last constraints. $\forall W_k(t) \in \Omega_{k,t}$, if $\exists$ P satisfies the first constraint, we have

$$\exists \boldsymbol{P}, \text{such that} \left(\sum_{j=1}^{N_d} D_{j,t} - \sum_{i=1}^{N_g} P_{i,t}\right) \in \sum_{k=1}^{N_w} \Omega_{k,t}; \quad t = 1, \ldots, T \tag{4.14}$$

If $\boldsymbol{P}$ satisfies the last constraint, we have

$$\left(\sum_{i=1}^{N_g} S_{l,i} P_{i,t} + \sum_{k=1}^{N_w} G_{l,k} W_{k,t} - \sum_{j=1}^{N_d} H_{l,j} D_{j,t}\right) \subseteq \left[-F_{l,t}^{\max}, F_{l,t}^{\max}\right] \tag{4.15}$$

$$\sum_{k=1}^{N_w} G_{l,k} \Omega_{k,t} \subseteq \left(\left[-F_{l,t}^{\max}, F_{l,t}^{\max}\right] + \sum_{j=1}^{N_d} H_{l,j} D_{j,t} - \sum_{i=1}^{N_g} S_{l,i} P_{i,t}\right) \tag{4.16}$$

Furthermore, it should be noted that $\Omega_{k,t}$ is a "if-else" interval number in (4.17). For that, we employ one binary variable $y_{k,t}$ and apply big M approach to

reformulate (4.17) as a simple interval number in (4.18) with some additional constraints by (4.19).

$$\Omega_{k,t} = \begin{cases} \left[W_{k,t}^{-}, W_{k,t}^{r}\right] & if\ W_{k,t}^{r} \geq W_{k,t}^{-} \\ W_{k,t}^{r} & else \end{cases}, \text{with } W_{k,t}^{r} \leq W_{k,t}^{+} \tag{4.17}$$

$$\Omega_{k,t} = \left[W_{k,t}^{-}\left(1 - y_{k,t}\right) + W_{k,t}^{r} y_{k,t}, W_{k,t}^{r}\right] \tag{4.18}$$

with additional constraints

$$\begin{cases} 0 \leq W_{k,t}^{r} \leq W_{k,t}^{+} \\ -My_{k,t} + W_{k,t}^{-} \leq W_{k,t}^{r} \leq W_{k,t}^{-} + M\left(1 - y_{k,t}\right) \end{cases} \tag{4.19}$$

where M is a large number.

Take (4.18) into (4.13) and it yields (4.20). Hence, if we can find a feasible solution $\boldsymbol{P}$ which satisfies (4.20), (4.13) will hold.

$$\sum_{k=1}^{N_w}\left(W_{k,t}^{-}\left(1 - y_{k,t}\right) + W_{k,t}^{r} y_{k,t}\right) \leq \sum_{j=1}^{N_d} D_{j,t} - \sum_{i=1}^{N_g} P_{i,t} \leq \sum_{k=1}^{N_w} W_{k,t}^{r} \tag{4.20}$$

Seminally, take (4.18) into (4.15) and it yields (4.21).

$$\sum_{k=1}^{N_w} G_{l,k}\left[W_{k,t}^{-}\left(1 - y_{k,t}\right) + W_{k,t}^{r} y_{k,t}, W_{k,t}^{r}\right] \subseteq \left(\left[-F_{l,t}^{max}, F_{l,t}^{max}\right] + \sum_{j=1}^{N_d} H_{l,j} D_{j,t} - \sum_{i=1}^{N_g} S_{l,j} P_{i,t}\right) \tag{4.21}$$

From the additional constraints (4.19), it is known that the upper and lower bound of $\Omega_{k,t}$ are always positive. Then, (4.21) can be furthermore simplified as

$$\begin{cases} \sum_{k=1}^{N_w}\left\{\max\left(G_{l,k}, 0\right) W_{k,t}^{r} + \min\left(G_{l,k}, 0\right)\left(W_{k,t}^{-}\left(1 - y_{k,t}\right) + W_{k,t}^{r} y_{k,t}\right)\right\} \\ \qquad \leq F_{l,t}^{\max} + \sum_{j=1}^{N_d} H_{l,j} D_{j,t} - \sum_{i=1}^{N_g} S_{l,i} P_{i,t} \\ \sum_{k=1}^{N_w}\left\{\min\left(G_{l,k}, 0\right) W_{k,t}^{r} + \max\left(G_{l,k}, 0\right)\left(W_{k,t}^{-}\left(1 - y_{k,t}\right) + W_{k,t}^{r} y_{k,t}\right)\right\} \\ \qquad \geq -F_{l,t}^{\max} + \sum_{j=1}^{N_d} H_{l,j} D_{j,t} - \sum_{i=1}^{N_g} S_{l,i} P_{i,t} \end{cases} \tag{4.22}$$

Note that the bilinear term $W_{k,t}^r y_{k,t}$ in (4.20) and (4.22) is difficult to deal with. Fortunately, this bilinear term is made by one continuous and one binary variable, and thus the big M approach can be reutilized to obtain simpler constraints:

$$\sum_{k=1}^{N_w}\left(W_{k,t}^-\left(1-y_{k,t}\right)+z_{k,t}\right)\le\sum_{j=1}^{N_d}D_{j,t}-\sum_{i=1}^{N_g}P_{i,t}\le\sum_{k=1}^{N_w}W_{k,t}^r \tag{4.23}$$

$$\begin{cases}\sum\limits_{k=1}^{N_w}\left\{\max\left(G_{l,k},0\right)W_{k,t}^r+\min\left(G_{l,k},0\right)\left(W_{k,t}^-\left(1-y_{k,t}\right)+z_{k,t}\right)\right\}\le F_{l,t}^{\max}+\sum\limits_{j=1}^{N_d}H_{l,j}D_{j,t}-\sum\limits_{i=1}^{N_g}S_{l,i}P_{i,t}\\ \sum\limits_{k=1}^{N_w}\left\{\min\left(G_{l,k},0\right)W_{k,t}^r+\max\left(G_{l,k},0\right)\left(W_{k,t}^-\left(1-y_{k,t}\right)+z_{k,t}\right)\right\}\ge -F_{l,t}^{\max}+\sum\limits_{j=1}^{N_d}H_{l,j}D_{j,t}-\sum\limits_{i=1}^{N_g}S_{l,i}P_{i,t}\end{cases} \tag{4.24}$$

with the additional constraints

$$\begin{cases}W_{k,t}^r-M\left(1-y_{k,t}\right)\le z_{k,t}\le W_{k,t}^r+M\left(1-y_{k,t}\right)\\ -My_{k,t}\le z_{k,t}\le My_{k,t}\end{cases} \tag{4.25}$$

For $y_{k,t}=1$, (4.24) is equal to $\begin{cases}W_{k,t}^r\le z_{k,t}\le W_{k,t}^r\\ -M\le z_{k,t}\le M\end{cases}$, in which the second constraint is redundant and $z_{k,t}=W_{k,t}^r$. Meanwhile, (4.18) and (4.19) become $\Omega_{k,t}=\left[W_{k,t}^r,W_{k,t}^r\right]$ and $\begin{cases}0\le W_{k,t}^r\le W_{k,t}^+\\ -M+W_{k,t}^-\le W_{k,t}^r\le W_{k,t}^-\end{cases}$; respectively, which leads to $0\le W_{k,t}^r\le W_{k,t}^-$.

Similarly, for $y_{k,t}=0$, (4.25) states $\begin{cases}W_{k,t}^r-M\le z_{k,t}\le W_{k,t}^r+M\\ 0\le z_{k,t}\le 0\end{cases}$, in which the first constraint is redundant and $z_{k,t}=0$. Then, (4.18) and (4.19) become $\Omega_{k,t}=\left[W_{k,t}^r,W_{k,t}^r\right]$ and $\begin{cases}0\le W_{k,t}^r\le W_{k,t}^+\\ W_{k,t}^-\le W_{k,t}^r\le W_{k,t}^-+M\end{cases}$, respectively, and we have $W_{k,t}^-\le W_{k,t}^r\le W_{k,t}^+$.

Now, we can construct a MILP model as follows

$$\min_{\boldsymbol{W}^r,\boldsymbol{P},\boldsymbol{y}}\quad\sum_{k=1}^{N_w}\sum_{t=1}^{T}c_{k,t}\left(W_{k,t}^+-W_{k,t}^r\right) \tag{4.26}$$

$$s.t.\quad\sum_{k=1}^{N_w}\left(W_{k,t}^-\left(1-y_{k,t}\right)+z_{k,t}\right)\le\sum_{j=1}^{N_d}D_{j,t}-\sum_{i=1}^{N_g}P_{i,t}\le\sum_{k=1}^{N_w}W_{k,t}^r,\quad t=1,\ldots,T \tag{4.27}$$

$$P_{i,t}^{\min} \le P_{i,t} \le P_{i,t}^{\max}, \quad i = 1, \ldots, N_g, \quad t = 1, \ldots, T \tag{4.28}$$

$$-Rd_{i,t} \le P_{i,t} - P_{i,t-1} \le Ru_{i,t}, \quad i = 1, \ldots, N_g, \quad t = 1, \ldots, T \tag{4.29}$$

$$\begin{aligned} &\sum_{k=1}^{N_w} \left\{ \max\left(G_{l,k}, 0\right) W_{k,t}^{r} + \min\left(G_{l,k}, 0\right) \left(W_{k,t}^{-}\left(1 - y_{k,t}\right) + z_{k,t} \right) \right\} \le F_{l,t}^{\max} + \sum_{j=1}^{N_d} H_{l,j} D_{j,t} \\ &\quad - \sum_{i=1}^{N_g} S_{l,i} P_{i,t}, \\ &\quad t = 1, \ldots, T, \quad l = 1, \ldots, N_l \end{aligned} \tag{4.30}$$

$$\begin{aligned} &\sum_{k=1}^{N_w} \left\{ \min\left(G_{l,k}, 0\right) W_{k,t}^{r} + \max\left(G_{l,k}, 0\right) \left(W_{k,t}^{-}\left(1 - y_{k,t}\right) + z_{k,t} \right) \right\} \ge \\ &\quad - F_{l,t}^{\max} + \sum_{j=1}^{N_d} H_{l,j} D_{j,t} - \sum_{i=1}^{N_g} S_{l,i} P_{i,t}, \\ &\quad t = 1, \ldots, T, \quad l = 1, \ldots, N_l \end{aligned} \tag{4.31}$$

$$\begin{cases} 0 \le W_{k,t}^{r} \le W_{k,t}^{+} \\ -My_{k,t} + W_{k,t}^{-} \le W_{k,t}^{r} \le W_{k,t}^{-} + M\left(1 - y_{k,t}\right) \end{cases}, \quad k = 1, \ldots, N_w, \; t = 1, \ldots, T \tag{4.32}$$

$$\begin{cases} W_{k,t}^{r} - M\left(1 - y_{k,t}\right) \le z_{k,t} \le W_{k,t}^{r} + M\left(1 - y_{k,t}\right) \\ -My_{k,t} \le z_{k,t} \le My_{k,t} \end{cases}, \; k = 1, \ldots, N_w, \; t = 1, \ldots, T \tag{4.33}$$

where $c_{k,t}$ is the curtailment cost of wind farm k at time period t.

4.3.1.2 Numerical Results and Discussion

In this section, the proposed approach is tested in WSCC 9-bus and IEEE 118-bus systems [3], respectively. The test is performed using MATLAB and CPLEX 12.5 on a personal computer with an Intel® Core™ i5 Duo Processor T420 (2.50 GHz) and 4 GB RAM (32 bit system). Besides, we assume $c_{k,t}$ to be the same, so the objective is essentially to minimize the total curtailment of wind power.

In the 9-bus system, Generator 3 is replaced by a wind farm, in which the forecasted wind power generation and three load demands over 24 h are depicted in Fig. 4.7, where the curves are similar to the real operating condition of the Jilin province in northern China. In addition, $c_{k,t}$ in (4.27) is assumed to be identical to simplify the problem, the wind power uncertainty level α is set to 20 % of the

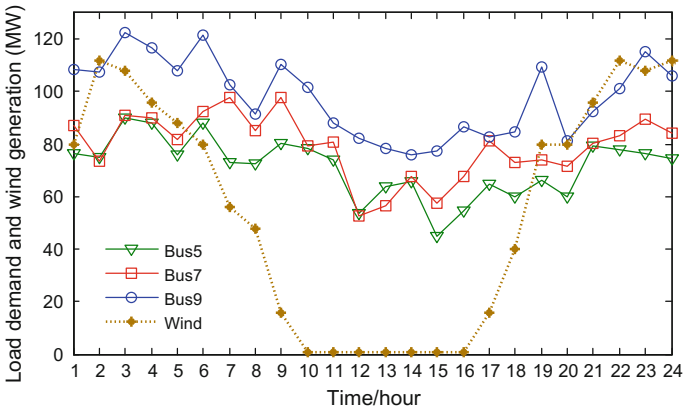

Fig. 4.7 The forecasted load demands and wind power generation

forecasted value, and different transmission capacities are used to simulate the solutions of different levels.

In one test, we adopt Monte Carlo simulation for the SCED model and find several infeasible cases, three of which are presented in Fig. 4.8. Then, the proposed method is implemented with different transmission capacity ratios β to the original values and the corresponding optimal curtailment values are presented in Figs. 4.9, 4.10 and 4.11 respectively.

As shown in Figs. 4.9, 4.10 and 4.11, the SCED needs 648 MW curtailment for $\beta = 1$, 136 MW curtailment for $\beta = 1.5$, and no curtailment for $\beta = 2$. The simulation results imply that (i) the SCED may be infeasible due to the uncertain wind power output, (ii) the curtailment values and the transmission capacities exhibit an

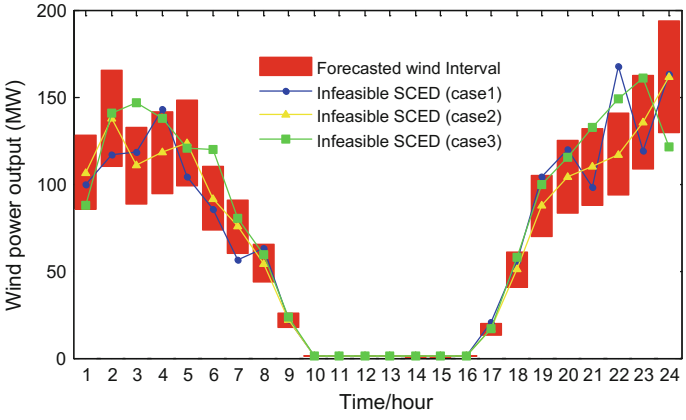

Fig. 4.8 Infeasible SCED cases

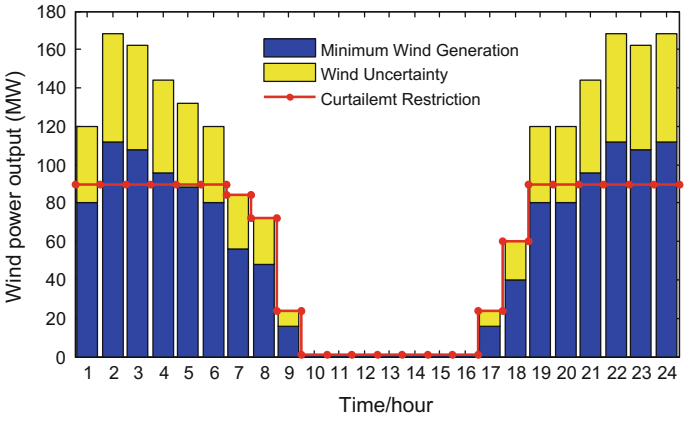

Fig. 4.9 Optimal curtailment for β = 1.0

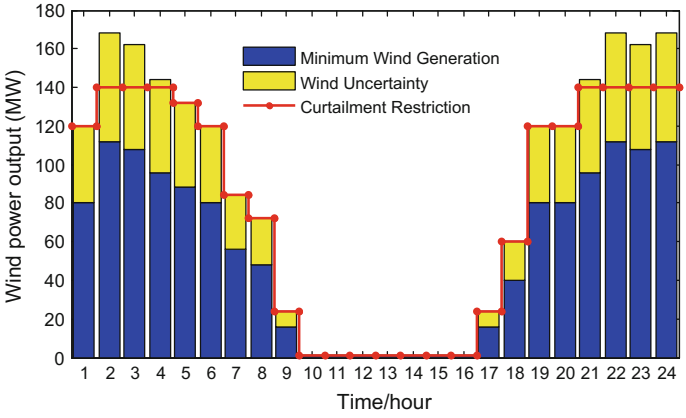

Fig. 4.10 Optimal curtailment for β = 1.5

inverse relationship, and (iii) when $\beta > 2$, the SCED is always feasible under various wind power variations within the uncertainty set.

Furthermore, the curtailment of wind power with respect to uncertainty levels α and transmission capacity ratios β is studied in Fig. 4.12. It is shown that for a given transmission capacity ratio, the curtailment increases with the incremental of the uncertainty level; whereas for a given uncertainty level, the curtailment decreases with the incremental of the transmission capacity ratio. In particular, there will be no curtailment when the transmission capacity expands to certain scale.

Another test is performed on IEEE 118-bus system. Note that the increase of the time periods and/or wind farms in (4.27) leads to the growth of binary variables, and the increasing number of the binary variables may affect the computational performance of the proposed model. Therefore, different scenarios are tested and

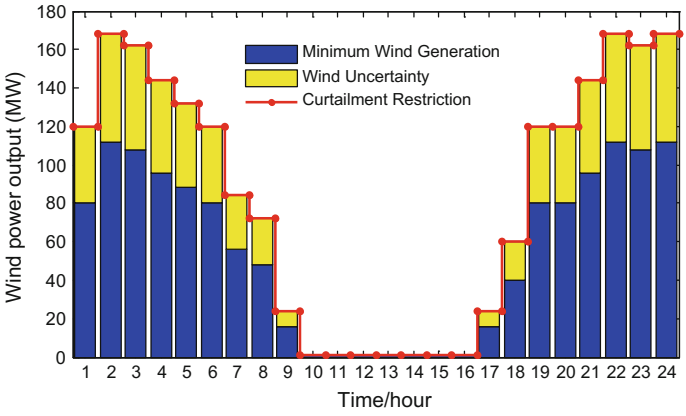

Fig. 4.11 Optimal curtailment for β = 2.0

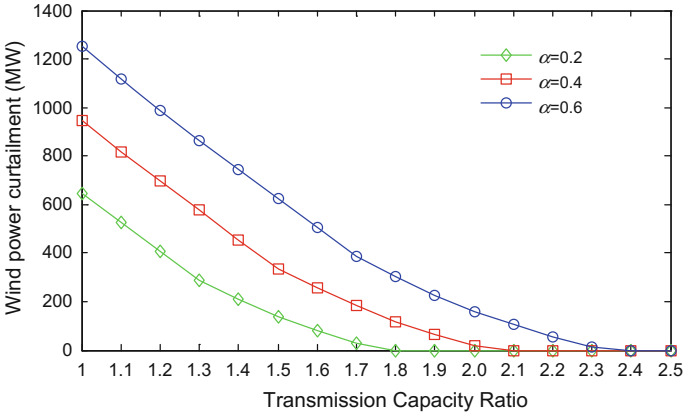

Fig. 4.12 Quantitive curtailment under different α and β

the corresponding results are presented in Table 4.2. It can be found that the increasing time periods and/or wind farms require more computing time, but the proposed model can still be efficiently handled by the branch and bound method even for the case with 96 time periods and 15 wind farms.

Table 4.2 Computational time using the proposed method (seconds)

	T = 4	T = 12	T = 24	T = 48	T = 96
N_w = 3	0.1496	0.3429	0.8801	1.4870	4.3241
N_w = 6	0.1600	0.4364	0.9903	1.8377	5.4446
N_w = 9	0.1904	0.6526	1.1403	2.2344	6.1579
N_w = 12	0.2256	0.6779	1.3906	2.7376	6.9643
N_w = 15	0.2581	0.7411	1.9039	3.0243	7.3526

4.3.2 Exact Penalty Function Model

4.3.2.1 Mathematical Theory of Exact Penalty Function

In the last chapter, we have proposed an optimal curtailment model to ensure the feasibility of the multi-period economic dispatch model, which is utilized in the day-ahead SCED model. Moreover, we have presented the reasonable curtailment-constrained curves to ensure the feasibility of the SCED. However, in real time market, the forecasted generation output of the wind farms will be updated with short-term forecasted results, so the forecasted intervals may be different from the forecasted results of the day-ahead market. Therefore, we need to modify the input parameters of SCED in real-time market with renewed wind generation output, so as to modify the scheduling plan in the day-ahead market. The real time single-period ED can be mathematically formulated as a quadratic programming (QP) problem, the objective is to minimize the traditional generation cost with the consideration of specific constraints such as generator physical limits and transmission line capacity limits. Obviously it is a quadratic programming problem, but the uncertain wind generation output can become the input parameters of the model.

$$\min \quad \sum_{i=1}^{N_g} \left(c_i + b_i P_i + a_i P_i^2\right) \tag{4.34}$$

$$s.t. \quad \sum_{i=1}^{N_g} P_{g,i} + \sum_{i=1}^{N_w} P_{w,i} = \sum_{i=1}^{N_l} P_{l,i} \tag{4.35}$$

$$\boldsymbol{P}_T^{\min} \le \boldsymbol{T}\left(\boldsymbol{P}_g + \boldsymbol{P}_w - \boldsymbol{P}_l\right) \le \boldsymbol{P}_T^{\max} \tag{4.36}$$

$$\boldsymbol{P}_g^{\min} \le \boldsymbol{P}_g \le \boldsymbol{P}_g^{\max},\ given \quad \boldsymbol{P}_w \subset \left[\boldsymbol{P}_w^{\min}, \boldsymbol{P}_w^{\max}\right] \tag{4.37}$$

Where $\boldsymbol{P}_g$ Pg is the conventional dispatchable (non-wind) generation; $\boldsymbol{P}_w$ is the wind power generation and $\boldsymbol{P}_l$ is the load; N_g, N_w and N_l denote the total number of generators, wind units and loads, respectively; (a_i, b_i, c_i) are the triplet coefficients of quadratic cost function of generator i; T is the generation shift factors. $\boldsymbol{P}_g^{min}$ and $\boldsymbol{P}_g^{max}$ are the minimum and maximum limit of generator output, respectively; and $\boldsymbol{P}_T^{min}$ and $\boldsymbol{P}_T^{max}$ are the lower and upper limit of transmission capabilities, respectively.

In real time market, the forecasted intervals of the wind generation output may not be the same as the day-ahead forecasted results. Intuitively, for any given Pw in the range of $[\boldsymbol{P}_g^{min}, \boldsymbol{P}_g^{max}]$, we may solve the QP problem to get the corresponding optimal solution, which is therefore a function of $\boldsymbol{P}_w$. However, with wind output being an uncertain variable with stochastic features, sometimes the OPF model can be unsolvable because the feasible region defined by those hard constraints becomes empty. That is because in the above OPF model, all constraints are

considered as "hard" constraints, which cannot be violated. In practice, some constraints can be violated, which are called "soft" constraints, to reach a feasible solution. When soft constraints are allowed, a slack variable for each of the soft constraints is added in the OPF model, and the optimization objective function includes an additional term to represent the cost of constraint violations through penalty factors. To justify the OPF model with soft constraints, three principles are presented as follows:

(1) Soft constraints should be physically meaningful and safe in practice for a short duration.
(2) Soft constraint violation should not be too big.
(3) The OPF with soft constraints should yield the same optimal solution as that of the original OPF, when the original OPF itself has feasible solutions.

From (4.35)–(4.38) we can see that, the energy balance constraints can be selected as soft constraints and the objective function can be modified with curtailment of the demand load being selected as penalty function; we can also select transmission capacity constraints as soft constraints and the objective function can be modified with the violation of the transmission capacity being selected as penalty function. From the respective of solving the mathematical model, no matter what kinds of soft constraints are, the solving method of the optimization model and exact penalty function are the same.

Based on the above principles, we introduce the OPF with constraint relaxation as follows:

$$\min \quad \sum_{i=1}^{N_g} \left(c_i + b_i P_i + a_i P_i^2\right) + \rho \|\boldsymbol{\varepsilon} \otimes \boldsymbol{\delta}\|_{\infty} \tag{4.38}$$

$$s.t. \quad \sum_{i=1}^{N_g} P_{g,i} + \sum_{i=1}^{N_w} P_{w,i} = \sum_{i=1}^{N_l} P_{l,i} \tag{4.39}$$

$$\boldsymbol{P}_T^{\min} - \boldsymbol{\varepsilon} \otimes \boldsymbol{\delta} \le \boldsymbol{T}\left(\boldsymbol{P}_g + \boldsymbol{P}_w - \boldsymbol{P}_l\right) \le \boldsymbol{P}_T^{\max} + \boldsymbol{\varepsilon} \otimes \boldsymbol{\delta} \tag{4.40}$$

$$\boldsymbol{P}_g^{\min} \le \boldsymbol{P}_g \le \boldsymbol{P}_g^{\max}, \ given \quad \boldsymbol{P}_w \subset \left[\boldsymbol{P}_w^{\min}, \boldsymbol{P}_w^{\max}\right] \tag{4.41}$$

$$0 \le \boldsymbol{\varepsilon} \le \boldsymbol{\varepsilon}^{\max}, \ \boldsymbol{\delta} \in \{0, 1\}, \ \boldsymbol{\varepsilon} \otimes \boldsymbol{\delta} = [\varepsilon_1 \delta_1, \ldots, \varepsilon_m \delta_m]^T \tag{4.42}$$

where δ is a pre-determined vector of binary variables and δ_i if constraint i can be softened and $\delta_i = 0$ otherwise; ε is a relaxation vector; ρ is the penalty factor for violation; and m is the number of transmission lines.

The OPF model in (4.38)–(4.42) attempts to minimize the total production cost and the cost of constraint violation. According to principle (1), some transmission constraints are chosen as soft constraints. Principle (2) is taken into account by (4.42).

Selection of penalty factor is the most critical and difficult to the OPF model with soft constraints for Principle (3). Applying an extremely big penalty factor in model (4.38)–(4.42) will make it equivalent to the original OPF model (4.35)–(4.37). However, when the penalty factor is too large, the cost of constraint violations may dominate the objective function during iterations, which may lead to slow convergence or even retain the no-solution issue for certain scenarios [4]. When the penalty factor is too small, the soft constraints will be easily violated and objective function value will be lowered at the expense of higher level of constraint violations, and dispatch results will therefore be skewed.

Therefore, an "exact penalty function" method is proposed in this book to arrive at a reasonable and justified penalty factor that meets the requirement set forth in Principle (3).

According to [5, 6], in order to guarantee the OPF problems with soft constraints produce the same solution as that of the original OPF problem for any feasible $\boldsymbol{P}_w$, penalty factor ρ must be greater than the 1-norm of the Lagrange multipliers of transmission constraints (4.38), denoted by λ, over all given feasible range of $\boldsymbol{P}_w$, which can be formulated in (4.43). To simplify the representation, model (4.35)–(4.37) is transformed into general formulation (4.44) using matrix expression.

Theorem 4.1: If the penalty factor $\rho \geq \max \lambda_p$ and original model is feasible, then for any given $\boldsymbol{P}_w$, the model of (4.38)–(4.42) is strictly equivalent to the model of (4.35)–(4.37), where Lagrange multipliers are denoted by λ, and $\frac{1}{p} + \frac{1}{q} = 1$ holds.

For example, if we take $\|\boldsymbol{\varepsilon} \otimes \boldsymbol{\delta}\|_\infty$ represent penalty function, then p needs to take norm-1 multiplier, that is $\|\lambda\|_1$; if we take $\|\boldsymbol{\varepsilon} \otimes \boldsymbol{\delta}\|_1$ represent penalty function, then p needs to take norm-∞ multiplier, that is $\|\lambda\|_\infty$. Furthermore, according to theorem4.1, when $\rho \geq \max\|\lambda\|_p$, the objective function denoted by (4.39) is called exact penalty function. And [6] pointed out that if we take $\|\boldsymbol{\varepsilon} \otimes \boldsymbol{\delta}\|_1$ represent penalty function, then the numbers of decision variables and constraint conditions will increase, while if we take $\|\boldsymbol{\varepsilon} \otimes \boldsymbol{\delta}\|_\infty$ represent penalty function, then the number of mere decision variables will increase. Therefore, from the respective of time computational complexity, taking $\boldsymbol{\varepsilon} \otimes \boldsymbol{\delta}_\infty$ as penalty function is better. So we will study penalty function with norm-∞ in this passange.

Then, (4.43) can be subsequently converted to a bi-level optimization problem in (4.45). The lower-level problem can be replaced by its Karush-Kuhn-Tucker (KKT) condition to obtain the lower bound of ρ.

$$\rho \geq \max_{\boldsymbol{P}_w} \|\boldsymbol{\lambda}\|_1 \tag{4.43}$$

General formulation:

$$\min_{\boldsymbol{P}_g} \quad 0.5\boldsymbol{P}_g^T \boldsymbol{A} \boldsymbol{P}_g \tag{4.44}$$

$$\begin{aligned} s.t. \quad & \boldsymbol{B}_E\boldsymbol{P}_g = \boldsymbol{C}_E\boldsymbol{P}_l + \boldsymbol{D}_E\boldsymbol{P}_w \\ & \boldsymbol{B}_I\boldsymbol{P}_g \le \boldsymbol{C}_I\boldsymbol{P}_l + \boldsymbol{D}_I\boldsymbol{P}_w \\ & given\ \boldsymbol{P}_w \subset \left[\boldsymbol{P}_w^{\min}, \boldsymbol{P}_w^{\max}\right] \end{aligned}$$

Maximum Lagrange:

$$\max_{\boldsymbol{P}_w} \quad \|\boldsymbol{\lambda}\|_1 \tag{4.45}$$

$$\begin{aligned} s.t. \quad & \overset{\min}{w} \le \boldsymbol{P}_w \le \boldsymbol{P}_w^{\max} \\ & \min_{\boldsymbol{P}_g} 0.5\boldsymbol{P}_g^T\boldsymbol{A}\boldsymbol{P}_g \ : \quad \boldsymbol{\lambda} \\ s.t. \quad & \boldsymbol{B}_E\boldsymbol{P}_g = \boldsymbol{C}_E\boldsymbol{P}_l + \boldsymbol{D}_E\boldsymbol{P}_w \\ & \boldsymbol{B}_I\boldsymbol{P}_g \le \boldsymbol{C}_I\boldsymbol{P}_l + \boldsymbol{D}_I\boldsymbol{P}_w \end{aligned}$$

where $\boldsymbol{A}$ denotes the quadratic cost matrix; $\boldsymbol{B}_E$, $\boldsymbol{C}_E$ and $\boldsymbol{D}_E$ are the coefficients of equality constraints; $\boldsymbol{B}_I$, $\boldsymbol{C}_I$ and $\boldsymbol{D}_I$ are the coefficients of inequality constraints.

We can find that (4.45) is actually a bi-level optimization model, for the lower-level problem we can use KKT condition and big M theory to transform it into a hybrid integer linear programming and we have:

$$\begin{aligned} & \boldsymbol{B}_E\boldsymbol{P}_g = \boldsymbol{C}_E\boldsymbol{D} + \boldsymbol{D}_E\boldsymbol{P}_w \\ & \boldsymbol{B}_I\boldsymbol{P}_g \le \boldsymbol{C}_I\boldsymbol{D} + \boldsymbol{D}_I\boldsymbol{P}_w \\ & \boldsymbol{A}\boldsymbol{P}_g + \boldsymbol{B}_I^T\lambda + \boldsymbol{B}_E^T\mu_1 = \boldsymbol{0} \\ & \left(\boldsymbol{C}_I\boldsymbol{D} + \boldsymbol{D}_I\boldsymbol{P}_w - \boldsymbol{B}_I\boldsymbol{P}_g\right) * \lambda = \boldsymbol{0} \\ & \lambda \ge 0, -\infty \le \mu_1 \le +\infty \end{aligned} \quad \Leftrightarrow \quad \begin{aligned} & \boldsymbol{B}_E\boldsymbol{P}_g = \boldsymbol{C}_E\boldsymbol{D} + \boldsymbol{D}_E\boldsymbol{P}_w \\ & \boldsymbol{A}\boldsymbol{P}_g + \boldsymbol{B}_I^T\lambda + \boldsymbol{B}_E^T\mu_1 = \boldsymbol{0} \\ & -\boldsymbol{M}(1-\boldsymbol{s}) \le \boldsymbol{B}_I\boldsymbol{P}_g - \boldsymbol{C}_I\boldsymbol{D} - \boldsymbol{D}_I\boldsymbol{P}_w \le \boldsymbol{0} \\ & 0 \le \lambda \le \boldsymbol{M}\boldsymbol{s} \quad \boldsymbol{s} \in \{0,1\} \end{aligned} \tag{4.46}$$

where M is a large number, $\boldsymbol{s}$ is an integer one dummy variable, the model in (4.45) can be transformed into:

$$\max_{\boldsymbol{P}_w} \lambda_1 \tag{4.47}$$

$$\text{s.t.} \boldsymbol{P}_w^{min} \le \boldsymbol{P}_w \le \boldsymbol{P}_w^{max}$$

$$\boldsymbol{B}_E\boldsymbol{P}_g = \boldsymbol{C}_E\boldsymbol{D} + \boldsymbol{D}_E\boldsymbol{P}_w$$

$$\boldsymbol{A}\boldsymbol{P}_g + \boldsymbol{B}_I^T\lambda + \boldsymbol{B}_E^T\mu_1 = \boldsymbol{0}$$

$$-\boldsymbol{M}(1-\boldsymbol{s}) \le \boldsymbol{B}_I\boldsymbol{P}_g - \boldsymbol{C}_I\boldsymbol{D} - \boldsymbol{D}_I\boldsymbol{P}_w \le \boldsymbol{0}$$

$$0 \le \lambda \le \boldsymbol{M}\boldsymbol{s} \quad \boldsymbol{s} \in \{0,1\}$$

From the respective view of mathematics, the sufficient and necessary condition "KKT condition is a convex quadric programming" is that the model is feasible, but the lower-level convex quadric programming in the model (4.45) may be infeasible. At present, KKT condition cannot guarantee the optimality, so that the Lagrange multiplier λ may not be determined solely. Therefore, we can transform (4.47) into (4.48) to guarantee the uniqueness of λ.

$$\max_{\boldsymbol{P}_w} \|\lambda\|_1 \tag{4.48}$$

$$\text{s.t.} \boldsymbol{P}_w^{min} \le \boldsymbol{P}_w \le \boldsymbol{P}_w^{max}$$

$$\boldsymbol{B}_E \boldsymbol{P}_g = \boldsymbol{C}_E \boldsymbol{D} + \boldsymbol{D}_E \boldsymbol{P}_w$$

$$-\boldsymbol{M}(1-\boldsymbol{s}) \le \boldsymbol{B}_I \boldsymbol{P}_g - \boldsymbol{C}_I \boldsymbol{D} - \boldsymbol{D}_I \boldsymbol{P}_w \le \boldsymbol{0}$$

$$\min 0.5\, \boldsymbol{\lambda}^T \boldsymbol{\lambda}$$

$$\boldsymbol{A}\boldsymbol{P}_g + \boldsymbol{B}_I^T \lambda + \boldsymbol{B}_E^T \mu_1 = \boldsymbol{0}$$

$$0 \le \boldsymbol{\lambda} \le \boldsymbol{M}\boldsymbol{s} \quad \boldsymbol{s} \in \{0,1\}$$

Then the KKT condition will be utilized again to transform the expression of convex quadric programming into a mixed integer programming, so we have:

$$\gamma = \max_{\boldsymbol{P}_w, \boldsymbol{\lambda}, \boldsymbol{P}_g, \boldsymbol{s}} 1^T \boldsymbol{\lambda} \tag{4.49}$$

$$\text{s.t.}\ \boldsymbol{0} \le \boldsymbol{\lambda} \le \boldsymbol{M}\boldsymbol{s} \tag{4.50}$$

$$\boldsymbol{B}_E \boldsymbol{P}_g = \boldsymbol{C}_E \boldsymbol{D} + \boldsymbol{D}_E \boldsymbol{P}_w \tag{4.51}$$

$$-\boldsymbol{M}(1-\boldsymbol{s}) \le \boldsymbol{B}_I \boldsymbol{P}_g - \boldsymbol{C}_I \boldsymbol{D} - \boldsymbol{D}_I \boldsymbol{P}_w \le \boldsymbol{0} \tag{4.52}$$

$$\boldsymbol{A}\boldsymbol{P}_g + \boldsymbol{B}_I^T \lambda + \boldsymbol{B}_E^T \mu_1 = \boldsymbol{0} \tag{4.53}$$

$$\boldsymbol{\lambda} + [-\boldsymbol{I}, \boldsymbol{I}]\boldsymbol{\theta} + \boldsymbol{B}_I \boldsymbol{\mu}_2 = \boldsymbol{0} \tag{4.54}$$

$$\boldsymbol{0} \le \boldsymbol{\theta} \le \mathbf{M} \begin{bmatrix} 1-\boldsymbol{s} \\ 1-\boldsymbol{s} \end{bmatrix} \tag{4.55}$$

$$\boldsymbol{P}_w^{min} \le \boldsymbol{P}_w \le \boldsymbol{P}_w^{max}, \boldsymbol{s} \in \{0,1\} \tag{4.56}$$

Obviously, the model in (4.49)–(4.56) is a simple mixed integer quadric programming model, and we can use = branch-and-bound algorithm to solve the model and get the global optimal goal γ, and it is just the lower bound of ρ.

4.3.2.2 Numerical Example

The proposed method based on exact penalty function has been verified on a six-bus test system shown in Fig. 4.13 and implemented with MATPOWER toolbox and CPLEX 12.

Solving model (4.47) gives the lower bound of ρ as 11.4265 $/MW. Assume the constraint maximum relaxation amount of each line capacity is $\varepsilon^{\max} = 10^T$ MW. When $P_{w1} = 30$ MW, the original OPF is feasible with the objective value $5261.77, and the constraint relaxation method using $\rho = 10^6$ gives the same solution. However, the iteration increases and numerical problems may occur when ρ is chosen 10^{10}. When a smaller ρ, such as 10, is selected which does not meet the criterion 11.4265, the hard constraint is softened and a different solution is produced. When $P_{w1} = 25$ MW, the original OPF is infeasible. Using the proposed method, the objective function value is $5351.02 with two soft constraints (SC), and $5342.84 with three SCs. Because of the lower penalty factor, lower objective function is achieved with one more SC. It should be pointed out that the same solution will be obtained for any ρ equal or greater than 11.4265. It demonstrates the exact penalty function can give the true lower bound of penalty factor ρ that satisfies Principle (3). Finally, tests on three large IEEE test systems with multiple wind farms show acceptable computational time (Tables 4.3 and 4.4).

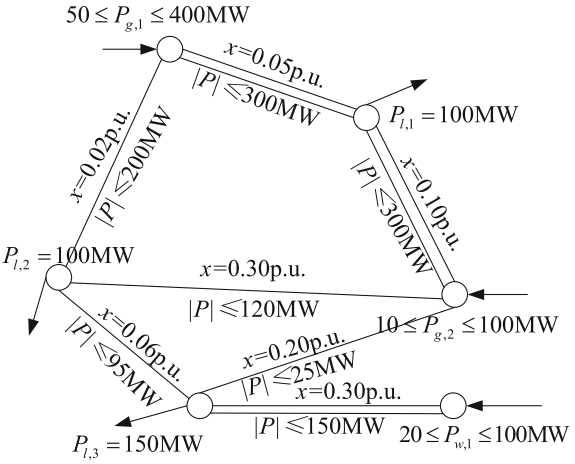

Fig. 4.13 A six-bus test system

Table 4.3 Solutions of feasible/infeasible OPF for different ρ

	Feasible OPF				Infeasible OPF	
P_{w1}(MW)	30				25	
ρ ($/MW)	×	10	11.4265	10^6	11.4265	10
# of SCs	0	1	0	0	2	3
Objective($)	5261.77	5259.39	5261.77	5261.77	5351.02	5342.84
Iteration	3	6	7	12	8	6

Note × denotes the penalty function is not considered

Table 4.4 Computational time of large systems with multiple wind farms

	IEEE 57-bus		IEEE 118-bus		IEEE 300-bus	
# of P_w	1	4	2	6	6	15
ρ ($/MW)	0	6.49	2.08	6.35	47.72	984.33
Time (s)	0.32	1.65	3.62	4.46	12.15	13.42

4.4 Conclusions

In this chapter, we have mainly addressed two questions: one is to apply the interval optimization theory into the power system economic dispatch model and establish the interval economic dispatch model; the other one is to study the methods to deal with infeasible economic dispatch when considering the stochastic of wind generation output. With interval economic dispatch model, we can extend the conventional determined economic dispatch model to uncertain interval model, as well as assume the uncertain wind generation output to be interval numbers as the inputs. Then we can get the optimization objectives as well as the varying ranges of optimal solutions. The interval results can be used to evaluate the influence of uncertainty of wind generation on the economic model and regarded as the extension of the sensitivity analysis of the economic dispatch optimization model. Generally speaking, sensitivity analysis is studying the influence of the disturbance of uncertain parameters on the optimal solutions, while interval optimization allows the parameters to vary in a large range and gets the interval results of the optimal solutions. Therefore, interval optimization has a wilder application range.

However, conventional economic dispatch model yields the optimal solutions under the given wind generation output forecasted values. When considering the uncertainty of wind generation outputs, we must not only guarantee the feasibility of the economic dispatch model under the given wind generation output forecasted values, but also pay attention to whether the economic dispatch model is always feasible when the wind generation outputs take arbitrary values within the given varying ranges. In this chapter we have studied two models for the infeasible economic dispatch model with wind generation outputs varying within the given ranges: the one is to minimize curtailment of wind generation, the other is to allow short term violation of transmission capacities. We can use the first solution into day-ahead dispatch and make a long term dispatch schedule while using the second one into real time dispatch model when considering the exact penalty function based constraint relaxation for the short time violation of constraints. Since power system is operating in the closed loop state, the original dispatch results can be updated in the next dispatch period and therefore the model may be feasible. So the economic dispatch model considering short term violation of the constraint can be used in real time dispatch.

Finally, through numerical results on many test systems, we have verified the effectiveness of the above methods proposed in this chapter. We have also tested

the time complexity on large-scale test system and the results illustrate the optimization model can be used in current real time dispatch and can provide some experience to decision makers.

References

1. Gu X, Ler T, Gross G (2007) Detection of island formation and identification of causal factors under multiple line outages. IEEE Trans Power Syst 22(2):505–513
2. Guo JC, Fu Y, Li ZY et al (2009) Direct calculation of line outage distribution factors. IEEE Trans Power Syst 24(3):1633–1634
3. Zimmerman RD, Murillo-Sa X, Nchez CE et al (2011) MATPOWER: steady-state operations, planning, and analysis tools for power systems research and education. IEEE Trans Power Syst 26(1):12–19
4. Fletcher R (1987) Practical methods of optimization. 2nd edn. Wiley, New York
5. Wills AG, Heath WP (2003) An exterior/interior-point approach to infeasibility in model predictive control
6. Gautam A, Yeng CS (2013) Soft-constrained model predictive control based on off-line-computed feasible sets. IEEE 52nd Annual Conference on Decision and Control. Firenze

Chapter 5
Robust Interval Economic Dispatch and the Price of Robustness

Abstract Interval economic dispatch only gives an interval solution, which cannot be used for the practical dispatch schedule, but only be used for evaluating the impact of wind power uncertainties. To find an optimal dispatch schedule from the interval solution while providing a "robust" solution for power system operators, interval robust optimization is proposed, including adaptive interval robust optimization and two-stage interval optimization models. The optimal solution from interval robust optimization is sacrificed by guaranteeing the whole security within the uncertainty set, which may lead to the conservatism comparing to the traditional deterministic economic dispatch. To reduce the conservatism, the price of robustness is introduced for decision makers.

5.1 Introduction

An interval economic dispatch model has been proposed in the last chapter. It's not hard to see that interval optimization solution calculated from this model only can be used for assessing the economic dispatch model considering uncertainty of wind power and observing the effect of wind power changing on the optimal objective function and optimal solutions of economic dispatch model. However, in the practical power system, interval optimization solution cannot be used for direct dispatch scheduling. In fact, a determined optimal value must be chosen from the interval solutions. Therefore, this chapter will research the robust interval economic dispatch model, which could get a robust economic dispatch optimization solution for decision makers.

The robust interval economic dispatch model can obtain an optimal solution to guarantee the security for any given realization of wind power output. In other words, the systems will reach the worst condition within the scope of wind power output and the robust interval economic dispatch model obtains an optimal solution in this situation. There are two models to be discussed in this chapter: adaptive

T. Ding, *Power System Operation with Large Scale Stochastic Wind Power Integration*, Springer Theses, DOI 10.1007/978-981-10-2561-7_5

robust interval economic dispatch model and two-stage robust interval economic dispatch model. The adaptive robust interval economic dispatch model considers the AGC control, where the AGC generators output will be adjusted to the imbalance power resulted from the wind power variation. In this situation, the objective of the adaptive robust interval economic dispatch model is to obtain the optimal scheduling, while satisfying all the security constraints after AGC control. The two-stage robust interval economic dispatch model considers the day-ahead network topology control. The generation output will be re-dispatched in response to the uncertainty of wind power output. In the worst wind power output situation, the objective of two-stage robust interval economic dispatch model is to obtain the optimal network topology, which ensures the system security. In the perspective of physical modeling, the two-stage robust interval economic dispatch model contains long and short time scales. This model obtains the optimization for topology control in the long time scale and considers the optimal scheduled generation in the short time scale situation.

Observe that the robust interval economic dispatch model is the coordination of security and economy, which fully ensures the security of power systems but the solutions might be conservative compared to the traditional economic dispatch model. In order to reduce the conservativeness, the price of robustness is introduced in this chapter, which proposes the optimal solution set under different robustness prices. This conception can be considered a new Paroto front. Finally, the flowchart of this chapter can be expressed in the Fig. 5.1.

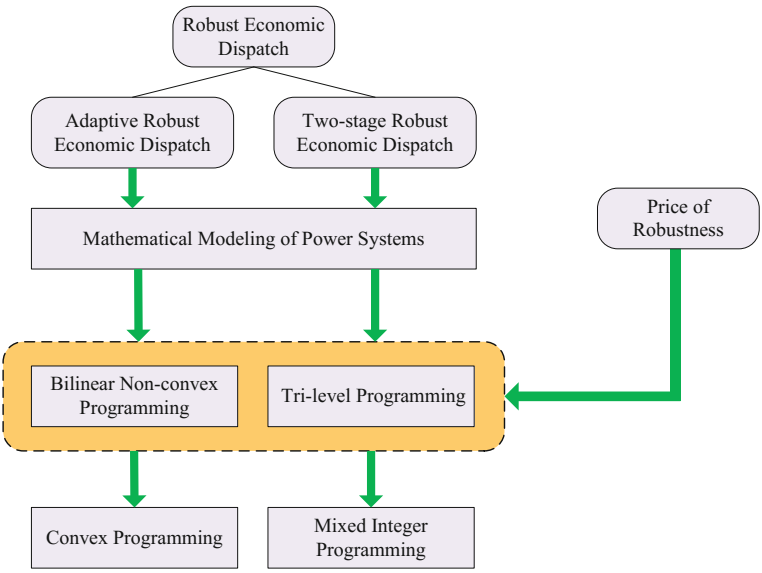

Fig. 5.1 Flowchart of this chapter

5.2 The Real-Time Robust Interval Economic Dispatch Model

5.2.1 The Adaptive Robust Interval Economic Dispatch Model Considering Uncertain Wind Power Output

Typically, the conventional dispatch model considering uncertainties of wind power is conducted under a single deterministic condition using the forecasted uncertain generation, which aims to minimize the total generation costs while guaranteeing the power balance and transmission security within the generator physical capacity. The fuel cost function usually adopts a quadratic function in electricity markets and security constraints are made up of several inequalities to ensure the loading of each transmission line within its capacity. According to the Sect. 4.2, the conventional dispatch model performs as follows:

$$(\text{Conventional model}) \min_{\boldsymbol{P}^{sch}} \sum_{i=1}^{N_g} \left(a_i \left(P_i^{sch} \right)^2 + b_i P_i^{sch} + c_i \right) \tag{5.1}$$

$$s.t. \sum_{j=1}^{N_d} D_j - \sum_{k=1}^{N_w} W_k^f = \sum_{i=1}^{N_g} P_i^{sch} \tag{5.2}$$

$$P_i^{\min} \le P_i^{sch} \le P_i^{\max}, \quad i = 1, \ldots, N_g \tag{5.3}$$

$$-F_l^{\max} \le \sum_{i=1}^{N_g} S_{l,i} P_i^{sch} + \sum_{k=1}^{N_w} G_{l,k} W_k^f - \sum_{j=1}^{N_d} H_{l,j} D_j \le F_l^{\max}, \quad l = 1, \ldots, N_l \tag{5.4}$$

where

P_i^{sch}	Scheduled generation of unit i
D_j	Forecasted load demand of site j
R_k^f	Forecasted generation of renewable resources unit k
(a_i, b_i, c_i)	Quadratic fuel cost coefficients of unit i
N_g	Total number of dispatchable units
N_d	Total number of load nodes
N_r	Total number of renewable resources units
N_l	Total number of transmission lines
$F_l^{\max}$	Transmission capacity of line l at period t
$G_{l,i}^P$	Distribution factor of dispatchable generation at bus i on line l
$G_{l,j}^D$	Distribution factor of load at bus i on line l
$G_{l,k}^R$	Distribution factor of renewable resource at bus k on line l
$P_i^{\min}/P_i^{\max}$	Maximum/minimum generation of unit i

Even with better understanding and modeling of both the meteorological and power conversion processes of renewable resources, an inherent and irreducible uncertainty will always occur in every forecast which may bring about challenge to the transmission security. In order to take the uncertainties into account for traditional DCOPF, the interval-based robust optimization method has been widely used in recent years, where the uncertainties were usually modeled as interval values. This can be given by

$$W_k \in \left[W_k^f - W_k^e, W_k^f + W_k^e\right], \quad k = 1, \ldots, N_w \tag{5.5}$$

where W_k^e represents the forecast error of renewable resource at bus k. Observe the model (5.1)–(5.4), the power balance equation constraints will be violated due to the imbalance resulted from the uncertain wind power output. Actually, the AGC generators can ensure the power balance through the true control based on the deviation. Therefore, an adaptive robust interval economic dispatch model is proposed in this paper to optimize the generation cost while ensuring the security of power systems.

Note that the balance between the total generation including thermal and renewable resources and the total load demand must be guaranteed at any time. So the generation of thermal units should be adjusted with the uncertain renewable resources output [1]. Let β_i denote the participation factor of unit i and the actual generation output can be expressed as in (5.6). Generally, it is desired that the participation factor is a nonnegative value, since the thermal generators will be adjusted by the participation factor to meet the energy balance. If a small increment of uncertainties is added to the studied power system, the generators must reschedule the output of appropriate generators to move to a new generation level within a short period of time.

$$\begin{aligned}
&\sum_{j=1}^{N_d} D_j - \sum_{k=1}^{N_w} W_k^f - \sum_{i=1}^{N_g} P_i^{sch} = 0, \\
&P_i = P_i^{sch} + \beta_i \varepsilon, \\
&\varepsilon = \sum_{j=1}^{N_d} D_j - \sum_{k=1}^{N_w} W_k - \sum_{i=1}^{N_g} P_i^{sch} = \sum_{k=1}^{N_w} \left(W_k^f - W_k\right)
\end{aligned} \tag{5.6}$$

where $\sum_{i=1}^{N_g} \beta_i = 1$ and $0 \le \beta_i \le 1$. $\mathrm{E}(\varepsilon) = 0$ implies that the expectation of wind power prediction error is 0; P_i is the actual power output of generator i after the AGC control. Equation (5.7), obtained through (5.6), explains that the generation and electricity can always be balanced by the participation factor.

$$\sum_{i=1}^{N_g} P_i = \sum_{i=1}^{N_g} \left(P_i^{sch} + \beta_i \varepsilon\right) = \sum_{i=1}^{N_g} P_i^{sch} + \varepsilon \sum_{i=1}^{N_g} \beta_i = \sum_{i=1}^{N_g} P_i^{sch} + \varepsilon = \sum_{j=1}^{N_d} D_j - \sum_{k=1}^{N_w} W_k \tag{5.7}$$

Taking the P_i in (5.6), the expected value of objective function is

$$\begin{aligned} \mathrm{E}\left(\sum_{i=1}^{N_g} \left(a_i (P_i)^2 + b_i P_i + c_i\right)\right) &= \mathrm{E}\left(\sum_{i=1}^{N_g} \left(a_i \left(P_i^{sch} + \beta_i \varepsilon\right)^2 + b_i \left(P_i^{sch} + \beta_i \varepsilon\right) + c_i\right)\right) \\ &= \mathrm{E}\left(\sum_{i=1}^{N_g} \left(a_i \left(P_i^{sch} + \beta_i \varepsilon\right)^2 + b_i \left(P_i^{sch} + \beta_i \varepsilon\right) + c_i\right)\right) \\ &= \sum_{i=1}^{N_g} \left(a_i \left(P_i^{sch}\right)^2 + b_i P_i^{sch} + c_i\right) + \mathrm{E}\left(\sum_{i=1}^{N_g} \left(a_i \beta_i^2 \varepsilon^2 + b_i \beta_i \varepsilon\right)\right) \end{aligned} \tag{5.8}$$

$$\begin{aligned} \mathrm{E}\left(\sum_{i=1}^{N_g} \left(a_i \beta_i^2 \varepsilon^2 + b_i \beta_i \varepsilon\right)\right) &= \mathrm{E}\left(\sum_{i=1}^{N_g} a_i \beta_i^2 \varepsilon^2\right) + \mathrm{E}\left(\sum_{i=1}^{N_g} a_i \beta_i^2 \varepsilon^2\right) = \mathrm{E}\left(\varepsilon^2\right) + 0 \\ &= \mathrm{E}(\varepsilon - \mathrm{E}(\varepsilon))^2 = \mathrm{E}\left(\sum_{k=1}^{N_w} \left(W_k - W_k^f\right)\right)^2 = \mathrm{E}\left(\left(\boldsymbol{e}^T \boldsymbol{W}\right)\left(\boldsymbol{e}^T \boldsymbol{W}\right)^T\right) \\ &= \mathrm{E}\left(\boldsymbol{e}^T \boldsymbol{W} \boldsymbol{W} \boldsymbol{e}^T\right) = \boldsymbol{e}^T E(\boldsymbol{W}\boldsymbol{W}) \boldsymbol{e}^T = \boldsymbol{e}^T \boldsymbol{\Lambda} \boldsymbol{e}^T = \sum_{k=1}^{N_w} \sum_{j=1}^{N_w} \Lambda_{kj} \end{aligned} \tag{5.9}$$

Finally, the objective function is as follows:

$$\min_{\boldsymbol{P}^{sch}} \sum_{i=1}^{N_g} \left(a_i \left(P_i^{sch}\right)^2 + b_i P_i^{sch} + c_i + a_i \beta_i^2 \sum_{k=1}^{N_w} \sum_{j=1}^{N_w} \Lambda_{kj}\right) \tag{5.10}$$

where $\boldsymbol{\Lambda}$ denotes the covariance matrix of renewable resource generation, which can be obtained from the historical data. Then taking P_i into (5.4) and (5.4), the roust DCOPF can be formulated as:

$$\text{(Robust model)} \quad \min_{\boldsymbol{P}^{sch}} \sum_{i=1}^{N_g} \left(a_i \left(P_i^{sch}\right)^2 + b_i P_i^{sch} + c_i + a_i \beta_i^2 \sum_{k=1}^{N_w} \sum_{j=1}^{N_w} \Lambda_{kj}\right) \tag{5.11}$$

$$s.t. \sum_{j=1}^{N_d} D_j - \sum_{k=1}^{N_w} W_k^f = \sum_{i=1}^{N_g} P_i^{sch} \tag{5.12}$$

$$P_i^{\min} \le P_i^{sch} + \beta_i \sum_{k=1}^{N_r} \left(W_k^f - W_k \right) \le P_i^{\max}, \quad i = 1, \ldots, N_g \tag{5.13}$$

$$\begin{aligned} -F_l^{\max} \le & \sum_{i=1}^{N_g} S_{l,i} \left(P_i^{sch} + \beta_i \sum_{k=1}^{N_w} \left(W_k^f - W_k \right) \right) \\ & + \sum_{k=1}^{N_r} G_{l,k} W_k - \sum_{j=1}^{N_d} H_{l,j} D_j \le F_l^{\max}, \quad l = 1, \ldots, N_l \end{aligned} \tag{5.14}$$

$$\sum_{i=1}^{N_g} \beta_i = 1, \quad 0 \le \beta_i \le 1, \ \forall W_k \in \left[W_k^f - W_k^e, W_k^f + W_k^e \right], \ k = 1, \ldots, N_w \tag{5.15}$$

5.2.2 *The Adaptive Robust Interval Economic Dispatch Model Considering the Price of Robustness*

It is widely considered in robust optimization research that the robust optimization model always produces over conservative solutions in the sense that it gives up too much optimality for the nominal problem in order to ensure robustness. Therefore, the price of robustness was proposed in [2–6] to reduce the conservatism, where the scaled deviations are assumed to belong to a polyhedral uncertainty set such that

$$W_k = W_k^f + W_k^e y_k, \quad k = 1, \ldots, N_w, \ \Omega = \left\{ \boldsymbol{y} | \sum_{k=1}^{N_w} |y_k| \le \Gamma, |y_k| \le 1, \forall k \right\} \tag{5.16}$$

where Γ is a parameter to adjust the robustness against the conservation level of the solution and $\Gamma \in [0, N_w]$. Equation (5.16) implies that only a subset of the uncertainties will change in order to adversely affect the solution. According to the Central Limit Theory, the arithmetic mean of a sufficiently large number of iterations of independent random variables will be approximately normally distributed. That is, assuming that a sample is obtained containing a large number of observations, each observation is randomly generated in a way that is independent on the values of the other observations, and then the arithmetic average of the observed values is calculated. In this approach, the worst scenario in robust optimization that all the uncertainties take their worst cases is reduced.

(i) If $\Gamma = 0$, uncertain polyhedral set Ω contains only the zero point such that the robust optimization equals to traditional deterministic counterpart.
(ii) If $\Gamma = N_w$, all the uncertainties take their worst cases, which is the robust optimization model in (5.11)–(5.15).
(iii) If $0 < \Gamma < N_w$, the conservative robustness is protected and can allow the decision-maker to make a trade-off.

With the consideration of the price of robustness, the original adaptive robust optimal power flow in (5.11)–(5.15) can be reformulated as:

$$\min_{\boldsymbol{P}^{sch}} \sum_{i=1}^{N_g} \left(a_i \left(P_i^{sch}\right)^2 + b_i P_i^{sch} + c_i + a_i \beta_i^2 \sum_{k=1}^{N_w} \sum_{j=1}^{N_w} \Lambda_{kj} \right) \tag{5.17}$$

$$s.t. \quad \sum_{j=1}^{N_d} D_j - \sum_{k=1}^{N_w} W_k^f = \sum_{i=1}^{N_g} P_i^{sch} \tag{5.18}$$

$$P_i^{\min} \le P_i^{sch} + \beta_i \sum_{k=1}^{N_w} \left(W_k^f - W_k^f - W_k^e y_k \right) \le P_i^{\max}, \quad i = 1, \ldots, N_g \tag{5.19}$$

$$\begin{aligned} -F_l^{\max} \le & \sum_{i=1}^{N_g} S_{l,i} \left(P_i^{sch} + \beta_i \sum_{k=1}^{N_w} \left(W_k^f - W_k^f - W_k^e y_k \right) \right) \\ & + \sum_{k=1}^{N_w} G_{l,k} \left(W_k^f + W_k^e y_k \right) - \sum_{j=1}^{N_d} H_{l,j} D_j \le F_l^{\max}, \quad l = 1, \ldots, N_l \end{aligned} \tag{5.20}$$

$$\sum_{i=1}^{N_g} \beta_i = 1, \quad 0 \le \beta_i \le 1, \ \forall \boldsymbol{y} \in \Omega = \left\{ \boldsymbol{y} \middle| \sum_{k=1}^{N_w} |y_k| \le \Gamma, |y_k| \le 1, \forall k \right\} \tag{5.21}$$

5.2.3 Simplification of the Proposed Model

It can be observed that the robust optimal power flow model in (5.17)–(5.21) is actually to find an optimal solution while satisfying the constraints for any given uncertain parameter, $\boldsymbol{y}$. Generally, the "for any" constraint is difficult to deal with. In order to solve this model, the proposed model is reformulated as a bi-level optimization model, such that

$$\min_{\boldsymbol{P}^{sch}, \boldsymbol{\beta}} \sum_{i=1}^{N_g} \left(a_i \left(P_i^{sch}\right)^2 + b_i P_i^{sch} + c_i + a_i \beta_i^2 \sum_{k=1}^{N_w} \sum_{j=1}^{N_w} \Lambda_{kj} \right) \tag{5.22}$$

$$s.t. \ \sum_{j=1}^{N_d} D_j - \sum_{k=1}^{N_w} W_k^f = \sum_{i=1}^{N_g} P_i^{sch} \tag{5.23}$$

$$\begin{cases} \max\limits_{\boldsymbol{y}\in\Omega}\left(P_i^{sch}-\beta_i\sum\limits_{k=1}^{N_w}W_k^e y_k\right)\le P_i^{\max} \\ P_i^{\min}\le\min\limits_{\boldsymbol{y}\in\Omega}\left(P_i^{sch}-\beta_i\sum\limits_{k=1}^{N_w}W_k^e y_k\right) \end{cases},\quad i=1,\ldots,N_g \tag{5.24}$$

$$\begin{cases} \max\limits_{\boldsymbol{y}\in\Omega}\left(\sum\limits_{i=1}^{N_g}S_{l,i}\left(P_i^{sch}-\beta_i\sum\limits_{k=1}^{N_w}W_k^e y_k\right)\right. \\ \quad\left.+\sum\limits_{k=1}^{N_w}G_{l,k}\left(W_k^f+W_k^e y_k\right)-\sum\limits_{j=1}^{N_d}H_{l,j}D_j\right)\le F_l^{\max} \\ -F_l^{\max}\le\min\limits_{y\in\Omega}\left(\sum\limits_{i=1}^{N_g}S_{l,i}\left(P_i^{sch}-\beta_i\sum\limits_{k=1}^{N_w}W_k^e y_k\right)\right. \\ \quad\left.+\sum\limits_{k=1}^{N_w}G_{l,k}\left(W_k^f+W_k^e y_k\right)-\sum\limits_{j=1}^{N_d}H_{l,j}D_j\right) \end{cases},\quad l=1,\ldots,N_l \tag{5.25}$$

$$\sum_{i=1}^{N_g}\beta_i=1,\quad 0\le\beta_i\le 1 \tag{5.26}$$

For (5.22), we derive

$$\begin{cases} \max\limits_{\boldsymbol{y}\in\Omega}\left(P_i^{sch}+\beta_i\sum\limits_{k=1}^{N_r}\left(W_k^f-W_k^f-W_k^e y_k\right)\right)=P_i^{sch}-\beta_i\max\limits_{\sum_{k=1}^{N_r}y_k=\Gamma,\,0\le y_k\le 1}\sum\limits_{k=1}^{N_r}W_k^e y_k \\ \min\limits_{\boldsymbol{y}\in\Omega}\left(P_i^{sch}+\beta_i\sum\limits_{k=1}^{N_r}\left(W_k^f-W_k^f-W_k^e y_k\right)\right)=P_i^{sch}+\beta_i\max\limits_{\sum_{k=1}^{N_r}y_k=\Gamma,\,0\le y_k\le 1}\sum\limits_{k=1}^{N_r}W_k^e y_k \end{cases} \tag{5.27}$$

It can be observed that the last term in (5.27) is a special linear programming that has only one equality constraint and variable bound constraints. Before any further discussion, first, we give a corollary as follows.

Corollary 5.1 [7]: *For the linear programming model* (5.28), *let* i_1, …, i_n *be a permutation of* 1,…,*n*, *such that* $c_{i_1}\ge\cdots\ge c_{i_n}$. *The optimal objective function value is given by* (5.29)

$$f=\max_{\boldsymbol{x}}\ \sum_{i=1}^{n}c_i x_i\quad s.t.\ \sum_{i=1}^{n}x_i=b,\quad 0\le x_i\le\bar{x}_i \tag{5.28}$$

$$f^* = \sum_{m=1}^{k-1} (c_{i_m} - c_{i_k})\bar{x}_{i_m} + c_{i_k} b \tag{5.29}$$

where $k(1 \le k \le n)$ is an integer number, such that $\sum_{m=1}^{k-1} \bar{x}_{i_m} \le b \le \sum_{m=1}^{k} \bar{x}_{i_m}$.

Based on Corollary 5.1, the optimal solution of the optimization model (5.27) is given by

$$\theta = \max_{\sum_{k=1}^{N_w} y_k = \Gamma, 0 \le y_k \le 1} \sum_{k=1}^{N_w} W_k^e y_k = \sum_{m=1}^{k-1} \left(W_{i_m}^e - W_{i_k}^e \right) + W_{i_k}^e \Gamma \tag{5.30}$$

where $i_1, \ldots, i_{N_r}$ is a permutation of 1,..., N_r, such that $R_{i_1}^e \ge \cdots \ge R_{i_{N_r}}^e$ and k $(1 \le k \le N_r)$ is an integer number, such that $k - 1 \le \Gamma \le k$. Therefore, (5.24) can be simplified as

$$P_i^{\min} + \beta_i \theta \le P_i^{sch} \le P_i^{\max} - \beta_i \theta, \quad i = 1, \ldots, N_g \tag{5.31}$$

For (5.25), we derive

$$\begin{aligned}
&\max_{y \in \Omega} \left(\sum_{i=1}^{N_g} S_{l,i} \left(P_i^{sch} + \beta_i \sum_{k=1}^{N_w} W_k^e y_k \right) + \sum_{k=1}^{N_w} G_{l,k} \left(W_k^f + W_k^e y_k \right) - \sum_{j=1}^{N_d} H_{l,j} D_j \right) \\
&= \sum_{i=1}^{N_g} S_{l,i} P_i^{sch} + \sum_{k=1}^{N_w} G_{l,k} W_k^f - \sum_{j=1}^{N_d} H_{l,j} D_j + \max_{y \in \Omega} \left(\sum_{k=1}^{N_w} G_{l,k} W_k^e y_k - \sum_{i=1}^{N_g} S_{l,i} \left(\beta_i \sum_{k=1}^{N_w} W_k^e y_k \right) \right) \\
&= \sum_{i=1}^{N_g} S_{l,i} P_i^{sch} + \sum_{k=1}^{N_w} G_{l,k} W_k - \sum_{j=1}^{N_d} H_{l,j} D_j + \max_{\sum_{k=1}^{N_w} y_k = \Gamma, 0 \le y_k \le 1} \left(\sum_{k=1}^{N_w} \left[W_k^e y_k \left(\sum_{i=1}^{N_g} S_{l,i} \beta_i + G_{l,k} \right) \right] \right)
\end{aligned} \tag{5.32}$$

$$\begin{aligned}
&\min_{y \in \Omega} \left(\sum_{i=1}^{N_g} S_{l,i} \left(P_i^{sch} + \beta_i \sum_{k=1}^{N_w} W_k^e y_k \right) + \sum_{k=1}^{N_w} G_{l,k} \left(W_k^f + W_k^e y_k \right) - \sum_{j=1}^{N_d} H_{l,j} D_j \right) \\
&= \sum_{i=1}^{N_g} S_{l,i} P_i^{sch} + \sum_{k=1}^{N_w} G_{l,k} W_k^f - \sum_{j=1}^{N_d} H_{l,j} D_j + \min_{y \in \Omega} \left(\sum_{k=1}^{N_w} G_{l,k} W_k^e y_k - \sum_{i=1}^{N_g} S_{l,i} \left(\beta_i \sum_{k=1}^{N_w} W_k^e y_k \right) \right) \\
&= \sum_{i=1}^{N_g} S_{l,i} P_i^{sch} + \sum_{k=1}^{N_w} G_{l,k} W_k - \sum_{j=1}^{N_d} H_{l,j} D_j - \max_{\sum_{k=1}^{N_w} y_k = \Gamma, 0 \le y_k \le 1} \left(\sum_{k=1}^{N_w} \left[W_k^e y_k \left(\sum_{i=1}^{N_g} S_{l,i} \beta_i + G_{l,k} \right) \right] \right)
\end{aligned} \tag{5.33}$$

Theorem 5.2 [3]: *The following robust optimization formulation in* (5.34)–(5.36) is equivalent to (5.37)–(5.40).

$$\max \boldsymbol{c}'\boldsymbol{x} \tag{5.34}$$

$$\text{s.t.} \sum_{j=1}^{n} a_{ij}x_j + \max_{\sum_{j=1}^{n} z_{ij}=\Gamma,\, 0\le z_{ij}\le 1} \left\{ \sum_{j=1}^{n} \bar{a}_{ij} z_{ij} x_j \right\} \le b_i, \quad i = 1, \ldots, n \tag{5.35}$$

$$x \in X \tag{5.36}$$

$$\max \boldsymbol{c}'\boldsymbol{x} \tag{5.37}$$

$$\text{s.t.} \sum_{j=1}^{n} a_{ij}x_j + t_i\Gamma_i + \sum_{j=1}^{n} p_{ij} \le b_i \quad i = 1, \ldots, n \tag{5.38}$$

$$t_i + p_{ij} \ge \bar{a}_{ij}x_j \quad i = 1, \ldots, n,\ j = 1, \ldots, n \tag{5.39}$$

$$x \in X, \quad p_{ij} \ge 0, t_i \ge 0 \quad i = 1, \ldots, n,\ j = 1, \ldots, n \tag{5.40}$$

Based on the above theorem, the robust counterpart of (5.32) yields

$$\sum_{i=1}^{N_g} S_{l,i}P_i^{sch} + \sum_{k=1}^{N_w} G_{l,k}W_k^f - \sum_{j=1}^{N_d} H_{l,j}D_j + t_l\Gamma + \sum_{k=1}^{N_w} p_{lk} \le F_l^{\max} \quad k = 1, \ldots, N_w \tag{5.41}$$

$$t_l + p_{lk} \ge W_k^e \left(\sum_{i=1}^{N_g} S_{l,i}\beta_i + G_{l,k} \right) \quad l = 1, \ldots, N_l,\ k = 1, \ldots, N_w \tag{5.42}$$

$$p_{lk} \ge 0, \quad t_l \ge 0 \quad l = 1, \ldots, N_l,\ k = 1, \ldots, N_w \tag{5.43}$$

Thus, the original bi-level adaptive robust optimal power flow considering the price of robustness can be simplified as a traditional convex quadratic programming model as:

$$(\textbf{Robust model}') \quad \min_{\boldsymbol{P}^{sch},\boldsymbol{\beta},\boldsymbol{t},\boldsymbol{p}} \sum_{i=1}^{N_g} \left(a_i \left(P_i^{sch}\right)^2 + b_i P_i^{sch} + c_i + a_i\beta_i^2 \sum_{k=1}^{N_w}\sum_{j=1}^{N_w} \Lambda_{kj} \right) \tag{5.44}$$

$$s.t. \sum_{j=1}^{N_d} D_j - \sum_{k=1}^{N_w} W_k^f = \sum_{i=1}^{N_g} P_i^{sch} \tag{5.45}$$

$$P_i^{\min} + \beta_i\theta \le P_i^{sch} \le P_i^{\max} - \beta_i\theta, \quad i = 1, \ldots, N_g \tag{5.46}$$

$$-F_l^{\max}+\left(t_l\Gamma+\sum_{k=1}^{N_w}p_{lk}\right)\le\sum_{i=1}^{N_g}S_{l,i}P_i^{sch}+\sum_{k=1}^{N_w}G_{l,k}W_k^f - \sum_{j=1}^{N_d}H_{l,j}D_j\le F_l^{\max}-\left(t_l\Gamma+\sum_{k=1}^{N_w}p_{lk}\right),\quad l=1,\ldots,N_l \tag{5.47}$$

$$t_l+p_{lk}\ge W_k^e\left(\sum_{i=1}^{N_g}S_{l,i}\beta_i+G_{l,k}\right),\quad l=1,\ldots,N_l,\ k=1,\ldots,N_w \tag{5.48}$$

$$p_{lk}\ge 0,\quad t_l\ge 0,\quad l=1,\ldots,N_l,\ k=1,\ldots,N_w \tag{5.49}$$

$$\sum_{i=1}^{N_g}\beta_i=1,\quad 0\le\beta_i\le 1 \tag{5.50}$$

where

$$\theta=\max_{\sum_{k=1}^{N_r}y_k=\Gamma,\,0\le y_k\le 1}\sum_{k=1}^{N_r}R_k^e y_k=\sum_{m=1}^{k-1}\left(R_{i_m}^e-R_{i_k}^e\right)+R_{i_k}^e\Gamma\quad\text{and}\quad k-1\le\Gamma\le k.$$

5.2.4 Numerical Results

First, the uncertainty degree and conservatism degree are well defined to study their impacts on the proposed robust interval economic dispatch model.

Uncertainty Degree η: $\eta=\frac{W_k^e}{W_k^f}$, where $W_k\in\left[W_k^f-W_k^e,W_k^f+W_k^e\right]$.

Conservatism Degree α: $\alpha=\frac{f^r-f^u}{f^u}\times 100\,\%$, where f^r and f^u are the optimal objective values calculated by robust optimal power flow and traditional deterministic optimal power flow, respectively.

It should be noted that f^r is always greater than f^u, because the optimal solution of robust model is obtained under the worst-case scenarios. The price of robustness is employed to avoid the optimal solution overly "robust" such that it is far from the real world and leads to a solution which is unnecessarily too conservative.

A. **IEEE 14-bus test system with 2 wind farms**

The IEEE-14 bus test system [8] with two wind farms is studied, where the wind farms are installed at bus #3 and #6 to replace the original thermal generators and the rated capacity of the two farms are 20 and 30 MW, respectively. Thus, the test

system consists of 14 buses, 3 thermal generators, 2 wind farms and 20 transmission lines. The spatial covariance matrix between the two wind farms is assumed to be $\begin{bmatrix} 0.8 & 0.2 \\ 0.2 & 0.9 \end{bmatrix}$.

It can be easily known that when $\Gamma = 0$, the proposed robust optimal model is equivalent to the traditional deterministic optimal power flow. When $\Gamma = N_w = 2$, the proposed robust model is just the robust optimal power flow without considering the price of robustness. Therefore, the above two models are the special cases of the proposed model. Taking Γ from 0 to 2, we obtain the optimal Γ curves. Figure 5.2a shows the Γ curve of the optimal value of the objective function, where it is apparent that the objective value of the DCOPF model is the objective value of DCOPF model is \$6443 (i.e., choosing Γ to be 0) and the objective value of R-DCOPF model is \$6558 (i.e., choosing Γ to be 2). In other words, the conservatism degree α increases from 0 to 1.8 %. It implies that the generation cost rises with the increase of Γ and more robustness is taken into account using large Γ while sacrificing more optimality of the solution.

Moreover, with the increase of uncertainty degree η, more generation cost will be sacrificed for the same Γ. It can be observed from Fig. 5.2b that conservatism degree α is about 0.4 % when $\Gamma = 2$ and $\eta = 0.1$, while α is around 1.8 % when $\Gamma = 2$ and $\eta = 0.4$.

In addition, the optimal generation and participation factor of the three generators are presented in Figs. 5.3, 5.4 and 5.5. With the increase of Γ, both the power output of generators 1 and 2 increase but the generator 3 output decreases. As for participation factors, both generator 1 and 2 are close to 0, while generator 3 tends to be 1.

The Γ curve offers a tradeoff between the generation cost and the uncertainty robustness. The decision maker has the flexibility of adjusting the robustness of the uncertainty against the level of conservatism of the optimal solution.

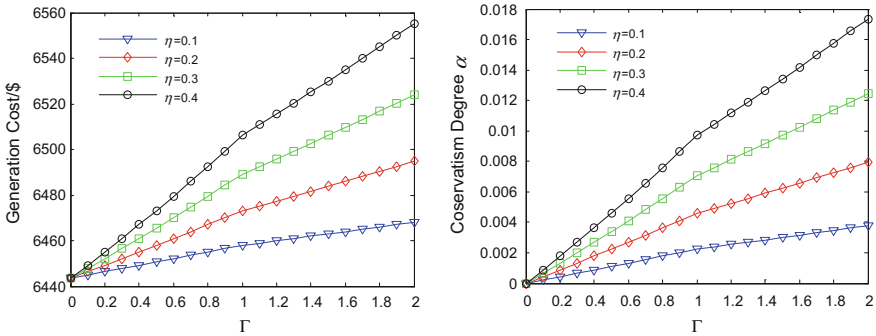

(a) Γcurve of objective value (b) Γcurve of conservatism degree

Fig. 5.2 Objective function and conservative factor Γ with different η

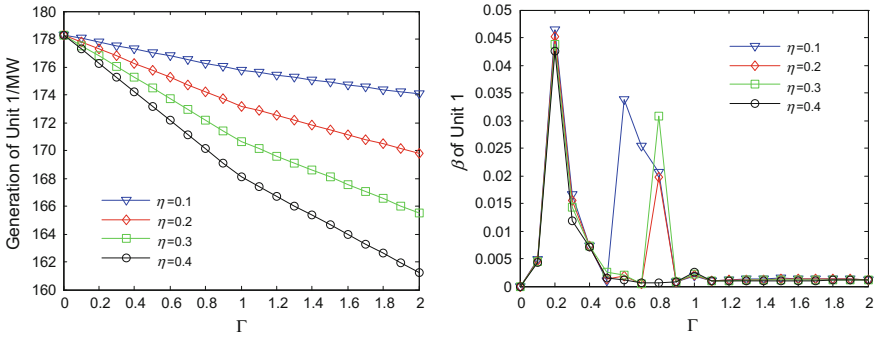

(a) Γcurve of objective value (b) Γcurve of conservatism degree

Fig. 5.3 Optimum output and conservative factor Γ of generator 1 with different η

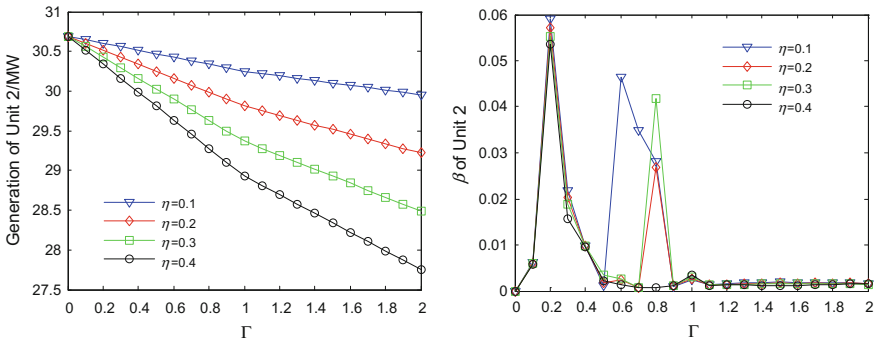

(a) Γcurve of objective value (b) Γcurve of conservatism degree

Fig. 5.4 Optimum output and conservative factor Γ of generator 2 with different η

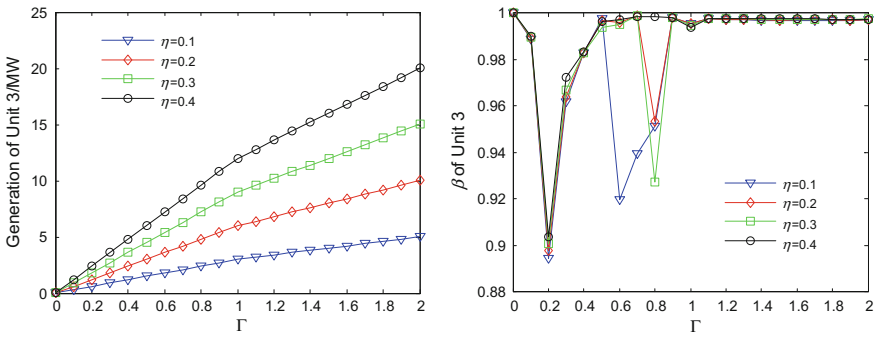

(a) Γcurve of objective value (b) Γcurve of conservatism degree

Fig. 5.5 Optimum output and conservative factor Γ of generator 3 with different η

Table 5.1 Probability of constraint satisfaction using Monte Carlo simulation

Γ	UD-iid (η)			ND-iid (η)			ND-C (η)		
	0.1 (%)	0.2 (%)	0.3 (%)	0.1 (%)	0.2 (%)	0.3 (%)	0.1 (%)	0.2 (%)	0.3 (%)
0.0	49.8	50.1	50.2	53.6	52.3	53.3	62.3	60.2	63.1
0.2	60.2	60.6	60.3	65.4	67.7	66.6	71.5	71.8	72.4
0.4	69.4	70.6	69.2	72.9	73.3	75.7	86.5	87.8	85.4
0.6	77.3	78.9	78.6	89.4	90.1	89.8	92.8	93.4	93.2
0.8	85.2	85.6	86.6	91.2	93.2	92.8	98.7	98.7	98.9
1.0	91.8	92.0	91.3	97.3	97.5	97.6	99.8	99.9	99.9
1.2	94.4	94.9	95.2	98.8	98.8	99.5	99.9	99.9	99.9
1.4	97.1	97.2	97.3	99.6	99.4	99.9	100	99.9	100
1.6	98.6	98.6	98.2	99.9	99.9	99.9	100	100	100
1.8	99.7	99.8	99.6	100	100	100	100	100	100
2.0	100	100	100	100	100	100	100	100	100

Furthermore, the probability of satisfying all constraints using 5000 Monte Carlo simulations based on different probability distribution models is investigated. Here, we choose three probability distribution models: multivariate uniform distribution with independent and identical distribution (UD-iid); multivariate normal distribution with independent and identical distribution (ND-iid) with a correlation matrix of $\begin{bmatrix} 0.8 & 0.2 \\ 0.2 & 0.9 \end{bmatrix}$; and multivariate normal distribution with correlation (ND-C) with a correlation matrix of $\begin{bmatrix} 0.8 & 0 \\ 0 & 0.9 \end{bmatrix}$. The results are reported in Table 5.1, where the probability of constraint satisfaction increases with the increase of Γ and all constraints can be satisfied when $\Gamma = Nw = 2$, i.e., the traditional robust optimal power flow model (R-DCOPF).

In addition, the comparison between UD-iid and ND-iid shows that in order to achieve 100 % constraint satisfaction, different probability distribution models lead to different choice of the price of robustness Γ. The comparison between ND-iid and ND-C shows that the correlation of wind farms also affects the price of robustness Γ in order to achieve 100 % constraint satisfaction.

B. **Medium-scale test systems with 10 wind farms**

Furthermore, the IEEE 118-bus system is studied which contains 118 buses and 186 branches as well as 10 wind farms which are located at bus #100, #103, #104, #105, #107, #110, #111, #112, #113 and #116.

Here, different transmission line capacity limits are chosen as 150 and 100 MW, respectively, and the corresponding Γ curves of the objective value and

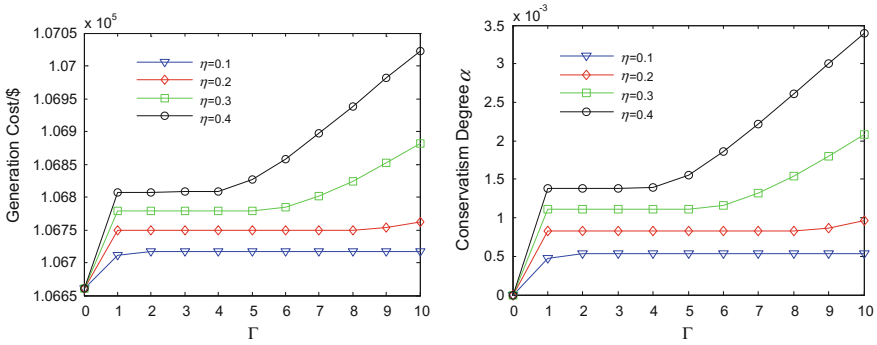

(a) Γcurveof objective value (b) Γcurve of conservatism degree

Fig. 5.6 Objective function and conservative factor Γ with different η (150 WM)

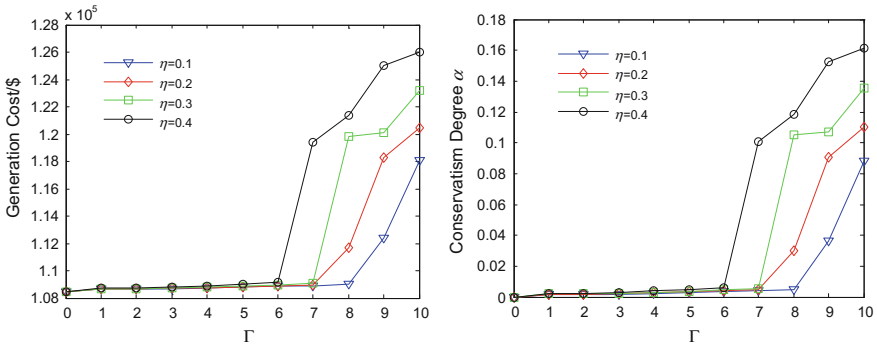

(a) Γcurve of objective value (b) Γcurve of conservatism degree

Fig. 5.7 Objective function and conservative factor Γ with different η (100 WM)

conservatism degree α are shown in Figs. 5.6 and 5.7. It can be observed that a tighter line capacity limit will lead to higher generation cost and conservatism degree α. In addition, for the case of tighter line capacity limit, the conservatism degree α may reach 18 % without considering the price of robustness, while the conservatism degree α is no more than 1 % for the case of higher line capacity limit. The Γ curve of conservatism degree w.r.t. to α increases slowly at first and then sharply after a "turning point". The "turning points" decrease with the increase of the uncertainty degree. For instance, as shown in Fig. 5.6, the "turning point" is at $\Gamma = 8$ when $\eta = 0.1$ and at $\Gamma = 6$ when $\eta = 0.4$.

5.3 The Day-Ahead Robust Interval Economic Dispatch Model

5.3.1 The Two-Stage Robust Interval Economic Dispatch Model Considering the Network Topology Control

In the day-ahead market, the adaptive robust interval economic dispatch model can also be used. However, the difference is that the coupling between multiple time periods should be considered. With the development of power systems, the network topology control presented by some researchers could reduce the cost of power generation to some extent. Therefore, this method is widely used in economic dispatch [9–13]. The general optimal transmission switching problem aims to minimize the total generation cost while satisfying all the operational constraints, which can be formulated as a mixed integer linear programming (MILP) in a matrix form as follows:

$$\min_{\boldsymbol{P}_t,\boldsymbol{Z}_t,\boldsymbol{\theta}_t,\boldsymbol{y}_t} \quad \sum_{t=1}^{T} \left(\boldsymbol{b}^T \boldsymbol{P}_t + \mathrm{sum}(\boldsymbol{c})\right) \tag{5.51}$$

$$s.t.\ \boldsymbol{C}_f^T \boldsymbol{Z}_t = \boldsymbol{C}_g \boldsymbol{P}_t - \boldsymbol{C}_d \boldsymbol{D}_t + \boldsymbol{C}_w \boldsymbol{W}_t^f \tag{5.52}$$

$$\boldsymbol{P}^{\min} \le \boldsymbol{P}_t \le \boldsymbol{P}^{\max}, \quad \boldsymbol{Rd} \le \boldsymbol{P}_t - \boldsymbol{P}_{t-1} \le \boldsymbol{Ru}, \quad \theta_t(ref) = 0 \tag{5.53}$$

$$-\boldsymbol{F}^{\max} \circ \boldsymbol{y}_t \le \boldsymbol{Z}_t \le \boldsymbol{F}^{\max} \circ \boldsymbol{y}_t \tag{5.54}$$

$$-M(1-\boldsymbol{y}_t) \le \boldsymbol{Z}_t - \boldsymbol{B}\boldsymbol{C}_f \boldsymbol{\theta}_t \le M(1-\boldsymbol{y}_t) \tag{5.55}$$

$$\boldsymbol{y}_t \in \{0,1\} \tag{5.56}$$

where T means the number of times; $\boldsymbol{P}_t$ and $\boldsymbol{D}_t$ represent the generation variables and the load level at time t; $(\boldsymbol{b}, \boldsymbol{c})$ are the linear and constant coefficients of cost function of generator; $\boldsymbol{\theta}_t$ is the $n_b \times 1$ voltage angle variables at time t and "*ref*" refers to the reference bus; $\boldsymbol{B}$ is an diagonal $n_l \times n_l$ electrical susceptance matrix of transmission element; $\boldsymbol{Z}_t$ is an $l \times 1$ branch flow variables at time t; M is a big number; $\boldsymbol{C}_f$ is a sparse $n_l \times n_b$ incidence matrix of directed power network, such that $S(i, j) = +1$, if the branch i is connected to its "from" bus j, $\boldsymbol{C}_f(i, j) = -1$, if the branch i is connected to its "to" bus j, and 0 otherwise (i.e., not connected); $\boldsymbol{P}^{\min}$ and $\boldsymbol{P}^{\max}$ are the minimum and maximum limits of generator output, respectively; vector $\boldsymbol{F}^{\max}$ represents the transmission line limits. $\boldsymbol{C}_g$ is a sparse $n_b \times n_g$ generator connection matrix, which can be defined such that its (i, j)-th element is 1 if generator j is located at bus i and 0 otherwise. Similarly, $\boldsymbol{C}_d$ is a sparse $n_b \times n_d$ load

connection matrix. $\boldsymbol{C}_w$ is a sparse $n_b \times n_d$ wind farm connection matrix. n_b, n_g, n_d and n_l denote the total number of buses, generators, load sites and transmission lines, respectively. $\boldsymbol{y}$ is an $n_l \times 1$ binary variables for transmission line state (0 open, 1 closed); The operator $\circ$ represents the Hadamard product (or entrywise product) that is an operation taking two vectors of the same length, and producing another vector where each element i is the product of elements i of the original two vectors.

It's important to note that the constraints (5.54) and (5.55) are complementary constraints in this model. They are obtained through the big M theory. These constraints imply that only one condition is active, and the other is always inactive. If $\boldsymbol{y} = 1$, we can get $\begin{cases} -\boldsymbol{F}^{\max} \le \boldsymbol{Z} \le \boldsymbol{F}^{\max} \\ 0 \le \boldsymbol{Z} - \boldsymbol{B}\boldsymbol{C}_f\boldsymbol{\theta} \le 0 \end{cases}$, which is equivalent to $-\boldsymbol{F}^{\max} \le \boldsymbol{B}\boldsymbol{C}_f\boldsymbol{\theta} \le \boldsymbol{F}^{\max}$. This means the line is service, which is limited by line transmission capacity constraints. If $\boldsymbol{y} = 0$, we can get $\begin{cases} 0 \le \boldsymbol{Z} \le 0 \\ -M \le \boldsymbol{Z} - \boldsymbol{B}\boldsymbol{C}_f\boldsymbol{\theta} \le M \end{cases}$, which is equivalent to $\begin{cases} \boldsymbol{Z} = 0 \\ -M \le \boldsymbol{B}\boldsymbol{C}_f\boldsymbol{\theta} \le M \end{cases}$. This means the line is out-of-service and its transmission power is 0.

Interval model is used in this paper due to the uncertainties of the wind power output. When the power balance constraints are destroyed, the generators will be rescheduled according to the new wind power output to ensure the real-time balance of power. To hedge against the contingency uncertainties, in this paper, a two-stage robust optimization model is formulated to minimize the total cost under the worst-case contingency scenario. The variable of first stage is the network topology and which of the second stage is optimal generation output. The robust optimization focuses on the optimal solution of first stage. The optimal solution of the second stage changes when the wind power output changed. A comparison of two optimal transmission switching problems with and without the consideration of corrective actions by SPSs for N-1 contingency is presented in Fig. 5.8, where it shows that

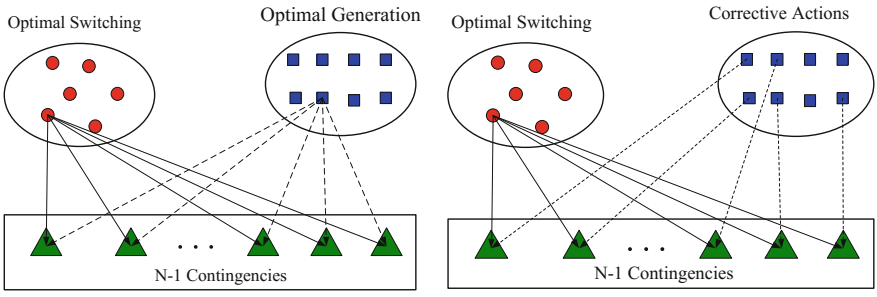

Fig. 5.8 Traditional economic dispatch considering network reconfiguration

the optimal switching strategy and generation decision are obtained at the same time to satisfy all the sets of constraints in each contingency. Therefore, for the second case, different contingency scenarios lead to different optimal corrective generation strategies.

The interval expression in Sect 5.2 also can be used for the uncertainties of wind power, which means the wind power output is the random value in the interval $\boldsymbol{W}_t \in \left[\boldsymbol{W}_t^f - \boldsymbol{W}_t^e, \boldsymbol{W}_t^f + \boldsymbol{W}_t^e\right]$, where the W_t^f and W_t^e is the predicted value and predicted error of wind power output at the time t. The two-stage robust optimal economic dispatch model is as follows:

$$\min_{\boldsymbol{y}_t \in \{0,1\}} \max_{\boldsymbol{W}_t \in \left[\boldsymbol{W}_t^f - \boldsymbol{W}_t^e, \boldsymbol{W}_t^f + \boldsymbol{W}_t^e\right]} \min_{\boldsymbol{P}_t, \boldsymbol{Z}_t, \boldsymbol{\theta}_t} \quad \sum_{t=1}^{T} \left(\boldsymbol{b}^T \boldsymbol{P}_t + \text{sum}(\boldsymbol{c})\right) \tag{5.57}$$

$$s.t.\ \boldsymbol{C}_f^T \boldsymbol{Z}_t = \boldsymbol{C}_g \boldsymbol{P}_t - \boldsymbol{C}_d \boldsymbol{D}_t + \boldsymbol{C}_w \boldsymbol{W}_t \tag{5.58}$$

$$\boldsymbol{P}^{\min} \le \boldsymbol{P}_t \le \boldsymbol{P}^{\max}, \quad \boldsymbol{C}_f^T \boldsymbol{Z}_t = \boldsymbol{C}_g \boldsymbol{P}_t - \boldsymbol{C}_d \boldsymbol{D}_t + \boldsymbol{C}_w \boldsymbol{W}_t, \theta_t(ref) = 0 \tag{5.59}$$

$$-\boldsymbol{F}^{\max} \circ \boldsymbol{y}_t \le \boldsymbol{Z}_t \le \boldsymbol{F}^{\max} \circ \boldsymbol{y}_t \tag{5.60}$$

$$-M(1 - \boldsymbol{y}_t) \le \boldsymbol{Z}_t - \boldsymbol{B}\boldsymbol{C}_f \boldsymbol{\theta}_t \le M(1 - \boldsymbol{y}_t) \tag{5.61}$$

It is obviously to see that the two-stage robust interval economic dispatch model is much different from the adaptive robust interval economic dispatch model in the Sect. 5.2. Compared from the mathematical model, the adaptive robust model is a bi-level optimal model but the two-stage robust model is a three-level programming model. Besides, the adaptive robust model only contains continuous variable, which can be converted into a convex quadratic programming model. But the two-stage robust model contains the discrete variable in the first stage and the continuous variable in the second stage, which is a mixed integer programming model. Therefore, the solution of the two-stage robust model is much more difficult from the adaptive robust model. An acceleration algorithm is needed for improving the efficiency of the proposed model, such as the Benders decomposition Method proposed in Sect. 2.3.4, with adding the primary cuts and dual cuts.

5.3.2 Numerical Results

The proposed method is tested on the IEEE 30-bus system, whose topology is shown in Fig. 5.9 and the detailed parameters can be found in MATPOWER [8]. Besides, there are six generators and the coefficients of the cost function given in Table 5.2. The convergence tolerance is assigned to 0.01 %. In addition, to test the

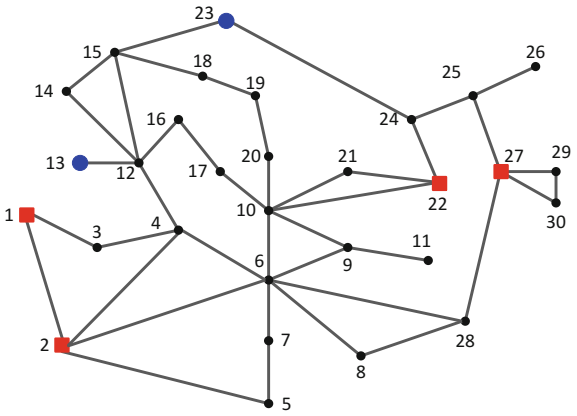

Fig. 5.9 IEEE 30-bus test system

Table 5.2 Cost efficient of each unit

Cost coefficients	Gen 1	Gen 2	Gen 3	Gen 4
b ($/MW)	0.8333	0.7292	1.250	0.4167
c ($)	12.5000	16.6667	14.5833	14.5833

proposed model and method under different scenarios, let γ be transmission capacity factor which simulates different transmission capacity as $\boldsymbol{F}^{\max} = \gamma \boldsymbol{F}^{0,\max}$, where $\boldsymbol{F}^{0,\max}$ is the normal capacity. Furthermore, 24 h are considered in this paper, and the load and wind power output curves in 24 h are given in Sect. 4.2.2.

A. **Comparison of the economical dispatch considering network reconfiguration and the traditional economical dispatch**

Firstly, we assume that the wind power output is certain, which means the uncertainty is 0. At this moment, the two-stage robust optimal economical dispatch model degrades into an optimal economical dispatch model containing network reconfiguration. Compared with the traditional optimal economical dispatch model, the results are shown in Fig. 5.10. As shown in this figure, if $\gamma < 1.3$, the optimal objective value of optimal economical dispatch model considering network reconfiguration is better than the traditional optimal economical dispatch model with the γ decreasing. If $\gamma < 1.3$, the optimal objective value of optimal economical dispatch model considering network reconfiguration is the same as the traditional optimal economical dispatch model. Especially, if $\gamma < 0.8$, the optimal economical dispatch model considering network reconfiguration have feasible solutions, however, the traditional optimal economical dispatch model does not. For example,

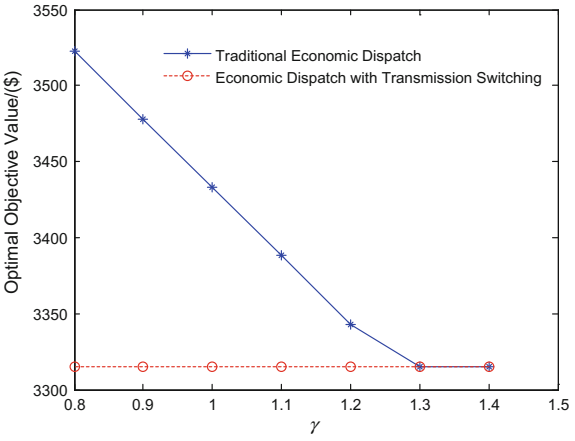

Fig. 5.10 Comparison of the economical dispatch considering network reconfiguration and the traditional economical dispatch

when $\gamma = 0.7$, the target value is \$3327, when $\gamma = 0.6$, the target value is \$3494. Therefore, compared with the traditional optimal economical dispatch model, the optimal economical dispatch model considering network reconfiguration have more feasible region. It can get better optimal solutions and may even change an infeasibility problem to a feasibility problem.

B. The influences of wind power uncertainties to the robust optimization model

Furthermore, we consider the influences of wind power uncertainties to the optimal economical dispatch model considering network reconfiguration. Adopting the conception of η and α in Sect. 4.2, the solutions of robust optimal model are shown in Figs. 5.11 and 5.12 considering different uncertainties. It shows that the optimal solutions will be worse and the α will increase as the uncertainties increasing. At the same time, the optimal solutions will be better and the α will increase as the γ increasing. When the transmission power of lines is smaller, the value of robust optimal model can be better, but the α increases. Therefore, the conception of robustness price is needed for decreasing the conservatism of robust optimal model.

C. The robust optimization model considering robustness price

After considering the robustness price, the optimal solutions of the two-stage robust model are shown as Table 5.3. It shows that, the robustness price can decrease the conservatism of robust optimal model to some degree. For example, when $\Gamma = 1$, the results is between $\Gamma = 0$ and $\Gamma = 2$. $\Gamma = 0$ is the solution of traditional optimal economical dispatch model. Even though this result is the most optimal solution, it does not consider the robustness. It means that the transmission power of lines may be out-of-limit in the worst situation of wind power output. $\Gamma = 2$ is the solution of

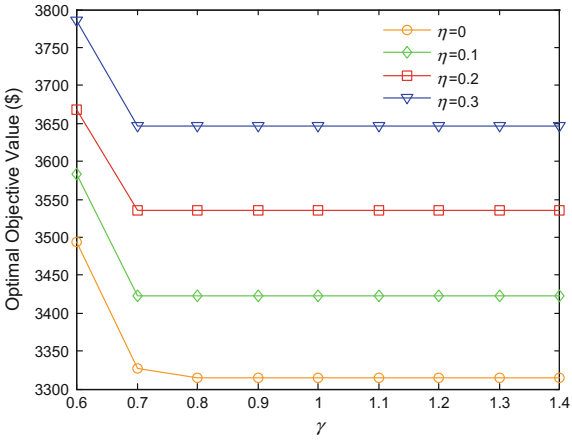

Fig. 5.11 Optimal values of robust model in different uncertainties

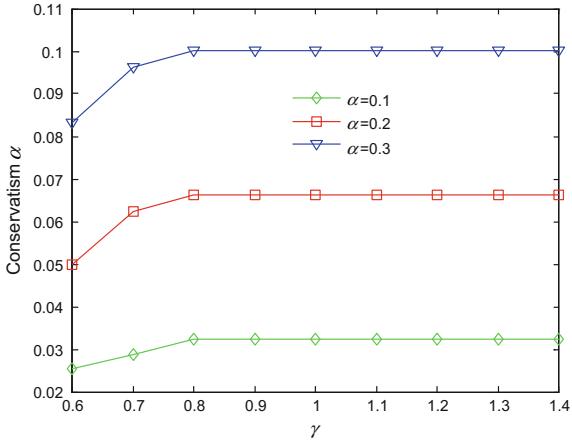

Fig. 5.12 The α in different uncertainties

robust optimal economical dispatch model, which does not consider the robustness price. Even though this result is the most secure solution, it does not consider the economics. The meaning of robustness price is to balance the security and economics for the decision maker. From Figs. 5.13 and 5.14, it can be seen that the security is better and the conservatism is less than the previous robust optimal model after $\Gamma = 1$. And they are both less than 5 %.

Table 5.3 Optimal values of robust model considering robustness price

$\alpha = 0.1$		Transmission capacity factor γ								
		1.4	1.3	1.2	1.1	1.0	0.9	0.8	0.7	0.6
Γ	2	3422.4	3422.4	3422.4	3422.4	3422.4	3422.4	3422.4	3422.4	3583.2
	1	3366.2	3366.2	3366.2	3366.2	3366.2	3366.2	3366.2	3372.6	3540.6
	0	3315	3315	3315	3315	3315	3315	3315	3327	3494
$\alpha = 0.2$		Transmission capacity factor γ								
		1.4	1.3	1.2	1.1	1.0	**0.9**	0.8	0.7	0.6
Γ	2	3534.8	3534.8	3534.8	3534.8	3534.8	3534.8	3534.8	3534.8	3668.7
	1	3411.2	3411.2	3411.2	3411.2	3411.2	3411.2	3411.2	3411.2	3574.7
	0	3315	3315	3315	3315	3315	3315	3315	3327	3494
$\alpha = 0.3$		Transmission capacity factor γ								
		1.4	1.3	1.2	1.1	1.0	0.9	0.8	0.7	0.6
Γ	2	3647.2	3647.2	3647.2	3647.2	3647.2	3647.2	3647.2	3647.2	3784.8
	1	3478.6	3478.6	3478.6	3478.6	3478.6	3478.6	3478.6	3478.6	3625.4
	0	3315	3315	3315	3315	3315	3315	3315	3327	3494

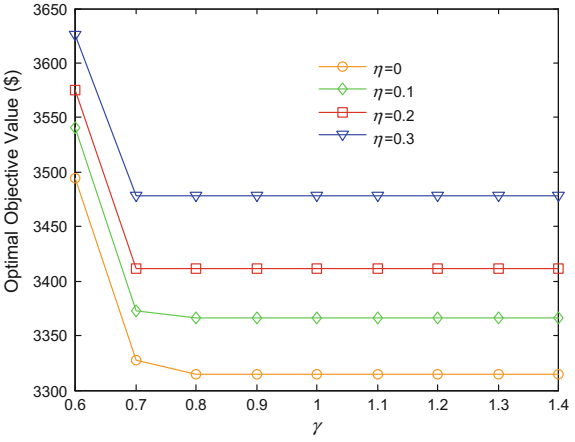

Fig. 5.13 Optimal values in different uncertainties (Γ = 1)

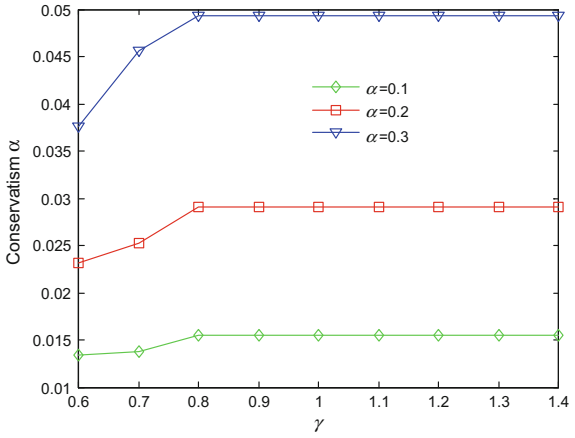

Fig. 5.14 The α in different uncertainties (Γ = 1)

5.4 Discussion

5.4.1 The Adaptive Robust Interval Economic Dispatch Model Containing Prohibited Zones

In the actual power system operation, bearing vibration will be magnified within some certain range because of the limitation of generator physical conditions. The prohibited zones are needed for the generators, because bearing vibration has the negative impact on the security and longevity of generators. According to the current generator operation conditions, these prohibited zones should be avoided. In

order to guarantee the optimal objective, the economic dispatch model with prohibited zones is studied [14–27].

It can be seen that the economic dispatch model with prohibited zones is not the convex programming problem anymore. Up to now, the most popular methods to solve this model are AI methods, such as genetic algorithm [14], evolutionary algorithm [15], particle swarm optimization [16–19], chaotic particle swarm optimization [20–22], anti-predator particle swarm optimization [23], improved particle swarm optimization [25], cross particle swarm optimization [26], neural network algorithm [27], artificial immune algorithm [21] and tabu search algorithm [24]. Nevertheless, these algorithms above are influenced by the parameters and iterations, which make the results random. A mixed integer programming method is presented in Appendix C, which can solve this problem effectively.

Furthermore, there are two aspects should be noticed in the economic dispatch model with prohibited zones. Firstly, how to set up and solve the model with prohibited zones properly. Secondly, the prohibited zones may jump from one to another under the uncertain wind power output. This "jump" should be considered, which increase the volatility of generator output.

5.4.2 *Two-Stage Robust Interval Economic Dispatch Model Considering Reliability Constraints*

The economic dispatch model considering network reconfiguration control can improve the operation cost of economic dispatch by switching some transmission lines under certain circumstances. But from the perspective of security and reliability of power grid, switching the line can be termed as the occurrence of $N-1$ contingency, which could reduce the reliability of power grid. To balance the security and reliability of power grid, lots of literatures have studied the two following strategies [9, 10]:

(i) Build the optimal scheduling model considering N-1 security constraints, which means adding N-1 security constraints to economic dispatch model considering network reconfiguration described in (5.57)–(5.61). Furthermore, consider the uncertainty of wind power output, and find the robust optimal solutions while satisfying all the $N-1$ security constraints, whose mathematical optimization model is described in Appendix D.

(ii) Increase the constraints for limiting the number of transmission lines available for switching to guarantee the reliability of systems. The constraints sets for line switching can be obtained by lots of off-line reliability simulation tests. The detailed mathematical model is described in Appendix D.

However, there are two problems considering all the N-1 security constraints into one model. First, from the view of computation complexity, the number of constraints would substantially increase by considering all the N-1 security

constraints, forming a larger-scale combinatorial optimization model which leads to much computational difficulties. Second, from the view of physical modeling, the model only considers the N-1 contingencies occurring on lines, but in practice, the N-1 contingencies could also occurs on generators and therefore the power balance would be broken. To guarantee the real-time power balance, the generator must be re-dispatched. In traditional N-1 models, it is difficult to consider re-dispatch, which will lead to a big deviation from the practical operation so that the computed results are quite conservative. Therefore, the second strategy is widely applied. The simulation results of strategy (ii) are given in Appendix D.

5.4.3 Multi-solution Problem and Goal Programming of Two-Stage Robust Interval Optimization Model

In essence, two-stage interval robust interval optimization model can be considered as a mixed integer-programming problem. It can be solved by benders decomposition method to decompose into the master and sub problems, and some existing matured commercial software, such as CPLEX, GUROBI, MOSEK, can provide solutions effectively. However, multi-solution phenomenon may occur in the mixed integer programming, which means that there are many optimal solutions corresponding to the same optimal objective. Sometimes, decision makers hope to want to find all the multiple solutions, and then choose the most acceptable and effective optimal solution based on the operation indices and the actual operation rules of the power grid. So how to get all the optimal solutions of the model is worth studying. What's more, taking network reconfiguration as an example, if the proposed optimization model has multiple solutions, it means that there are a variety of combination schemes for line switching. Some schemes need to switch a lot of lines while others need to switch a few, although all the schemes have the same optimal objective function. Considering the security and reliability of power grid, it is naturally expected to switch lines as few as possible while obtaining the same optimal objective, but sometimes there are hundreds of multiple solutions. At this point, how to fast obtain the multiple solutions set with switching the least number of lines is the most concerned by decision makers. The multiple solution problem of two-stage interval robust optimization model is discussed in detail in Appendix E, and the method of goal programming is used to obtain all the multi-solution sets.

5.5 Summary

In this chapter, the robust interval optimization method mentioned in Chap. 2 is introduced to the economic dispatch model with uncertainties of large-scale wind power integration. In the process of robust interval economic dispatch, different

robust interval optimization methods can be used in different timescale. For the day-ahead dispatch model, this chapter adopts two-stage robust interval optimization model, for finding the most robust network topology while ensuring the security of power grid operation under uncertainty of wind power in one day. In real-time economic dispatch models, this chapter presents an adaptive robust interval optimization model, for finding the most robust unit output scheduling value while ensuring that in the process of real-time output balancing, AGC can still meet the constraints of the unit and the network even under arbitrary disturbance of wind power output. However, the essence of robust optimization is to optimize the system in the worst situation, and therefore it is inevitable to make the result relatively conservative comparing to the results of traditional deterministic optimization. Thus, this chapter introduces the concepts of the price of robustness, providing the decision-makers with the balance of economy and security, and yielding an optimal solution set similar to the Pareto frontier.

What's more, it should be noted that, on studying adaptive robust optimization in the real-time dispatch, the participation factor of generator is introduced to allocation unbalanced power for AGC units, and the overall volatility and economic optimization of the generator should be ensured in the optimal selection of participation factor, and consequently a multi-objective optimization model is obtained.

At last, through the simulation of IEEE test systems, the validity and applicability of the proposed optimization method are verified. But note that the robust optimization on a large-scale test system could increase the computation complexity. For day-ahead dispatch, the computational time is not very important, but for the real-time dispatch in 5–15 min, the computational time should be ensured, which will be studied mainly in the next chapter.

References

1. Jabr RA (2013) Adjustable robust OPF with renewable energy sources. Power Syst IEEE Trans 28(4):4742–4751
2. Cicerone S, D'Angelo G, Di Stefano G et al (2009) Recoverable robustness for train shunting problems. Algorithmic Oper Res 4(2):102–116
3. Bertsimas D, Sim M (2004) The price of robustness. Oper Res 52(1):35–53
4. Changhyeok L, Cong L, Mehrotra S et al (2014) Modeling transmission line constraints in two-stage robust unit commitment problem. Power Syst IEEE Trans 29(3):1221–1231
5. Martinez-Mares A, Fuerte-Esquivel CR (2013) A robust optimization approach for the interdependency analysis of integrated energy systems considering wind power uncertainty. Power Syst IEEE Trans 28(4):3964–3976
6. Ahuja RK, Hring RHM, Zaroliagis CD (2009) Robust and online large-scale optimization. Springer, Berlin
7. Zhai QZ, Guan XH, Cheng JH et al (2010) Fast identification of inactive security constraints in SCUC problems. Power Syst IEEE Trans 25(4):1946–1954

8. Zimmerman RD, Murillo-Sa X, Nchez CE et al (2011) MATPOWER: steady-state operations, planning, and analysis tools for power systems research and education. Power Syst IEEE Trans 26(1):12–19
9. Khanabadi M, Ghasemi H, Doostizadeh M (2013) Optimal transmission switching considering voltage security and N-1 contingency analysis. Power Syst IEEE Trans 28(1):542–550
10. Villumsen JC, Bronmo G, Philpott AB (2013) Line capacity expansion and transmission switching in power systems with large-scale wind power. Power Syst IEEE Trans 28(2):731–739
11. Makela O, Warrington J, Morari M et al (2014) Optimal transmission line switching for large-scale power systems using the alternating direction method of multipliers. In: Power systems computation conference (PSCC), Wroclaw
12. Soroush M, Fuller JD (2014) Accuracies of optimal transmission switching heuristics based on DCOPF and ACOPF. Power Syst IEEE Trans 29(2):924–932
13. Ostrowski J, Wang JH, Liu C (2014) Transmission switching with connectivity-ensuring constraints. Power Syst IEEE Trans 29(6):2621–2627
14. Orero SO, Irving MR (1996) Economic dispatch of generators with prohibited operating zones: a genetic algorithm approach. Gener Transm Distrib IEE Proc 143(6):529–534
15. Jayabarathi T, Sadasivam G, Ramachandran V (1999) Evolutionary programming based economic dispatch of generators with prohibited operating zones. Electr Power Syst Res 52(3):261–266
16. Zwe-Lee G (2003) Particle swarm optimization to solving the economic dispatch considering the generator constraints. Power Syst IEEE Trans 18(3):1187–1195
17. Naresh R, Dubey J, Sharma J (2004) Two-phase neural network based modelling framework of constrained economic load dispatch. IEE Proc Gener Transm Distrib 151(3):373–378
18. Pereira-Neto A, Unsihuay C, Saavedra OR (2005) Efficient evolutionary strategy optimisation procedure to solve the nonconvex economic dispatch problem with generator constraints. Gener Transm Distrib IEE Proc 152(5):653–660
19. Jeyakumar DN, Jayabarathi T, Raghunathan T (2006) Particle swarm optimization for various types of economic dispatch problems. Int J Electr Power Energy Syst 28(1):36–42
20. Cai J, Ma X, Li L et al (2007) Chaotic particle swarm optimization for economic dispatch considering the generator constraints. Energy Convers Manag 48(2):645–653
21. Panigrahi BK, Yadav SR, Agrawal S et al (2007) A clonal algorithm to solve economic load dispatch. Electr Power Syst Res 77(10):1381–1389
22. Coelho LDS, Lee C (2008) Solving economic load dispatch problems in power systems using chaotic and Gaussian particle swarm optimization approaches. Int J Electr Power Energy Syst 30(5):297–307
23. Selvakumar AI, Thanushkodi K (2008) Anti-predatory particle swarm optimization: solution to nonconvex economic dispatch problems. Electr Power Syst Res 78(1):2–10
24. Pothiya S, Ngamroo I, Kongprawechnon W (2008) Application of multiple tabu search algorithm to solve dynamic economic dispatch considering generator constraints. Energy Convers Manag 49(4):506–516
25. Chandram K, Subrahmanyam N, Sydulu M (2009) Secant method combined with PSO for economic dispatch with prohibited operating zones. In: IEEE/PES power systems conference and exposition, Seattle, WA
26. Khamsawang S, Jiriwibhakorn S (2009) Solving the economic dispatch problem using novel particle swarm optimization. Int J Electr Comput Syst Eng 3(1):41–46
27. Ding T, Bo R, Gu W et al (2014) Big-M based MIQP method for economic dispatch with disjoint prohibited zones. Power Syst IEEE Trans 29(2):976–977

Chapter 6
Acceleration Strategies for Large-Scale Economic Dispatch Models

Abstract It should be noted that for the economic dispatch model for the practical large-scale power system with multiple time periods is a combinatorial problem and have a great challenge to solve, especially for the robust optimization model. In this book, spatial reduction and temporal decomposition strategies are proposed to improve the computational efficiency, where spatial reduction is to identify the redundant constraints before solving the model and temporal decomposition is to decompose the multi-period problem into several single-period problems that can be parallel handled.

6.1 Introduction

In general, there are thousands of buses and transmission lines in the real power system, so the economic dispatch optimization model is actually a large-scale combination optimization model. In particular, when the robust optimization model with the price of robustness is adopted in Chap. 5, constraints will increase sharply. With respect to the multi-period dynamic economic dispatch, the increasing number of the time periods results in a time-consuming calculation and it will bring about a great challenge for on-line applications. Hence, this chapter will study the acceleration strategies for large-scale economic dispatch problems by reducing spatial-dimension and temporal decoupling. For reducing spatial-dimension, most transmission capacity constraints are inactive and the inactive constraint reduction strategy is proposed to quickly identify the inactive constraints and then eliminate them from the model before solving the proposed model. Furthermore, the multi-period economic dispatch is composed of several single-period economic dispatch models with inter-temporal constraints such as unit ramp rate constraints. For temporal decoupling, assuming that the single-period economic dispatch can be solved quickly, temporal decoupling is studied for decomposed the multi-period economic dispatch into several independent single-period economic dispatch problems for parallel computation. The book is organized as follows (Fig. 6.1).

T. Ding, *Power System Operation with Large Scale Stochastic Wind Power Integration*, Springer Theses, DOI 10.1007/978-981-10-2561-7_6

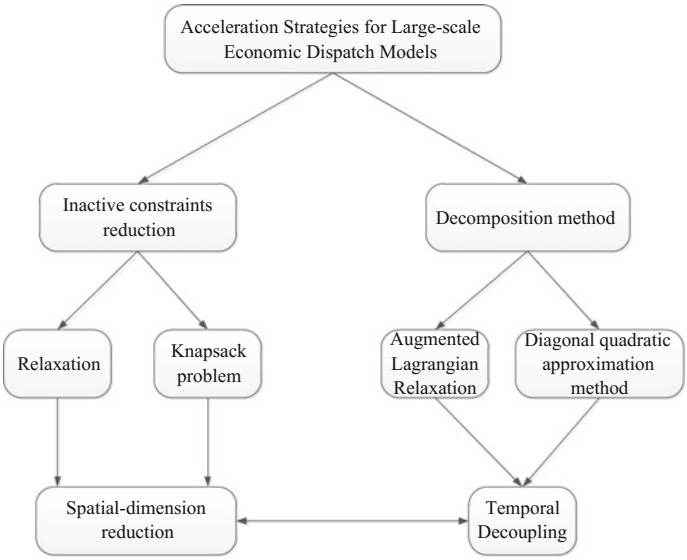

Fig. 6.1 Framework of this chapter

6.2 Redundant Security Constraints Fast Identification

6.2.1 Redundant Constraints Description and Definition

Recall the interval economic dispatch model defined in Sect. 4.2.1, where Eqs. (4.8–4.12) construct the feasible region of the security constrained economic dispatch.

$$\sum_{i=1}^{N_g} P_i(t) + \left[\sum_{k=1}^{N_w} W_k^-(t), \sum_{k=1}^{N_w} W_k^+(t)\right] = \sum_{j=1}^{N_d} D_j(t), \quad t = 1, \ldots T \tag{6.1}$$

$$P_i^{\min}(t) \le P_i(t) \le P_i^{\max}(t), \quad i = 1, \ldots, N_g, \ t = 1, \ldots T \tag{6.2}$$

$$-Rd_i \le P_i(t) - P_i(t-1) \le Ru_i, \quad i = 1, \ldots, N_g, \ t = 1, \ldots T \tag{6.3}$$

$$-F_l^{\max} \le \sum_{i=1}^{N_g} S_{l,i} P_i(t) + \sum_{k=1}^{N_w} G_{l,k}\left[W_k^-(t), W_k^+(t)\right] - \sum_{j=1}^{N_d} H_{l,j} D_j(t) \le F_l^{\max}, \quad t = 1, \ldots T, \ l = 1, \ldots, N_l \tag{6.4}$$

where the definition of variables can be found in Sect. 4.2.1. The feasible region consists of linear constraints, which is defined as a Polyhedron. Equations (6.1) and (6.4) show the uncertainty of the Polyhedron resulted from the uncertain wind

power output. Here, we assume the load demand is constant, so the uncertain wind power and the deterministic load demand can be combined as the net load, giving

$$\Omega = \begin{cases} \boldsymbol{e}^T \boldsymbol{P}_g + \boldsymbol{e}^T \boldsymbol{P}_b = \boldsymbol{0} \\ \boldsymbol{Rd}^{\min} \le \boldsymbol{EP}_g \le \boldsymbol{Ru}^{\max}, \boldsymbol{P}_g^{\min} \le \boldsymbol{P}_g \le \boldsymbol{P}_g^{\max} \\ \boldsymbol{F}^{\min} \le \boldsymbol{GP}_g - \boldsymbol{HP}_b \le \boldsymbol{F}^{\max} \\ \forall \boldsymbol{P}_b \in \left[\boldsymbol{P}_b^-, \boldsymbol{P}_b^+\right] \end{cases} \tag{6.5}$$

where $\boldsymbol{P}_b$ is the the net load of load demand plus the wind power. The first constraints in (6.5) response to the energy balance constraints in (6.1). The second constraints refer to the ramp rate constraints in (6.3) and the generation limits in (6.2). The third constraints are the network security constraints in (6.4). The last constraints give the stochastic disturbances of the injected power due to $\forall W_k \in \left[W_k^-(t), W_k^+(t)\right]$.

A large-scale SCED model contains plenty of security constraints. If all security constraints are considered in the model, the efficiency will be greatly reduced. Hence, identigying and eliminating redundant constraints will be studied to improve the efficiency, provide necessary messages for decision-makers, and recognize active lines.

Note that inactive constraint identification should be a fast algorithm. It is less meaningful if solving time is longer than that by solving a convex quadratic programming directly. In general, the interior-point method is adopted to solve a convex quadratic programming, whose time complexity is $\mathcal{O}(n^3)$. So the time complexity of the inactive constraint identification must be lower than $\mathcal{O}(n^3)$.

Note that a constraint is inactive if the feasible region remains the same after this constraint is eliminated. Figure 6.2 shows a inactive constraint description: there is no intersection between inactive constraints and the feasible region or there is a peak point of the Polyhedron in the intersection. Firstly, the inactive constraints are studied under the certain condition. Assuming that a Polyhedron is represented as

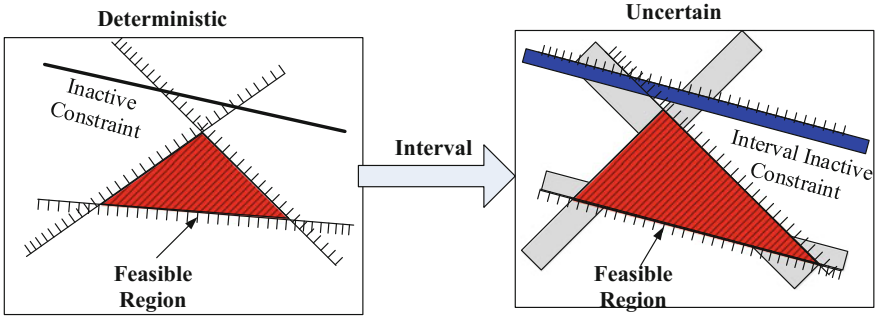

Fig. 6.2 Certainty and uncertainty of redundant constraint definition

$\Omega = \{\boldsymbol{x} \in \mathrm{R}^n | \boldsymbol{A}\boldsymbol{x} \le \boldsymbol{b}\}$, $\boldsymbol{A}^i\boldsymbol{x} \le \boldsymbol{B}^i$ is defined as i-th constraint of Ω, and the Polyhedron $\Omega^{i-} = \{\boldsymbol{x} \in \mathrm{R}^n | \boldsymbol{A}^{i-}\boldsymbol{x} \le \boldsymbol{b}^{i-}\}$ is represented as a new feasible region without i-th constraint. Then, the necessary and sufficient condition of $\boldsymbol{A}^i\boldsymbol{x} \le \boldsymbol{B}^i$ as an inactive constraint of Ω is $\Omega = \Omega^{i-}$. However, it is difficult to judge the equality of these two Polyhedrons. So another necessary and sufficient condition to identify inactive constraint will be provided.

A Polyhedron $\Omega^* = \{\boldsymbol{x} \in \mathrm{R}^n | \boldsymbol{A}^{i-}\boldsymbol{x} \le \boldsymbol{b}^{i-}, \boldsymbol{A}^i\boldsymbol{x} = \boldsymbol{b}^i\}$ is built. The necessary and sufficient condition to identify i-th constraint to be inactive is that Ω^* is an empty set or a single-point set. So the original problem is converted into a judgement problem of an empty set or a single-point set. There are many methods to recognize like Farkas lemma, which turns self-variables into a nonnegative space as well as inequality constraints into equality constraints, and then recognizes by Fourier-Monzkin Elimination Method [1]. B-rule based iteration method can also be used to recoginze the problem [2]. Furthermore, an optimization problem is adopted based on the simplex. Among these methods, the optimization method is faster in time complexity [3]. Since Ω^* can be representd as $\Omega^* = \{\boldsymbol{x} \in \mathrm{R}^n | \boldsymbol{A}\boldsymbol{x} \le \boldsymbol{b}, \boldsymbol{A}^i\boldsymbol{x} \ge \boldsymbol{b}^i\}$, we have

Theorem 6.1 (necessary and sufficient): *In an optimization problem* $Z = \max_{x \in \Omega^{i-}} \boldsymbol{A}^i\boldsymbol{x}$,, *if* $Z \le \boldsymbol{b}^i$ *is satisfied, i-th constraint is an inactive constraint.*

The uncertainty of $\boldsymbol{y}$ is considered. We assume that feasible region of a Polyhedron is represented as $\Omega = \{\boldsymbol{x} \in \mathrm{R}^n, \boldsymbol{y} \in \mathrm{R}^m | \boldsymbol{A}\boldsymbol{x} + \boldsymbol{B}\boldsymbol{y} \le \boldsymbol{b}, \boldsymbol{C}\boldsymbol{x} \le \boldsymbol{d}, \forall \boldsymbol{y} \in [\boldsymbol{y}^{\min}, \boldsymbol{y}^{\max}]\}$. Based on Theorem 6.1, i-th constraint is an inactive constraint if $Z = \max_{\forall \boldsymbol{y}, \boldsymbol{x} \in \Omega^{i-}} \boldsymbol{A}^i\boldsymbol{x} + \boldsymbol{B}^i\boldsymbol{y}$ and $Z \le \boldsymbol{b}^i$ is satisfied. However, uncertain variables are randomized. So the model can be turned into a bi-level optimization problem based on (6.6). For optimization of "max-max", the dimension of variables will be increased. The bi-level optimization problem can be turned into a single-level optimization problem.

$$\max_{\forall \boldsymbol{y}, \boldsymbol{x} \in \Omega^{i-}} \boldsymbol{A}^i\boldsymbol{x} + \boldsymbol{B}^i\boldsymbol{y} = \max_{\boldsymbol{y}^{\min} \le \boldsymbol{y} \le \boldsymbol{y}^{\max}} \max_{\boldsymbol{x} \in \Omega^{i-}} \boldsymbol{A}^i\boldsymbol{x} + \boldsymbol{B}^i\boldsymbol{y} \tag{6.6}$$

"max-max" in (6.6) are combined to "max". n-dimension variable $\boldsymbol{x}$ can be expanded to $(n + m)$-dimension variable $\boldsymbol{z} = (\boldsymbol{x}^T, \boldsymbol{y}^T)^T \in \mathrm{R}^{n+m}$, that is, the uncertain variable is regarded as an optimization variable. Later, (6.6) is rewrited as $Z = \max_{z \in \Pi^{i-}} \boldsymbol{D}^i\boldsymbol{z}$, $\Pi = \{\boldsymbol{z} \in \mathrm{R}^{n+m} | \boldsymbol{D}\boldsymbol{z} \le \boldsymbol{f}\}$ after increasing dimensions. We have

$$\boldsymbol{D} = \begin{bmatrix} \boldsymbol{A} & \boldsymbol{B} \\ \boldsymbol{C} & \boldsymbol{0} \\ \boldsymbol{0} & \boldsymbol{I} \\ \boldsymbol{0} & -\boldsymbol{I} \end{bmatrix}, \quad \boldsymbol{f} = \begin{bmatrix} \boldsymbol{b} \\ \boldsymbol{d} \\ \boldsymbol{y}^{\max} \\ -\boldsymbol{y}^{\min} \end{bmatrix} \tag{6.7}$$

where $\boldsymbol{I}$ is an m–dimension unit matrix. So i-th constraint is an inactive constraint if $Z \le \boldsymbol{f}^i$ is satisfied.

6.2.2 Greedy-Algorithm Based Fast Relaxation Identification

In the feasible region of SCED, the third term of (6.4) shows the transmission capacity constraints, which are bilateral. Bilateral constraints can be converted into two unilateral constraints and variable dimensions will be increased from N_g to (N_g + N_d). Moreover, according to the necessary and sufficient conditions above, the bilateral constraint is inactive if these two unilateral constraints are inactive.

$$\boldsymbol{GP}_g - \boldsymbol{HP}_b \le \boldsymbol{F}^{\max} \text{ 且 } -\boldsymbol{GP}_g + \boldsymbol{HP}_b \le -\boldsymbol{F}^{\min} \tag{6.8}$$

However, 2N optimization problem need to be solved for N security constraints, which is time-consuming. Considering a large transimission capacity in real power systems. Reference [4] applied a relaxaiton method, which expanded the feasible region, considered energy balance constraints as well as generation limits, and neglected the ramp rate constraints. T time periods can be decoupled and l-th bilateral security constraint can be converted into two unilateral constraints according to (6.8)

$$\max_{\boldsymbol{P}_g, \boldsymbol{P}_b} \overline{Z}^l_+ = \sum_{i=1}^{N_g} G_{l,i} P_{g,i} - \sum_{j=1}^{N_b} H_{l,j} P_{b,j} \tag{6.9}$$

$$\max_{\boldsymbol{P}_g, \boldsymbol{P}_b} \overline{Z}^l_- = -\sum_{i=1}^{N_g} G_{l,i} P_{g,i} + \sum_{j=1}^{N_b} H_{l,j} P_{b,j} \tag{6.10}$$

$$s.t. \sum_{i=1}^{N_g} P_{g,i} = \sum_{j=1}^{N_b} P_{b,j} \tag{6.11}$$

$$P^{\min}_{g,i} \le P_{g,i} \le P^{\max}_{g,i}, \quad P^{\min}_{b,j} \le P_{b,j} \le P^{\max}_{b,j} \tag{6.12}$$

where N_b is the bus number. The result of the optimization model of (6.9), (6.11) and (6.12) is $\bar{Z}^l_+$, and the result of the optimization model of (6.10)–(6.12) is $\overline{Z}^l_-$. Based on Theorem 6.1, the results are Z^l_+ and Z^l_-, respectively. It is obvious that $\overline{Z}^l_+ \ge Z^l_+$ and $\overline{Z}^l_- \ge Z^l_-$ are satisfied. l-th bilateral security constraint is inactive if $\overline{Z}^l_+ \le F^{\max}_l$ and $\overline{Z}^l_- \le -F^{\min}_l$ are satisfied at the same time. Otherwise, we cannot identify if $\overline{Z}^l_+ \le F^{\max}_l$ and $\overline{Z}^l_- \le -F^{\min}_l$ cannot be satisfied at the same time. So this method only gives sufficient but not necessary conditions.

In addition, the optimization model (6.9)–(6.12) can be directly solved by the simplex algorithm, but this may take much time since the calculation of the inverse matrix in the simplex method is time-consuming. Note that the optimization model of (6.9)–(6.12) is particular, where there is one equality constraint as well as upper

and lower bounds of variables. This problem is similar to a "knapsack problem" in mathematical programming which can be solved very fast.

Firstly, we have $\boldsymbol{P}_g = \boldsymbol{P}_g + \Delta\boldsymbol{P}_g$ and $\boldsymbol{P}_b = \boldsymbol{P}_b^{\max} - \Delta\boldsymbol{P}_b$. The $(N_g + N_b)$ dimensions optimization model can be converted into $(N_g + N_b)$ dimensions increment vector space. We have $(\boldsymbol{P}_g^T, \boldsymbol{P}_d^T)^T \rightarrow (\Delta\boldsymbol{P}_g^T, \Delta\boldsymbol{P}_d^T)^T$. The objective function is (6.9). Equation (6.13) is represented as a equivalent form. Later, we have (6.14). Equation (6.10) can also be converted into (6.15)

$$\sum_{i=1}^{N_g} G_{l,i}P_{g,i} - \sum_{j=1}^{N_b} H_{l,j}P_{b,j} = \sum_{i=1}^{N_g} G_{l,i}\left(P_{g,i}^{\min} + \Delta P_{g,i}\right) + \sum_{j=1}^{N_b} -H_{l,j}\left(P_{b,j}^{\max} - \Delta P_{b,j}\right) \tag{6.13}$$

$$\overline{Z}_+^l = \sum_{i=1}^{N_g} G_{l,i}P_{g,i}^{\min} - \sum_{j=1}^{N_b} H_{l,j}P_{b,j}^{\max} + \sum_{i=1}^{N_g} G_{l,i}\Delta P_{g,i} + \sum_{j=1}^{N_b} H_{l,j}\Delta P_{b,j} \tag{6.14}$$

$$\overline{Z}_-^l = \sum_{j=1}^{N_b} H_{l,j}P_{b,j}^{\max} - \sum_{i=1}^{N_g} G_{l,i}P_{g,i}^{\min} + \sum_{i=1}^{N_g} -G_{l,i}\Delta P_{g,i} + \sum_{j=1}^{N_b} -H_{l,j}\Delta P_{b,j} \tag{6.15}$$

Equality constraints can be represented as (6.16) and then converted into (6.17).

$$\sum_{i=1}^{N_g}\left(P_{g,i}^{\min} + \Delta P_{g,i}\right) = \sum_{j=1}^{N_b}\left(P_{b,j}^{\max} - \Delta P_{b,j}\right) \tag{6.16}$$

$$\sum_{i=1}^{N_g}\Delta P_{g,i} + \sum_{j=1}^{N_b}\Delta P_{b,j} = \sum_{j=1}^{N_b} P_{b,j}^{\max} - \sum_{i=1}^{N_g} P_{g,i}^{\min} \tag{6.17}$$

The generation limits and load demand inequality constraints can be represented as (6.18), and then converted into (6.19).

$$P_{g,i}^{\min} \le P_{g,i}^{\min} + \Delta P_{g,i} \le P_{g,i}^{\max}, \quad P_{b,j}^{\min} \le P_{b,j}^{\max} - \Delta P_{b,j} \le P_{b,j}^{\max} \tag{6.18}$$

$$0 \le \Delta P_{g,i} \le P_{g,i}^{\max} - P_{g,i}^{\min}, \quad 0 \le \Delta P_{b,j} \le P_{b,j}^{\max} - P_{b,j}^{\min} \tag{6.19}$$

From what has been discussed above, the optimization result is $\Delta\bar{Z}_+^l$ based on the optimization model of (6.20), (6.22), and (6.23), and the optimization result is $\overline{Z}_-^l$ based on the optimization model of (6.21)–(6.23). We have $Q = \sum_{i=1}^{N_g} G_{l,i}P_{g,i}^{\min} - \sum_{j=1}^{N_b} H_{l,j}P_{b,j}^{\max}$. Theorem 6.2 is given.

Theorem 6.2 (sufficient but not necessary): *l-th bilateral security constraint is inactive, if* $\Delta\overline{Z}^{l}_{+} + Q \le F_l^{\max}$ and $\Delta\overline{Z}^{l}_{-} - Q \le -F_l^{\min}$ *are satisfied at the same time.*

Obviously, ramp rate constraints are relaxed to decouple the time periods and convert a large problem into a small problem for improving the efficiency. Another relaxed constraints are the rest N_l-1 security constraints except the present security constraint. This deduction is only sufficient due to relaxation.

$$\max_{\boldsymbol{P}_g,\boldsymbol{P}_b} \Delta\overline{Z}^{l}_{+} = \sum_{i=1}^{N_g} G_{l,i}\Delta P_{g,i} + \sum_{j=1}^{N_b} H_{l,j}\Delta P_{b,j} \tag{6.20}$$

$$\max_{\boldsymbol{P}_g,\boldsymbol{P}_b} \Delta\overline{Z}^{l}_{-} = \sum_{i=1}^{N_g} -G_{l,i}\Delta P_{g,i} + \sum_{j=1}^{N_b} -H_{l,j}\Delta P_{b,j} \tag{6.21}$$

$$s.t. \sum_{i=1}^{N_g} \Delta P_{g,i} + \sum_{j=1}^{N_b} \Delta P_{b,j} = \sum_{j=1}^{N_b} P_{b,j}^{\max} - \sum_{i=1}^{N_g} P_{g,i}^{\min} \tag{6.22}$$

$$0 \le \Delta P_{g,i} \le P_{g,i}^{\max} - P_{g,i}^{\min}, \quad 0 \le \Delta P_{b,j} \le P_{b,j}^{\max} - P_{b,j}^{\min} \tag{6.23}$$

The Increment optimization model of (6.20)–(6.23) is similar to the model of a "knapsack problem" [5]. The difference is that the optimization variables of a "knapsack problem" are integers, and the optimization variables of an increment model are continuous. When (6.20) is the optimization target, the optimization variables are represented as (6.24), and the objective price coefficients are represented as (6.25).

$$\Delta\boldsymbol{P} = \left(\Delta P_{g,1}, \Delta P_{g,2}, \ldots, \Delta P_{g,N_g}, \Delta P_{b,N_g+1}, \Delta P_{b,N_g+2}, \ldots, \Delta P_{b,N_g+N_b}\right)^T \tag{6.24}$$

$$\boldsymbol{c} = \left(G_{l,1}, G_{l,2}, \ldots, G_{l,N_g}, H_{l,N_g+1}, H_{l,N_g+2}, \ldots, H_{l,N_g+N_b}\right)^T \tag{6.25}$$

From the view of a "knapsack problem", this problem can be described as follows: There are $N_g + N_b$ kinds of things. The weight of i-th is ΔP_i. The price of unit weight is c_i. The knapsack can carry the weight of $\sum_{j=1}^{N_b} P_{b,j}^{\max} - \sum_{i=1}^{N_g} P_{g,i}^{\min}$. How to load things to get the maximum price? The Greedy Algorithm can solve this problem efficiently. Moreover, it can be called as the continuous Greedy Algorithm due to continuous and adjustable variables. That is, we can order the price of the unit weight and load things that have a higher unit weight price first until the limit is reached.

The procedure of the greedy-algorithm based fast relaxation identification can be described as below.

From what has been discussed above, we need to order an $N_g + N_d$—dimensions vector as well as identify and the summation for $N_g + N_b$ times. We will have $\Delta\bar{Z}^{l}_{+}$.

So the time complexity is $(N_g + N_d)\log(N_g + N_d)$, that is, $\mathcal{O}(n \log n)$. $\Delta\bar{Z}_-^l$ can be obtained for the same reason. Based on Theorem 6.2, the fast identification can be made.

6.2.3 *Inactive Constraint Elimination of Rubost Optimization Models*

It can be easily observed that the original robust optimal power flow model of Sect. 5.2 can be converted into a simple convex quadratic programming on the condition that the description of redundant constraints of Sect. 6.2.1 is applied in the robust optimization models of Sect. 5.2, but the difference from the traditional deterministic optimal power flow model is that the number of the security constraints increases significantly from N_l to $N_l \times N_r$, which may affect the efficiency of the optimization model. In order to achieve a more applicable solution for on-line applications, we can identify the inactive constraints before solving the model and only consider the active constraints in the computation, which is called "inactive constraint identification technique". In this context, we consider

Corollary 6.3 *For each security constraint, if* (6.26) *holds, this security constraint is an inactive constraint.*

$$\begin{cases} f_l^{\max} = \max\limits_{\boldsymbol{P}^{sch}\in\Theta} \max\limits_{W_k^f - R_k^e \le W_k \le W_k^f + W_k^e} \left(\sum\limits_{i=1}^{N_g} G_{l,i}^P P_i^{sch} + \sum\limits_{k=1}^{N_w} G_{l,k}^W W_k - \sum\limits_{k=1}^{N_d} G_{l,j}^D D_j \right) \le F_l^{\max} \\ f_l^{\min} = \min\limits_{\boldsymbol{P}^{sch}\in\Theta} \min\limits_{W_k^f - R_k^e \le W_k \le W_k^f + W_k^e} \left(\sum\limits_{i=1}^{N_g} G_{l,i}^P P_i^{sch} + \sum\limits_{k=1}^{N_w} G_{l,k}^W W_k - \sum\limits_{k=1}^{N_d} G_{l,j}^D D_j \right) \ge F_l^{\max} \end{cases} \tag{6.26}$$

where Θ *is the feasible region of the optimal power flow.*

Obviously, Corollary 6.3 needs to solve $N_l \times N_r$ linear programming to find all the inactive constraints. It is desired that the inactive constraint identification process is not very time-consuming. In order to quickly solve the optimization model, we can relax the feasible region Θ with the help of relaxation models of (6.26), which gives a upper bound for "max" model and lower bound for "min" model. If the feasible region is overly relaxed, only a small amount of inactive constraints will be identified; but if the feasible region is not relaxed, it costs a lot of computational efforts to find all the inactive constraints. Therefore, a promising relaxation method is of the most importance. Section 6.2.2 presents that only the energy balance constraints and generation limits should be kept which is a good choice to relax. It has been used in the UC problem [4].

Therefore, this relaxation method of Sect. 6.2.2 is employed in this book, where the relaxed model for each security constraint l is given by

$$\begin{cases} f_l^{\max} = \max\limits_{\substack{\sum_{j=1}^{N_d} D_j - \sum_{k=1}^{N_r} R_k^f = \sum_{i=1}^{N_g} P_i^{sch} \\ P_i^{\min} \le P_i^{sch} \le P_i^{\max}}} \max\limits_{R_k^f - R_k^e \le R_k \le R_k^f + R_k^e} \left(\sum_{i=1}^{N_g} G_{l,i}^P P_i^{sch} + \sum_{k=1}^{N_r} G_{l,k}^R R_k - \sum_{j=1}^{N_d} G_{l,j}^D D_j \right) \\ \quad = \max\limits_{\substack{\sum_{j=1}^{N_d} D_j - \sum_{k=1}^{N_r} R_k^f = \sum_{i=1}^{N_g} P_i^{sch} \\ P_i^{\min} \le P_i^{sch} \le P_i^{\max}}} \left(\sum_{i=1}^{N_g} G_{l,i}^P P_i^{sch} \right) + \max\limits_{R_k^f - R_k^e \le R_k \le R_k^f + R_k^e} \left(\sum_{k=1}^{N_r} G_{l,k}^R R_k \right) - \sum_{j=1}^{N_d} G_{l,j}^D D_j \\ f_l^{\min} = \min\limits_{\substack{\sum_{j=1}^{N_d} D_j - \sum_{k=1}^{N_r} R_k^f = \sum_{i=1}^{N_g} P_i^{sch} \\ P_i^{\min} \le P_i^{sch} \le P_i^{\max}}} \min\limits_{R_k^f - R_k^e \le R_k \le R_k^f + R_k^e} \left(\sum_{i=1}^{N_g} G_{l,i}^P P_i^{sch} + \sum_{k=1}^{N_r} G_{l,k}^R R_k - \sum_{j=1}^{N_d} G_{l,j}^D D_j \right) \\ \quad = \min\limits_{\substack{\sum_{j=1}^{N_d} D_j - \sum_{k=1}^{N_r} R_k^f = \sum_{i=1}^{N_g} P_i^{sch} \\ P_i^{\min} \le P_i^{sch} \le P_i^{\max}}} \left(\sum_{i=1}^{N_g} G_{l,i}^P P_i^{sch} \right) + \min\limits_{R_k^f - R_k^e \le R_k \le R_k^f + R_k^e} \left(+ \sum_{k=1}^{N_r} G_{l,k}^R R_k \right) - \sum_{j=1}^{N_d} G_{l,j}^D D_j \end{cases} \tag{6.27}$$

Compared with (6.27) and (6.26), the difference is that the feasible region consists of energy balance constraints and generation limits changed from the feasible region Θ in the first model of the bi-level model.

On the other hand, the model of (6.27) is a bi-level optimization problem whose optimization variables are separable and objective function is linear. So, the model can be in fact separated into two parts. That means, we can have two models, the inner model and the outer model, which can be optimized separately. This optimization model can be called as Separable Programming. Greedy Algorithm in Sect. 6.2.2 can solve the outer model which is of course the same as Theorem 5.1 in Sect. 5.2.3. Therefore, we have the "max" model by using the exact closed forms in Theorem 5.1, yielding

$$f_l^{\max,1} = \sum_{m=1}^{h-1} \left(G_{l,s_m} - G_{l,s_h} \right) P_{g,s_m}^{\max} + G_{l,s_h} \left(\sum_{j=1}^{N_d} D_j - \sum_{k=1}^{N_w} W_k^f \right) + \sum_{m=h+1}^{N_g} D_j \left(G_{l,s_m} - G_{l,s_h} \right) P_{g,s_m}^{\min} \tag{6.28}$$

where $h (1 \le h \le N_g)$ is an integer number, such that

$$\sum_{m=1}^{h-1} \left(P_{g,s_m}^{\max} - P_{g,s_m}^{\min} \right) \le \sum_{j=1}^{N_d} D_j - \sum_{k=1}^{N_w} W_k^f - \sum_{i=1}^{N_g} P_{g,i}^{\min} \le \sum_{m=1}^{h} \left(P_{g,s_m}^{\max} - P_{g,s_m}^{\min} \right) \tag{6.29}$$

where $S_1, \ldots, S_{N_g}$ is a permutation of 1,…,N_g, such that $G_{l,s_1} \ge \cdots \ge G_{l,s_{N_g}}$.

Similarly, the first part of "min" model also can be obtained as follows:

$$f_l^{\min,1} = \sum_{m=1}^{h-1} \left(G_{l,s_m} - G_{l,s_h}\right) P_{g,s_m}^{\min} + G_{l,s_h} \left(\sum_{j=1}^{N_d} D_j - \sum_{k=1}^{N_w} W_k^f \right) + \sum_{m=h+1}^{N_g} \left(G_{l,s_m} - G_{l,s_h}\right) P_{g,s_m}^{\min} \tag{6.30}$$

where $h(1 \le h \le N_g)$ is an integer number, such that

$$\sum_{m=1}^{h-1} \left(P_{g,s_m}^{\max} - P_{g,s_m}^{\min} \right) \le \sum_{j=1}^{N_d} D_j - \sum_{k=1}^{N_w} W_k^f - \sum_{i=1}^{N_g} P_{g,i}^{\min} \le \sum_{m=1}^{h} \left(P_{g,s_m}^{\max} - P_{g,s_m}^{\min} \right) \tag{6.31}$$

It should be noted that the difference between solving "max" and "min" model is in the permutation of $S_1, \ldots, S_{N_g}$. The proposed inactive constraint identification method only needs two permutations, i.e., descending order and ascending order computation for each security constraint, which can be handled in a very fast speed.

It can be found that the inner model is much easier to solve, compared with the outer model, since it only contains the upper and lower bound constraints of the uncertain wind power $\boldsymbol{W}$. Thus, we have

$$f_l^{\max,2} = \sum_{k=1}^{N_w} G_{l,k}^W W_k^f + \sum_{k=1}^{N_w} \left| G_{l,k}^W W_k^e \right| \tag{6.32}$$

$$f_l^{\min,2} = \sum_{k=1}^{N_w} G_{l,k}^W W_k^f - \sum_{k=1}^{N_w} \left| G_{l,k}^W W_k^e \right| \tag{6.33}$$

Finally, we can conbine the inner model and outer model. If it holds for $\begin{cases} f_l^{\max,1} + f_l^{\max,2} - \sum_{j=1}^{N_d} G_{l,j}^D D_j \le F_l^{\max} \\ f_l^{\max,1} + f_l^{\max,2} - \sum_{j=1}^{N_d} G_{l,j}^D D_j \ge -F_l^{\max} \end{cases}$, the constraint l is inactive and can be eliminated.

Permuting each security constraint only once will generate the set of active constraints. Then, the active constraints are kept and the inactive constraints are eliminated. Let the set of active constraints be Φ and the robust optimization model considering the eliminated redundant constraints can be finally presented as:

$$\min_{\boldsymbol{P}^{sch}, \boldsymbol{\beta}, t, \boldsymbol{p}} \sum_{i=1}^{N_g} \left(a_i \left(P_i^{sch}\right)^2 + b_i P_i^{sch} + c_i + a_i \beta_i^2 \sum_{k=1}^{N_w} \sum_{j=1}^{N_w} \Lambda_{kj} \right) \tag{6.34}$$

$$s.t. \ \sum_{j=1}^{N_d} D_j - \sum_{k=1}^{N_w} W_k^f = \sum_{i=1}^{N_g} P_i^{sch} \tag{6.35}$$

$$P_i^{\min} + \beta_i \theta \le P_i^{sch} \le P_i^{\max} - \beta_i \theta, \quad i = 1, \ldots, N_g \tag{6.36}$$

$$\begin{aligned} -F_l^{\max} = \left(t_l \Gamma + \sum_{k=1}^{N_w} p_{lk} \right) \le \sum_{i=1}^{N_g} G_{l,i}^P P_i^{sch} \\ + \sum_{k=1}^{N_w} G_{l,k}^W W_k^f - \sum_{j=1}^{N_d} G_{l,j}^D D_j \le F_l^{\max} - \left(t_l \Gamma + \sum_{k=1}^{N_w} p_{lk} \right), \quad l \in \Phi \end{aligned} \tag{6.37}$$

$$t_l + p_{lk} \ge W_k^e \left(\sum_{i=1}^{N_g} G_{l,i}^P \beta_i + G_{l,k}^W \right), \quad l \in \Phi, \quad k = 1, \ldots, N_w \tag{6.38}$$

$$p_{lk} \ge 0, \quad t_l \ge 0, \quad l \in \Phi \quad k = 1, \ldots, N_w \tag{6.39}$$

$$\sum_{i=1}^{N_g} \beta_i = 1, \quad 0 \le \beta_i \le 1 \tag{6.40}$$

where

$$\theta = \max_{\sum_{k=1}^{N_w} y_k = \Gamma, 0 \le y_k \le 1} \sum_{k=1}^{N_w} W_k^e y_k = \sum_{m=1}^{k-1} \left(W_{i_m}^e - W_{i_k}^e \right) + W_{i_k}^e \Gamma \quad \text{and} \quad k - 1 \le \Gamma \le k.$$

6.2.4 Simulation Analysis

A. **Test on a simple example**

The feasible region is Ω which represents a simple single time period economic dispatch model with energy balance constraints, transmission security constraints and generation limits.

$$\underset{x_1, x_2}{\Omega'} = \begin{cases} x_1 + x_2 = [6, 14] & \text{Power Balance} \\ x_1 + 2x_2 + 2[6, 14] \le 55 & \text{Security Constraint} \\ 2x_1 + x_2 + [6, 14] \le 22 & \text{Security Constraint} \\ -x_1 + 2x_2 + [6, 14] \le -4 & \text{Security Constraint} \\ x_1, x_2 \in [0, 10] & \text{Generation Limit} \end{cases}$$

$$\underset{x_1,x_2,y}{\Omega'} = \begin{cases} x_1 + x_2 - y = 0 & \text{Power Balance} \\ x_1 + 2x_2 + 2y \le 55 & \text{Security Constraint} \\ 2x_1 + x_2 + y \le 22 & \text{Security Constraint} \\ -x_1 + 2x_2 + y \le -4 & \text{Security Constraint} \\ 0 \le x_1, x_2 \le 10, \quad 6 \le y \le 14 & \text{Generation Limit} \end{cases}$$

The new feasible region Ω' is obtained after variables increase dimensions. Based on Theorem 6.2, taking the first transmission security constraint for illustration, the relaxation model in the increment space is as follows:

$$\begin{aligned} &\Delta\overline{Z}^1 = \max \Delta x_1 + 2\Delta x_2 - 2\Delta y \\ &s.t.\ \Delta x_1 + \Delta x_2 + \Delta y = 14 \\ &0 \le \Delta x_1, \Delta x_2 \le 10, 0 \le \Delta y \le 8 \end{aligned}$$

The coefficient permutation of the targets is $2 \rightarrow 1 \rightarrow -2$ based on the continuous Greedy Algorithm. Late, the optimal results are $\Delta x_2 = 10$, $\Delta x_1 = 4$, $\Delta x_3 = 0$. The objective increment is $\Delta\overline{Z}^1 = 24$. $Q^1 = 28$. $\overline{Z}^1 = \Delta\overline{Z}^1 + Q^1 = 52 < 55$. This constraint is inactive.

It is the same to have $\bar{Z}^2 = 38 > 22$ and $\bar{Z}^3 = 30 > -4$. So we cannot identify these constraints. Furthermore, the second security constraint is active and the third one is inactive based on Theorem 6.1.

In Fig. 6.3, the feasible region of (a) is a sub-set of energy balance constraints. The first security constraint and the third one have no intersection with the feasible region. That means the original feasible region does not change when these constraints are eliminated. Only the second constraint is active. When the energy balance constraint is kept in the relaxed feasible region based on Theorem 6.2, the constraint is inactive if the constraint has no intersection with the feasible region (Theorem 6.2 holds) like the first security constraint. Otherwise, we cannot identify constraints like the second and the third ones.

When there is an intersection between the third constraint and the relaxed feasible region, but there is no intersection with the original feasible region. Based on Theorem 6.1, we need to identify whether the new feasible region without the second one and the third one is the same as the original feasible region or not, respectively. It is not difficult to find that the second one is active.

B. **24-h IEEE nine-bus test systems economic dispatch**

The simulation analysis of 9-bus systems in MATPOWER [6] is studied where there are three generators and nine lines. The first generator is wind power. Load demand and wind power are obtained like those in Sect. 4.2.2. There are $2 \times 9 \times 24 = 432$ constraints in all when a bilateral security constraint are transformed into two unilateral security constraints.

Assume that the bus uncertainty is 5 %. There are 1 and 0.9 times transmission capacity. Theorem 6.1 and Theorem 6.2 is used in the test system.

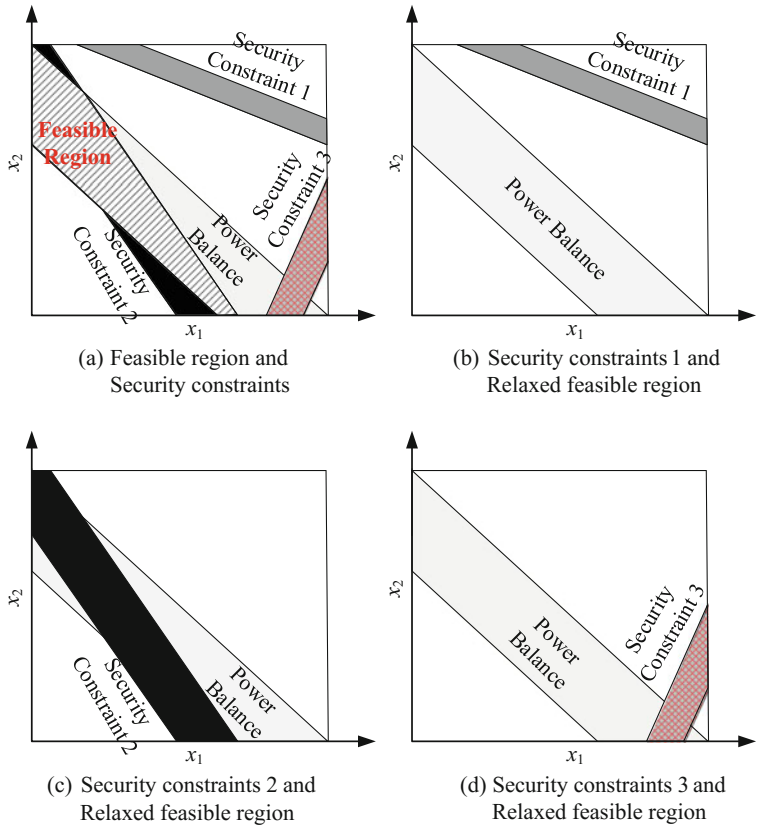

Fig. 6.3 Certainty and uncertainty of redundant constraints

In Table 6.1, all security constraints are inactive resulted from the original transmission capacity. They can be eliminated in SCED models. Based on Theorem 6.1 to identify all constraints, the total computational time is 20 s. However, the total computational time is 2.23 s by using Theorem 6.2 to identify and eliminate 193 constraints first and then using Theorem 6.1 to identify the other 23 constraints.

Moreover, the total computational time is 2.28 s by using both Theorem 6.1 and Theorem 6.2 to identify all inactive constraints. Compared with Theorem 6.1, the efficiency is improved. It is the same when the transmission capacity is 0.9 times. The results are shown in Table 6.2. There are nine active constraints in SCED models, and other constraints can be eliminated. The total computational time is 20 s by using Theorem 6.1 to identify all constraints. However, the total computational time is 3.7 s in all by using Theorem 6.2 to identify and eliminate 178 constraints first and then using Theorem 6.1 to identify the other 38 constraints. Nine active

Table 6.1 Greedy algorithm based fast relaxation identification

Algorithm : Greedy Algorithm Based Fast Relaxation Identification
Step 1: Order the price of $\boldsymbol{c}$ and have $S_1, S_2, \ldots, S_{N_g+N_b}$;
Step 2: $V \leftarrow 0$, $W \leftarrow 0$, $i \leftarrow 1$;
Step 3: $P_{S_i} = P_{S_i}^{\max} - P_{S_i}^{\min}$;
Step 4: **if** $V + P_{S_i} \le \sum_{j=1}^{N_b} P_{b,j}^{\max} - \sum_{i=1}^{N_g} P_{g,i}^{\min}$
Update W and V as $W \leftarrow W + c_{S_i} P_{S_i}$, $V \leftarrow V + P_{S_i}$, $i \leftarrow i+1$, and go to **Step 3**;
else
Update W as $W \leftarrow W + c_{S_i}\left(\sum_{j=1}^{N_b} P_{b,j}^{\max} - \sum_{i=1}^{N_g} P_{g,i}^{\min} - V\right)$, and go to **Step 5**;
end
Step 5: $\Delta \overrightarrow{Z}_+^l = W$;

Table 6.2 Results under the original transmission capacity (1 times)

Mehod	Theorem 6.1	Theorem 6.2	Theorem 6.1 + Theorem 6.2
Inactive security constraints	0	23	0
Time(s)	20.02	0.046	2.28

constraints are identified by using Theorem 6.1 and Theorem 6.2 which improves the efficiency compared with using Theorem 6.1 only. It takes only 3.76 s.

Compared with Tables 6.2 and 6.3, there are different active security constraints resulted from different transmission capacities. This method can identify and eliminate inactive constraints based on Theorem 6.2.

Moreover, active unilateral security constraints are transformed into active bilateral security constraints corresponding every line and time period. The array (t, i) is represented as i-th unit in t-th period. The set of active constraints resulted from the 0.9 times transmission capacity is given in Table 6.4. They may reach the bounds and be active in 5-th period.

C. 118-bus test systems economic dispatch in 96 periods

There are 54 generators and 186 lines in IEEE 118-bus test system. There are $2 \times 186 \times 96 = 35712$ unilateral security constraints. The uncertainty of bus injection is 10 % and the transmission capacity is original. In Table 6.5, it takes 3 h to identify 74 active constraints based on Theorem 6.1. However, it takes only 8.79 s to identify 881 active constraints based on Theorem 6.2. The computational

Table 6.3 Results under the transmission capacity (0.9 times)

Method	Theorem 6.1	Theorem 6.2	Theorem 6.1 + Theorem 6.2
Inactive security constriants	9	38	9
Time(s)	20.13	0.051	3.76

Table 6.4 Transmission lines and time periods

Method	The array (t, i)
Theorem 6.1	(11,5); (13,5); (15,5); (16,5); (17,5); (18,5); (21,5); (22,5); (23,5)
Theorem 6.2	(1,5); (1,3); (2,5); (2,3); (3,5); (3,3); (4,5); (4,3); (5,5); (5,3); (6,5); (6,3); (7,5); (7,3); (8,5); (8,3); (9,5); (9,3); (10,5); (10,3); **(11,5)**; (11,3); **(13,5)**; (14,5); (14,3); **(15,5)**; (15,3); **(16,5)**; (16,3); **(17,5)**; **(18,5)**; **(21,5)**; **(22,5)**; (22,3); **(23,5)**; (23,3); (24,5); (24,3)

Table 6.5 Results under the original transmission capacity (with 10 % uncertainty)

Method	Theorem 6.1	Theorem 6.2	Theorem 6.1 + Theorem 6.2
Inactive security constriants	74	881	74
Time	3 h	8.79 s	4.88 min

time is 4.88 min by using Theorem 6.2 to eliminate the inactive constraints first and then using Theorem 6.1 to identify the others. The number of identified constraints is the same. When the uncertainty of bus injection is 20 %, Table 6.6 shows that it takes 3 h to solve 35712 linear programming problems based on Theorem 6.1. However, it takes 9.13 s when Theorem 6.2 is used to eliminate 34772 inactive constraints first (97 % of all security constraints) and Theorem 6.1 is used to identify active constraints later.

D. Acceleration for robust optimization algorithm

IEEE 118-bus systems in Sect. 5.2.4 B is studied, where there are 118 buses in 24-h periods. Considering different transmission capacity limits under uncertainty degree $\eta = 0.4$, the numbers of inactive constraints found by the proposed inactive constraint reduction method are shown in Figs. 6.4 and 6.5. In Fig. 6.4, the black rectangle denotes the index of inactive lines. According to Fig. 6.5a, all constraints are inactive which can be eliminated in the model when constraint limit is greater than 1100 MW.

Active constraints are considered in the model. In addition, there are more active constraints when the line capacity limit is tighter. From Fig. 6.5b, it can be found that the computational efficiency is improved with the help of the proposed inactive constraint reduction strategy. For example, for 1100 MW line capacity limit, the computational time of the solution process drops from 3.13 to 0.12 s with the proposed strategy. In addition, the implementation of the inactive constraint reduction strategy takes only about 0.09226 s. The total time is 0.13 and is improved

Table 6.6 Results under 0.9 times transmission capacity (with 20 % uncertainty)

Method	Theorem 6.1	Theorem 6.2	Theorem 6.1 + Theorem 6.2
Inactive security constriants	96	940	96
Time	3 h	9.13 s	5.21 min

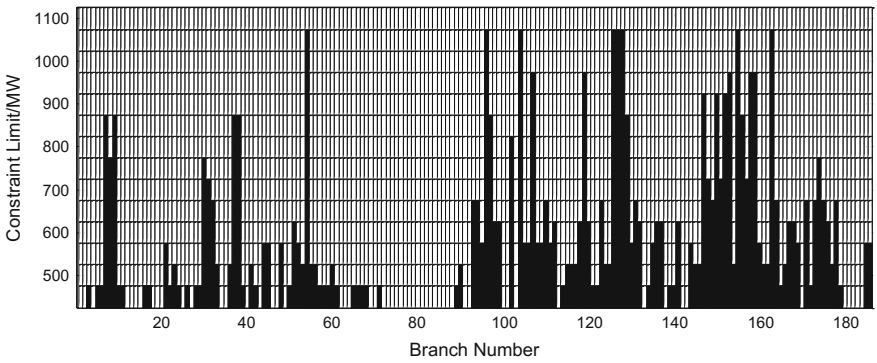

Fig. 6.4 Inactive constraints sets with different constraint limits

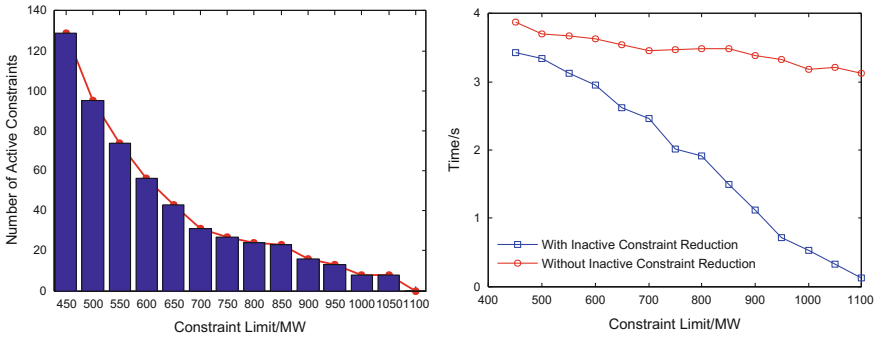

(a) Number of active constraints found by the proposed method
(b) Comparison of time consumption with/without inactive constraint reduction

Fig. 6.5 Simulation results

25 times than solving directly. Note that inactive constraint identification is applied once and can be used again in real-time markets. It will contribute to the large-scale system operation.

To further demonstrate the effectiveness of the proposed method and show the computational performance with the introduced inactive constraints reduction strategy, simulations are performed on six real-world Polish systems with more than 2000 buses and 2500 lines which are available in MATPOWER. The computational time of the systems is shown in Table 6.6, where *Time1* and *Time2* denote the time for solving the robust model without and with using the inactive constraint reduction strategy, respectively; *Time3* represents the time for identifying the inactive constraint. It can be observed that the robust models may not be directly handled by commercial solvers because the solver is out of memory resulted from large amount of dummy variables and additional constraints. In contrast, the

Table 6.7 Computational time on six large systems

Test systems	# of security constraints	# of active security constraints	Ratio of active constraints (%)	Time 1 (s)	Time 2 (s)	Time 3 (s)
2383-bus	2896	99	3.42	×	3.3242	2.4364
2736-bus	3269	14	0.43	×	0.9189	2.8456
2746-bus	3279	10	0.30	×	0.8333	2.8357
3012-bus	3572	103	2.88	×	3.657	3.2596
3120-bus	3693	211	5.73	×	9.4453	3.3521
3375-bus	4161	176	4.23	×	6.2381	3.5213

Note: "×" means that the problem is unsolvable due to the lack of enough memory space

proposed inactive constraint reduction strategy can help the solver obtain the optimal solution and the total computational time is less than 10 s. The time to identify inactive constraints is less than 5 s. It will contribute to the real-time operation. Interestingly, it can be also found that in real-world power systems, the number of active constraints only takes a small proportion. For the Polish power systems showed in Table 6.7, the number of inactive constraints is more than 94 % of all the transmission lines. Especially in 2736-bus systems and 2746-bus systems, the ratio of active constraints is less than 1 %. Therefore, the inactive constraint reduction strategy can greatly improve the computational efficiency.

6.3 Decomposition Method for Multi-period Economic Dispatch

6.3.1 Mathematical Modeling and Theoretical Method

As an ED model, the economic dispatch (ED) model is widely used in the Energy Management System (EMS) of RTOs/ISOs, and can be generally expressed as follows:

$$Z = \min_{P_{i,t}} \sum_{i=1}^{N} \sum_{t=1}^{T} f\left(P_{i,t}\right) \tag{6.41}$$

$$s.t. \sum_{i=1}^{N_g} P_{i,t} = \sum_{j=1}^{N_d} D_{j,t} - \sum_{k=1}^{N_w} W_{k,t}^{f}, \quad t = 1, \ldots T \tag{6.42}$$

$$P_{i,t}^{\min} \le P_{i,t} \le P_{i,t}^{\max}, \quad i = 1, \ldots N_g, \; t = 1, \ldots T \tag{6.43}$$

$$-Rd_{i,t} \le P_{i,t} - P_{i,t-1} \le Ru_{i,t}, \quad i = 1, \ldots N_g, \ t = 1, \ldots T \tag{6.44}$$

$$-F_l^{\max} \le \sum_{i=1}^{N_g} S_{l,i} P_{i,t} - \sum_{j=1}^{N_d} H_{l,j} D_{j,t} + \sum_{k=1}^{N_w} G_{l,k} W_{k,t}^f \le F_l^{\max}, \quad l = 1, \ldots, N_l, \ t = 1, \ldots T \tag{6.45}$$

where the definitions can be found in Sect. 4.2.1. $f(\bullet)$ is the fuel cost function, which is usually presented as a quadratic or piece-wise linear function, leading to a quadratic or linear programming techniques correspondingly. Equations (6.42), (6.43), (6.44), and (6.45) represent the energy balance constraints, generator capacity constraints, generator ramp rate constraints, and transmission capacity constraints, respectively. The feasible region of the ED model is a polyhedron enclosed by T equalities, $N_g T + N_l T$ inequalities and $N_g T$ element-wise constraints with $N_g T$ variables. It is an extremely large-scale optimization problem with coupled structure, whose size grows quickly with the increase of time periods T. Moreover, we are interested in the case when T is very large, which introduces further computational challenges.

In fact, the objective function (6.41) and the constraints except (6.44) are separable in terms of the decision vectors $\boldsymbol{x}_1, \boldsymbol{x}_2, \ldots, \boldsymbol{x}_T$, but the linear constraint (6.44) links them together. To overcome the issue of nonseparability of the linking constraint (6.44), we consider the augmented Lagrangian relaxation approach to put it into objective function and solve the dual problem, where the new model by the augmented Lagrangian relaxation can be decomposed into several decoupled sub-problems and computed in parallel. This will greatly alleviate the computational complexity and may be applied to on-line applications, such as dynamic economic dispatch, multi-period look-ahead dispatch and so on.

Model (6.41)–(6.45) can be mathematically formulated as a convex optimization model in matrix form as:

$$\min_{\boldsymbol{x}_1, \ldots, \boldsymbol{x}_T} \ f(\boldsymbol{x}_i) \tag{6.46}$$

$$s.t. \ \sum_{i=1}^{T} \boldsymbol{A}_i \boldsymbol{x}_i = \boldsymbol{b} \tag{6.47}$$

$$\boldsymbol{x}_i \in \Omega_i, \quad i = 1, \ldots, T \tag{6.48}$$

where Ω_i is a convex and closed set for decision vector $\boldsymbol{x}_i$; the objective function f is a separable convex function which satisfies

$$f(\boldsymbol{x}_i) = \sum_{i=1}^{T} f_i(\boldsymbol{x}_i) \tag{6.49}$$

The augmented Lagrangian function can be constructed as

$$L(\boldsymbol{x}_i, \boldsymbol{\pi}) = f(\boldsymbol{x}_i) + \boldsymbol{\pi}^T \left(\sum_{i=1}^{T} \boldsymbol{A}_i \boldsymbol{x}_i - \boldsymbol{b} \right) + \frac{r}{2} \left(\sum_{i=1}^{T} \boldsymbol{A}_i \boldsymbol{x}_i - \boldsymbol{b} \right)^T \left(\sum_{i=1}^{T} \boldsymbol{A}_i \boldsymbol{x}_i - \boldsymbol{b} \right) \tag{6.50}$$

Furthermore, the dual function can be formulated as

$$g(\boldsymbol{\pi}) = \min_{\boldsymbol{x}_1, \ldots, \boldsymbol{x}_T} L(\boldsymbol{x}_i, \boldsymbol{\pi}) \tag{6.51}$$

$$s.t.\ \boldsymbol{x}_i \in \Omega_i, \quad i = 1, \ldots, T \tag{6.52}$$

where $\boldsymbol{\pi} \in \mathrm{R}^{m \times 1}$ is the Lagrange multipliers corresponding to (6.47), r is a penalty parameter and $r > 0$.

Correspondingly, the dual problem is written as

$$\max_{\boldsymbol{\pi} \in \mathrm{R}^{m \times 1}} \ g(\boldsymbol{\pi}) \tag{6.53}$$

If the model is a feasible convex model, there is no gap between the primary and dual problem, so (6.53) and (6.46)–(6.48) are strictly equivalent. According to the optimality conditions, we have

$$\begin{cases} \sum_{i=1}^{T} \boldsymbol{A}_i \boldsymbol{x}_i^* - \boldsymbol{b} = \boldsymbol{0} \\ \nabla f_{\boldsymbol{x}_i}(\boldsymbol{x}_i^*) + \boldsymbol{A}_i^T \left(\boldsymbol{\pi}^* + r \left(\sum_{i=1}^{T} \boldsymbol{A}_i \boldsymbol{x}_i^* - \boldsymbol{b} \right) \right) = \boldsymbol{0}, \quad i = 1, \ldots, T \end{cases} \tag{6.54}$$

Since the optimal solution of the primary model $\boldsymbol{x}^k$ at k-th iteration is to minimize the augmented Lagrangian function with a given Lagrange multiplier at k-th iteration, we can easily derive that

$$\begin{aligned} \nabla_{\boldsymbol{x}_i} L(\boldsymbol{x}_i, \boldsymbol{\pi}^k) &= \nabla f_{\boldsymbol{x}_i}(\boldsymbol{x}_i^{k+1}) + \boldsymbol{A}_i^T \left(\boldsymbol{\pi}^k + r \left(\sum_{i=1}^{T} \boldsymbol{A}_i \boldsymbol{x}_i^{k+1} - \boldsymbol{b} \right) \right) \\ &= \nabla f_{\boldsymbol{x}_i}(\boldsymbol{x}_i^{k+1}) + \boldsymbol{A}_i^T \boldsymbol{\pi}^{k+1} \end{aligned} \tag{6.55}$$

As a result, the Lagrange multipliers can be updated by (6.56)

$$\boldsymbol{\pi}^{k+1} = \boldsymbol{\pi}^k + r \left(\sum_{i=1}^{T} \boldsymbol{A}_i \boldsymbol{x}_i^{k+1} - \boldsymbol{b} \right) \tag{6.56}$$

The stopping condition can be defined if the infeasibility of KKT optimality condition is small enough, such that

$$\left\| \sum_{i=1}^{T} \boldsymbol{A}_i \boldsymbol{x}_i^{k+1} - \boldsymbol{b} \right\| + \sum_{i=1}^{T} \left\| \nabla f_{\boldsymbol{x}_i}\left(\boldsymbol{x}_i^{k+1}\right) + \boldsymbol{A}_i^T \boldsymbol{\pi}^{k+1} \right\| \le \varepsilon \tag{6.57}$$

where ε is a given precision. Now, the procedure of the augmented Lagrangian relaxation method can be described in Table 6.8.

But unfortunately, the augmented Lagrangian function introduces a quadratic penalty, which is not separable for the whole objective function. Therefore, it greatly challenges the application of parallel computation to solving the problem at the Step 3. Now, we will employ the diagonal quadratic approximation method (DQAM) to provide a separable approximation for the third part of the augmented Lagrangian function in the Step 3. Let $(\boldsymbol{x}_1, \ldots, \boldsymbol{x}_T) = \left(\boldsymbol{x}_1^k + \boldsymbol{h}_1, \ldots, \boldsymbol{x}_T^k + \boldsymbol{h}_T\right)$, we have

$$\begin{aligned} v(\boldsymbol{x}) &= \frac{r}{2}\left(\sum_{i=1}^{T} \boldsymbol{A}_i \boldsymbol{x}_i - \boldsymbol{b}\right)^T \left(\sum_{i=1}^{T} \boldsymbol{A}_i \boldsymbol{x}_i - \boldsymbol{b}\right) \\ &= \frac{r}{2}\left(\sum_{i=1}^{T} \boldsymbol{A}_i \left(\boldsymbol{x}_i^k + \boldsymbol{h}_i\right) - \boldsymbol{b}\right)^T \left(\sum_{i=1}^{T} \boldsymbol{A}_i \left(\boldsymbol{x}_i^k + \boldsymbol{h}_i\right) - \boldsymbol{b}\right) \\ &= r\left(\sum_{i=1}^{T} \boldsymbol{A}_i \boldsymbol{x}_i^k - \boldsymbol{b}\right)^T \sum_{i=1}^{T} \boldsymbol{A}_i \boldsymbol{h}_i + \frac{r}{2} \sum_{i=1}^{T} \left(\left(\boldsymbol{A}_i \boldsymbol{h}_i\right)^T \boldsymbol{A}_i \boldsymbol{h}_i\right) \\ &\quad + \frac{r}{2} \sum_{i \ne j} \left(\left(\boldsymbol{A}_j \boldsymbol{h}_j\right)^T \left(\boldsymbol{A}_i \boldsymbol{h}_i\right)\right) + v\left(\boldsymbol{x}_i^k\right) \end{aligned} \tag{6.58}$$

Table 6.8 Procedure of augmented Lagrangian relaxation method

Augmented Lagrangian Relaxation	
Step 1:	Given π^0 and $k \leftarrow 0$;
Step 2:	**while** 1
Step 3:	Fix the π^k and solve model (6), such that $\left(\boldsymbol{x}_1^{k+1}, \ldots, \boldsymbol{x}_T^{k+1}\right) \leftarrow \min_{\boldsymbol{x}_1, \ldots, \boldsymbol{x}_T} L\left(\boldsymbol{x}_i, \pi^k\right) \quad s.t \quad \boldsymbol{x}_i \in \Omega_i$
Step 4:	Update the multipliers by (10) as $\pi^{k+1} \leftarrow \pi^k + r\left(\sum_{i=1}^{T} \boldsymbol{A}_i \boldsymbol{x}_i^{k+1} - \boldsymbol{b}\right)$
Step 5:	**if** the KKT condition has not been met Update $k \leftarrow k+1$ and go to **Step2**; **else** Return $\left(\boldsymbol{x}_1^{k+1}, \ldots, \boldsymbol{x}_T^{k+1}\right)$ and π^{k+1}; stop. **end**
end	

Observe that only the third term in (6.58) is not separable, and we can ignore this term and get a separable approximation, which is referred to (DQAM). Furthermore, the augmented Lagrangian function can be approximated by

$$\begin{aligned} L(\boldsymbol{x}_i, \boldsymbol{\pi}) \approx \widetilde{L}(\boldsymbol{x}_i, \boldsymbol{\pi}) = & f\left(\boldsymbol{x}_i^k + \boldsymbol{h}_i\right) + \boldsymbol{\pi}^T \left(\sum_{i=1}^{T} \boldsymbol{A}_i \left(\boldsymbol{x}_i^k + \boldsymbol{h}_i\right) - \boldsymbol{b} \right) \\ & + v\left(\boldsymbol{x}_i^k\right) + r \left(\sum_{i=1}^{T} \boldsymbol{A}_i \boldsymbol{x}_i^k - \boldsymbol{b} \right)^T \sum_{i=1}^{T} \boldsymbol{A}_i \boldsymbol{h}_i + \frac{r}{2} \sum_{i=1}^{T} \left((\boldsymbol{A}_i \boldsymbol{h}_i)^T \boldsymbol{A}_i \boldsymbol{h}_i \right) \end{aligned} \tag{6.59}$$

It should be noted that in optimization problems, the constant numbers in the objective function can be omitted, so we have

$$g(\boldsymbol{\pi}) = \min_{\boldsymbol{x}_1, \ldots, \boldsymbol{x}_T} \widetilde{L}(\boldsymbol{x}_i, \boldsymbol{\pi}) \Leftrightarrow g(\boldsymbol{\pi}) = \min_{\boldsymbol{h}_1, \ldots, \boldsymbol{h}_T} K(\boldsymbol{h}_i, \boldsymbol{\pi}) \tag{6.60}$$

where

$$\begin{aligned} K(\boldsymbol{h}_i, \boldsymbol{\pi}) = & f\left(\boldsymbol{x}_i^k + \boldsymbol{h}_i\right) + \boldsymbol{\pi}^T \left(\sum_{i=1}^{T} \boldsymbol{A}_i \boldsymbol{h}_i - \boldsymbol{b} \right) \\ & + \frac{r}{2} \sum_{i=1}^{T} \left((\boldsymbol{A}_i \boldsymbol{h}_i)^T \boldsymbol{A}_i \boldsymbol{h}_i \right) + r \left(\sum_{i=1}^{T} \boldsymbol{A}_i \boldsymbol{x}_i^k - \boldsymbol{b} \right)^T \sum_{i=1}^{T} \boldsymbol{A}_i \boldsymbol{h}_i \end{aligned} \tag{6.61}$$

By the use of DQAM, it can be easily found from (6.61) that the whole function of K is separable. It yields

$$K(\boldsymbol{h}_i, \boldsymbol{\pi}) = \sum_{i=1}^{T} K_i(\boldsymbol{h}_i, \boldsymbol{\pi}) - \boldsymbol{\pi}^T \boldsymbol{b} \tag{6.62}$$

where

$$\begin{aligned} K_i(\boldsymbol{h}_i, \boldsymbol{\pi}) = & f_i\left(\boldsymbol{x}_i^k + \boldsymbol{h}_i\right) + \boldsymbol{\pi}^T \boldsymbol{A}_i \boldsymbol{h}_i \\ & + \frac{r}{2} (\boldsymbol{A}_i \boldsymbol{h}_i)^T \boldsymbol{A}_i \boldsymbol{h}_i + r \left(\sum_{i=1}^{T} \boldsymbol{A}_i \boldsymbol{x}_i^k - \boldsymbol{b}^T \right)^T \boldsymbol{A}_i \boldsymbol{h}_i \end{aligned} \tag{6.63}$$

Moreover, the last term of (6.63) will become a constant number which can be eliminated when solving the model at the Step 3. Thus, Step 3 can be replaced by the following flowchart (Table 6.9).

Table 6.9 Procedure of parallel DQAM

Parallel DQAM	
for $i=1,\ldots,T$	
Step 3-1:	Parallel solve for $\boldsymbol{h}_i^k \leftarrow \min_{\boldsymbol{h}_i} \; K_i\left(\boldsymbol{h}_i, \pi^k\right) \quad s.t \quad \boldsymbol{x}_i^k + \boldsymbol{h}_i \in \Omega_i$
Step 3-2:	$\boldsymbol{x}_i^{k+1} \leftarrow \boldsymbol{x}_i^k + \boldsymbol{h}_i^k$
end	

Another issue that should be carefully addressed is the choice of the penalty parameter r in the augmented Lagrangian function (6.50). However, it has been proved in [7] that the augmented Lagrangian relaxation method can converge for any fixed penalty parameter r, as long as r is strictly positive i.e., $r > 0$ and the original convex model (1) is a feasible problem. Note, it is found that small r may result in many iterations to converge. Therefore, we can use an increasing sequence $\{r^k\}$ to remedy r, but keep in mind that the difference between augmented Lagrangian relaxation and the penalty function method is that the sequence of $\{r^k\}$ in the penalty function method should tend to grow infinitely which may lead to an ill-conditioning problem. In contrast, the augmented Lagrangian relaxation method does not require $\{r^k\}$ to be infinite, since for any penalty parameter, the method can converge. It is the advantage of the augmented Lagrangian relaxation method that the ill-conditioning problem could be alleviated.

In this term, we can set an upper bound for $\{r^k\}$ based on the one used for augmented Lagrangian relaxation to avoid numerical performance. On the other hand, it is not difficult to find that if the constraint violation is too small, we should increase the penalty r^k. In this term, the scheme for parameter choice can be presented in the Table 6.10, where τ belongs to [1, $+\infty$] and Π is a large number that relies on the computer performance. The suggested values can be chosen as $\tau = 5$, $\Pi = 10^6$ and $r^0 = 0.5$.

Then in order to analyze the convergence proper of the DQAM method and discuss the possible problem in DQAM method solution, we will first give some basic definitions:

Table 6.10 The choice of penalty parameters

Parameter Choice	
Step 4-1:	**if** $\left\|\sum_{i=1}^{T} \boldsymbol{A}_i \boldsymbol{x}_i^{k+1} - \boldsymbol{b}\right\| \le \eta^k$
	Update the multipliers and penalty as
	$\pi^{k+1} \leftarrow \pi^k + r^k\left(\sum_{i=1}^{T} \boldsymbol{A}_i \boldsymbol{x}_i^{k+1} - \boldsymbol{b}\right)$ and $r^{k+1} \leftarrow r^k$;
	else
	Update the multipliers and penalty as
	$\pi^{k+1} \leftarrow \pi^k$ and $r^{k+1} \leftarrow \min\left(\tau r^k, \Pi\right)$;
end	
Step 4-2:	Update $\eta^{k+1} = \left(r^k\right)^{-0.1-0.9k}$;

Partial Separability [8]: A smooth convex function f: R$n \rightarrow$ R is partially separable of degree ω if there exists a collection $\mathcal{J}$ of subsets of {1, 2,..,n} such that

$$f(\boldsymbol{x}) = \sum_{J \in \mathcal{J}} f_J(\boldsymbol{x}) \quad \text{和} \quad \max_{J \in \mathcal{J}} |J| \leq \omega \tag{6.64}$$

where for each J, fJ is a smooth convex function that depends on $\boldsymbol{x}i$ for $i \in J$ only; $|\cdot|$ is the cardinality of a set.

Theorem 6.4 [8]: *For convex quadratic function given by*

$$f(\boldsymbol{x}) = \frac{r}{2}(\boldsymbol{A}\boldsymbol{x} - \boldsymbol{b})^T(\boldsymbol{A}\boldsymbol{x} - \boldsymbol{b}) = \frac{r}{2}\sum_{i=1}^{m}\left(b_i - \sum_{j=1}^{n} a_{ij}x_j\right) \tag{6.65}$$

where $A \in \mathrm{R}^{m \times n}$, $b \in \mathrm{R}^{n \times 1}$ and $x \in \mathrm{R}^{n \times 1}$. *Let*

$$\omega_i = \left|\left\{j : a_{ij} \neq 0\right\}\right|, \quad i = 1, 2, \ldots, m \tag{6.66}$$

we conclude that f is partially separable of degree

$$\omega = \max_{i \in \{1,2,\ldots,m\}} \omega_i \tag{6.67}$$

According to the definition of partial separability with the Theorem 6.4, the convergence analysis can be given as

Theorem 6.5 [8]: *Let* $f(\boldsymbol{x}) = \frac{r}{2}(\boldsymbol{A}\boldsymbol{x} - \boldsymbol{b})^T(\boldsymbol{A}\boldsymbol{x} - \boldsymbol{b})$ *be partially separable of degree* $\omega > 1$. *If f is strongly convex, DQAM converges linearly, that is* $f\left(\boldsymbol{x}^{k+1}\right) \leq qf\left(\boldsymbol{x}^k\right)$, *where q is*

$$q = 1 - \frac{u}{16L(\omega - 1)^3 + 4(\omega - 1)u} \tag{6.68}$$

and $L = \max_{1 \leq i \leq n} r\left\|\boldsymbol{A}_{i,\cdot}\right\|$; μ *is a positive number that depends on the f.*

Remarks When (6.42) and (6.45) are relaxed, there are at less N_g nonnegative variables in every row of the coefficient matrix of the quadratic term of the augmented Lagrangian function. Hence, the transforming distribution factor is a full-matrix and there is strong coupling among units. In contrast, when (6.44) is relaxed, there are two nonnegative variables in every row of the coefficient matrix of the quadratic term of the augmented Lagrangian function. The matrix with a smaller separable degree ω which is generated by relaxing (6.44) leads to a better convergence property theoretically. In addition, the augmented Lagrangian function is regarded as a separable fuction using Diagonal Quadratic Approximation Method. Many messages will be losed if "hard constraints" of (6.45) is relaxed,

which may result in many iterations to converge. Based on the discussion of ramp rate constraints, relaxing these constraints will have a better parallel performance.

From what has been discussed above, the augmented Lagrangian relaxation approach of (6.41)–(6.45) is employed to solve the ED models, in which the ramp rate constraints are chosen as the hard constraints to be relaxed. Note that the relaxed constraints in the augmented Lagrangian relaxation formulation are generally utilized for the equalities. As a result, we can introduce dummy variables to ramp rate constraints, such that

$$\begin{cases} P_{i,t} - P_{i,t-1} - u_{i,t} = 0 \\ -Rd_{i,t} \le u_{i,t} \le Ru_{i,t} \end{cases}, \quad t = 1, \ldots T, \quad i = 1, \ldots N_g \tag{6.69}$$

Consequently, the augmented Lagrangian relaxation of the original DED model can be formulated as

$$Z(\lambda_{i,t}) = \min_{P_{i,t}, u_{i,t}} L\left(P_{i,t}, u_{i,t}, \lambda_{i,t}\right) \tag{6.70}$$

$$s.t. \sum_{i=1}^{N_g} P_{i,t} + \sum_{k=1}^{N_w} W_{k,t} = \sum_{j=1}^{N_d} D_{j,t}, \quad t = 1, \ldots T \tag{6.71}$$

$$P_{i,t}^{\min} \le P_{i,t} \le P_{i,t}^{\max}, \quad i = 1, \ldots N_g \tag{6.72}$$

$$-Rd_{i,t} \le u_{i,t} \le Ru_{i,t}, \quad i = 1, \ldots N_g \tag{6.73}$$

$$\begin{aligned} -F_l^{\max} \le & \sum_{i=1}^{N_g} S_{l,i} P_{i,t} - \sum_{j=1}^{N_d} H_{l,j} D_{j,t} \\ & + \sum_{k=1}^{N_w} G_{l,k} W_{k,t}^f \le F_l^{\max}, \quad l = 1, \ldots N_l, t = 1, \ldots T \end{aligned} \tag{6.74}$$

where

$$L\left(P_{i,t}, u_{i,t}, \lambda_{i,t}\right) = \sum_{t=1}^{T} \sum_{i=1}^{N} \left(f(P_{i,t}) + \lambda_{i,t}\left(P_{i,t} - P_{i,t-1} - u_{i,t}\right) + \frac{r}{2}\left(P_{i,t} - P_{i,t-1} - u_{i,t}\right)^2 \right) \tag{6.75}$$

The dual problem of (6.70)–(6.74) can be cast as

$$Z = \max_{\lambda_{i,t}} Z(\lambda_{i,t}) \tag{6.76}$$

For k-th iteration, we have

$$K\left(hp_{i,t}, hu_{i,t}, \lambda_{i,t}^{k}\right) = \sum_{t=1}^{T}\left(\sum_{i=1}^{N} f_i(P_{i,t}^{k} + hp_{i,t}) + \sum_{i=1}^{N}\left(\lambda_{i,t}^{k} - \lambda_{i,t+1}^{k}\right)hp_{i,t} - \sum_{i=1}^{N}\lambda_{i,t}^{k} hu_{i,t}\right) + \frac{r}{2}(\boldsymbol{Ah})^{T}(\boldsymbol{Ah}) + r(\boldsymbol{Ax}^{k})\boldsymbol{Ah} \tag{6.77}$$

where

$$\boldsymbol{hp} = \left(\underbrace{hp_{1,1}, \ldots, hp_{N,1}}_{\boldsymbol{hp}_1}, \underbrace{hp_{1,1}, \ldots, hp_{N,2}}_{\boldsymbol{hp}_2}, \ldots, \underbrace{hp_{1,T}, \ldots, hp_{N,T}}_{\boldsymbol{hp}_T}\right)^{T} \tag{6.78}$$

$$\boldsymbol{hu} = \left(\underbrace{hu_{1,1}, \ldots, hu_{N,1}}_{\boldsymbol{hu}_1}, \underbrace{hu_{1,1}, \ldots, hu_{N,2}}_{\boldsymbol{hu}_2}, \ldots, \underbrace{hu_{1,T}, \ldots, hu_{N,T}}_{\boldsymbol{hu}_T}\right)^{T} \tag{6.79}$$

$$\boldsymbol{h} = \left(\boldsymbol{hp}^{T}, \boldsymbol{hu}^{T}\right)^{T} = \left(\boldsymbol{hp}_1^{T}, \ldots, \boldsymbol{hp}_T^{T}, \boldsymbol{hu}_1^{T}, \ldots, \boldsymbol{hu}_T^{T}\right)^{T} \tag{6.80}$$

$$\boldsymbol{P} = \left(\underbrace{P_{1,1}, \ldots, P_{N,1}}_{\boldsymbol{P}_1}, \underbrace{P_{1,1}, \ldots, P_{N,2}}_{\boldsymbol{P}_2}, \ldots, \underbrace{P_{1,T}, \ldots, P_{N,T}}_{\boldsymbol{P}_T}\right)^{T} \tag{6.81}$$

$$\boldsymbol{u} = \left(\underbrace{u_{1,1}, \ldots, u_{N,1}}_{u_1}, \underbrace{u_{1,1}, \ldots, u_{N,2}}_{u_2}, \ldots, \underbrace{u_{1,T}, \ldots, u_{N,T}}_{u_T}\right)^{T} \tag{6.82}$$

$$\boldsymbol{x} = \left(\boldsymbol{P}^{T}, \boldsymbol{u}^{T}\right)^{T} = \left(\boldsymbol{P}^{T}, \ldots, \boldsymbol{P}_T^{T}, \boldsymbol{u}_1^{T}, \ldots, \boldsymbol{u}_T^{T}\right)^{T} \tag{6.83}$$

$$\boldsymbol{B} = \begin{bmatrix} \boldsymbol{I}_{N\times N} & & & & \\ -\boldsymbol{I}_{N\times N} & \boldsymbol{I}_{N\times N} & & & \\ & -\boldsymbol{I}_{N\times N} & \boldsymbol{I}_{N\times N} & & \\ & & & \ddots & \\ & & & -\boldsymbol{I}_{N\times N} & \boldsymbol{I}_{N\times N} \end{bmatrix} \tag{6.84}$$

$$\boldsymbol{A} = [\boldsymbol{B} - \boldsymbol{I}] = \begin{bmatrix} \boldsymbol{I}_{N\times N} & & & & & -\boldsymbol{I}_{N\times N} & & & & \\ -\boldsymbol{I}_{N\times N} & \boldsymbol{I}_{N\times N} & & & & & -\boldsymbol{I}_{N\times N} & & & \\ & -\boldsymbol{I}_{N\times N} & \boldsymbol{I}_{N\times N} & & & & & -\boldsymbol{I}_{N\times N} & & \\ & & & \ddots & & & & & \ddots & \\ & & & -\boldsymbol{I}_{N\times N} & \boldsymbol{I}_{N\times N} & & & & & -\boldsymbol{I}_{N\times N} \end{bmatrix} \tag{6.85}$$

Keep in mind that the model (6.41)–(6.45) is within T time periods, i.e., $t = 1,\ldots, T$, so we always assume $\lambda_{i,t+1}^{k}$ in (6.77) to be zero. Furthermore, we have

$$\boldsymbol{Ah} = [\boldsymbol{B} - \boldsymbol{I}]\left(\boldsymbol{hp}^T, \boldsymbol{hu}^T\right)^T = \boldsymbol{Bhp} - \boldsymbol{hu} \tag{6.86}$$

The third term of (6.77) can be reformulated as

$$\begin{aligned} (\boldsymbol{Ax}^k)\boldsymbol{Ah} &= (\boldsymbol{Ax}^k)(\boldsymbol{Bhp} - \boldsymbol{hu}) \\ &= (\boldsymbol{Ax}^k)\sum_{t=1}^{T}(\boldsymbol{B}_t\boldsymbol{hp}_t - \boldsymbol{hu}_t) \\ &= (\boldsymbol{Bp}^k - \boldsymbol{u}^k)\sum_{t=1}^{T}(\boldsymbol{B}_t\boldsymbol{hp}_t - \boldsymbol{hu}_t) \end{aligned} \tag{6.87}$$

The fourth term of (6.77) can be reformulated as

$$\begin{aligned} (\boldsymbol{Ah})\boldsymbol{Ah} &= (\boldsymbol{Bhp} - \boldsymbol{hu})^T(\boldsymbol{Bhp} - \boldsymbol{hu}) \\ &= \sum_{t=1}^{T}(\boldsymbol{B}_t\boldsymbol{hp}_t - \boldsymbol{hu}_t)^T(\boldsymbol{B}_t\boldsymbol{hp}_t - \boldsymbol{hu}_t) \\ &= \sum_{t=1}^{T}(\boldsymbol{B}_t\boldsymbol{hp}_t)^T\boldsymbol{B}_t\boldsymbol{hp}_t + \sum_{t=1}^{T}(\boldsymbol{hu}_t)^T\boldsymbol{u}_t - 2\sum_{t=1}^{T}(\boldsymbol{B}_t\boldsymbol{hp}_t)^T\boldsymbol{hu}_t \end{aligned} \tag{6.88}$$

where

$$\boldsymbol{B}_t = \begin{cases} \left[\underbrace{\boldsymbol{0}_{N\times N}}_{1}, \ldots, \underbrace{\boldsymbol{I}_{N\times N}}_{t}, \underbrace{-\boldsymbol{I}_{N\times N}}_{t+1}, \underbrace{\boldsymbol{0}_{N\times N}}_{i+2}, \ldots, \underbrace{\boldsymbol{0}_{N\times N}}_{T}\right]^T & t = 1,\ldots, T-1 \\ \left[\underbrace{\boldsymbol{0}_{N\times N}}_{1}, \ldots \underbrace{\boldsymbol{0}_{N\times N}}_{t}, \ldots, \underbrace{\boldsymbol{0}_{N\times N}}_{T-1}, \underbrace{-\boldsymbol{I}_{N\times N}}_{T}\right]^T & t = T \end{cases} \tag{6.89}$$

It can be observed that $\boldsymbol{hp}$ and $\boldsymbol{hu}$ can be decomposed into T separable parts and (6.77) can be decomposed as

$$K\left(hp_{i,t}, hu_{i,t}, \lambda_{i,t}^{k}\right) = \sum_{t=1}^{T} K_t\left(hp_{i,t}, hu_{i,t}, \lambda_{i,t}^{k}\right) \tag{6.90}$$

where

$$K_t\left(hp_{i,t}, hu_{i,t}, \lambda_{i,t}^{k}\right) = \sum_{i=1}^{N} f_i\left(P_{i,t}^{k} + hp_{i,t}\right) + \sum_{i=1}^{N}\left(\lambda_{i,t}^{k} - \lambda_{i,t+1}^{k}\right)hp_{i,t} + \frac{r}{2}(\boldsymbol{B}_t\boldsymbol{hp}_t)^T\boldsymbol{B}_t\boldsymbol{hp}_t$$
$$+ r\left(\boldsymbol{BP}^k - \boldsymbol{u}^k\right)\boldsymbol{B}_t\boldsymbol{hp}_t - \sum_{i=1}^{N}\lambda_{i,t}^{k}hu_{i,t} - r\left(\boldsymbol{BP}^k - \boldsymbol{u}^k\right)\boldsymbol{hu}_i + \frac{r}{2}(\boldsymbol{hu}_t)^T\boldsymbol{hu}_t + r(\boldsymbol{B}_t\boldsymbol{hp}_t)^T\boldsymbol{hu}_t \tag{6.91}$$

Furthermore, the **Step 3-1** in the Table 6.8 can be presented as

$$\left(\boldsymbol{hp}_t^k, \boldsymbol{hu}_t^k\right) \leftarrow \min_{\boldsymbol{hp}_t, \boldsymbol{hu}_t} \quad K_t\left(\boldsymbol{hp}_t, \boldsymbol{hu}_t, \boldsymbol{\lambda}^k\right) \tag{6.92}$$

$$s.t. \quad \sum_{i=1}^{N_g}\left(P_{i,t}^{k} + hp_{i,t}\right) = \sum_{j=1}^{N_d} D_{j,t} - \sum_{k=1}^{N_w} W_{k,t}^{f} \tag{6.93}$$

$$P_{i,t}^{\min} \le P_{i,t}^{k} + hp_{i,t} \le P_{i,t}^{\max}, \quad i = 1, \ldots .N_g \tag{6.94}$$

$$-Rd_{i,t} \le u_{i,t}^{k} + hu_{i,t} \le Ru_{i,t}, \quad i = 1, \ldots .N_g \tag{6.95}$$

$$-F_l^{\max} \le \sum_{i=1}^{N_g} S_{l,i}P_{i,t} - \sum_{j=1}^{N_d} H_{l,j}D_{j,t} + \sum_{\mathrm{k}=1}^{N_w} G_{l,k}W_{k,t}^{f} \le F_l^{\max}, \quad l = 1, \ldots .N_l \tag{6.96}$$

However, the $\boldsymbol{hp}_t$ and $\boldsymbol{hu}_t$ are coupled at each time period and we should solve (6.92)–(6.96), so that $\boldsymbol{hp}_t$ and $\boldsymbol{hu}_t$ can be obtained at the same time. However, we can adopt the idea of the alternating direction method of multipliers method (alternating direction method of multipliers method, ADMM) [9–12], where $\boldsymbol{hp}_t$ and $\boldsymbol{hu}_t$ can be decoupled. Likewise, solving (6.92)–(6.96) can be transformed to solve two decoupled sub-problems:

$$(\mathbf{Sub-P1}) \quad \boldsymbol{hp}_t^k \leftarrow \min_{\boldsymbol{hp}_t} \quad K_t\left(\boldsymbol{hp}_t, \boldsymbol{hu}_t^k, \boldsymbol{\lambda}^k\right) \tag{6.97}$$

$$s.t. \quad \sum_{i=1}^{N_g}\left(P_{i,t}^{k} + hp_{i,t}\right) = \sum_{j=1}^{N_d} D_{j,t} - \sum_{k=1}^{N_w} W_{k,t}^{f} \tag{6.98}$$

Table 6.11 The proposed method for multi-period dynamic economic dispatch

The proposed method for multi-period dynamic economic dispatch
Step 1: Given $\boldsymbol{\lambda}^0$, r^0, $\eta^0 \leftarrow (r^0)^{-0.1}$, $P_t^0 \leftarrow 0$, $u_t^0 \leftarrow 0$ and $k \leftarrow 0$;
Step 2: **while** 1
Step 3: Fix the multipliers $\boldsymbol{\lambda}^k$;
Step 4: **for** t=1,..,T
Parallel solve model (6-97)-(6-100) and obtain $\boldsymbol{hp}_t^k$; $\boldsymbol{P}_t^{k+1} \leftarrow \boldsymbol{P}_t^k + \boldsymbol{hp}_t^k$;
end
Step 5: **for** t=1,..,T
Parallel solve model (6-101)-(6-102) and obtain $\boldsymbol{hu}_t^k$;
$\boldsymbol{u}_t^{k+1} \leftarrow \boldsymbol{u}_t^k + \boldsymbol{hu}_t^k$;
end
Step 6: Construct $\boldsymbol{P}^{k+1} = \left[\left(\boldsymbol{P}_1^{k+1}\right)^T, \left(\boldsymbol{P}_2^{k+1}\right)^T, ..., \left(\boldsymbol{P}_T^{k+1}\right)^T \right]^T$
and $\boldsymbol{u}^{k+1} = \left[\left(\boldsymbol{u}_1^{k+1}\right)^T, \left(\boldsymbol{u}_2^{k+1}\right)^T, ..., \left(\boldsymbol{u}_T^{k+1}\right)^T \right]^T$;
Step 7: **if** $\left\| \sum_{i=1}^{T} \boldsymbol{A}_i \boldsymbol{x}_i^{k+1} - \boldsymbol{b} \right\| \le \eta^k$
$\lambda^{k+1} \leftarrow \lambda^k + r^k \left(\boldsymbol{BP}^{k+1} - \boldsymbol{u}^{k+1} \right)$ and $r^{k+1} \leftarrow r^k$;
else
$\lambda^{k+1} \leftarrow \lambda^k$ and $r^{k+1} \leftarrow \min\left(\tau r^k, \Pi\right)$;
end
Update $\eta^{k+1} = \left(r^k\right)^{-0.1-0.9k}$;
Step 8: **if** $\left\| \boldsymbol{BP}^{k+1} - \boldsymbol{u}^{k+1} \right\| + \sum_{i=1}^{T} \left\| \nabla f_{P_i}\left(\boldsymbol{P}_i^{k+1}\right) + \boldsymbol{A}_i^T \lambda^{k+1} \right\| \le \varepsilon$
Stop and return ($\boldsymbol{P}_t^{k+1}$, $\boldsymbol{u}_t^{k+1}$, λ^{k+1});
else
Update $k \leftarrow k+1$ and go to **Step2**;
end
end

$$P_{i,t}^{\min} \le P_{i,t}^k + hp_{i,t} \le P_{i,t}^{\max}, \quad i = 1, \ldots N_g \tag{6.99}$$

$$-F_l^{\max} \le \sum_{i=1}^{N_g} S_{l,i} P_{i,t} - \sum_{j=1}^{N_d} H_{l,j} D_{j,t} + \sum_{k=1}^{N_w} G_{l,k} W_{k,t}^f \le F_l^{\max}, \quad l = 1, \ldots N_l \tag{6.100}$$

$$(\mathbf{Sub} - \mathbf{P2}) \quad \boldsymbol{hu}_t^k \leftarrow \min_{\boldsymbol{hu}_t} K_t\left(\boldsymbol{hp}_t^k, \boldsymbol{hu}_t, \lambda^k\right) \tag{6.101}$$

$$s.t. \ -Rd_{i,t} \le u_{i,t}^k + hu_{i,t} \le Ru_{i,t}, \quad i = 1, \ldots N_g \tag{6.102}$$

The whole procedure of the augmented Lagrangian method using DQAM for multi-period dynamic economic dispatch can be presented in Table 6.11.

6.3.2 *Simulation Analysis*

The proposed PALR method using DQAM has been tested on the IEEE 118-bus and the Polish 2383-bus system with several different time periods. The topology

parameter and normal load demand can be found in MATPOWER [6]. The 24-h load demand and wind power can be derived by the use of the load factor shown in Sect. 3.3.2. The convergence tolerance is assigned as 0.01 %. The tests were implemented using MATLAB and CPLEX 12.5, and performed on an Intel® Core™ i5 Duo Processor T420 (2.50 GHz) PC with 4 GB RAM.

A. IEEE 118-bus test systems

For the proposed method, the impact of a ramp rate limit on the total number of iterations. We choose the ramp rate σ as 5, 10, 15, 20 and 50 % of the capacity of generators per hour respectively.

The results on IEEE 118-bus systems are shown in Table 6.12. It is observed that the ramp rate limits have a great impact on the convergence performance of the proposed method. When the ramp rate is faster, the number of iterations will be less. When σ is greater than 20 %, only one iteration is needed for convergence. That means that the ramp rate is so fast that the time coupling can be ignored. Multi-period ED can be split into T single-period period ED. In addition, Table 6.12 show the comparison of ALR and LR method. For a fast ramp rate, PALR and LR both converge fast, but for a small ramp rate, LR may need large number of iterations, whereas PALR can be much faster.

It should be noted that the benchmark ED solver for a 118-bus system considering all the security constraints needs no more than 0.1 s. Furthermore, the computational time for ALR and DED which is solved directly by CPLEX is presented in Table 6.13. It can be observed that with the increase of T, the scale of DED becomes large which takes more time using CPLEX. Moreover, with the

Table 6.12 Impact of ramp rate limits on iterations

σ (%)	T = 24		T = 48		T = 96		T = 288	
	ALR	LR	ALR	LR	ALR	LR	ALR	LR
5	7	63	8	67	11	76	14	89
10	3	21	3	26	4	29	6	33
15	1	6	1	8	2	11	2	18
20	1	3	1	4	1	6	1	8
50	1	1	1	1	1	1	1	1

Table 6.13 Comparison of computational time between ALR and DED

σ (%)	T = 24 (s)		T = 48 (s)		T = 96 (s)		T = 288 (s)	
	ALR	DED	ALR	DED	ALR	DED	ALR	DED
5	0.70	0.29	0.80	0.37	1.10	0.92	1.40	5.10
10	0.30	0.27	0.30	0.33	0.40	0.79	0.60	4.78
15	0.10	0.24	0.10	0.33	0.20	0.78	0.20	4.67
20	0.10	0.24	0.10	0.32	0.10	0.78	0.10	4.69
50	0.10	0.24	0.10	0.32	0.10	0.78	0.10	4.63

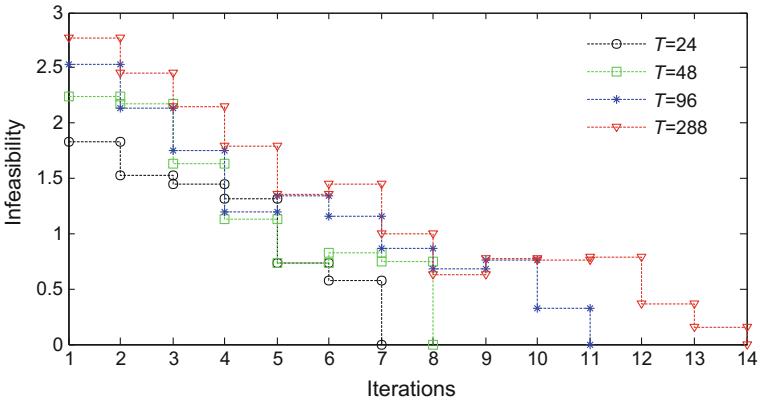

Fig. 6.6 Iterations of the proposed method under β = 5 %

increase of σ, ALR needs fewer iterations, but the time used to directly solve DED by CPLEX is nearly the same. Even when the ramp rate is large, directly solving DED by CPLEX cannot be accelerated. In this term, the proposed PALR method is fairly applicable to the DED with a large number of time periods and a fast ramp rate.

Figure 6.6 depicts the solution process of the proposed method under σ = 5 % over iterations. There needs to be 14 iterations for DED with 288 time periods and 7 iterations for DED with 24 time periods. In general, more iterations are needed based on the increase of the number of time periods.

B. **Polish 2383-bus test systems**

In order to further verify our proposed method on large-scale systems, we have performed tests on the Polish 2383-bus system, where there are 2896 transmission lines and 323 generators in service. Generally, in practical power systems, the generator ramp rates per hour are about 20–40 % of the maximum capacity for coal turbines and 50–80 % for gas turbines. In this book, we choose the slow ramp rate of coal turbines to be 20 % * $P^{\max}$/h and the fast ramp rate of gas turbines to be 50 % * $P^{\max}$/h. It takes 0.3 s to solve the single-period ED model for CPELX solver. However, the multi-period ED model cannot be solved by CPLEX directly for $T \geq 24$ due to the lack of enough memory space. Considering all transmission security, the transforming distribution matrix is 2383×2383 full matrix. $2896 \times 2383 \times 24 \times 8$ bit $\approx$ 1.234 GB DRAM will be need for all transmission security. The personal computer with 4 GB RAM has a great challenge to solve 24-h real ED using 1 G RAM due to operating systems and other softwares like MATLAB. For the same test system, since each sub-problem takes $2896 \times 2383 \times 8$ bit $\approx$ 52.65 MB RAM, we can use PALR to separate a multi-period ED problem into T single-period ED sub-problems simultaneously, in which the memory requirement can be greatly reduced for each of those computers.

Here, we use 96 time periods in the following study. If all the units are coal turbines (i.e., σ = 20 %), it needs 10 iterations for convergence; if all the units are gas turbines (i.e., σ = 50 %), it needs 4 iterations for convergence. As a result, the number of fast-ramping gas turbines has a large impact on the convergence performance of the ALR method.

However, it should be noted that the location and the number of generators may have a great impact on the convergence performance of the algorithm. Hence, we define the Γ index of i-th generator as (6.103). Obviously, a large Γ implies that the unit needs a high generators' ramp up/down requirement and heavy ramp pressure. Particularly, if the generators with large Γ are gas turbines, the proposed method can be accelerated.

$$\Gamma_i = \frac{1}{P_i^{\max}} \sqrt{\sum_{t=2}^{T} \left(P_{i,t} - P_{i,t-1}\right)^2} \tag{6.103}$$

For convenience, let the number of gas turbines be N_{Gas}. At first, when $N_{\text{Gas}} = 0$, it needs 10 iterations and the Γ index can be shown in Fig. 6.7. Furthermore, we sort Γ in descending order and assume N_{Gas} units with large Γ to be gas turbines, the convergence performance is shown in Fig. 6.8. When $11 \geq N_{\text{Gas}} \geq 8$, the number of iterations will reduce from 10 to 5 and furthermore, when $N_{\text{Gas}} \geq 12$, the number of iteration will reduce to 4 which is the same as that with all units being gas turbines. For comparison, we choose 20 generators ($N'_{Gas} = 20$) with small Γ to be gas turbines, and the proposed algorithm still needs 9 iterations before convergence. This illustrates that, even if a small number of generators have fast ramp rate, the proposed method can still achieve the same best convergence as the case with all units being gas turbines.

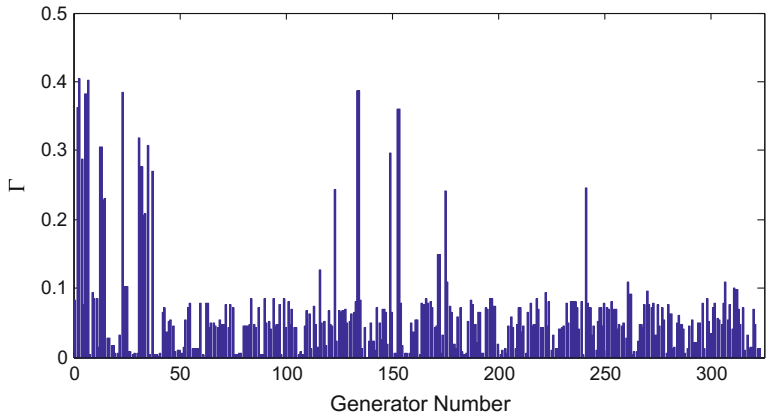

Fig. 6.7 Γ index of each unit

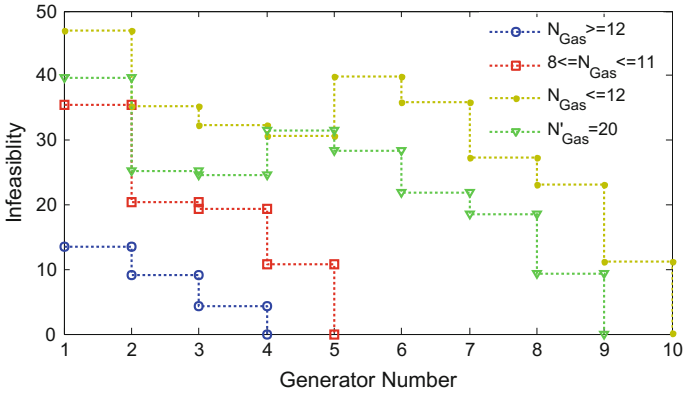

Fig. 6.8 Iterations of the proposed method with fast ramp rate units

6.4 Conclusion

This Chapter studied two acceleration strategies for multi-period large-scale economic dispatch problems: spatial-dimension reduction and time decoupling. Spatial-dimension reduction is used by identifying inactive security constraints. Inactive constraint elimination will reduce the complexity of the optimization problem. Time decoupling is used through the augmented Lagrangian relaxation approach to relax ramp rate constraints. In this term, the multi-period economic dispatch model is decomposed into several single-period economic dispatch problems that can be efficiently handled in parallel. The Lagrange multipliers can be updated by the augmented Lagrangian dual model. The optimization results will be obtained. The spatial-dimension reduction can be used in the robust optimization problem in the last chapter to reduce the computational time. Moreover, time decoupling can be used in day-ahead multi-period optimization problems, especially in the optimization problems with large fast ramp rate generators.

References

1. Duffin RJ (1974) On Fourier's analysis of linear inequality systems. Pivoting and extension. Springer, Berlin, pp 71–95
2. Bland RG (1977) New finite pivoting rules for the simplex method. Math Oper Res 2(2):103–107
3. Schrijver S (1998) Theory of linear and integer programming. Wiley, New york
4. Zhai QZ, Guan XH, Cheng JH et al (2010) Fast identification of inactive security constraints in SCUC problems. Power Syst IEEE Trans 25(4):1946–1954
5. Devore RA, Temlyakov VN (1996) Some remarks on greedy algorithms. Adv Comput Math 5(1):173–187

6. Zimmerman RD, Murillo-Sa X, Nchez CE et al (2011) MATPOWER: steady-state operations, planning, and analysis tools for power systems research and education. Power Syst IEEE Trans 26(1):12–19
7. Boyd S, Parikh N, Chu E et al (2011) Distributed optimization and statistical learning via the alternating direction method of multipliers. Found Trends Mech Learn 3(1):1–122
8. Richtárik P, Takáč M (2012) Parallel coordinate descent methods for big data optimization. arXiv preprint. arXiv:1212.0873
9. Kekatos V, Giannakis GB (2013) Distributed robust power system state estimation. Power Syst IEEE Trans 28(2):1617–1626
10. Dzung P, Kalagnanam J (2014) Some efficient optimization methods for solving the security-constrained optimal power flow problem. Power Syst IEEE Trans 29(2):863–872
11. Erseghe T (2014) Distributed optimal power flow using ADMM. Power Syst IEEE Trans 29 (5):2370–2380
12. Loukarakis E, Bialek JW, Dent CJ (2014) Investigation of maximum possible OPF problem decomposition degree for decentralized energy markets. Power Syst IEEE Trans, 1–13

Chapter 7
Conclusions and Prospects

Abstract This chapter gives the conclusion and further works.

Using the interval analysis method, this paper mainly studied on the power flow analysis and optimization decisions considering the uncertain large scale wind power integration from the modeling and algorithm design point of view. In particular, the technique summarized in Chap. 2 is of generality, which can be applied to the analysis under interval uncertainty in any other areas. The innovations and key results are summarized as follows:

1. A novel algorithm for solving linear and nonlinear interval equations and its employment on the interval power flow model

The key of solving interval power flow relies on solving the linear and nonlinear interval equations. In this paper in terms of the linear equations, the Krawczyk iteration method, including approximate inverse preconditioner using Frobenius norm minimization was proposed to guarantee the convergence of the iterative method. It was then employed to the DC power flow and extended DistFlow-based interval radial power flow. As for the nonlinear equations, a solving method for optimization problem was proposed, especially for the interval quadratic nonlinear equations. The nonconvex feasible region was relaxed to the convex one, which was then followed by binding the boundaries to approximate the exact solution in the interval AC power flow model. Furthermore, as the slack bus may not charge of all the uncertainties, the uncertainties were therefore dispatched among all the generators to form the interval dynamic power flow model.

2. A novel interval optimization algorithm including right hand uncertainties and its implements on the interval economic dispatch model

To address the effect of interval uncertainty of wind power output on the optimal results of security constrained economic dispatch (SCED), the interval SCED model was proposed to acquire the optimal objective function and interval values. The SCED model is mathematically an interval optimal problem including right hand uncertainty. It can be converted into a bi-level deterministic model, namely,

T. Ding, *Power System Operation with Large Scale Stochastic Wind Power Integration*, Springer Theses, DOI 10.1007/978-981-10-2561-7_7

"max-min" model, which however challenges to find the global solution. Fortunately, the paper proved that the "max-min" model is of particularity, which can be established as a mixed integer linear programming after it is transformed into the bilinear programming according to the strong duality theorem. Finally, the general algorithm for solving the interval optimum problem was proposed and applied to the interval SCED model. It will also bring application value to other areas when solving the interval optimum problem.

3. A proposed technique dealing with SCED model infeasible for wind power in the uncertainty set

This paper presented the relaxation technique to tackle with the infeasible SCED model under the wind power uncertainty set which results in the control failure due to the lack of instructions in the close-loop control. Two relaxation methods were given: Considering the optimal wind curtailment in a long time horizon, the curtailment is utilized to guarantee the SCED to be feasible; the other is the relaxation on short-term power limit of the transmission lines based on the real-time scheduling. An economic dispatch model with an exact penalty function was then established which can be transformed to a three-level programming model, obtaining the global solution by reformulating a mixed integer programming model according to the KKT condition due to its convexity.

4. Proposing adaptable and two-stage interval robust SCED models in different time scales respectively

In practice, the dispatching order and schedule cannot be obtained directly by the interval solution. Two interval robust SCED models, that is, the adaptable optimization model and the two-stage optimization model, were proposed within this paper to find a robust optimal value contributing to dispatching schedule while guaranteeing the wind power in the interval within security constraints. The adaptable interval robust optimization is characterized by the generation governed by automatic generation control (AGC) to balance the power in real time in response to the wind power variation, while guaranteeing all the constraints after adjustment. The two-stage interval robust optimization model is essentially a scheduling optimization problem which considers various network topologies. To address the uncertainties of wind power output, the model is established to find the optimal network topology to guarantee the transmission security under the worst wind power variation condition. Mathematically, the adaptable model is termed as a special bi-level optimization model which can be transformed into the convex optimization through dummy variables in a high dimensional space; and the two-stage model is the three-level mixed integer optimization model which can be solved by Benders decomposition. In this paper, two general techniques were given to design the Benders cut to enhance the efficiency.

Furthermore, as the interval robust economic dispatch was dealt with under the worst uncertain condition to guarantee the system security, the solution obtained was conservative compared with the one from non-robust model. The robust cost

was therefore introduced to reduce its conservative property, providing the optimal scheduling solution as the new Pareto front under different robust costs for decision makers.

5. A proposed spatial dimensional reduction and time decoupling algorithm for a large scale SCED model

In practical, the real power system is a large scale combined optimal model. When it is applied with the proposed interval robust optimization model with robust cost, its constraints scale will increase, which challenges its online application. Therefore, this paper investigated the acceleration techniques for solving large scale economic dispatch model in two aspects, which are dimension reduction and time decoupling. From the dimension reducing point of view, most transmission line constraints are redundant due to the few congested lines in practical, which shows less influence on the optimal solution. By use of continuous knapsack algorithm after relaxing the feasible region, the redundant constraints are excluded so that the complexity of solving is significantly reduced. In terms of time decoupling, the multi-period economic dispatch model refers to combine the economic dispatch models in several periods together constrained by unit ramping constraints. Augmented Lagrangian relaxation and diagonal quadratic approximation technique enhance the efficiency for solving the unit commitment model by splitting the multi-period model into several independent models which can be solved in parallel.

Finally, future works are put forward:

1. Correlation of uncertainties to be considered in interval arithmetic

It is known in Chap. 2 that interval numbers are set in mutual independently without considering the correlation of interval uncertain variables (i.e. wind power output). However, the interval power flow with correlation of wind power cannot be solved using iteration methods like Krawczyk iteration whereas the optimal based interval power flow technique is able to solve it, just including the correlation constraint in the optimization model. But it is still worthy to further study on how to model the correlation of wind power properly and its application on the proposed optimization model.

2. AC Power Flow Model has yet to determine to be applied to the economic dispatch optimization

Traditional economic dispatch model was based on the DC power flow in the linear network to approximate the AC model, enhancing its convergence and global optimality. In particular, existing robust commercial software enables DC economic dispatch to be used widely in the practical production and operation.

AC economic dispatch model reflects the nonlinear network characteristics as well as system reactive power and voltage, modeling the real power system operation. However, the AC economic dispatch model is complex and difficult to solve due to its nonlinearity and non-convexity: first, its global optimality is hard to

guarantee; second, the initial value to obtain optimal solution which is however local is hard to set; third, the existing commercial software for solving nonlinear non-convex problem is not robust, where convergence problem may occur.

Fortunately, optimization techniques have been developed, especially for the nonlinear and non-convex power flow, and methods for convexification have been widely studied as well. Although those methods are able to find the global optimal solution in the polynomial time, the challenge is how to revert the optimal solution of convexification to the one in the original non-convex AC economic dispatch model.

3. Unit commitment problem

The proposed economic dispatch model and algorithm were achieved after the optimal unit commitment start-up but without discussion on the unit commitment. In fact, the unit commitment is an important research topic in the market. The network reconfiguration considering unit commitment and the unit commitment considering $N - 1$ wind farms are deserved to be further studies in the future. It is mentioned that the economic dispatch model is a convex optimization problem whereas the unit commitment is termed as a mixed integer programming problem which is non-convex. Although the mixed integer programming has been developed rapidly, the computational efficiency to solve large scale unit commitment is still a challenge. Therefore, how to solve a large scale unit commitment optimization problem efficiently is to worth studying in the future work.

4. Further study on a combined research of wind power and electricity market

The paper mainly focused on incorporating the large scale uncertain wind power generation from the power system point of view without considering electricity market. However, as the electricity market is complete in Europe and North America, combined study of wind power integration and electricity market is a work of important application value. Instead of tracing wind power uncertainty passively, it is active to offset the wind uncertainty to use wind power in financial ways such as futures, contracts and so on. However, it is deserved to study on how to establish the electric market considering wind power uncertainties.

5. Research on Reactive power uncertainties

This paper studied on the uncertain real power economic dispatch considering but without considering reactive power. As reactive power is a main research task in power system, the proposed interval optimization and robust optimization method can be applied to such area in the future.

Appendix A

Solutions of interval linear equations

Set interval linear equations as $\langle \boldsymbol{A} \rangle \langle \boldsymbol{x} \rangle = \langle \boldsymbol{b} \rangle$, given $\langle \boldsymbol{A} \rangle \in \mathrm{IR}^{n \times n}$ and $\langle \boldsymbol{b} \rangle \in \mathrm{IR}^{n \times 1}$, solve $\langle \boldsymbol{x} \rangle$. To solve interval linear equations, the solution methods are presented following:

A. Interval Gaussian Elimination

Interval Gaussian elimination is similar to traditional Gaussian elimination, the difference is to use interval operations. It notes that Gauss elimination method eliminates the coefficient matrix into the upper triangular matrix and the elimination of each column needs pivoting. The traditional Gauss elimination is to select the maximum elements below the column diagonal elements as the pivot. For interval Gaussian elimination, column magnitude pivoting can be used to choose a pivot as the contender with the largest magnitude, where we recall that the magnitude of x is defined as $\mathrm{mig}(\langle \boldsymbol{x} \rangle) = \begin{cases} \min\{|\underline{x}|, |\overline{x}|\} & \text{if } 0 \notin \langle \boldsymbol{x} \rangle \\ 0 & \text{otherwise} \end{cases}$. The flow chart of Gaussian elimination is shown in Table A.1.

B. Kraw operator iteration method

The nature of Kraw operator iteration method is an iteration method, given an initial value $\langle \boldsymbol{x}^0 \rangle$, the iterations are formulated as

$$\langle \boldsymbol{x}^{i+1} \rangle = \left(\boldsymbol{C} \langle \boldsymbol{b} \rangle + (\boldsymbol{I} - \boldsymbol{C} \langle \boldsymbol{A} \rangle) \langle \boldsymbol{x}^i \rangle \right) \cap \langle \boldsymbol{x}^i \rangle \tag{A.1}$$

where $\boldsymbol{C}$ is a constant matrix.

To use Kraw operator iteration method, two points should be considered:

(1) Selection problem of initial value

The initial value choice of Kraw operator iteration method requires $\langle \boldsymbol{x}^0 \rangle \in \mathrm{IR}$ and satisfy $\langle \boldsymbol{x}^* \rangle \subseteq \langle \boldsymbol{x}^0 \rangle$; due to $\langle \boldsymbol{x} \rangle \subseteq (\boldsymbol{C} \langle \boldsymbol{b} \rangle + (\boldsymbol{I} - \boldsymbol{C}\boldsymbol{A}) \langle \boldsymbol{x} \rangle)$,we know $\| \langle \boldsymbol{x} \rangle \| \leq \| \boldsymbol{C} \langle \boldsymbol{b} \rangle \| + \lambda \| \langle \boldsymbol{x} \rangle \|$. Therefore,$\| \langle \boldsymbol{x} \rangle \| \leq \alpha$, where $\alpha = \frac{\| \boldsymbol{C} \langle \boldsymbol{b} \rangle \|}{1 - \lambda}$.

T. Ding, *Power System Operation with Large Scale Stochastic Wind Power Integration*, Springer Theses, DOI 10.1007/978-981-10-2561-7

Table A.1 Interval linear equations based on interval Gaussian elimination

Interval Gaussian elimination	
Input:	Interval coefficient matrix is <***A***>, n is the dimension of <***A***>, interval vector is <***b***>
Output:	The interval solution of $\langle A\rangle\langle x\rangle=\langle b\rangle$ is $\langle x\rangle$
Step 1:	**for** i=1:n-1
Step 2:	[maxmig,index] = max(mig(<***A***(i:n,i)>);
Step 3:	**if** maxmig<=0
Step 4:	error('The problem is no solution')
Step 5:	**end**
Step 6:	k=index+i-1;
Step 7:	**if** $k \neq i$
Step 8:	<***A***([i k],i:n)>=<***A***([k i],i:n)>;
Step 9:	<***b***([i k])>=<***b***([k i])>;
Step 10:	**end**
Step 11:	**for** j = i+1:n
Step 12:	mult = <***A***(j,i)>/<***A***(i,i)>;
Step 13:	<***A***(j,i+1:n)> = <***A***(j,i+1:n)> –mult*<***A***(i,i+1:n)>;
Step 14:	<***b***(j)> = <***b***(j)>–mult*<***b***(i)>;
Step 15:	**end**
Step 16:	**end**
Step 17:	<***x***(n)> = <***b***(n)>/<***A***(n,n)>;
Step 18:	**for** i = n-1:-1:1;
Step 19:	<***x***(i)> = (<***b***(i)> –<***A***(i,i+1:n)>*<***x***(i+1:n,1)>)/<***A***(i,i)>;
Step 20:	**end**

The initial interval can be chosen as

$$\left\langle \boldsymbol{x}^0 \right\rangle = ([-\alpha, +\alpha], [-\alpha, +\alpha], \ldots, [-\alpha, +\alpha])^{\mathrm{T}} \tag{A.2}$$

(2) Selection problem of constant matrix $\boldsymbol{C}$

[1] proposes that if the constant matrix $\boldsymbol{C}$ is selected as the inverse central matrix of coefficient matrix, such that $\boldsymbol{C} = (\boldsymbol{A}^c)^{-1}$, then $\boldsymbol{C}\langle \boldsymbol{A}\rangle$is an H-matrix, which can generally guarantee the convergence of the algorithm.

The flow chart of interval linear equations based on Kraw operator iteration method is shown in Table A.2.

C. Interval hull method

In improve the convergence, the matrix transformation of interval linear equations is firstly carried out, and the equivalent equations are obtained, so that the coefficient matrix $\langle \boldsymbol{A}\rangle$ can be an H-matrix. Therefore, the two sides of interval linear equations $\langle \boldsymbol{A}\rangle\langle \boldsymbol{x}\rangle = \langle \boldsymbol{b}\rangle$ are multiplied by the inverse of the central matrix $\boldsymbol{A}$, and let

$$\langle \boldsymbol{M}\rangle = \boldsymbol{A}^{-1}\langle \boldsymbol{A}\rangle, \quad \langle \boldsymbol{r}\rangle = \boldsymbol{A}^{-1}\langle \boldsymbol{b}\rangle \tag{A.3}$$

Table A.2 Interval linear equations based on Kraw operator iteration method

	Kraw operator iteration method
Input:	ε is convergence precision, $\boldsymbol{A}$ is central matrix, n is the dimension of $\boldsymbol{A}$, η为approximation precision to 0 elements;
Output:	The interval solution of $\langle A\rangle\langle x\rangle=\langle b\rangle$ is $\langle x\rangle$
Step 1:	According to (2-11), compute δ, and obtain $\delta=1/\left\|A^T A\right\|_1$;
Step 2:	Let $\boldsymbol{C}\leftarrow\boldsymbol{A}^{-1}$, and $k\leftarrow 1$;
Step 3:	Let $\boldsymbol{b}\leftarrow\boldsymbol{Cb}$, $<\boldsymbol{A}>\leftarrow\boldsymbol{I}-\boldsymbol{C}<\boldsymbol{A}>$;
Step 4:	Compute $\lambda\leftarrow\|<\boldsymbol{A}>\|$ and $\alpha=\|\boldsymbol{C}\langle\boldsymbol{b}\rangle\|/(1-\lambda)$;
Step 5:	Obtain $\left\langle x^0\right\rangle\leftarrow([-\alpha,+\alpha],[-\alpha,+\alpha],\ldots,[-\alpha,+\alpha])^T$, $s^0\leftarrow 2n\alpha$, $\tau\leftarrow+\infty$ and $k\leftarrow 1$;
Step 6:	**while** $\tau\leq\varepsilon$
Step 7:	$\left\langle x^{k+1}\right\rangle\leftarrow\left(\boldsymbol{C}\langle\boldsymbol{b}\rangle+(\boldsymbol{I}-\boldsymbol{C}\langle\boldsymbol{A}\rangle)\left\langle x^k\right\rangle\right)\cap\left\langle x^k\right\rangle$
Step 8:	$s^{k+1}\leftarrow sum(length(\left\langle x^{k+1}\right\rangle))$;
Step 9:	$\tau\leftarrow(s^k-s^{k+1})/s^{k+1}$;
Step 10:	**end**

The original interval linear equations are equivalently transformed into (A.4).

$$\langle \boldsymbol{M}\rangle\langle \boldsymbol{x}\rangle = \langle \boldsymbol{r}\rangle \tag{A.4}$$

Obviously, if coefficient matrix $\langle \boldsymbol{A}\rangle$ is degenerated into a real matrix which upper bound and lower bound are the same, then $\langle \boldsymbol{M}\rangle$ is degenerated into a real identity matrix and the original problem can be solved precisely; however, if range of intervals in the coefficient matrix $\langle \boldsymbol{A}\rangle$ is not very wide, then $\langle \boldsymbol{M}\rangle$ is approximate a real identity where matrix diagonal elements are the intervals around 1 and the non-diagonal elements are intervals around 0, so coefficient matrix $\langle \boldsymbol{M}\rangle$ is an H-matrix.

It notes that in the equivalence transformation of (A.3), the inverse $\boldsymbol{A}^{-1}$ of real central matrix needs to be solved, but central matrix may be degenerated, which can not solve the inverse. Actually, the inverse of central matrix does not need to solve precisely, we only need to obtain the approximate inverse of central matrix to make coefficient matrix $\langle \boldsymbol{M}\rangle$ to be an H-matrix. Therefore, in the process of inversion, a larger number of diagonal elements in $\boldsymbol{A}$ can be added to make the $\boldsymbol{A}$ diagonally dominant, which can solve the inverse problem when $\boldsymbol{A}$ is degenerated.

Additionally, in the process of interval coefficient matrix transformed into an H-matrix, because two sides are both multiplied by the inverse of the central matrix which increases interval operations and may lead to conservatism of solutions. It also has such problem when using Kraw operator iteration method directly, but interval hull method can overcome conservatism in some extent and has a certain robustness. With the increase of the coefficient matrix disturbance, interval hull method can obtain a smaller range of interval than Gaussian elimination and Kraw operator iteration method, which is proved in [1].

Theorem A.1[2] *If interval matrix* $\langle \boldsymbol{M} \rangle \in \mathrm{IR}^{n\times n}$ *is an H-matrix,* $\langle r \rangle \in \mathrm{IR}^{n}$ *is an interval constant vector, then the approximate hull solution is expressed as x:*

$$x_i = \frac{\langle r_i \rangle + [-\beta_i, -\beta_i]}{\langle M_{ii} \rangle + [-\alpha_i, -\alpha_i]} \tag{A.5}$$

$$\boldsymbol{t} = (\boldsymbol{M}^c)^{-1}\mathrm{mag}(\langle \boldsymbol{x} \rangle) \tag{A.6}$$

$$d_i = (\boldsymbol{M}^c)_{ii}^{-1} \tag{A.7}$$

$$\alpha_i = (\boldsymbol{M}^c)_{ii}^{-1} - 1/d_i \tag{A.8}$$

$$\beta_i = t_i/d_i - \mathrm{mag}(\langle r_i \rangle) \tag{A.9}$$

where $\langle M_{ii} \rangle \in \langle \boldsymbol{M} \rangle$; $\langle r_i \rangle \in \langle \boldsymbol{r} \rangle$; $\mathbf{t} \in \mathrm{R}^{n}$; $\mathbf{d} \in \mathrm{R}^{n}$; $\boldsymbol{\alpha} \in \mathrm{R}^{n}$; $\boldsymbol{\beta} \in \mathrm{R}^{n}$; $\mathbf{M}^{c}$ is the *comparison matrix of* $\langle \boldsymbol{M} \rangle$.

According to (A.5) and (A.6), to obtain approximate hull solution $\boldsymbol{x}$, the inverse of comparison matrix must be solved first. Therefore, a method to solve $(\boldsymbol{M}^c)^{-1}$ is introduced next. To obtain the precise hull of $\boldsymbol{x}$, we should find the supremum of $\boldsymbol{\alpha}$ and $\boldsymbol{\beta}$ as precisely as possible. Because coefficient matrix $\langle \boldsymbol{M} \rangle$ is an H-matrix, the inverse $(\boldsymbol{M}^c)^{-1}$ of comparison matrix is positive semidefinite, which means a real matrix $\boldsymbol{S} \in \mathrm{R}^{n\times n}$ is existed to be the supremum of $(\boldsymbol{M}^c)^{-1}$ and it can be formulated as (A.10) and (A.11). Therefore, if we can find approximate matrix $\boldsymbol{D}$ and two vectors $\boldsymbol{v}$ and $\boldsymbol{w}$, the supremum $\boldsymbol{S}$ is obtained. Because the precise inverse of comparison matrix is hard to obtain, the approximate inverse matrix is introduced. Combined with interval operations, the error will be increased, so the approximate inverse matrix should be corrected.

$$\boldsymbol{I} - \boldsymbol{M}^c\boldsymbol{D} \le \boldsymbol{M}^c\boldsymbol{v}\boldsymbol{w}^T \tag{A.10}$$

$$\boldsymbol{S} = \boldsymbol{D} + \boldsymbol{v}\boldsymbol{w}^T \tag{A.11}$$

where $\boldsymbol{D} \in \mathrm{R}^{n\times n}$ is the approximate value of $(\boldsymbol{M}^c)^{-1}$; $\boldsymbol{v} \in \mathrm{R}^{n}$; $\boldsymbol{w} \in \mathrm{R}^{n}$.

Because $\langle \boldsymbol{M} \rangle$ is an H-matrix, according to its definition, a vector $\boldsymbol{v} \in \mathrm{R}^{n}$ must exist and satisfy $\boldsymbol{v} > \mathbf{0}$ and $\boldsymbol{u} = \boldsymbol{M}^c\boldsymbol{v} > \mathbf{0}$. Therefore, let $\boldsymbol{v}$ to be the vector satisfied with (A.10), and vector $\boldsymbol{w}$ satisfied with (A.11) is:

$$w_k = \max_i \frac{-K_{ik}}{u_i} \tag{A.12}$$

$$\boldsymbol{K} = \boldsymbol{M}^c\boldsymbol{D} - \boldsymbol{I} \tag{A.13}$$

Therefore, if vector $\boldsymbol{v}$ is obtained, then according to (A.10)–(A.12), we can get the supremum $\boldsymbol{S}$ of $(\boldsymbol{M}^c)^{-1}$. Due to $\boldsymbol{u} = \boldsymbol{M}^c\boldsymbol{v}$, $\boldsymbol{u}$ is free variable with any value, so $\boldsymbol{v} = (\boldsymbol{M}^c)^{-1}\boldsymbol{u}$. Because $(\boldsymbol{M}^c)^{-1}$ is hard to solve precisely, it is necessary to replace

$(\boldsymbol{M}^c)^{-1}$ by approximate inverse $\boldsymbol{D}$. Considering $(\boldsymbol{M}^c)^{-1}$ is positive semidefinite, then let the all elements of $\boldsymbol{u}$ are 1 to guarantee the non-negative $\boldsymbol{v}$. To guarantee $\boldsymbol{u} = \boldsymbol{M}^c\boldsymbol{v}$ is strictly satisfied, the obtained $\boldsymbol{v}$ is taken in again to compute $\boldsymbol{u}$. obviously, if approximate inverse is good enough, $\boldsymbol{u}$ is greatly close to the vector of full 1 elements:

$$\boldsymbol{v} = \boldsymbol{D}(1, 1, \ldots, 1)^{\mathrm{T}} \approx (\boldsymbol{M}^c)^{-1}(1, 1, \ldots, 1)^{\mathrm{T}} > \boldsymbol{0} \tag{A.14}$$

Finally, to guarantee the precision of supremum matrix $\boldsymbol{S}$, (A.5), (A.14) need to be computed with different approximate methods, where $\boldsymbol{v}$ and the approximate inverse $\boldsymbol{D}$ of comparison can be computed by rounding-off method; $\boldsymbol{u}$ and $\boldsymbol{K}$ can be computed by downward approximation method; $\boldsymbol{w}$, $\boldsymbol{S}$ and (A.6)–(A.9) can be computed by upward approximation method. Downward approximation method denotes approximation is always approaching to negative infinity, for example, $1.7 \approx 1$, $-1.4 \approx -2$; Upward approximation method denotes approximation is always approaching to positive infinity, for example, $1.7 \approx 2$, $-1.4 \approx -1$.

The flow chart of interval linear equations based on interval hull method is shown in Table A.3.

Table A.3 Interval linear equations based on interval hull method

Interval Hull Method	
Input: $<\boldsymbol{A}> \in \mathrm{IR}^{n\times n}$, $<\boldsymbol{b}> \in \mathrm{IR}^{n}$	
Output: The solution of interval linear equations is $\boldsymbol{\sigma} \in \mathrm{IR}^{n}$	
Step 1:	n = dim(<***A***>); //solve interval matrix dimension
Step 2:	**C** = inv(mid(<***A***>)); //solve inverse of central matrix
Step 3:	**M** = **C***<***A***>; //solve coefficient matrix after preconditioning (H-matrix)
Step 4:	**r** = **C***<***b***>; // solve constant matrix after preconditioning
Step 5:	**dM** = diag(**M**); //preserve diagonal elements of coefficient matrix
Step 6:	**N** = compmat(**M**); //solve the comparison matrix of M
Step 7:	**D** = inv(**N**); // solve approximate inverse of comparison matrix
Step 8:	**v** = mag(**D***ones(n,1)); // solve **v** by (A-14)
Step 9:	SetroundDown; //downward approximation
Step 10:	**u** = **N***v; //solve **u**
Step 11:	**if** all(min(**u**)>0)
Step 12:	**dNc** = diag(**N**); // preserve diagonal elements of comparison matrix
Step 13:	**K** = **N***D - speye(n); // (A-13)
Step 14:	SetroundUp; // upward approximation
Step 15:	**w**=max(-**K**./(**u***ones(1,n))); // (A-12)
Step 16:	**S** = **D** + **v***w; // (A-11)
Step 17:	**t** = **S***mag(<***b***>); // (A-6)
Step 18:	**d** = diag(**S**); // (A-7)
Step 19:	**alpha** = **dNc** + (-1)./**d**; // (A-8)
Step 20:	**beta** = **t**./**d** - mag(**p**); // (A-9)
Step 21:	**σ** = (**p**+ [-**beta**, **beta**])./(**dM**+[-**alpha**, **alpha**]); // (A-10)
Step 22:	**end**
Step 23:	SetroundNeareast; // restore rounding-off

D. Optimality-based method

For interval linear equations $\langle \boldsymbol{A} \rangle \langle \boldsymbol{x} \rangle = \langle \boldsymbol{b} \rangle$, the interval$\langle \boldsymbol{x} \rangle$can be solved by optimality-based method. Introduce new dummy variable $\boldsymbol{A}$, the optimization model is formulated as following:

$$\min/\max_{\boldsymbol{x},\boldsymbol{A}} \quad x_i \quad i = 1, \ldots, n \tag{A.15}$$

$$s.t. \quad \underline{a_{ij}} \leq a_{ij} \leq \overline{a_{ij}} \quad i = 1, \ldots, n; j = 1, \ldots, n \tag{A.16}$$

$$\underline{b_j} \leq \sum_{i=1}^{n} a_{ij} x_i \leq \overline{b_j} \quad j = 1, \ldots, n \tag{A.17}$$

We can know the optimization above is a nonlinear programming, and the lower and upper bound of the ith variable can be obtained by solving the objective function of "min" and "max". Additionally, the solution of every variable is independent, so n optimizer can be used with parallel implement.

The advantage is this method can obtain the strict upper and lower bound of interval solution. However, it also has some disadvantages: first, for n variable, we should solve $2n$ optimization models, though these model can be parallelly computed, it also needs many parallel cores; second, the model is a nonlinear programming, and only global optimal solution can represent real upper and lower bound of interval, but it is a NP-hard problem for a nonlinear programming to search the global optimal solution.

References

[1] Neumeier A (2000) Erratum to: a simple derivation of the Hansen-Bliek-Rohn-Ning-Kearfott enclosure for linear interval equations. Reliable Comput 6(2):227

[2] Neumaier A (1999) A simple derivation of the Hansen-Bliek-Rohn-Ning-Kearfott enclosure for linear interval equations. Reliable Comput 5(2):131–136

Appendix B

Solutions of interval nonlinear equations solutions

Mathematically, the interval nonlinear equations are formulated as

$$\boldsymbol{F}(\langle \boldsymbol{x} \rangle) = \boldsymbol{0} \tag{B.1}$$

Assume $0 \notin F'(\langle \boldsymbol{x} \rangle)$, and let $\boldsymbol{y} = m(\langle \boldsymbol{x} \rangle)$, where $m(\langle \boldsymbol{x} \rangle)$ is the middle of interval $\langle \boldsymbol{x} \rangle$, then the Newton iteration of interval is formulated as $\langle \boldsymbol{x} \rangle = m(\langle \boldsymbol{x} \rangle) - f(m(\langle \boldsymbol{x} \rangle))/F^{-1}(\langle \boldsymbol{x} \rangle), \forall \boldsymbol{y} \in \langle \boldsymbol{x} \rangle$. Obviously, it is much more difficult to solve inverse $F(\langle \boldsymbol{x} \rangle)^{-1}$ of interval matrix than traditional real matrix. Therefore, Krawczyk-Moore iteration method is proposed and the iteration is formulated as following:

$$K(\boldsymbol{y}, \langle \boldsymbol{x} \rangle) = \boldsymbol{y} - \boldsymbol{Y} f(\boldsymbol{y}) - \left(\boldsymbol{I} - \boldsymbol{Y} F'(\langle \boldsymbol{x} \rangle)\right)(\langle \boldsymbol{x} \rangle - \boldsymbol{y}) \tag{B.2}$$

$\forall \boldsymbol{y} \in \langle \boldsymbol{x} \rangle$, $\forall \boldsymbol{Y} \in n \times n$ nonsingular matrix, where $\boldsymbol{y}$ and $\boldsymbol{Y}$ are defined as

$$\begin{cases} \langle \boldsymbol{x}^{i+1} \rangle = \langle \boldsymbol{x}^{i} \rangle \cap K\left(\langle \boldsymbol{x}^{i} \rangle\right) \\ K\left(\langle \boldsymbol{x}^{i} \rangle\right) = \boldsymbol{y}^{i} - \boldsymbol{Y}^{i} f\left(\boldsymbol{y}^{i}\right) - \left(\boldsymbol{I} - \boldsymbol{Y}^{i} F'\left(\langle \boldsymbol{x}^{i} \rangle\right)\right)\left(\langle \boldsymbol{x}^{i} \rangle - \boldsymbol{y}^{i}\right) \\ \boldsymbol{y}^{i} = m(\langle \boldsymbol{x}^{i} \rangle) \quad \boldsymbol{Y}^{i} = \left[m\left(F'(\langle \boldsymbol{x}^{i} \rangle)\right)\right]^{-1} \end{cases} \tag{B.3}$$

where $\boldsymbol{I}$ is an identity matrix; m is the middle of the interval. Therefore, $\boldsymbol{y}$ is actually a deterministic vector, and $\boldsymbol{Y}^{i}$ is the inverse of the deterministic matrix. It notes that the same variable of Kraw operator iteration method of nonlinear equations is used in $F'(\langle x \rangle)$ for many times which will expand the range of interval.

T. Ding, *Power System Operation with Large Scale Stochastic Wind Power Integration*, Springer Theses, DOI 10.1007/978-981-10-2561-7

Appendix C

Economic Dispatch Model with Prohibited Zones

C.1 Modeling of Economic Dispatch with Prohibited Zones

As shown in (D.1), the range of the generation output will be divided into several feasible sub-regions. Suppose that there are 2 prohibited zones, the original continuous feasible region will be divided into three disjoint sub regions in which only one is allowed to operate, and the output power could continuously operate within each chosen sub feasible region. Besides, the beginning and end are always feasible regions. If not, the region should be cut off. Then, the prohibited zones and feasible regions are alternating, and the number of feasible regions is one more than that of prohibited zones. So the economic dispatch model with prohibited zones can be presented as

$$\min \quad \sum_{i=1}^{N_g} \left(a_i P_i^2 + b_i P_i + c_i\right) \tag{C.1}$$

$$s.t. \quad \sum_{i=1}^{N_g} P_i + \sum_{k=1}^{N_g} W_k^f = \sum_{j=1}^{N_d} D_j \tag{C.2}$$

$$\begin{cases} \max\left(P_i^0 - DR_i, P_i^{\min}\right) \le P_i \le \min\left(P_i^0 + UR_i, P_i^{\max}\right) \\ P_i \in \left[P_{i,1}^{\min}, P_{i,1}^{\max}\right], or \ldots, \left[P_{i,j}^{\min}, P_{i,j}^{\max}\right], or \ldots, or \left[P_{i,m_i}^{\min}, P_{i,m_i}^{\max}\right], \end{cases} \quad i = 1, \ldots, N_g \tag{C.3}$$

$$-F_l^{\max} \le \sum_{i=1}^{N_g} G_{l,i}^P P_i + \sum_{k=1}^{N_w} G_{l,k}^W W_k^f - \sum_{k=1}^{N_d} G_{l,j}^D D_j \le F_l^{\max}, \quad l = 1, \ldots, N_l \tag{C.4}$$

T. Ding, *Power System Operation with Large Scale Stochastic Wind Power Integration*, Springer Theses, DOI 10.1007/978-981-10-2561-7

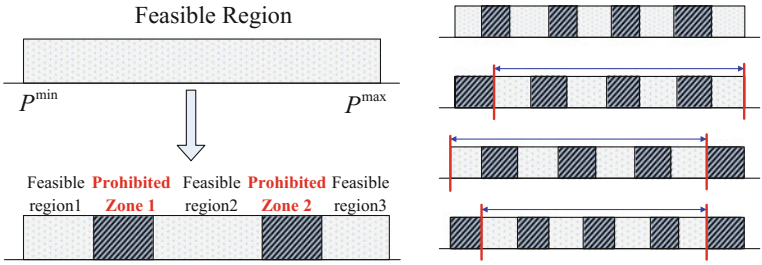

Fig. C.1 Feasible regions and prohibited zones

$$\sum_{i=1}^{N_g} R_i^+ \geq SU, \quad \sum_{i=1}^{N_g} R_i^- \geq SD \tag{C.5}$$

where the parameters are the same as that in Sect. 4.2.1. The differences are including: (C.3) is the ramp constraints; UR_i and DR_i are the ramp up and ramp down constraint of ith generator; P_i^0 is the generation output of ith generator; m_i represents the number of sub-regions of ith generator; $P_{i,j}^{\min}$ and $P_{i,j}^{\max}$ are the lower and upper bound of jth sub-region for ith generator; "or" implies that only one sub-region could be chosen. (C.4) the reserve constraints of generators; R_i^+ and R_i^- are up and down spanning reserve of ith generator; SU and SD total reserve requirement of up and down spanning reserve (Fig. C.1).

C.1.1 Simplification of the Modeling for Prohibited Zones

Figure C.1 illustrates a binary coding scheme applied on a generator with two prohibited zones. The shaded areas represent three disjoint feasible zones, and the gaps among the feasible zones are two disjoint prohibited zones. We assign one binary variable to each of the two prohibited zones, namely, x_1 and x_2. If the binary variable takes 0, the zone to the right of the prohibited zone upper bound is selected; otherwise, the zone to the left of the prohibited zone lower bound is selected. The zones selected by the two binary variables may or may not have intersections. When the intersection exists, it aligns with one feasible zone; otherwise, the feasible zone is empty. For instance in Fig. C.1, when both binary variables takes 1, the intersection will be the first feasible zone from left; when x_1 takes 1 and x_2 takes 0, there is no feasible zone. As such, each feasible zone can be uniquely represented by a binary code. For example, the three feasible regions in Fig. C.1 can be denoted by {11}, {01} and {00} respectively.

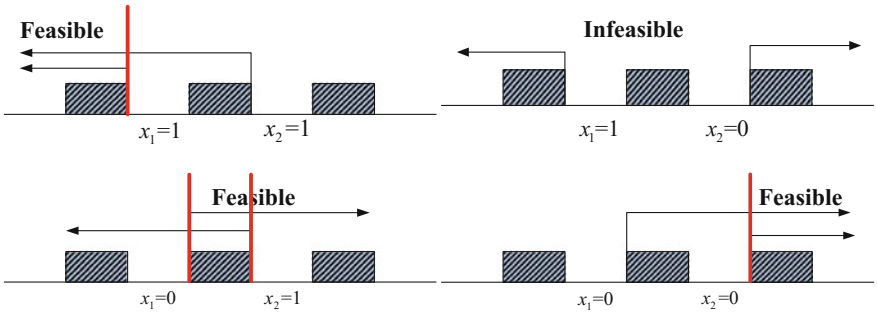

Fig. C.2 Binary coding example for two disjoint prohibited zones

Note that the binary variable assigned to any prohibited zone must be equal to or larger than the binary variable associated with the prohibited zone to its left. Otherwise, the intersection feasible zone will be empty. For instance, as shown in second scenario in Fig. C.1, the binary code is {10} and the resulting feasible zone is empty. Therefore, for generator i with n_i feasible zones, we will create m_i-1 binary variables, and the binary code for each of the feasible zones will be $\underbrace{000\ldots000}_{m_i-1}$, $\underbrace{000\ldots001}_{m_i-1}$, $\underbrace{000\ldots011}_{m_i-1}$, $\underbrace{000\ldots111}_{m_i-1}, \cdots,$ $\underbrace{001\ldots111}_{m_i-1}$, $\underbrace{011\ldots111}_{m_i-1}$, $\underbrace{111\ldots111}_{m_i-1}$, respectively. Not coincidentally, these m_i binary-coded sequences represent the feasible zones from right to left on P_i horizon, respectively (Fig. C.2).

For N_g generators, with m_i prohibited zones for ith generator, constraints (C.3) can be equivalently converted to (C.6)

$$\begin{cases} \max\left(P_i^0 - DR_i, P_i^{\min}\right) \le P_i \le \min\left(P_i^0 + UR_i, P_i^{\max}\right) \\ P_i \le P_{i,j}^{\max} + M\left(1 - x_{i,j}\right) \\ -P_i \le -P_{i,j+1}^{\min} + Mx_{i,j} \\ x_{i,j} \le x_{i,j+1} \end{cases}, \quad \begin{cases} j = 1, 2, \ldots, m_i - 1 \\ i = 1, 2, \ldots, N_g \end{cases} \tag{C.6}$$

where M is a big real number; $x_{i,j}$ denotes the binary variable associated with jth prohibited zone of ith generator. When M is selected such that second and third constraints are satisfied, the solution is insensitive to the actual value of M. M can be conservatively selected as $M = max\left\{P_i^{max}\right\} + 1$, which is a sufficient but not necessary condition. It should also be pointed out that, in practice M should not be selected to be extremely big. Otherwise, it may cause numerical instability.

Besides, it should be noted that the system spinning reverse constraints can also be taken into consideration. Reserve is essential to deal with uncertainties and unexpected system conditions. However, the prohibited zones strictly limited units' ability to regulate load if the load regulation falls into certain prohibited zones. Therefore, only the units without prohibited zones are taken into account for the

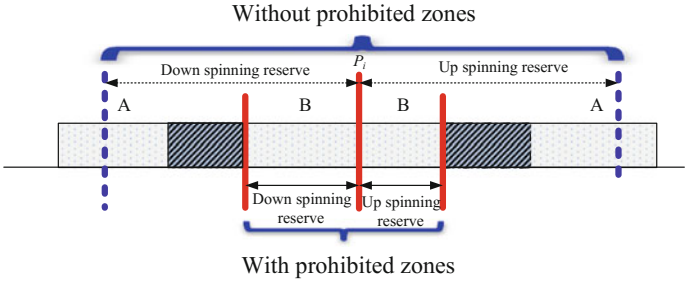

Fig. C.3 Spinning reserve of unit with/without prohibited zones

system spinning reserve requirement. Theoretically, the unit with prohibited zones can still provide spinning reserve within its sub feasible region. The down/up spinning reserve of a unit is illustrated in Fig. C.3. When the unit has no prohibited zone, its reserve capability can reach feasible region A; while with prohibited zones, its reserve capability shrinks to sub feasible region B to prevent the load regulation from prohibited operation (Fig. C.3).

The spinning reserve of units with prohibited zones will shrink to its sub feasible region. In addition, only one sub feasible regions is allowed to operate. Therefore, the spinning reserve of each unit can be expressed as

Let Θ denote the set of all units with prohibited zones and Ψ denote the set of all units without prohibited zones. For unit $i \in \Psi$, the up and down spinning reserve R_i^u/R_i^d can be formulated as (C.7), whereas for unit $i \in \Theta$, the up and down spinning reserve R_i^+/R_i^- can be cast as (C.8). Here, we let $y_{i,0} = 0$ and $y_{i,m_i+1} = 1$.

$$R_i^u = \min\left\{UR_i, P_{\mathrm{g},i}^{\max} - P_{\mathrm{g},i}\right\}, \quad i \in \Psi \tag{C.7a}$$

$$R_i^d = \min\left\{DR_i, P_{\mathrm{g},i} - P_{\mathrm{g},i}^{\min}\right\}, \quad i \in \Psi \tag{C.7b}$$

$$R_i^+ = \min\left\{UR_i, \sum_{j=1}^{m_i+1} P_{\mathrm{g},i,j}^{\max}\left(y_{i,j} - y_{i,j-1}\right) - P_{\mathrm{g},i}\right\}, \quad i \in \Theta \tag{C.8a}$$

$$R_i^- = \min\left\{DR_i, P_{\mathrm{g},i} - \sum_{j=1}^{m_i+1} P_{\mathrm{g},i,j}^{\min}\left(y_{i,j} - y_{i,j-1}\right)\right\}, \quad i \in \Theta \tag{C.8b}$$

C.1.2 Mathematical Model

Finally, taking (C.6) into (C.3), and taking (C.7)–(C.8) into (C.5), we can obtain the final mathematical model with consideration of uncertain wind power and prohibited zones, such that

$$\min \quad \sum_{i=1}^{N_g} \left(a_i P_i^2 + b_i P_i + c_i\right) \tag{C.9}$$

$$s.t. \quad \sum_{i=1}^{N_g} P_i + \sum_{k=1}^{N_w} W_k^f = \sum_{j=1}^{N_d} D_j \tag{C.10}$$

$$\max\left(P_i^0 - DR_i, P_i^{\min}\right) \le P_i \le \min\left(P_i^0 + UR_i, P_i^{\max}\right), \quad i \in \Omega_\Psi \tag{C.11}$$

$$\begin{cases} \max\left(P_i^0 - DR_i, P_i^{\min}\right) \le P_i \le \min\left(P_i^0 + UR_i, P_i^{\max}\right) \\ P_i \le P_{i,j}^{\max} + M\left(1 - x_{i,j}\right) \\ -P_i \le -P_{i,j+1}^{\min} + M x_{i,j} \\ x_{i,j} \le x_{i,j+1} \end{cases}, \quad \begin{cases} j = 1, 2, \ldots, m_i - 1 \\ i \in \Omega_\Theta \end{cases} \tag{C.12}$$

$$-F_l^{\max} \le \sum_{i=1}^{N_g} G_{l,i}^P P_i + \sum_{k=1}^{N_w} G_{l,k}^W W_k^f - \sum_{j=1}^{N_d} G_{l,j}^D D_j \le F_l^{\max}, \quad l = 1, \ldots, N_l \tag{C.13}$$

$$\begin{aligned} &\sum_{i=1}^{N_g} \left(\min\left\{ UR_i, \sum_{j=1}^{m_i+1} P_{i,j}^{\max}\left(y_{i,j+1} - y_{i,j}\right) - P_i \right\} \right) \ge SU \\ &\sum_{i=1}^{N_g} \left(\min\left\{ DR_i, P_i - \sum_{j=1}^{m_i+1} P_{i,j}^{\min}\left(y_{i,j+1} - y_{i,j}\right) \right\} \right) \ge SD \end{aligned} \tag{C.14}$$

where Ω_Ψ is the set of generators without prohibited zones and Ω_Θ is the set of generators with prohibited zones.

In order to eliminate the "min" constraints in the above, we should give a transformation. Since the "min" operator in (C.11) and (C.12) is for a constant number, which is actually a predetermined number before solving the model. In contrast, the "min" operator is for the variable P_i in (C.14), which can be termed as a bi-level optimization model. Bur fortunately, the "min" operators are always at the left side of the inequalities "≥", which can be transformed to a convex optimization model by introducing some dummy variables. It should be noted that this transformation is exact when "min" operator is at the left side of "≥" or "max" operator is at the left side of "≤", which gives

$$\min \quad \sum_{i=1}^{N_g} \left(a_i P_i^2 + b_i P_i + c_i\right) \tag{C.15}$$

$$\text{s.t.} \quad \sum_{i=1}^{N_g} P_i + \sum_{k=1}^{N_w} W_k^f = \sum_{j=1}^{N_d} D_j \tag{C.16}$$

$$\max\left(P_i^0 - DR_i, P_i^{\min}\right) \le P_i \le \min\left(P_i^0 + UR_i, P_i^{\max}\right), \quad i \in \Omega_\Psi \tag{C.17}$$

$$\begin{cases} \max\left(P_i^0 - DR_i, P_i^{\min}\right) \le P_i \le \min\left(P_i^0 + UR_i, P_i^{\max}\right) \\ P_i \le P_{i,j}^{\max} + M\left(1 - x_{i,j}\right) \\ -P_i \le P_{i,j+1}^{\min} + M x_{i,j} \\ x_{i,j} \le x_{i,j+1} \end{cases}, \quad \begin{cases} j = 1, 2, \ldots, m_i - 1 \\ i \in \Omega_\Theta \end{cases} \tag{C.18}$$

$$-F_l^{\max} \le \sum_{i=1}^{N_g} G_{l,i}^P P_i + \sum_{k=1}^{N_w} G_{l,k}^W W_k^f - \sum_{j=1}^{N_d} G_{l,i}^D D_j \le F_l^{\max}, \quad l = 1, \ldots, N_l \tag{C.19}$$

$$\begin{cases} \sum\limits_{i \in \Omega_\Psi} Z_{1,i} + \sum\limits_{i \in \Omega_\Theta} Z_{2,i} \ge Su \\ \sum\limits_{i \in \Omega_\Psi} Z_{3,i} + \sum\limits_{i \in \Omega_\Theta} Z_{4,i} \ge Sd \end{cases} \tag{C.20}$$

$$\begin{cases} Z_{1,i} \le UR_i, Z_{1,i} \le \min\left(P_i^0 + UR_i, P_i^{\max}\right) - P_i & i \in \Omega_\Psi \\ Z_{2,i} \le UR_i, Z_{2,i} \le \sum\limits_{j=1}^{m_i+1} P_{i,j}^{\max}\left(y_{i,j} - y_{i,j-1}\right) - P_i & i \in \Omega_\Theta \\ Z_{3,i} \le DR_i, Z_{3,i} \le P_i - \max\left(P_i^0 + DR_i, P_i^{\min}\right) & i \in \Omega_\Psi \\ Z_{4,i} \le DR_i, Z_{4,i} \le P_i - \sum\limits_{j=1}^{m_i+1} P_{i,j}^{\max}\left(y_{i,j} - y_{i,j-1}\right) & i \in \Omega_\Theta \end{cases} \tag{C.21}$$

C.2 Adaptive Robust Interval Economic Dispatch with Prohibited Zones

Since the wind power output is usually stochastic, the thermal generation will be changed at each time period to guarantee the power balance. Due to the existence of prohibited zones, the generation output may operate in the prohibited zones under the wind power disturbances. In order to prevent the prohibited zones, the generation output may jump from one to another under the uncertain wind power output. This "jump" should be considered, which increases the volatility of generator output.

To address this problem, an adaptive robust optimization model is set up by extending the proposed model in Sect. 5.2. In addition, the price of the robustness is also taken into consideration, such that

$$W_k = W_k^f + W_k^e y_k, \ldots k = 1, \ldots, N_w, \quad \Omega = \left\{ \boldsymbol{y} \middle| \sum_{k=1}^{N_w} |y_k| \le \Gamma, \quad |y_k| \le 1, \quad \forall k \right\} \tag{C.22}$$

Furthermore, the deterministic model (C.15)–(C.21) can be extended to the robust optimization model (C.23)–(C.32). This robust optimization model implies that for the given feasible sub-regions of each generator, the participation factors can be employed to guarantee the real-time power balance. Moreover, the physical constraints of each generator should be strictly guaranteed when the generation output is adjusted by the participation factors for any wind power output variation, which gives

$$\min_{\boldsymbol{P}^{sch}} \quad \sum_{i=1}^{N_g} \left(a_i \left(P_i^{sch}\right)^2 + b_i P_i^{sch} + c_i + a_i \beta_i^2 \sum_{k=1}^{N_w} \sum_{j=1}^{N_w} \Lambda_{kj} \right) \tag{C.23}$$

$$s.t. \quad \sum_{j=1}^{N_d} D_j - \sum_{k=1}^{N_w} W_k^f = \sum_{i=1}^{N_g} P_i^{sch} \tag{C.24}$$

$$\max\left(P_i^0 - DR_i, P_i^{\min}\right) + \beta_i \theta \le P_i^{sch} \le \min\left(P_i^0 + UR_i, P_i^{\max}\right) - \beta_i \theta, \quad i \in \Omega_\Psi \tag{C.25}$$

$$\begin{cases} \max\left(P_i^0 - DR_i, P_i^{\min}\right) + \beta_i \theta \le P_i^{sch} \le \min\left(P_i^0 + UR_i, P_i^{\max}\right) - \beta_i \theta \\ P_i^{sch} + \beta_i \theta \le P_{i,j}^{\max} + M\left(1 - x_{i,j}\right) \\ -P_i^{sch} + \beta_i \theta \le -P_{i,j+1}^{\min} + M x_{i,j} \\ x_{i,j} \le x_{i,j+1} \\ \begin{cases} j = 1, 2, \ldots, m_i - 1 \\ i \in \Omega_\Theta \end{cases} \end{cases}, \tag{C.26}$$

$$\begin{aligned} -F_l^{\max} + \left(t_l \Gamma + \sum_{k=1}^{N_w} P_{lk} \right) \le \sum_{i=1}^{N_g} G_{l,i}^P P_i^{sch} + \sum_{k=1}^{N_w} G_{l,k}^R W_k^f - \sum_{j=1}^{N_d} G_{l,i}^D D_j \le F_l^{\max} \\ - \left(t_l \Gamma + \sum_{k=1}^{N_w} P_{lk} \right), \\ l = 1, \ldots, N_l \end{aligned} \tag{C.27}$$

$$t_l + p_{lk} \geq W_k^e \left(\sum_{i=1}^{N_g} G_{l,i}^P \beta_i + G_{l,k}^W \right), \quad l = 1, \ldots, N_l,\ k = 1, \ldots, N_w \tag{C.28}$$

$$p_{lk} \geq 0,\ t_l \geq 0, \quad l = 1, \ldots, N_l,\ k = 1, \ldots, N_w \tag{C.29}$$

$$\sum_{i=1}^{N_g} \beta_i = 1, \quad 0 \leq \beta_i \leq 1 \tag{C.30}$$

$$\begin{cases} \sum\limits_{i \in \Omega_\Psi} Z_{1,i} + \sum\limits_{i \in \Omega_\Theta} Z_{2,i} \geq Su \\ \sum\limits_{i \in \Omega_\Psi} Z_{3,i} + \sum\limits_{i \in \Omega_\Theta} Z_{4,i} \geq Sd \end{cases} \tag{C.31}$$

$$\begin{cases} Z_{1,i} \leq UR_i, Z_{1,i} \leq \min\left(P_i^0 + UR_i, P_i^{\max}\right) - P_i^{sch} & i \in \Omega_\Psi \\ Z_{2,i} \leq UR_i, Z_{2,i} \leq \sum\limits_{j=1}^{m_i+1} P_{i,j}^{\max}\left(y_{i,j} - y_{i,j-1}\right) - P_i^{sch} & i \in \Omega_\Theta \\ Z_{3,i} \leq DR_i, Z_{3,i} \leq P_i^{sch} - \max\left(P_i^0 + DR_i, P_i^{\min}\right) & i \in \Omega_\Psi \\ Z_{4,i} \leq DR_i, Z_{4,i} \leq P_i^{sch} - \sum\limits_{j=1}^{m_i+1} P_{i,j}^{\min}\left(y_{i,j} - y_{i,j-1}\right) & i \in \Omega_\Theta \end{cases} \tag{C.32}$$

where $\theta = \max\limits_{\sum_{k=1}^{N_w} y_k = \Gamma, 0 \leq y_k \leq 1} \sum_{k=1}^{N_w} W_k^e y_k = \sum_{m=1}^{k-1} \left(W_{i_m}^e - W_{ik}^e \right) + W_{i_k}^e \Gamma$ and $k - 1 \leq \Gamma \leq k$ are constants; $\boldsymbol{\beta}$ is the participation factors, $\boldsymbol{P}^{sch}$ is the scheduled generation output and other parameters can be found in Sect. 4.2.

Appendix D

Two-Stage Robust Interval Economic Dispatch with Reliability Constraints

D.1 Two-Stage Robust Interval Economic Dispatch with N − 1 Contingencies Constraints

Putting the N − 1 contingency constraints into the original robust transmission switching model (5.57)–(5.61), we can obtain a new two-stage robust interval economic dispatch model. This model aims to find an optimal topology that satisfies all the N − 1 contingencies. When one contingency occurs, the generation output cannot be changed while the power flow will change. Therefore, we should set up some new variables for describing the power flow after the contingency, yielding

$$\min_{\boldsymbol{P}_t,\boldsymbol{Z}_t,\boldsymbol{\theta}_t,\boldsymbol{y}_t,\boldsymbol{Z}_{c,t},\boldsymbol{\theta}_{c,t}} \quad \sum_{t=1}^{T}\left(\boldsymbol{b}^T\boldsymbol{P}_t + \mathrm{sum}(\boldsymbol{c})\right) \tag{D.1}$$

$$s.t. \quad \boldsymbol{C}_f^T\boldsymbol{Z}_t = \boldsymbol{C}_g\boldsymbol{P}_t - \boldsymbol{C}_d\boldsymbol{D}_t + \boldsymbol{C}_w\boldsymbol{W}_t^f \tag{D.2}$$

$$\boldsymbol{P}^{\min} \le \boldsymbol{P}_t \le \boldsymbol{P}^{\max},\ \boldsymbol{Rd} \le \boldsymbol{P}_t - \boldsymbol{P}_{t-1} \le \boldsymbol{Ru},\ \theta_t(ref) = 0 \tag{D.3}$$

$$-\boldsymbol{F}^{\max} \circ \boldsymbol{y}_t \le \boldsymbol{Z}_t \le \boldsymbol{F}^{\max} \circ \boldsymbol{y}_t \tag{D.4}$$

$$-M(\boldsymbol{1} - \boldsymbol{y}_t) \le \boldsymbol{Z} - \boldsymbol{B}\boldsymbol{C}_f\boldsymbol{\theta}_t \le M(\boldsymbol{1} - \boldsymbol{y}_t) \tag{D.5}$$

T. Ding, *Power System Operation with Large Scale Stochastic Wind Power Integration*, Springer Theses, DOI 10.1007/978-981-10-2561-7

$$\boldsymbol{C}_f^T \boldsymbol{Z}_{c,t} = \boldsymbol{C}_g \boldsymbol{P}_t - \boldsymbol{C}_d \boldsymbol{D}_t + \boldsymbol{C}_d \boldsymbol{W}_t^f, \quad \theta_{c,t}(ref) = 0 \tag{D.6}$$

$$-\boldsymbol{F}^{\max} \circ N1_c \le \boldsymbol{Z}_{c,t} \le \boldsymbol{F}^{\max} \circ N1_c \tag{D.7}$$

$$-M(\mathbf{2} - \boldsymbol{y}_t - N1_c) \le \boldsymbol{Z}_{c,t} - \boldsymbol{B}\boldsymbol{C}_f \boldsymbol{\theta}_{c,t} \le M(\mathbf{2} - \boldsymbol{y}_t - N1_c) \tag{D.8}$$

$$\boldsymbol{y}_t \in \{0, 1\} \tag{D.9}$$

where $\boldsymbol{\theta}_{c,t}$ and $\boldsymbol{Z}_{c,t}$ are $n_b \times 1$ angle vector and $n_l \times 1$ branch flow vector under the contingence c at time t; $N1_c$ is an $n_l \times 1$ binary vector, and it is 0 when this is a contingency, 1 otherwise. Furthermore, the robust interval optimization model can be presented as:

$$\min_{\boldsymbol{y}_t \in \{0,1\}} \max_{\boldsymbol{W}_t \in \left[\boldsymbol{W}_t^f - \boldsymbol{W}_t^e, \boldsymbol{W}_t^f + \boldsymbol{W}_t^e\right]} \min_{\boldsymbol{P}_t, \boldsymbol{Z}_t, \boldsymbol{\theta}_t} \sum_{t=1}^{T} \left(\boldsymbol{b}^T \boldsymbol{P}_t + \mathrm{sum}(\boldsymbol{c})\right) \tag{D.10}$$

$$s.t. \quad \boldsymbol{C}_f^T \boldsymbol{Z}_t = \boldsymbol{C}_g \boldsymbol{P}_t - \boldsymbol{C}_d \boldsymbol{D}_t + \boldsymbol{C}_w \boldsymbol{W}_t \tag{D.11}$$

$$\boldsymbol{P}^{\min} \le \boldsymbol{P}_t \le \boldsymbol{P}^{\max}, \ \boldsymbol{R}\boldsymbol{d} \le \boldsymbol{P}_t - \boldsymbol{P}_{t-1} \le \boldsymbol{R}\boldsymbol{u}, \ \theta_t(ref) = 0 \tag{D.12}$$

$$-\boldsymbol{F}^{\max} \circ \boldsymbol{y}_t \le \boldsymbol{Z}_t \le \boldsymbol{F}^{\max} \circ \boldsymbol{y}_t \tag{D.13}$$

$$-M(\mathbf{1} - \boldsymbol{y}_t) \le \boldsymbol{Z} - \boldsymbol{B}\boldsymbol{C}_f \boldsymbol{\theta}_t \le M(\mathbf{1} - \boldsymbol{y}_t) \tag{D.14}$$

$$\boldsymbol{S}^T \boldsymbol{Z}_{c,t} = \boldsymbol{C}_g \boldsymbol{P}_t - \boldsymbol{C}_d \boldsymbol{D}_t + \boldsymbol{C}_d \boldsymbol{W}_t^f, \quad \theta_{c,t}(ref) = 0 \tag{D.15}$$

$$-\boldsymbol{F}^{\max} \circ N1_c \le \boldsymbol{Z}_{c,t} \le \boldsymbol{F}^{\max} \circ N1_c \tag{D.16}$$

$$-M(\mathbf{2} - \boldsymbol{y}_t - N1_c) \le \boldsymbol{Z}_{c,t} - \boldsymbol{B}\boldsymbol{C}_f \boldsymbol{\theta}_{c,t} \le M(\mathbf{2} - \boldsymbol{y}_t - N1_c) \tag{D.17}$$

D.2 Budget of the N − 1 contingencies

If taking all the N − 1 contingencies into one optimization model, the result may be much too conservative. In order to trade off the security and economy, we can design a budget to have a balance. In this book, we will limit the number of

transmission lines that can be used for switching and the corresponding model can be written as

$$\min_{\boldsymbol{P}_t,\boldsymbol{Z}_t,\boldsymbol{\theta}_t,\boldsymbol{y}_t} \quad \sum_{t=1}^{T}\left(\boldsymbol{b}^T\boldsymbol{P}_t+\text{sum}(\boldsymbol{c})\right) \tag{D.18}$$

$$s.t. \quad \boldsymbol{C}_f^T\boldsymbol{Z}_t=\boldsymbol{C}_g\boldsymbol{P}_t-\boldsymbol{C}_d\boldsymbol{D}_t+\boldsymbol{C}_w\boldsymbol{W}_t \tag{D.19}$$

$$\boldsymbol{P}^{\min}\le\boldsymbol{P}_t\le\boldsymbol{P}^{\max},\ \boldsymbol{Rd}\le\boldsymbol{P}_t-\boldsymbol{P}_{t-1}\le\boldsymbol{Ru},\ \theta_t(ref)=0 \tag{D.20}$$

$$-\boldsymbol{F}^{\max}\circ\boldsymbol{y}_t\le\boldsymbol{Z}_t\le\boldsymbol{F}^{\max}\circ\boldsymbol{y}_t \tag{D.21}$$

$$-M(\boldsymbol{1}-\boldsymbol{y}_t)\le\boldsymbol{Z}_t-\boldsymbol{BC}_f\boldsymbol{\theta}_t\le M(\boldsymbol{1}-\boldsymbol{y}_t) \tag{D.22}$$

$$\boldsymbol{y}_t\in\{0,1\},\ \boxed{\sum_{l=1}^{N_l}(1-y_l)\le\Delta} \tag{D.23}$$

where N_l is the number of transmission lines, Δ is the maximum number of transmission lines that is allowed to be switched. The robust optimization model with this budget can be reformulated as

$$\min_{\boldsymbol{y}\in\{0,1\},\sum_{l=1}^{N_l}(1-y_l)\le\Delta}\ \max_{\boldsymbol{W}_t\in\left[\boldsymbol{W}_t^f-\boldsymbol{W}_t^e,\boldsymbol{W}_t^f+\boldsymbol{W}_t^e\right]}\ \min_{\boldsymbol{P}_t,\boldsymbol{Z}_t,\boldsymbol{\theta}_t}\quad\sum_{t=1}^{T}\left(\boldsymbol{b}^T\boldsymbol{P}_t+\text{sum}(\boldsymbol{c})\right) \tag{D.24}$$

$$s.t. \quad \boldsymbol{C}_f^T\boldsymbol{Z}_t=\boldsymbol{C}_g\boldsymbol{P}_t-\boldsymbol{C}_d\boldsymbol{D}_t+\boldsymbol{C}_w\boldsymbol{W}_t \tag{D.25}$$

$$\boldsymbol{P}^{\min}\le\boldsymbol{P}_t\le\boldsymbol{P}^{\max},\ \boldsymbol{Rd}\le\boldsymbol{P}_t-\boldsymbol{P}_{t-1}\le\boldsymbol{Ru},\ \theta_t(ref)=0 \tag{D.26}$$

$$-\boldsymbol{F}^{\max}\circ\boldsymbol{y}_t\le\boldsymbol{Z}_t\le\boldsymbol{F}^{\max}\circ\boldsymbol{y}_t \tag{D.27}$$

$$-M(\boldsymbol{1}-\boldsymbol{y}_t)\le\boldsymbol{Z}_t-\boldsymbol{BC}_f\boldsymbol{\theta}_t\le M(\boldsymbol{1}-\boldsymbol{y}_t) \tag{D.28}$$

Furthermore, the price of robustness introduced in Sect. 5.2 also can be used in the proposed robust optimization model with the consideration of the transmission line budget. Thus, the model (D.24)–(D.28) becomes

$$\min_{\boldsymbol{y}\in\{0,1\},\sum_{l=1}^{N_l}(1-y_l)\le\Delta}\ \boxed{\max_{W_k=W_k^f+W_k^e y_k,\ \sum_{k=1}^{N_w}|y_k|\le\Gamma,|y_k|\le1}}\ \min_{\boldsymbol{P}_t,\boldsymbol{Z}_t,\boldsymbol{\theta}_t}\quad\sum_{t=1}^{T}\left(\boldsymbol{b}^T\boldsymbol{P}_t+\text{sum}(\boldsymbol{c})\right) \tag{D.29}$$

$$s.t.\ \boldsymbol{C}_f^T \boldsymbol{Z}_t = \boldsymbol{C}_g \boldsymbol{P}_t - \boldsymbol{C}_d \boldsymbol{D}_t + \boldsymbol{C}_w \boldsymbol{W}_t \tag{D.30}$$

$$\boldsymbol{P}^{\min} \le \boldsymbol{P}_t \le \boldsymbol{P}^{\max}, \boldsymbol{Rd} \le \boldsymbol{P}_t - \boldsymbol{P}_{t-1} \le \boldsymbol{Ru}, \theta_t(ref) = 0 \tag{D.31}$$

$$-\boldsymbol{F}^{\max} \circ \boldsymbol{y}_t \le \boldsymbol{Z}_t \le \boldsymbol{F}^{\max} \circ \boldsymbol{y}_t \tag{D.32}$$

$$-M(\boldsymbol{1} - \boldsymbol{y}_t) \le \boldsymbol{Z}_t - \boldsymbol{B}\boldsymbol{C}_f \boldsymbol{\theta}_t \le M(\boldsymbol{1} - \boldsymbol{y}_t) \tag{D.33}$$

where N_w is the number of wind farms and Γ is the price of robustness.

D.3 Numerical Results

The same 30-bus test system as used in Sect. 5.3 is utilized, where Δ is chosen from 0 to 4. The model is solved by the CPLEX 12.5 and the results are shown in Table D.1. It can be observed that different Δ leads to different results. Note that

Table D.1 Robust optimal solution for switching with the budget set

α=0.1		Transmission capacity factor γ								
		1.4	1.3	1.2	1.1	1.0	0.9	0.8	0.7	0.6
Δ	4	{∅}	{2, 5, 7, 18}	{2, 26, 32, 35}	{2, 3, 6, 35}	{2, 10, 25, 41}	{5, 11, 28, 33}	{2, 6, 12, 33}	{7, 21, 23, 31}	{19, 22, 31, 41}
	3	{∅}	{9, 17, 29}	{1, 6, 7}	{2, 12, 35}	{2, 3, 35}	{1, 7, 33}	{19, 22, 31}	{5, 15, 33}	{15, 33, 41}
	2	{∅}	{1, 31}	{15, 31}	{15, 35}	{15}	{15, 33}	{15, 33}	{15, 33}	{33, 41}
	1	{∅}	{7}	{31}	{33}	{33}	{33}	{33}	{33}	×
	0	{∅}	{∅}	{∅}	{∅}	{∅}	{∅}	{∅}	×	×
α=0.2		Transmission capacity factor γ								
		1.4	1.3	1.2	1.1	1.0	0.9	0.8	0.7	0.6
Δ	4	{∅}	{1, 3, 28, 29}	{1, 20, 32, 35}	{2, 12, 30, 31}	{2, 5, 10, 41}	{1, 3, 11, 33}	{1, 31, 32}	{7, 19, 23, 31}	{9, 22, 31, 41}
	3	{∅}	{3, 9, 10}	{1, 6, 7}	{9, 11, 35}	{2, 3, 35}	{1, 17, 33}	{15, 31, 32}	{19, 22, 31}	{2, 33, 41}
	2	{∅}	{1, 7}	{11, 31}	{14, 35}	{11, 35}	{5, 33}	{31, 32}	{1, 33}	{33, 41}

(continued)

Table D.1 (continued)

α=0.1		Transmission capacity factor γ								
		1.4	1.3	1.2	1.1	1.0	0.9	0.8	0.7	0.6
			{31}	{31}	{33}	{33}	{∅}	{33}	{33}	×
	0	{∅}	{∅}	{∅}	{∅}	{∅}	{∅}	{∅}	×	×
α=0.3		Transmission capacity factor γ								
		1.4	1.3	1.2	1.1	1.0	0.9	0.8	0.7	0.6
Δ	4	{∅}	{2, 6, 7, 27}	{2, 7, 18, 35}	{4, 7, 8, 31}	{2, 3, 14, 33}	{3, 18, 30, 31}	{2, 3, 31, 32}	{7, 19, 23, 31}	{19, 22, 31, 41}
	3	{∅}	{4, 6, 30}	{2, 3, 31}	{2, 12, 35}	{1, 3, 35}	{1, 3, 33}	{15, 31, 32}	{28, 29, 32}	{2, 33, 41}
	2	{∅}	{1, 31}	{11, 31}	{15, 35}	{2, 35}	{14, 33}	{31, 32}	{29, 33}	{33, 41}
	1	{∅}	{33}	{33}	{33}	{35}	{33}	{33}	{33}	×
	0	{∅}	{∅}	{∅}	{∅}	{∅}	{∅}	{∅}	×	×

"×" represents that the model is infeasible. Besides, the robust objective value considering transmission line switching set is shown in Table D.2. When α = 0.2 without the price of robustness, the objective value is always \$3534.8 under any transmission capacity factor γ from 1.4 to 0.7. When transmission capacity factor γ becomes larger, Δ doesn't affect the optimal objective value, whereas when transmission capacity factor γ becomes smaller, Δ will affect the optimal objective value. In fact, Δ can be termed as the tradeoff between economy and reliability. Smaller Δ implies that the number of transmission lines available for switching is limited, so that the reliability is higher; larger Δ will affect the system's reliability but is more economic.

Table D.2 Robust optimal objective value for switching with the budget set ($)

$\alpha = 0.1$		Transmission capacity factor γ								
		1.4	1.3	1.2	1.1	1.0	0.9	0.8	0.7	0.6
Δ	4	3422.4	3422.4	3422.4	3422.4	3422.4	3422.4	3422.4	3428.1	3594.9
	3	3422.4	3422.4	3422.4	3422.4	3422.4	3422.4	3422.4	34774	3615.4
	2	3422.4	3422.4	3422.4	3422.4	3422.4	3422.4	3437.4	3477.4	3689.3
	1	3422.4	3422.4	3422.4	3422.4	3422.4	3422.4	3437.4	3477.4	×
	0	3422.4	3426.9	3471.8	3516.6	3561.5	3606.3	3651.2	×	×
$\alpha = 0.2$		Transmission capacity factor γ								
		1.4	1.3	1.2	1.1	1.0	0.9	0.8	0.7	0.6
Δ	4	3.5348	3.5348	3.5348	3.5348	3.5348	3.5348	3.5348	3.5350	3.6811
	3	3.5348	3.5348	3.5348	3.5348	3.5348	3.5348	3.5348	3.5657	3.7278
	2	3.5348	3.5348	3.5348	3.5348	3.5348	3.5348	3.5348	3.5898	3.7278
	1	3.5348	3.5348	3.5348	3.5348	3.5348	3.5348	3.5498	3.5898	×
	0	3422.4	3426.9	3471.8	3516.6	3561.5	3606.3	3651.2	×	×
$\alpha = 0.3$		Transmission capacity factor γ								
		1.4	1.3	1.2	1.1	1.0	0.9	0.8	0.7	0.6
Δ	4	3.6472	3.6472	3.6472	3.6472	3.6472	3.6472	3.6472	3.6472	3.8254
	3	3.6472	3.6472	3.6472	3.6472	3.6472	3.6472	3.6472	3.6572	3.8402
	2	3.6472	3.6472	3.6472	3.6472	3.6472	3.6472	3.6472	3.7022	3.8402
	1	3.6472	3.6472	3.6472	3.6472	3.6472	3.6472	3.6622	3.7022	×
	0	3422.4	3426.9	3471.8	3516.6	3561.5	3606.3	3651.2	×	×

Appendix E

Multiple Solution Set for Two-Stage Robust Interval Optimization Model

E.1 Method for Multiple Solution Set

The general mathematical model can be expressed as

$$(\textbf{MILP}) \qquad F_1 = \min_{\boldsymbol{w}\in \mathrm{R}, \boldsymbol{v}\in Z} \ \boldsymbol{c}^T\boldsymbol{w} \ \ s.t. \quad (\boldsymbol{w}, \boldsymbol{v}) \in \Theta \tag{E.1}$$

First, let one optimal solution and the corresponding objective value of (E.1) be $\boldsymbol{u}^{opt} = (\boldsymbol{w}^{opt}, \boldsymbol{v}^{opt})$ and F^{opt}, respectively. In order to find another optimal solution with the same objective value, we add an objective cut that constrains the new objective value through its current optimal value in (E.2).

$$F_1^{opt} \le \boldsymbol{c}^T\boldsymbol{w} \le F_1^{opt} + \varepsilon \tag{E.2}$$

We can also find the approximate optimal solution as (E.3), which has a small difference from the exact optimal solution.

$$F_1^{opt} \le \boldsymbol{c}^T\boldsymbol{w} \le F_1^{opt} + \varepsilon \tag{E.3}$$

where ε is a small gap to the optimal solution, which can be adjusted by decision makers. If ε is chosen as 0, (E.3) is the same with (E.2).

Because the current optimal solution satisfies all constraints in an inconsequential manner, it has to be precluded, explicitly, from the new search. To address this issue, we introduce a new constraint, $\boldsymbol{v} \neq \boldsymbol{v}^{opt}$, where $\boldsymbol{v}$ is a binary variable. The logic expression "exclusive" or (XOR, $\oplus$) can be employed to formulate "$\neq$" in the following expression.

T. Ding, *Power System Operation with Large Scale Stochastic Wind Power Integration*, Springer Theses, DOI 10.1007/978-981-10-2561-7

$$\sum_{i=1}^{m} \left(v_i \oplus v_i^{opt}\right) \geq 1 \tag{E.4}$$

Since XOR yields $v \oplus 0 = y$, and $v \oplus 1 = 1 - v$ for any binary variable v, (E.4) can be split into two parts by (E.4), as follows

$$\sum_{i=1 \text{ and } v_i^{opt}=0}^{m} v_i + \sum_{i=1 \text{ and } v_i^{opt}=1}^{m} (1 - v_i) \geq 1 \tag{E.5}$$

Later, let Γ^0 and Γ^1 denote index sets of the optimal integer solution $\boldsymbol{v}^{opt}$ valued at zero and one, respectively. Then, we have

$$\sum_{i \in \Gamma^0} v_i + \sum_{i \in \Gamma^1} (1 - v_i) \geq 1 \tag{E.6}$$

It has been established that (E.6) is cast as an integer cut that should be appended in (E.1). Hence, a different optimal solution can be computed.

Based on the above analysis, a recursive process is proposed to capture other optimal solutions with the same or nearly the same objective value.

Step 1: Solve the model (E.1), which gives the optimal solution $\boldsymbol{u}^{0,opt} = (\boldsymbol{w}^{0,opt}, \boldsymbol{v}^{0,opt})$ and optimal objective value F^{opt}; let $k \leftarrow 1$, $\Omega \leftarrow \{\boldsymbol{u}^{0,opt}\}$.

Step 2: Generate an objective cut in (E.3) and solve the minimum number of switched branches problem as follows.

$$\left(\mathbf{MILP}^{'}\right) \qquad F_2 = \max_{\boldsymbol{w} \in \mathrm{R}, \boldsymbol{v} \in Z} \sum_{i=1}^{m} v_i \tag{E.7a}$$

$$s.t. \quad (\boldsymbol{w}, \boldsymbol{v}) \in \Theta \tag{E.7b}$$

$$F_1^{opt} \leq \boldsymbol{c}^T \boldsymbol{w} \leq F_1^{opt} + \varepsilon \tag{E.7c}$$

Step 3: Calculate the optimal solution of (E.7) F_2^{opt} and generate an integer cut through (E.6) to find the MOSs with minimum switched transmission lines.

$$\left(\mathbf{MILP}^{'}\right) \qquad F_2 = \max_{\boldsymbol{w} \in \mathrm{R}, \boldsymbol{v} \in Z} \sum_{i=1}^{m} v_i \tag{E.8a}$$

$$s.t. \quad (\boldsymbol{w}, \boldsymbol{v}) \in \Theta \tag{E.8b}$$

$$F_1^{opt} \leq \boldsymbol{c}^T \boldsymbol{w} \leq F_1^{opt} + \varepsilon \tag{E.8c}$$

$$F_2^{opt} = \sum_{i=1}^{m} v_i \tag{E.8d}$$

$$\sum_{i \in \Gamma^{j,0}} v_i + \sum_{i \in \Gamma^{j,1}} (1 - v_i) \geq 1 \quad j = 1, 2, \ldots, k \tag{E.8e}$$

where $\Gamma^{j,0}$ and $\Gamma^{j,1}$ are the index sets of jth optimal integer solution $\boldsymbol{v}^{j,opt}$, valued at zero and one, respectively.

Step 4: Solve (E.7) by the same MILP solver and achieve a new optimal solution as $\boldsymbol{u}^{k+1,opt} = (\boldsymbol{w}^{k+1,opt}, \boldsymbol{v}^{k+1,opt})$.

Step 5: If the problem is infeasible, **stop**; otherwise, let $k \leftarrow k + 1$, $\Omega \leftarrow \{\Omega, \boldsymbol{u}^{k,opt}\}$, and go to **Step 3**.

According to the algorithm above, a new integer cut is generated at each iteration, which can be used to preclude the obtained MOSs in **Step 3**. Then, each integer cut is added into model (E.7). This algorithm can compute a new optimal solution with the same or approximate optimal objective values.

For instance, if the decision maker values branch l and hopes it not be switched, one constraint "$y_l = 1$" needs to be added. Now, we can give the following simple example to capture the multiple optimal solutions, where the gap is 10^{-6}.

$$\begin{aligned} \min \quad & 2x_1 + 2x_2 - x_3 \\ s.t. \quad & x_1 + x_2 + x_3 \geq 2 \\ & x_1, x_2, x_3 \in \{0, 1\} \end{aligned}$$

Since $x_1, x_2, x_3 \in \{0, 1\}$ and $x_1 + x_2 + x_3 \geq 2$, there are four feasible solutions: {0, 1, 1}, {1, 0, 1}, {1, 1, 0}, and {1, 1, 1}. The corresponding objective values are 1, 1, 4, 3. Therefore, the optimal value is 1 and there are two optimal solutions {0, 1, 1} and {1, 0, 1}.

If using the MILP solver we can find one optimal solution {0, 1, 1} with the optimal value 1, and then we set the model by (E.8) that

$$\begin{aligned} \min \quad & 2x_1 + 2x_2 - x_3 \\ s.t. \quad & x_1 + x_2 + x_3 \geq 2 \\ & x_1, x_2, x_3 \in \{0, 1\} \\ & 1 \leq 2x_1 + 2x_2 - x_3 \leq 1 + 10^{-6} \\ & x_1 + (1 - x_2) + (1 - x_3) \geq 1 \end{aligned} .$$

Then, the solution by the MILP solver is {1, 0, 1}, with the value 1.

Again, we construct a new model by (E.8), such that

$$\begin{aligned}
&\min \quad 2x_1 + 2x_2 - x_3 \\
&s.t. \quad x_1 + x_2 + x_3 \geq 2 \\
&\quad x_1, x_2, x_3 \in \{0, 1\} \\
&1 \leq 2x_1 + 2x_2 - x_3 \leq 1 + 10^{-6} \\
&x_1 + (1 - x_2) + (1 - x_3) \geq 1 \\
&(1 - x_1) + x_2 + (1 - x_3) \geq 1
\end{aligned}.$$

This is an infeasible model detected by the MILP solvers.

Therefore, the recursive process stops and we capture two MOSs in total, {0, 1, 1} and {1, 0, 1} with the optimal objective value 1.

E.2 Numerical Results

For the case in Sect. 5.3.2, if not considering the budget set Δ, the optimal solution by different solvers, such as CPLEX, GUROBI and MOSEK is shown in Table E.1, where different solvers gives different optimal solution but the same optimal objective value. This is because there are many kinds of heuristics in the branch and bound method of the mixed integer programming, such as depth-first and

Table E.1 Impact of different solvers on the optimal solution of two-stage robust interval transmission switching model

α = 0.1	Transmission capacity factor γ								
	1.4	1.3	1.2	1.1	1.0	0.9	0.8	0.7	0.6
Line switching no. (CPLEX)	{13}	{13}	{1, 2, 3, 6, 7, 13, 30, 33}	{1, 2, 3, 5, 7, 13, 18, 31, 35}	{1, 2, 3, 6, 10, 12, 13, 25, 27, 30, 41}	{1, 2, 5, 6, 11, 13, 14, 15, 18, 24, 26, 28, 31}	{3, 4, 6, 13, 18, 20, 21, 23, 28, 29}	{1, 2, 7, 13, 18, 21, 23, 28, 29}	{1, 6, 13, 18, 20, 22, 26, 28, 29, 31, 41}
Line Switching No. (MOSEK)	{1, 2, 3, 9, 28, 29, 31, 38, 41}	{2, 8, 12, 17, 18, 21, 23, 28, 35}	{7, 18, 20, 28, 31, 32, 37, 41}	{10, 14, 20, 25, 26, 29, 30, 33, 37}	{3, 4, 7, 9, 10, 14, 17, 23, 28, 29, 31, 32, 39}	{1, 2, 6, 8, 12, 15, 18, 24, 28, 29, 31, 33, 38}	{3, 5, 12, 18, 20, 23, 26, 28, 29, 31}	{2, 7, 12, 18, 21, 23, 29, 31}	{2, 9, 18, 20, 22, 26, 27, 31, 41}
Line Switching No. (MOSEK)	{1, 2, 10, 11, 13, 14, 15, 28, 37, 41}	{1, 2, 13, 19}	{1, 2, 6, 7, 9, 11, 13, 28, 39, 40}	{13, 35}	{1, 11, 13, 18, 25, 28, 29, 32, 40}	{1, 2, 6, 12, 13, 15, 24, 26, 28, 31, 39}	{3, 5, 8, 12, 13, 18, 19, 20, 23, 31, 39}	{2, 7, 12, 13, 18, 21, 23, 28, 29, 39}	{4, 5, 12, 13, 18, 20, 22, 26, 28, 29, 31, 41}

Table E.2 Multiple solution Set

Transmission capacity factor γ (%)	Number of multiple solutions	Number of minimum lines	
		Number of minimum lines	Number of multiple solutions
60	8	7	4
80	316	3	9
100	>3000	1	16

breadth-first methods. Since there are multiple optimal solutions, different solver adopted different search strategies may leads to different optimal solution.

Comparing Table E.1 with Table 5.2 in Sect. 5.3.2, we can find that different solvers lead to different optimal solution but the same optimal objective value. Moreover, when using different budget set Δ, the optimal solution is also different and the number of multiple optimal solutions will decrease.

Finally, the optimal solution with minimum switching line number can be computed by the proposed method. Take the uncertainty degree with 0.1 for instance and the results are shown in Table E.2. With the increase of transmission capacity factor γ, the number of multiple optimal solutions will increase. For $\gamma = 1$, the number of the multiple solutions is more than 3000. In fact, it needs only one switched transmission line to achieve the optimal objective value, but the solver may obtain the optimal solution more than one lines. Therefore, it is meaningful to find the optimal solution with minimum switching line number, which can more or less improves the reliability of the whole system. Meanwhile, the number of optimal solution with minimum switching line number is greatly reduced. For $\gamma = 1$, there are 16 optimal solutions with minimum switching line number, which only need to switch one transmission line.